Universidad de Valladolid

ESCUELA DE INGENIERÍAS INDUSTRIALES

DPTO. INGENIERÍA ENERGÉTICA Y FLUIDOMECÁNICA

TESIS DOCTORAL:

CONTRIBUCIÓN AL DESARROLLO E INTRODUCCIÓN DE COMBUSTIBLES GASEOSOS RENOVABLES MEDIANTE LA CARACTERIZACIÓN TERMODINÁMICA DE MEZCLAS DE SUS COMPONENTES UTILIZANDO UN DENSÍMETRO DE FLOTADOR DE SUSPENSIÓN MAGNÉTICA OPTIMIZADO

Presentada por

MARÍA ENGRACIA MONDÉJAR MONTAGUD

para optar al grado de doctora por la Universidad de Valladolid

Dirigida por:

DR. CÉSAR R. CHAMORRO CAMAZÓN

DR. ROLAND SPAN

Valladolid, Marzo 2012

Universidad de Valladolid

ESCUELA DE INGENIERÍAS INDUSTRIALES

DPTO. INGENIERÍA ENERGÉTICA Y FLUIDOMECÁNICA

PhD THESIS:

CONTRIBUTION TO THE DEVELOPMENT AND IMPLEMENTATION OF RENEWABLE GASEOUS FUELS THROUGH THE CHARACTERIZATION OF MIXTURES OF THEIR COMPONENTS BY USING AN OPTIMIZED SINGLE SINKER DENSIMETER WITH MAGNETIC SUSPENSION COUPLING

Submitted by

MARÍA ENGRACIA MONDÉJAR MONTAGUD

for the partial fulfillment of a Doctorate in Philosophy by the University of Valladolid

Directed by:
DR. CÉSAR R. CHAMORRO CAMAZÓN
DR. ROLAND SPAN

‘Sólo cuando el ultimo árbol haya sido talado,
sólo cuando el último río haya sido envenenado,
sólo cuando el último pez haya sido capturado,
sólo entonces te darás cuenta de que el dinero no se come’.

Proverbio de los Indios Cree.

‘Only when the last tree has been cut down;
Only when the last river has been poisoned;
Only when the last fish has been caught;
Only then will you find that money cannot be eaten.’

Cree Indian proverb.

ACKNOWLEDGMENTS

This thesis ends my phase as PhD student, full of work and learning, but also of fun. Simultaneously it begins a new phase that I wish to be as good as the first one. Without the help that I have received during this time, this thesis would have been, undoubtedly, more difficult.

Therefore I wish to thank Dr. César R. Chamorro, for helping me from the beginning of my PhD. For the guidance of this thesis, for his help, for his support, for his great dedication, for his great patience and for his advices, thanks a lot.

I also wish to thank Dr. Roland Span, for his help during my research stay at the Ruhr Universität Bochum and for the guidance of this thesis, *Danke schön!*

I would like to thank also to my colleagues of TERMOCAL research group, who helped me with my work and who supported me when I needed. For the good times in the laboratory, thanks.

I also thank my colleagues of the Lehrstuhl für Thermodynamik of the Ruhr Universität Bochum, for their hospitality and friendship. For the good times in Bochum, *Danke schön auch!*

I wish to thank, of course, my family and friends for supporting me in the difficult moments and for helping me to smile. For the good moments, thanks again.

And finally, I would like to thank the Programa Nacional de Formación del Profesorado Universitario (FPU) for providing the funding for my work.

Thanks to everyone who helped me!

“A los que me quieren y apoyan”

ABSTRACT

This thesis deals with the thermodynamic characterization of gaseous binary mixtures related with alternative fuels through accurate density measurements carried out with a single sinker densimeter with magnetic suspension coupling.

Several setup modifications affecting each of the measured magnitudes were performed to reduce the main uncertainty sources. After the improvements were executed the measurement uncertainty was thoroughly estimated.

Density measurements were carried out in a temperature range (250 – 400) K at pressures up to 20 MPa on the binary mixtures carbon dioxide with nitrogen, carbon monoxide with nitrogen, and carbon dioxide with methane.

The experimental data were compared with the density estimates calculated from the GERG-2004 reference equation of state for natural gases and related mixtures.

TABLE OF CONTENTS

LIST OF FIGURES

LIST OF TABLES

NOMENCLATURE

SYMBOLS

B	Buoyancy force, N
	second virial coefficient, $cm^3 \cdot mol^{-1}$
C	second order elastic constant
	third virial coefficient, $(cm^3 \cdot mol^{-1})^2$
E	Young modulus, Pa^{-1}
f	model function for the propagation of uncertainties law
g	gravity acceleration, $m \cdot s^{-2}$
k	coverage factor
K	compressibility modulus, MPa^{-1}
m	mass, kg
N	number of components of a mixture
p	pressure, MPa
r	correlation coefficient
R	resistance, Ω
s	standard deviation
T	temperature, K
u	standard uncertainty
U	expanded uncertainty
V	volume, m^3

W	resistance ratio, Ω/Ω balance reading, g
x	input quantity estimate
X	input quantity
y	output quantity estimate
Y	output quantity
Z	compressibility factor

GREEK SYMBOLS

α	reduced Helmholtz free energy thermal expansion coefficient, K^{-1}
δ	reduced density
ε_ρ	apparatus specific constant
ϕ_0	coupling factor
μ	mean
ν	degrees of freedom
ρ	density, $kg \cdot m^{-3}$
τ	reduced temperature
χ	magnetic susceptibility, $m^3 \cdot kg^{-1}$

SUBSCRIPTS

0	sinker volume calibration reference state
1	titanium sinker
2	silicon sinker
eff	effective degrees of freedom
em	electromagnet
exp	experimental data
EoS	calculated with the equation of state
i, j	input quantity numbers
MP	measuring point
n	number of independent repeated observations
N	total number of input quantities
oi	component i of a mixture
pm	permanent magnet
probe	temperature probe resistance
std	standard resistance
S	sinker
S0	sinker under vacuum
Sf	sinker immersed in fluid
TI	titanium calibrated weight
Ta	tantalum calibrated weight

ZP	zero point

SUPERSCRIPTS

r	residual behaviour
0	ideal gas behavior

ABBREVIATIONS

AAD	Average absolute deviation
Bias	Average deviation
CEM	Centro Español de Metrología (Spanish national metrology institute)
CF	Calibration factor
EA	European Co-operation for Accreditation
ENAC	Entidad Nacional de Acreditación de España (Spanish Institution of Accreditation)
EU	European Union
EURAMET	European Association of National Metrology Institutes
FTE	Force transmission error
GERG	European Gas Research Group
GUM	Guide to the Expression of Uncertainty in Measurement
IUPAC	International Union of Pure and Applied Chemistry
MaxD	Maximum relative deviation

MP	Measuring point, measuring position
NP	Null position
PC	Personal computer
PRT	platinum resistance thermometer
RMS	Root mean squared
SSMSD	Single sinker magnetic suspension densimeter
TSMSD	Two sinker magnetic suspension densimeter
ZP	Zero point

CHEMICAL SYMBOLS

CH_4	Methane
CO	Carbon monoxide
CO_2	Carbon dioxide
N_2	Nitrogen
O_2	Oxygen
Si	Silicon
Ta	Tantalum
Ti	Titanium

CHAPTER 1

INTRODUCTION AND MOTIVATION

1.1. MOTIVATION OF THE RESEARCH

The inspiration for the research project presented in this thesis is explained in the following sections.

Background: energy and environmental crisis

At the beginning of the 21st century the world must face two important threats: the deep crisis of the present energy model due to the depletion of oil and gas reserves and the increasing global warming caused by the greenhouse effect. These two problems, far from being uncorrelated, are two sides of the same coin: the current fossil fuel economy.

Fossil fuels, mainly coal, have long been used, together with other energy sources, to provide the necessary heat to cover human necessities. However, with the beginning of the Industrial Revolution at the end of the 18th century, there was a boom in fossil fuel consumption. The demand of coal and oil rose quickly and, in the early 19th century, coal was replaced by oil as the engine of economic growth. Since then it has been fuelling the development of the world up to the present day.

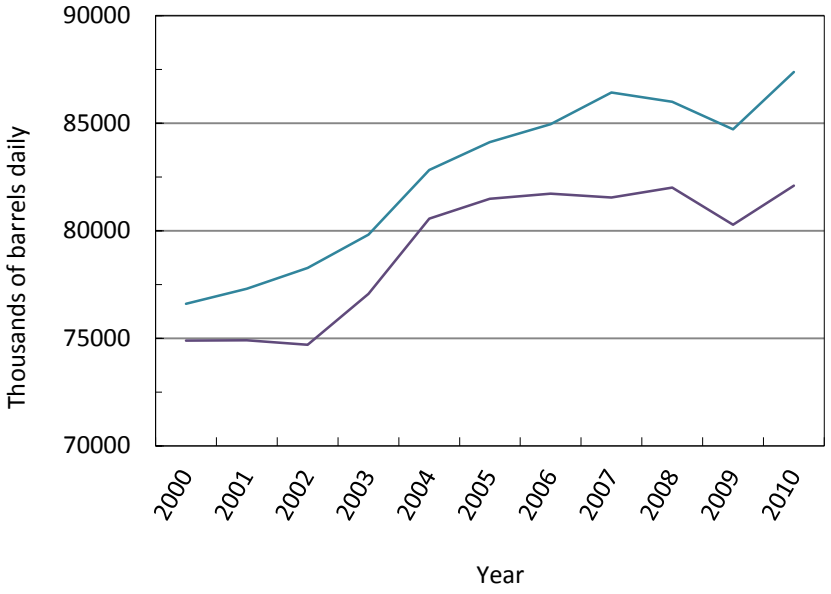

Figure 1.1. World oil production (—) and demand (—) in thousands of barrels per day for the last ten years (1).

Whether the so called 'peak oil' has already been reached or not, it is true that oil and gas resources are limited and are going into steady decline against the rising energy demands of the global population. Figures 1.1. and 1.2. show the world production and demand of oil and natural gas, respectively, for the last ten years (1). It can be observed that the consumption of both oil and natural gas has grown by approximately 15% and 30%, respectively, over the last ten years. This growing demand together with the increase in the exploitation of the oil and natural gas sources (which, in the case of oil, is lower than the world consumption) are accelerating the draining of the available reserves.

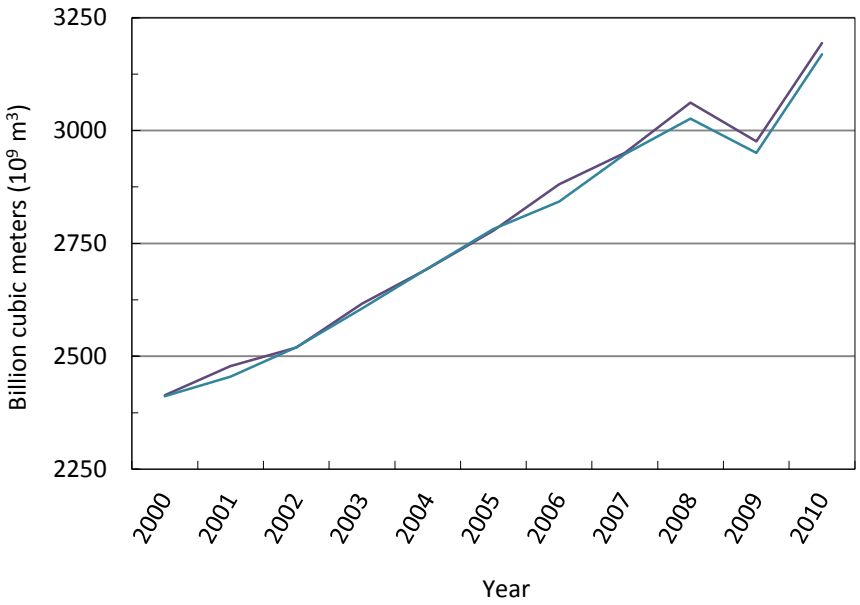

Figure 1.2. World natural gas production (—) and demand (—) in billion cubic meters (10^9 m^3) for the last ten years (1).

This unavoidable depletion of the fossil fuels production has contributed to the increase in the price of oil, which is setting record highs nowadays. In addition to this price rise, the important energy dependence of Europe questions more and more the sustainability of the current fossil fuel economy.

The replacement of the current fossil fuel economy

The difficult, but imperative, solution to this situation requires a world coalition to establish a new energy system to replace the actual fossil fuel economy. This transition

period, far from being unrealistic, is just one more of the transitions between different energy economies which have taken place since humanity has existed (2, 3). It is already known that the key transitions to alternative energies that have happened since the Middle Ages are always triggered by the erratic availability of the dominant energy supplies and the increase in energy prices.

In the 16th century the overuse of wood for heating and cooking purposes caused the deforestation of land which brought an energy and nutritional crisis. It was then that, coal arose as the solution to the declining wood economy.

In the early 19th century whale oil was the most common lubricant and fuel for lamps. The over-exploitation of this substance caused whales to be threatened with extinction. Thus, petroleum began to be commercialized as a substitute for whale oil.

Therefore, since the Industrial Revolution, which began between the end of the 18th and the beginning of the 19th century, the consumption of oil and carbon has increased to such an extent that the current world economy is based on these fuels together with natural gas (the so called 'fossil fuels'). Moreover, this situation has been accompanied by an increase in CO_2 emissions which is causing global warming, also called the greenhouse effect.

Since both the depletion of fossil fuels and global warming are evident facts, our current priority is the research focused on the development of new alternative energy resources. These alternative energies will have to replace fossil fuels by meeting, not only the energy requirements, but also environmental requirements in order to avoid an unsustainable economy.

Strategies towards a sustainable future

Strategies for the replacement of the current energy system by a new sustainable energy model are supported by three mainstays:

- The use of renewable energies. The use of renewable resources for the production of power and for transport facilities will result in a lower external dependence for energy supply and in lower emissions of carbon dioxide. Following this objective, the

European Union Parliament approved a resolution in the International Conference on Renewable Energy (Bonn, 2004) (4) by which the European Commission and Council were called to make the effort to reach a target of 20% for the contribution by renewable energy to the total primary energy consumption in the EU by 2020.

- The capture and storage of carbon dioxide. Since the transition to the new sustainable energy model requires a sufficient period of time, the capture and storage of carbon dioxide can help to reduce CO_2 emissions due to the use of fossil fuels and biomass. Regarding this topic, the European Council approved a compulsory energy plan by which a 20% drop of the total CO_2 emissions by 2020 was considered. This plan joined the previous Kyoto Protocol to the United Nations Framework Convention on Climate Change, by which the concentrations of greenhouse gases in the atmosphere are aimed to be controlled and reduced (5).

- Energy saving and efficiency. Since 'the cheapest and best energy is the saved energy', a significant effort must be focused on increasing the efficiency of energy processes and reducing energy losses to the minimum.

Alternative gas fuels as part of the new sustainable fuel economy

By alternative gas fuels, we mean those gases which are obtained from renewable sources but also the gas fuels coming from industrial by-products. The first group is those gases obtained from the gasification of different kinds of biomass (syngas) and from the anaerobic digestion or fermentation of biomass (biogas). The second group refers to those gases which are not obtained from renewable sources but are by-products of other industrial processes which can be exploited to increase the efficiency of the installations. An example of these gases would be the exhaust gases from coke ovens and blast furnaces. The use of these alternative gas fuels can play an important role in the new energy system, whether as renewable energy sources or by-products exploitation. Moreover these gas fuels can be used independently, but also injected in the existing natural gas networks, as is considered in several European projects such as Marcogaz (6), Bongo (7) and a research project for the characterization of energy gases of EURAMET (8), in which this work takes part.

Another advantage of the use of gas fuels would be the lower CO_2 emissions compared with the CO_2 emitted during the combustion of liquid or solid fuels.

The role of Thermodynamics in the development and exploitation of alternative gas fuels

Accurate knowledge concerning the thermodynamic behaviour of fuels is essential for the development and optimization of the exploitation, transport and storage processes in which the fuels are involved. This precise description of the thermodynamic properties of the fuel under determined physical conditions can be given by several correlations or, more extensively, by the equation of state of the fluid.

Nowadays, the thermodynamic behaviour of natural gas is known with a high accuracy thanks to extensive research work on the development of a reliable equation of state for natural gas, which began with Klimeck (9) in 2000 with a preliminary model for seven components and was continued by Kunz, Klimeck, Wagner and Jaeschke with the publication of the GERG-2004 equation of state (10) for natural gases and other related mixtures. This model was developed based on two principal mainstays: a new formulation based on multiparameter equations of state described by Span (11), and the extensive data base of various thermodynamic properties of pure gases, binary and multi-component mixtures.

Briefly, the basic formulation of the GERG-2004 for the estimation of the properties of mixtures consists of the sum of fundamental equations for each mixture component and functions which represent the mixture's behaviour.

The GERG equation of state is a fundamental equation explicit in the Helmholtz free energy a with the density ρ and temperature T as independent variables. Since the Helmholtz free energy, as a function of these two variables, is a fundamental form of an equation of state, all thermodynamic properties can be derived from it.

The Helmholtz free energy is usually expressed in its dimensionless form, as a sum of the Helmholtz free energy of the ideal gas α^0 and the residual behaviour term α^r, as indicated in Eq.1.1.

$$\alpha(\delta,\tau) = \alpha^0(\delta,\tau) + \alpha^r(\delta,\tau) \qquad \text{Eq.1.1.}$$

Here, $\tau=T/T_c$ is the inverse reduced temperature and $\delta=\rho/\rho_c$ is the reduced density, where T_c and ρ_c are the critical temperature and density for the considered fluid. While the first term of the Helmholtz energy as expressed in Eq.1.1. can be calculated by using the relations existing for ideal gas, the second term corresponding to the residual part of the real behaviour must be fitted with experimental data.

The Helmholtz energy is a magnitude which is not accessible by direct experimental measurements so it must be approximated by a mathematical expression whose coefficients are fitted by considering different experimental thermodynamic properties. Setzmann and Wagner (12) developed a methodology for the optimization of the structure of these mathematical expressions. These expressions contain a bank of terms combining polynomial terms and exponential terms of the two independent variables τ and ρ.

In the case of mixtures, both the ideal and the residual terms of the Helmholtz free energy are expressed as functions of the composition of the mixture, as expressed in Eq.1.2. and Eq.1.3.

$$\alpha^0(\rho,T,\bar{x}) = \sum_{i=1}^{N} x_i \left[\alpha_{oi}^0(\rho,T) + \ln x_i\right] \qquad \text{Eq.1.2.}$$

$$\alpha^r(\delta,\tau,\bar{x}) = \sum_{i=1}^{N} x_i \alpha_{oi}^r(\delta,\tau) + \Delta\alpha^r(\delta,\tau,\bar{x}) \qquad \text{Eq.1.3.}$$

In these expressions x_i is the molar fraction of each component of the mixture and $\triangle\alpha^r$ is the so-called departure function. The contribution of this last term is comparatively inferior to the contribution of the equations of each pure component and was only developed for some binary mixtures. For the rest of the mixtures or components, combining rules or adjusted reducing functions were used.

The importance of density data in the development of equations of state

The optimization of the residual term of the Helmholtz free energy is made by fitting it simultaneously to different thermodynamic properties so that the approach of the estimation of the equation is similar for all the properties.

However, of all the thermodynamic properties which can be measured to characterize the thermodynamic behaviour of a fuel, density data are especially important.

On the one hand, density is an accessible property through different experimental methodologies which are described in Chapter 2. For this reason, density data cover a great part of the current thermodynamic properties database. For example, from all the data collected concerning mixtures for the development and evaluation of the GERG 2004 equation of state, 69% were (p, ρ, T) data.

On the other hand, (p, ρ, T) data are preferable to other properties because of their 'linear behaviour'. The fitting of the parameters of the equation is made by minimizing the weighted residuum resulting from the deviations between the experimental and the estimated properties. When this minimization is made by using properties which are expressed as functions of the independent variables ρ and T (i.e. pressure as a function of density and temperature, $p(\rho, T)$) the resulting system of equations is linear, with the consequent simplification of the resolution and less computing time. The variables which accomplish this requirement are called the 'linear data'.

Here, the availability of high accuracy density data of several fluids is of great importance for the development and testing of the equations of state.

Moreover, experimental density data are used in several correlations for the indirect determination of other thermodynamic properties. For instance, density is one of the thermophysical properties involved in the determination of the Wobbe index. Following this line, the measurement of the density of different fuel mixtures is included in one of the activities of a current research project of the European Metrology Research Programme (EMRP), mentioned previously, concerning the characterization of alternative energy gases (8).

Density data are also used for the fitting of the virial coefficients of the virial equation of state, which are of great importance in the determination of other thermodynamic properties in the gaseous phase, especially near saturation (13).

In conclusion, density data, together with other experimental thermodynamic properties, are of great importance, since they can be used in several correlations for the indirect determination of less accessible properties (14).

The current reference equation of state for natural gases and related mixtures

The great interest in natural gas and, by extension other gas fuels, made it necessary to accurately characterize their thermodynamic behaviour over a wide range of conditions and compositions. Therefore, the AGA8-DC92 equation of state of Starling and Savidge (15) was developed as a prediction model for the properties of natural gases and mixtures containing natural gas components, in the gas phase. As new experimental data were reported and higher accuracies were demanded for new applications, the AGA8-DC92 model showed significant limitations, especially at low temperatures and for mixture compositions which differ significantly from that of natural gas. To overcome these limitations and to extend the range of validity of the equation to the entire fluid region, even if the available number of experimental data was poor in some regions, a new reference equation of state for natural gas and related mixtures, the GERG-2004 equation of state (10), was developed. However, the AGA8-DC92 model is still used as the current standard for natural gas in industry.

Recently, a new version of the GERG model, the GERG-2008 equation of state (16), has been released to extend the original number of components covered by the GERG-2004 (18 components) to 21 components. The new components are *n*-nonane, *n*-decane and hydrogen sulphide. Since none of these components are present in the compositions of the mixtures studied in this thesis, density data reported in this work are always compared with density values calculated from the GERG-2004 equation of state (10).

The new GERG-2008 equation of state is under consideration to be adopted as an ISO Standard (ISO 20765-2 and ISO 20765-3).

The GERG model was developed mainly for the estimation of the thermodynamic properties of natural gases, but also other related gas mixtures. In this way, a lack of data for mixtures containing minority components of natural gas is appreciable.

Table 1.1. gives typical values of the composition of alternative fuel gases, such as biogas or syngas, as compared to the composition of natural gas. As can be seen, biogases and syngases (from the gasification of biomass) have a lower methane content, but a higher content in other substances such as nitrogen, carbon dioxide, carbon monoxide and hydrogen. Only the gases produced from coal have higher contents in methane. Any binary mixture containing these components would be of great interest for study, since the contribution of new thermodynamic property data will be used to test and improve the current estimation models.

Table 1.1. Approximated composition of different fuel gases (6). CMM = coal mine methane. CBM = coal bed methane.

	Natural gas	Biogas Anaerobic digester	Biogas landfill	Coal CMM	Coal CBM	Biomass gasification with. O_2	Biomass gasification with air
CH_4	88.8	65.0	45.0	65.0	90.0	15.6	2.0
C_{2+}	8.3	0.0	0.0	1.5	2.2	5.8	0.0
H_2	0.0	0.0	1.5	0.0	0.0	22.0	20.0
CO	0.0	0.0	0.0	0.0	0.0	44.4	20.0
CO_2	2.3	35.0	40.0	16.0	3.3	12.2	7.0
N_2	1.1	0.2	15.0	18.0	4.5	0.0	50.0
O_2	0.0	0.0	1.0	0.5	0.0	0.0	0.0

1.2. OBJECTIVES OF THE THESIS

The main objectives of this thesis are enumerated as follows:

Improvement of the measurement uncertainty of the single sinker densimeter

The first objective of this thesis was to reduce the measurement uncertainty of the single sinker densimeter with magnetic suspension coupling, in order to accomplish the primary objective of this research work with the highest achievable accuracy and reliability.

To achieve the mentioned reduction in the measurement uncertainty of the three state point magnitudes (p, ρ, T) in the most optimized way and determine the most

important uncertainty sources, an uncertainty analysis was presented as the best method to determine the main uncertainty sources. This analysis could guide the modifications to perform on the single sinker densimeter in order to act only were necessary, from the uncertainty point of view.

Development of a control and data acquisition program

Both the measurement procedure control and the data acquisition needed to be controlled from the control computer to optimize the data acquisition time. New software accomplishing both ease of use and flexibility for modifications as per requirements was necessary.

Measurement of (p, ρ, T) data of binary mixtures of non-conventional fuels components

The main objective of this thesis is the accurate characterization of the (p, ρ, T) behaviour of different binary gas mixtures containing major components of alternative gaseous fuels, over a wide range of pressures and temperatures. This objective is accomplished via the measurement of experimental densities of the gas mixtures by using an accurate single sinker densimeter with magnetic suspension coupling. This objective is related with the above mentioned importance of accurate knowledge concerning the thermodynamic behaviour of alternative fuels. Therefore, binary mixtures containing nitrogen, carbon dioxide, carbon monoxide and methane were studied in this work.

Moreover, it can also be proved that the availability of experimental data in the literature for these mixtures was low, except for the case of mixtures of methane with carbon dioxide, or even very low in the case of mixtures of nitrogen with carbon monoxide.

Test of the current reference equation of state for natural gases

Another aim of this thesis was the test of the current reference equation of state for natural gases and related mixtures (17) when estimating the density of binary mixtures

containing gaseous fuels components. To this end, the experimental data measured for this work will be used to test the GERG-2004 equation of state.

Contribution to the density data base for the improvement of the mixture parameters in the reference equation of state for natural gas

Since the equations of state are under a continuous development and improvement process, the report of new accurate experimental data of any thermodynamic property is of great interest. Thus, the density data reported in this thesis will contribute not only to the test of the reference equation of state for natural gases and related mixtures, but also to the future improvement of its performance.

1.3. STRUCTURE OF THE THESIS

This thesis presents the improvement of the measurement uncertainty of a single sinker densimeter with magnetic suspension coupling and reports accurate and reliable density measurements for mixtures of carbon dioxide with nitrogen, carbon monoxide with nitrogen and carbon dioxide with methane.

The outline of this thesis is now described:

In the present **Chapter 1**, the importance of the density measurements of the mixtures studied in this work from the point of view of the actual energy perspective has been explained. The choice of the GERG 2004 equation of state for the estimation of thermodynamic properties for these mixtures has been described and the background of density measurement has been summarized.

Chapter 2 reviews the main methodologies used in the experimental determination of the density of fluids and the measuring principle of the single sinker densimeter with magnetic suspension balance used for the measurements presented in this work. The measuring technique and the equipment for the determination of each magnitude are described, and the control program developed and the automation of the measuring procedure are also detailed.

Chapter 3 describes the modifications which were performed on the single sinker densimeter for the improvement of the measurement uncertainty. The measurement uncertainty of the state point magnitudes is evaluated and the reduction in uncertainty achieved thanks to the improvements is studied and validated.

Chapter 4 presents density measurements for four mixtures of carbon dioxide with nitrogen containing 10, 15, 20 and 50 mole percent carbon dioxide. The agreement of the experimental density data with the calculated densities from the GERG-2004 equation of state is analyzed and compared with the experimental data reported by other authors. Second and third virial coefficients are reported for these mixtures.

Chapter 5 presents density measurements for two mixtures of carbon monoxide with nitrogen containing 5 and 10 mole percent carbon monoxide. The agreement of the experimental density data with the calculated densities from the GERG-2004 equation of state is analyzed and compared with the experimental data reported by other authors. Second and third virial coefficients are reported for these mixtures.

Chapter 6 presents density measurements for one mixture of carbon dioxide with methane containing 20 mole percent carbon dioxide. The agreement of the experimental density data with the calculated densities from the GERG-2004 equation of state is analyzed and compared with the experimental data reported by other authors.

Finally, **Chapter 7** summarizes the conclusions and recommendations reached after this work and the directions for future work.

The **Appendix** collects all the (p, ρ, T) experimental data measured in this work and enumerates the publications in international journals and congresses derived from this thesis. The research stay certificate for the Mention of European Doctorate can also be found here.

REFERENCES

1. British Petroleum. *BP Statistical Review of World Energy June 2011,* 2011.

2. SCHEER, H. *Solare Weltwirtschaft: Strategie Für Die Ökologische Moderne,* 2002.

3. SORENSEN, B.A History of Energy: Northern Europe from the Stone Age to the Present Day*. Earthscan Ltd*, 2011.

4. European Parliament. *European Parliament Resolution on the International Conference for Renewable Energies (Bonn,.* 2004.

5. *Kyoto Protocol,* 2011.

6. Marcogaz. *Final Recommendation - Injection of Gases from Non-Conventional Sources into Gas Networks,* 2006.

7. FLORRISSON, O. and PINCHBECK, D. *Biogas and Others in Natural Gas Operations (BONGO): A Project Under Development.* Burgel ed. 23 rd World Gas Conference, 2006.

8. HALOUA, F. et al. *Caloric Quantities and Density Measurement of Non-Conventional Gases,* 2011.

9. KLIMECK, R.; SPAN, R. and WAGNER, W. Development of a Reference Equation of State for Thermal and Caloric Properties of Natural Gases. Phase 1: Theoretical Results. *Report to GERG WG 1.34 (Lehrstuhl Für Thermodynamik, Ruhr-Universität Bochum)*, 1999.

10. KUNZ, O. et al. The GERG-2004 Wide-Range Reference Equation of State for Natural Gases and Other Mixtures*. GERG Technical Monograph Fortschr*, 2007.

11. SPAN, R. *Multiparameter Equations of State - an Accurate Source of Thermodynamic Property Data.* Berlin: Springer, 2000.

12. SETZMANN, U. and WAGNER, W. A New Method for Optimizing the Structure of Thermodynamic Correlation Equations. *International Journal of Thermophysics*, 1989, vol. 10, no. 6. pp. 1103-1126.

13. ICHIKURA, K.; KANO, Y. and SATO, H. Importance of Third Virial Coefficients for Representing the Gaseous Phase Based on Measuring PVT-Properties of 1,1,1-Trifluoroethane (R143a). *International Journal of Thermophysics*, 2006, vol. 27, no. 1. pp. 23-38.

14. ULBIG, P. and HOBURG, D. Determination of the Calorific Value of Natural Gas by Different Methods. *Thermochimica Acta*, 2002, vol. 382. pp. 27-35.

15. STARLING, K.E. and SAVIDGE, J.L. *Compressibility Factors of Natural Gas and Other Related Hydrocarbon Gases - AGA Transmission Measurement Committee Report 8.*, 1992.

16. KUNZ, O. and WAGNER, W. The GERG-2008 Wide-Range Equation of State for Natural Gases and Other Mixtures: An Expansion of GERG-2004. *To be Submitted to J. Chem. Eng. Data*, 2011.

17. KUNZ, O. et al. The GERG-2004 Wide-Rangereference Equation of State for Natural Gases. *GERG Technical Monograph and Fortschritt-Berichte VDI*, 2005.

CHAPTER 2

THE SINGLE SINKER DENSIMETER WITH MAGNETIC SUSPENSION COUPLING

2.1. STATE OF THE ART METHODS OF DENSITY MEASUREMENT

As mentioned in the first Chapter, density is one of the most important thermodynamic properties in the development of reference equations of state. Therefore very accurate experimental density values are essential for the fitting of the parameters of these equations of state as well as for the selection of appropriate departure functions.

Among all standard methods for density measurement the IUPAC (International Union of Pure and Applied Chemistry) (1) recognizes the measurement techniques showed in the scheme in Figure 2.1. as the most refined and accurate methods for density measurement of fluids.

As it can be seen, the techniques for the measurement of fluids density can be gathered in five main principles, which are described as follows:

- **Vibrating bodies:** these densimeters, commonly vibrating tube densimeters and vibrating wire densimeters, are basically a spring-mass system where the vibration frequency of a body is measured and subsequently related with the density of the fluid surrounding the body.

- **Buoyancy:** densimeters based on the buoyancy effect are based in the Archimedes's Principle and take into account the relation between the buoyancy force experimented by a body immersed in a fluid and the density of this fluid. The different types of buoyancy densimeters indicated in Figure 2.1. come from successive improvements of the hydrostatic balance densimeters.

- **Piezometers:** piezometers group three main methods for the determination of the density of fluids. In these three methods the temperature, pressure and amount of the fluid contained in a cell of known volume are measured. The main difference between the three methods lies in the way of determining the density. In fixed volume piezometers the density is usually calculated by determining gravimetrically the mass of fluid inside the cell. In variable volume piezometers the change in volume is

determined and related with the fluid pressure. Expansion piezometers relate the density of the fluid in two different volumes with the volume ratio.

- **Bellows volumetry:** these densimeters are a particular type of piezometer where the entire measuring cell which contains the fluid, or only a part of it, is a flexible bellows which transmits the pressure of the fluid with almost no loss in pressure. The displacement suffered by the bellow due to the volume change is measured and related with the pressure of the fluid.

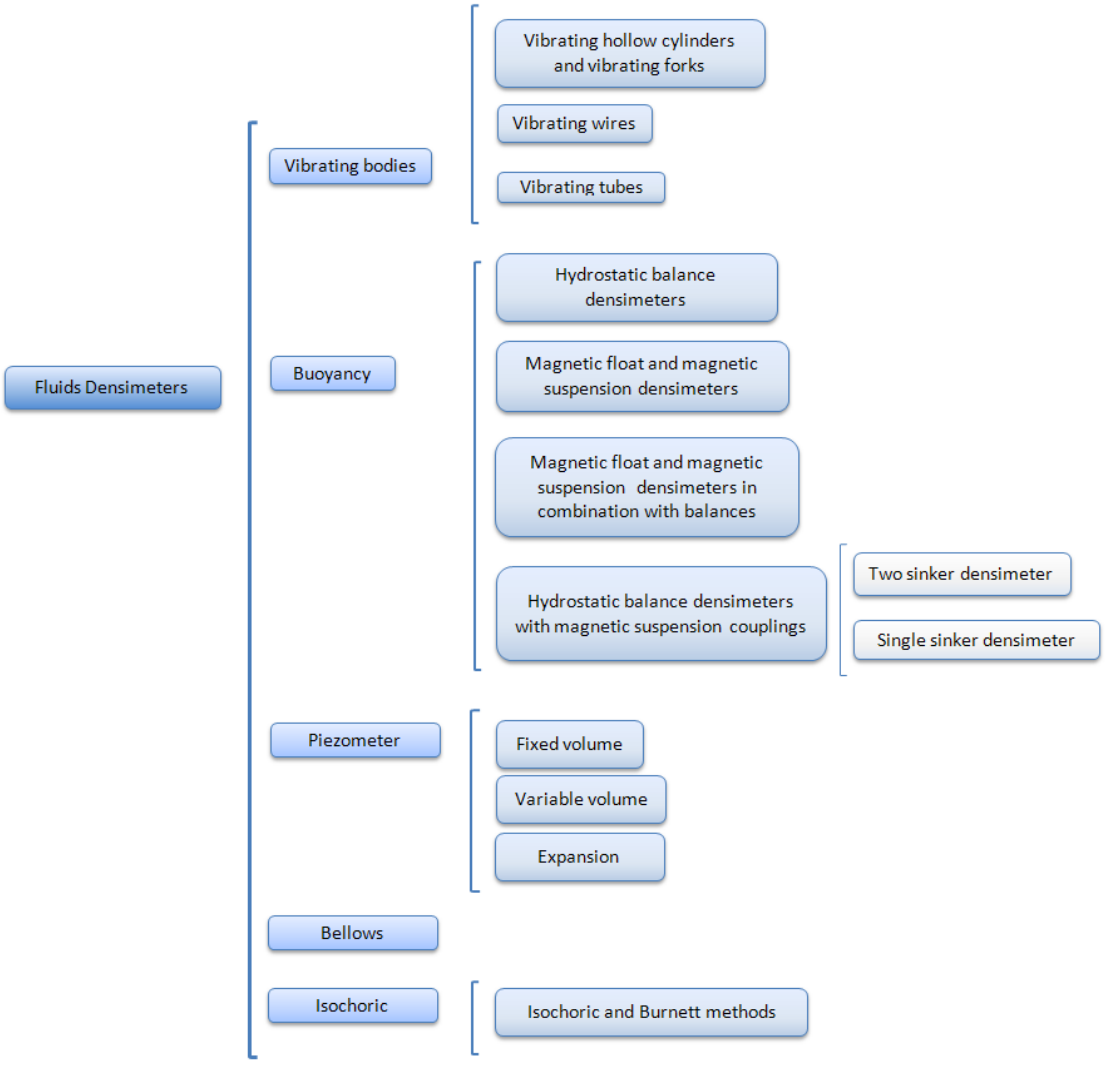

Figure 2.1. Densimetry methods schema.

- **Isochoric methods:** in these methods the measured fluid is contained in a high pressure vessel with constant volume which is immersed in a thermostatic bath. The

fluid is pressurized by means of a compressor and the density is obtained from the known vessel volume and the amount of fluid.

Despite bellows volumetry, piezometers and isochoric methods are techniques which have long been developed, the majority of density measurements are nowadays carried out with buoyancy or vibrating bodies based techniques. The measurement uncertainty of the former techniques has been reported to be around 0.1% (1), which is higher in value than the estimated uncertainty of sinker densimeters with magnetic suspension coupling which can reach values down to 0.01%. The estimated measurement uncertainty in density of vibrating tube and wire densimeters is typically 0.1%, but in some specific cases it can be reduced down to 0.01% by using selected reference liquids for calibration.

Table 2.1. collects the number of articles containing experimental densities of fluids for some of the densimetry methods showed in Figure 2.1. which has been published over the last five years (from 2007 to 2011).

Table 2.1. Number of articles containing density data of fluids for different densimetry methods, published over the last five years (2007-2011).

Densimetry method	Number of published articles
Vibrating wire	19
Vibrating tube	>100
Two sinker densimeter	11
Single sinker densimeter	13
Bellows volumetry	18
Piezometer	14
Isochoric	10

As it can be observed the most utilized methodology for density measurements is the vibrating tube densimeter. It was mentioned above that the uncertainty in density achieved with this method is not as low as that achieved with the sinker densimeters with magnetic suspension coupling. However, the extensive supply of commercial equipments based in this methodology (Anton Paar, Sodev Inc., ...), together with their ease of automation, make vibrating tube densimeters the most used technology for experimental determination of the density of fluids.

Wagner and Kleinrahm (2) concluded that only hydrostatic balance densimeters with magnetic suspension couplings could achieve very low uncertainties (in the order of a few parts per 10^4) covering large ranges of temperature and pressure over different fluid phases.

As indicated previously, hydrostatic densimeters use the Archimedes's Principle to determinate the density of a fluid by determining the buoyancy force acting on a body, the so called sinker. Initially, hydrostatic densimeters were used to measure the density of liquids at ambient pressure by weighting directly the mass of the sinker immersed in the liquid. Other kind of hydrostatic densimeters, the magnetic float and magnetic suspension densimeters, used a magnetic float immersed in the liquid in a stable position which was kept thanks to solenoids. The relation between the buoyancy force and the current needed to maintain the magnet stable was established with reference liquids. With this densimeter, liquids in a reduced pressure range could be measured.

Afterwards, magnetic float and magnetic suspension densimeters were combined with balances. In this new configuration, the cell containing the fluid or the magnetic buoy, respectively, was suspended from the balance. The magnet inside the cell could be magnetically suspended, so that the difference in mass of the cell containing the fluid, or the magnetic buoy, could be determined directly with the balance when the float was suspended or not. The main disadvantage of these densimeters was that the balance was in contact with the measured fluid and could be damaged.

Finally, the hydrostatic balance densimeters with magnetic suspension coupling were developed. In these densimeters the bodies supporting the buoyancy force of the fluid were not magnetic and their weight was transmitted without contact to an accurate balance by means of a new suspension coupling system. This methodology achieved the highest accuracies by avoiding significant side effects present in the former densimeters. Hydrostatic balance densimeters with magnetic suspension coupling are grouped by the number of sinkers used to determine the density as: two sinker densimeter with magnetic suspension coupling and single sinker densimeter with magnetic suspension coupling.

The two sinker densimeter, developed by Kleinrahm and Wagner (3) in the early 1980s, achieves currently the lowest uncertainties in density measurement in a wide density range. This high accuracy is obtained due to the contactless magnetic coupling, developed by Gast (4) and improved by Lösch et al.(5, 6), and to the application of Archimedes' principle as a differential method, which allows many of the disturbing side effects due to buoyant forces, surface-tension forces and gas adsorption to be avoided.

The measuring principle of the single sinker densimeter with magnetic suspension coupling used in this work is explained in the next section.

2.2. MEASURING PRINCIPLE OF THE SINGLE SINKER DENSIMETER WITH MAGNETIC SUSPENSION COUPLING

The single sinker densimeter with magnetic suspension coupling was firstly developed by Brachthäuser et al. (7) and described by Wagner et al. (8) in the early 1990s to simplify the complex design of the two sinker densimeter. This new densimeter lacked a sinker-changing device resulting in a less complex design and measurement process. However since some side effects, such as gas adsorption on the sinker surface, were not compensated for with the single sinker densimeter design, the measurement uncertainty in density was higher.

Afterwards, the original version of the single sinker densimeter was improved by Klimeck (9) in order to reduce the individual uncertainties in temperature, density and pressure measurement and to improve the performance of the densimeter. Thus, Klimeck introduced the two-stage thermostating system to improve the stability and uniformity of the cell temperature. Several compact versions of the single sinker densimeter, consisting in the unification of the coupling housing and the measuring cell, were afterwards developed.

The compact version of the single sinker densimeter with magnetic suspension coupling used and modified in this work was manufactured and supplied by Rubotherm Präzisionsmesstechnik GmbH, Germany. It is a compact version of the original single sinker densimeter and works in the gas phase in the temperature range

from 250 K to 400 K and pressures up to 20 MPa. The densimeter, together with the ancillary equipment supplied by other providers which are mentioned in the following sections, was assembled in our laboratory in 1996. The setup was described by Chamorro et al. in (10).

Several modifications have recently been performed on the densimeter in order to improve the measurement uncertainty in the three state point magnitudes: temperature, pressure and density. The uncertainty analysis and the reduction in the measurement uncertainty achieved after performing the modifications on the setup are presented in Chapter 3.

The single sinker densimeter with magnetic suspension coupling is based, as all buoyancy densimeters, on the Archimedes's Principle. The measuring principle of this densimeter consists in the measurement of the buoyancy force that experiments a sinker immersed in a fluid. This buoyancy force is proportional to the density of the fluid and the volume of the sinker. Therefore, if the sinker volume and the buoyancy force are known the density of the fluid surrounding the sinker can be obtained through Eq.2.1.

$$\rho(T,p) = \frac{B}{g \cdot V(T,p)} = \frac{m_{S0} - m_{Sf}}{V_S(T,p)} \qquad \text{Eq.2.1.}$$

, where $\rho(T,p)$ is the density of the fluid in kg·m^{-3}, as a function of its temperature and pressure, B is the buoyancy force in N, g is the gravity acceleration constant in m·s^{-2}, $V(T,p)$ is the sinker volume, in m^3, as a function of the fluid temperature and pressure. The buoyancy force acting on the sinker is determined by measuring the weight difference between the sinker mass in a vacuum m_{S0} and the sinker mass in the pressurized fluid m_{Sf}.

Figure 2.2. shows a simplified schema of the measuring cell. As it can be observed, the cell consists of a cylinder with two hollows: the coupling housing and the measuring cell itself. In the first housing the electromagnet of the magnetic coupling is lodged. Inside the measuring cell the sinker, the sinker support and the permanent magnet of the magnetic coupling are located.

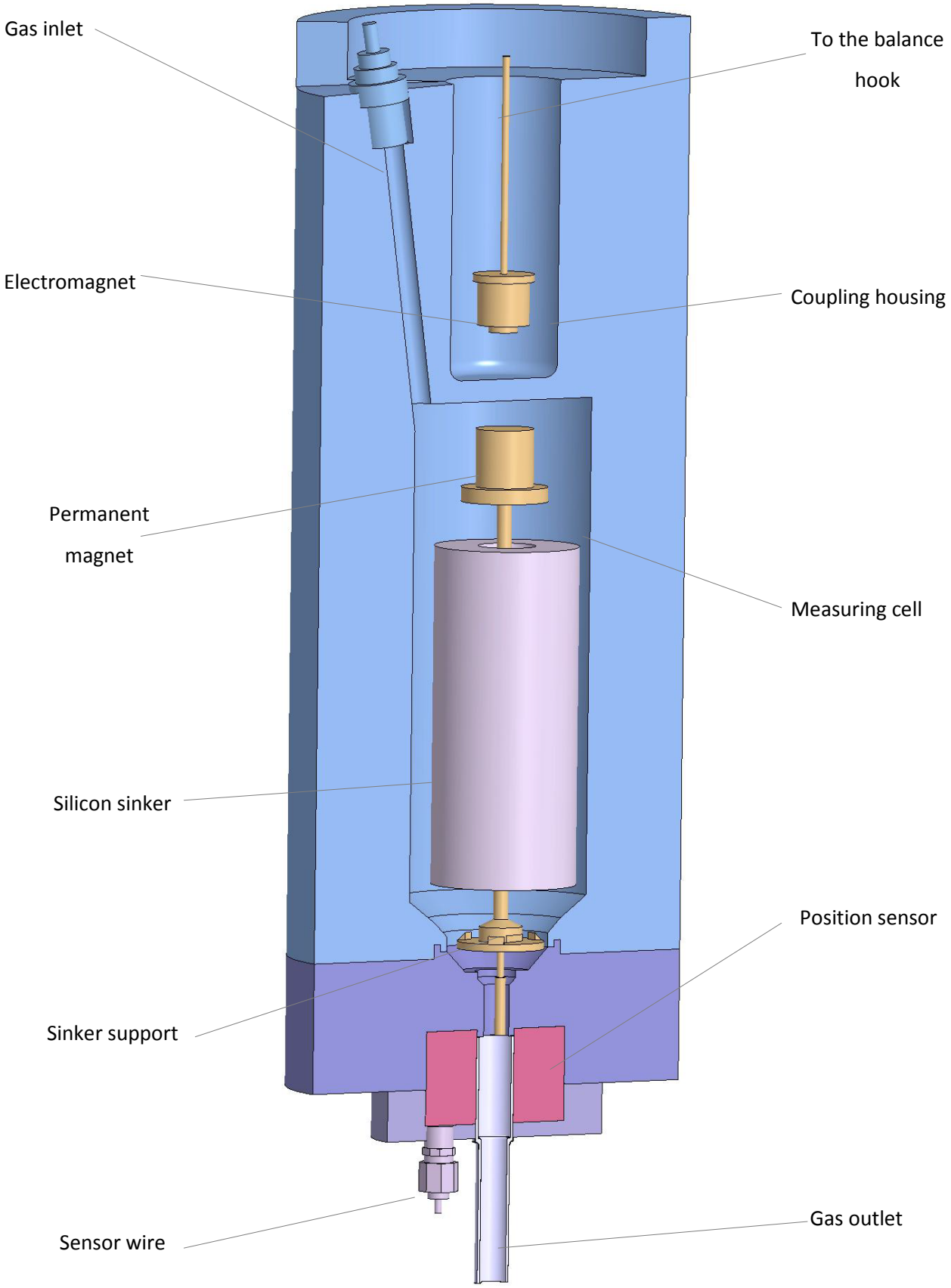

Figure 2.2. Schematic 3D view of the measuring cell.

When the magnetic suspension coupling switches the electromagnet, which is physically connected to the balance hook (as illustrated in figure 2.3.), it attracts the permanent magnet coupled to the sinker support. The position of the sinker support is controlled by a coil sensor allocated at the bottom of the measuring cell. Thus the sinker mass can be measured with an accurate balance avoiding any contact between the balance and the pressurized gas.

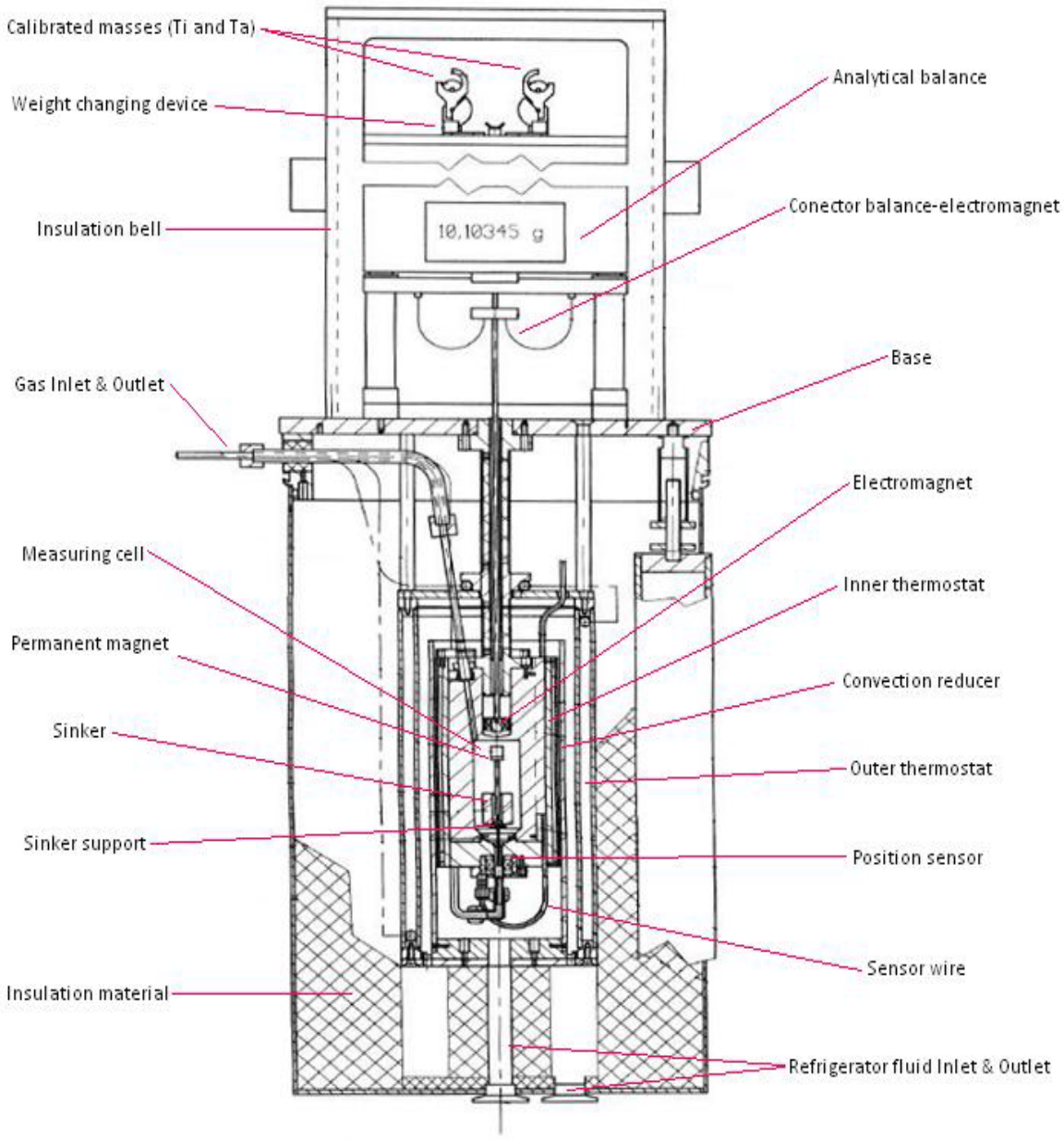

Figure 2.3. Schema of the single sinker densimeter.

The measuring cell cylinder is made of a copper-chromium-zirconium-alloy (CuCrZr) for two reasons: the quasi neutral magnetic behavior of this material and its high thermal resistance.

In the next sections, the measurement process of the single sinker densimeter and the ancillary equipment operation are described.

2.2.1. Pressure measurement

Pressure of the fluid is measured with two Digiquartz pressure transducers (Paroscientific 43KR-HHT-101 and Paroscientific 2300A-101, shown in Figure 2.4.) which work in the pressure ranges 2-20 MPa and 0-2 MPa, respectively. The two transducers are connected to two Digiquartz intelligent displays (730 and 735) and are connected to the filling system, depicted in Figure 2.5, far from the thermostat tubes to avoid the influence of the temperature of the refrigerator fluid. The pressure transducer which works in the pressure range up to 2 MPa is separated from the rest of the pressure network with a manual valve in order to avoid its exposition to an overpressure. This valve must be manually opened when the pressure of the fluid is below 2 MPa.

Figure 2.4. Pressure transducers used for the measurement of pressure in the range 0 – 2 MPa (down) and 2 – 20 MPa (up).

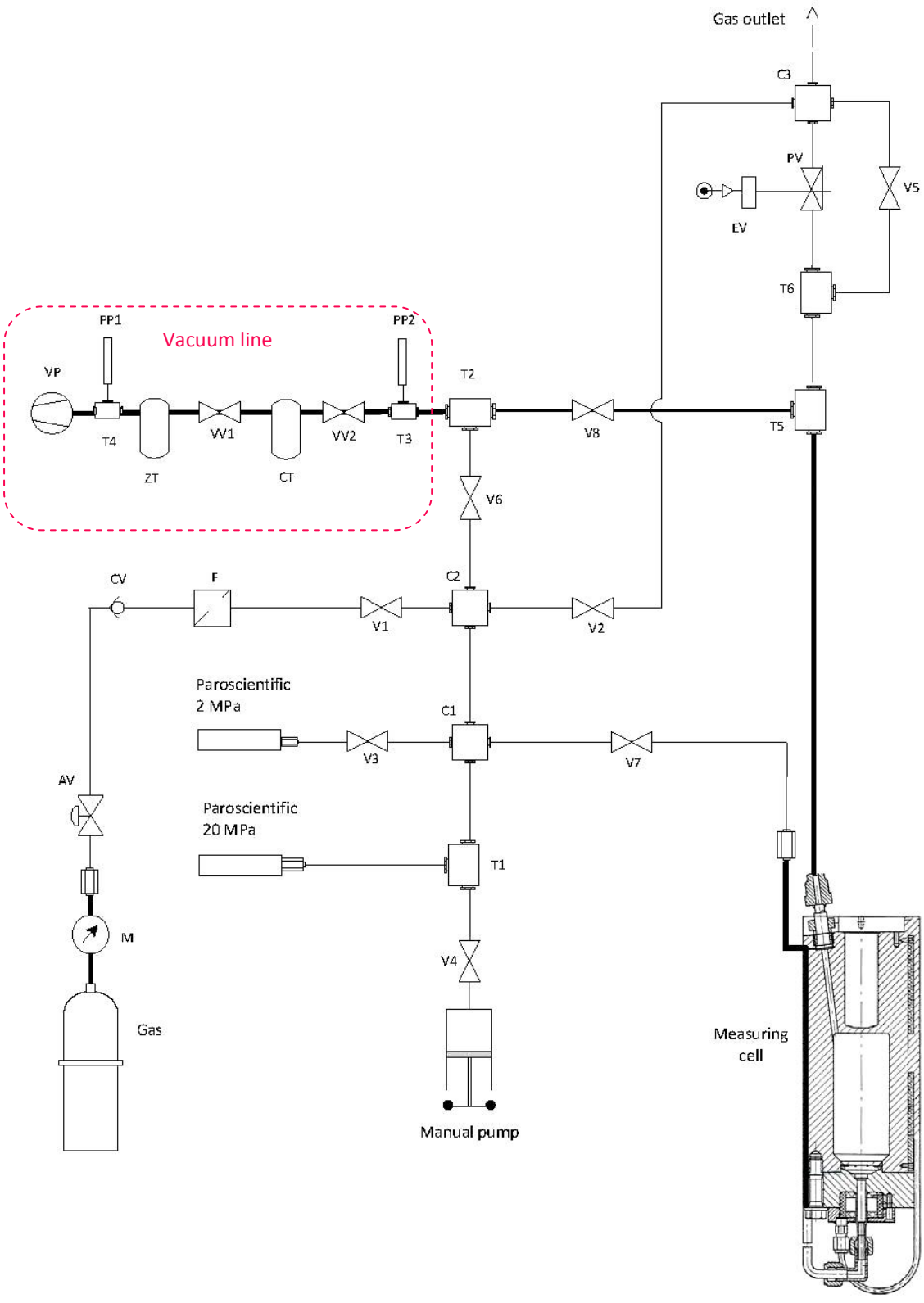

Figure 2.5. Schematic flow diagram of the pressure pipelines used to fill and evacuate the measuring cell of the single sinker densimeter. V1-V8: High pressure valves 20 MPa range. EV: Electrovalve. PV: Piston air operated valve. C1-C3 High pressure cross fittings. T1-T6: High pressure tee fittings. VP: Vacuum pump. M: Manometer. VV1-VV2: Vacuum line valves. ZT: Zeolites trap. CT: Cryogenic trap. PP1-PP2: vacuum probes.

a)

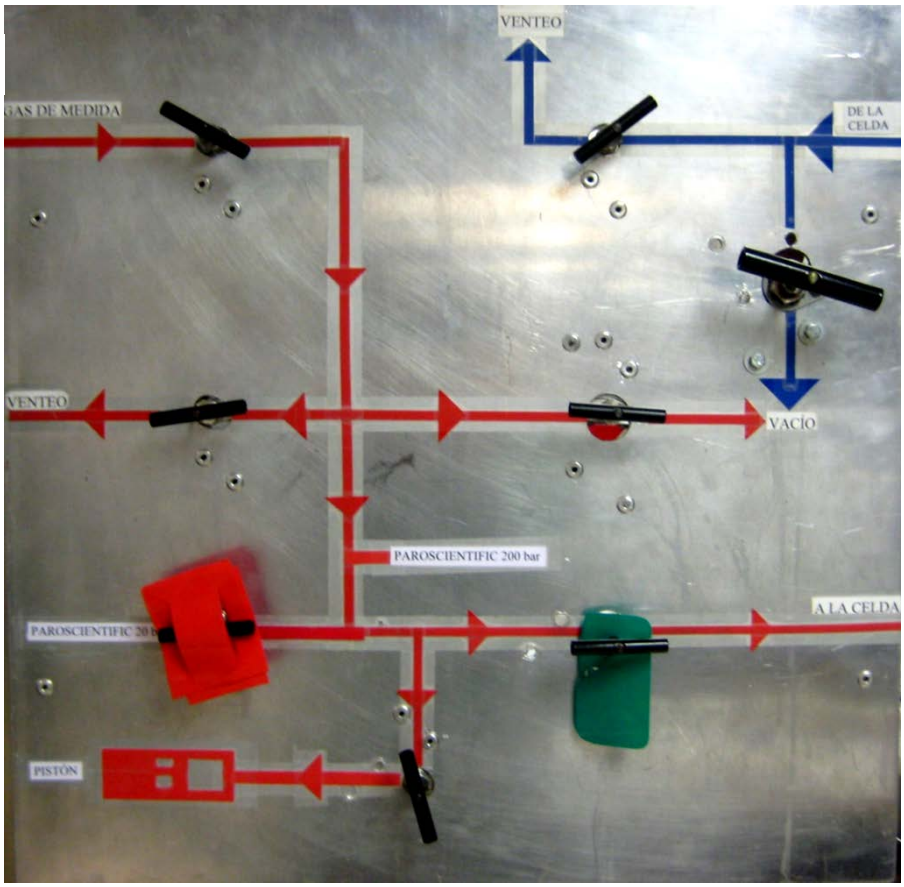

b)

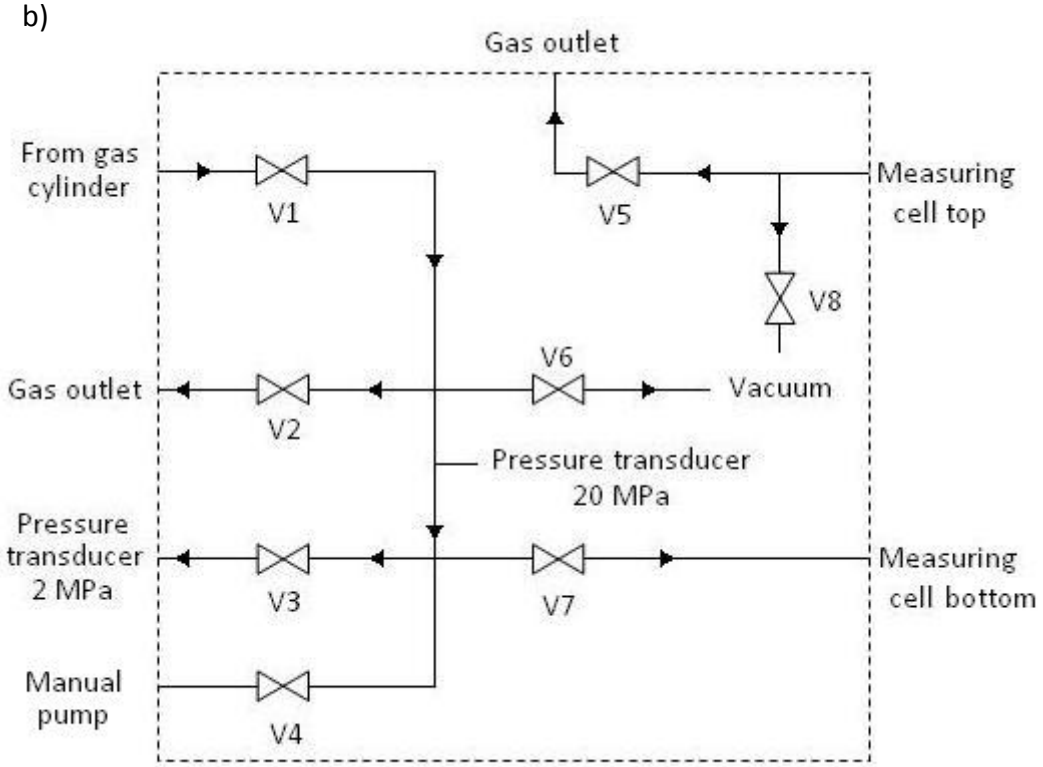

Figure 2.6. a) Valves panel. b) Schema of the pressure panel. Green cards are placed on opened valves and red cards indicate which valves must not be opened in order not to expose the pressure transducer for the range 0 – 2 MPa to an overpressure.

Pressure network

All the pipelines of the pressure network are made of stainless steel. Pipelines connecting the measuring cell with the pressure network and pipelines of the vacuum line had and inner diameter of 1/4”. Tubes connecting the gas cylinder with the pressure network have an inner diameter of 1/8”. The rest of the pipelines of the installation have inner diameters of 1/16”. All the valves used to connect the different parts of the pressure network and the tee and cross fittings were from HIP (High Pressure Equipment Company) and could work at pressures up to 15000 psi.

The manual pump utilized for the pressurizing of the measuring cell is a standard laboratory high pressure generator (HIP Model 87-6-5, 5000 psi) made of stainless steel.

Filling and pressurizing of the measuring cell

Filling of the measuring cell is accomplished manually through the valves panel represented and schematized in Figure 2.6.

The gas cylinder is connected to the pressure network by means of a needle valve which is used to control the gas flow during the filling of the measuring cell. Two cases are considered when filling the cell up to a pressure of 20 MPa:

- If the gas cylinder pressure is already 20 MPa or above, the measuring cell is filled by opening valves V1 and V7 with a continuous and moderate gas flow.

- If the gas cylinder pressure is below 20 MPa a filling cycle must be followed to increase the pressure of the fluid contained in the cell up to 20 MPa. In the first place, both the measuring cell and the manual pump are filled up to the gas cylinder pressure. Then, valve V1 is closed and the fluid is pressurized by using the manual pump. Next, valve V7 is closed and valve V1 is opened to fill the pipelines and the manual pump with gas. The pressure in the pipelines is increased up to the current pressure of the cell and then up to the limit. This cycle is repeated until the pressure inside the cell has the required value.

Pressure transducers were conveniently insulated to avoid deviations from the real pressure value due to sudden changes of the room temperature.

Evacuating of the measuring cell

The evacuation of the measuring cell can be accomplished manually, through one of the evacuation valves, or automatically through a pneumatic evacuation valve.

Manual evacuation

The manual evacuation of the cell which can be done to depressurize the cell before the measurement of the sinker mass in a vacuum or because of safety reasons is accomplished through one of the two evacuating valves (V2 and V5).

Automatic evacuation

The automatic evacuation of the cell is done to change the pressure to the next pressure step during the automatic measuring of an isotherm, but also if the pressure inside the cell exceeds 20 MPa. It is done thanks to a piston air operated valve (Mini-Hippo Piston air-operated valve 50 – 90 p.s.i.) which is controlled remotely from the control PC. When the last measurement point of a pressure step is finished, the piston air operated valve opens while the pressure transducer Paroscientific 43KR-HHT-101 controls the gas pressure. When the gas pressure reaches the next pressure step value, the automatic valve is closed.

Vacuum system

The vacuum system is connected to the pressure network through valves V6 and V8, to evacuate all the pressure pipelines or only the measuring cell, respectively. Vacuum in the cell is achieved with a two-stage rotator vacuum pump LEYBOLD model TRIVAC D8B, in Figure 2.7., which can create a vacuum of 0.5 Pa ($5 \cdot 10^{-3}$ mbar). Two traps are placed between the vacuum pump and the pressure network of the densimeter to prevent impurities and damaging vapors from entering into the measuring cell. The first trap, a zeolite trap LEYBOLD model FA 2-4, avoids the migration of water or

hydrocarbons molecules from the vacuum pump to the cell. The second trap consists in a cold trap LEYBOLD model TK 4-8, which protects the pump from damaging vapors. This cold trap must be filled with liquid nitrogen when the vacuum pump is working.

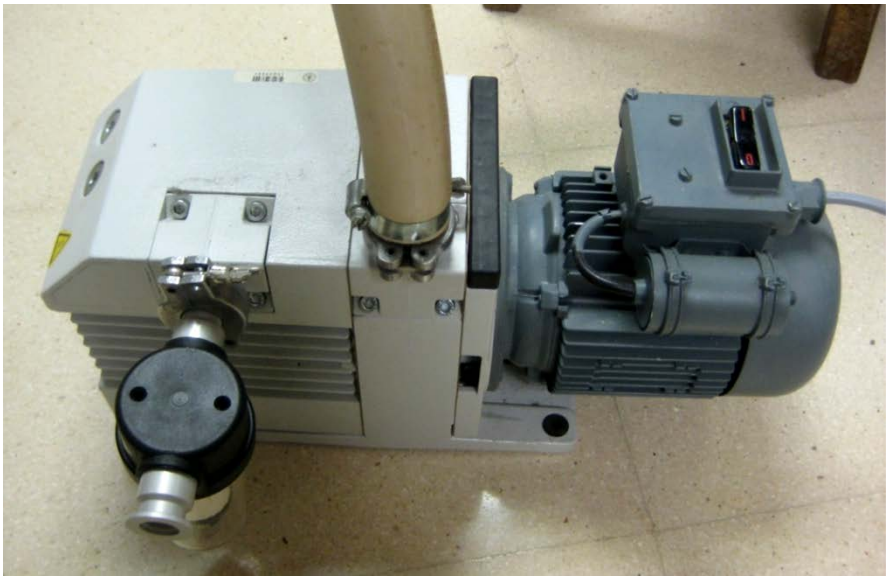

Figure 2.7. Leybold vacuum pump.

The vacuum was measured by means of two vacuum probes connected to a vacuometer THERMOVAC model TM22 which works in the pressure range from $5 \cdot 10^{-4}$ to atmospheric pressure.

2.2.2. Temperature measurement

Temperature inside the cell is determined by means of two PRT-25 probes (Minco S1059PJ5X6) which are placed diametrically opposed at half the height of the measuring cell. Another PRT-25 probe, Rosemount, is placed next to the coupling housing to determine if vertical temperature gradients exist. These probes, which locations are given in Figure 2.8., are connected to an AC comparator resistance bridge (Automatic Systems Laboratory model F700) through a Multichannel Switchbox (Automatic Systems Laboratory model SB 148/01). The bridge measures the resistance ratio between the PRT-25 probe and an external standard calibrated resistor (Tinsley model 5685A, 25 Ω). The external resistor is thermostatized at 36 ºC.

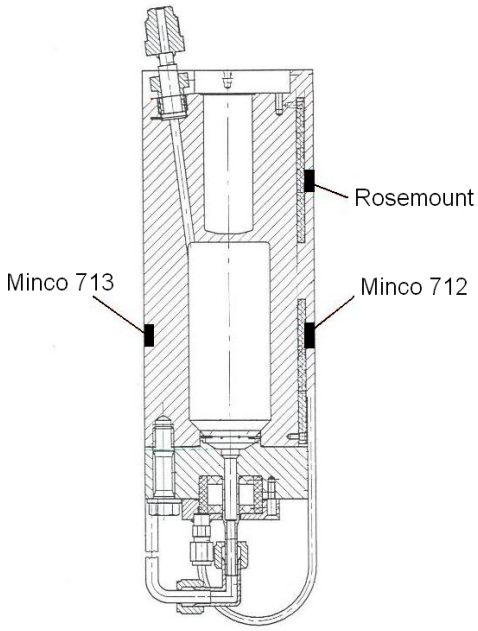

Figure 2.8. PRT-25 probes location in the measuring cell.

Thermostatization of the cell

The thermostatization of the measuring cell is accomplished thanks to two independent thermostating systems: the primary system, which consists of a double-walled stainless steel cylinder which surrounds the cell, and the secondary system, which consists of an electric resistance directly in contact with the measuring cell wall. To achieve a determined temperature of the fluid contained in the measuring cell, firstly the thermostatic bath is switched to a temperature slightly lower than that required and secondly the required temperature is achieved by using the electronic temperature regulator.

Outer thermostat system

The outer thermostat system, or primary system, consists of a double-walled steel cylinder through which a fluid (silicon oil Dow Corning 200 Fluid, viscosity 10 cst) is passed from an external temperature-controlled bath (Julabo model MV FP50). The working range of the thermostatic bath is (-50 – 200) ºC. A convection reducer, consisting in a copper cylinder, is placed between the double-walled cylinder and the inner electrical heating system to ensure a homogeneous heat transmission to the cell and avoid the convection of the fluid inside the measuring cell. Figure 2.9. shows the

steal double-walled cylinder of the outer thermostat during the assembly of the densimeter together with an schema of the measuring cell with the two stage thermostat and the copper cylinder.

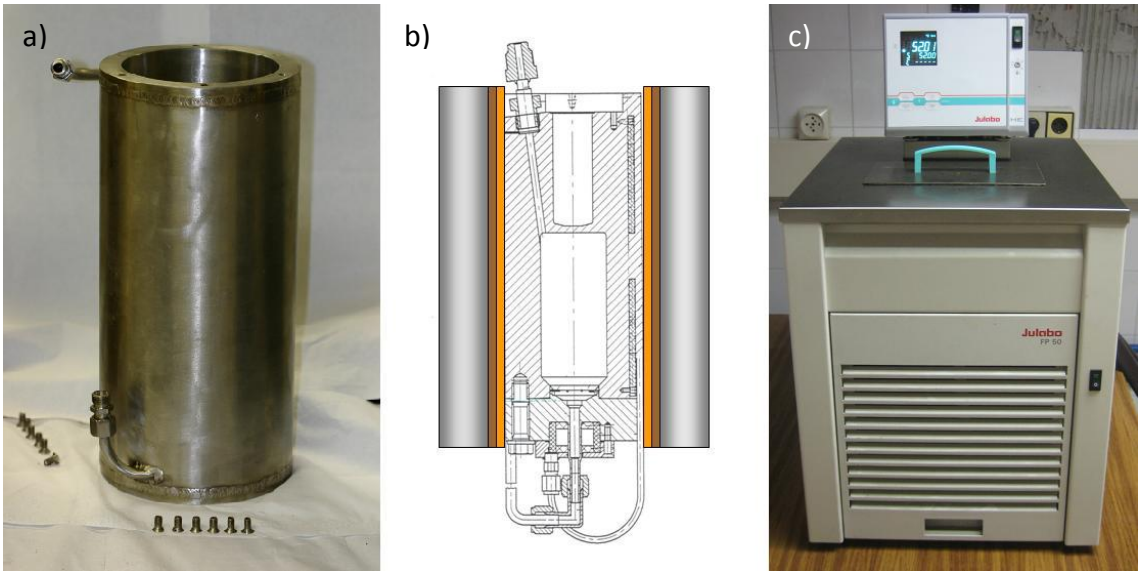

Figure 2.9. a) Steel cylinder during the assembly of the densimeter. b) Schema of the location of the steel cylinder with respect to the measuring cell and the electric resistance. c) Thermostatic bath Julabo MV FP 50.

Inner thermostat system

The inner thermostat, or secondary system, consists in an electrical heating system which is directly in contact with the measuring cell wall that is controlled by an electronic temperature controller (Julabo model MC-E). This electronic temperature controller is capable of controlling the temperature of the electrical resistance based on the temperatures values given by three PRT-100 probes A1, A2 and S. Probe S is a safety temperature probe and probe A2 is used for the temperature control. A1 is utilized for a secondary temperature control which is not used in this configuration. Figure 2.10. shows the electrical heating cylinder during the assembly of the densimeter together with an schema of the measuring cell and the location of the secondary stage thermostat, and the thermostatic bath.

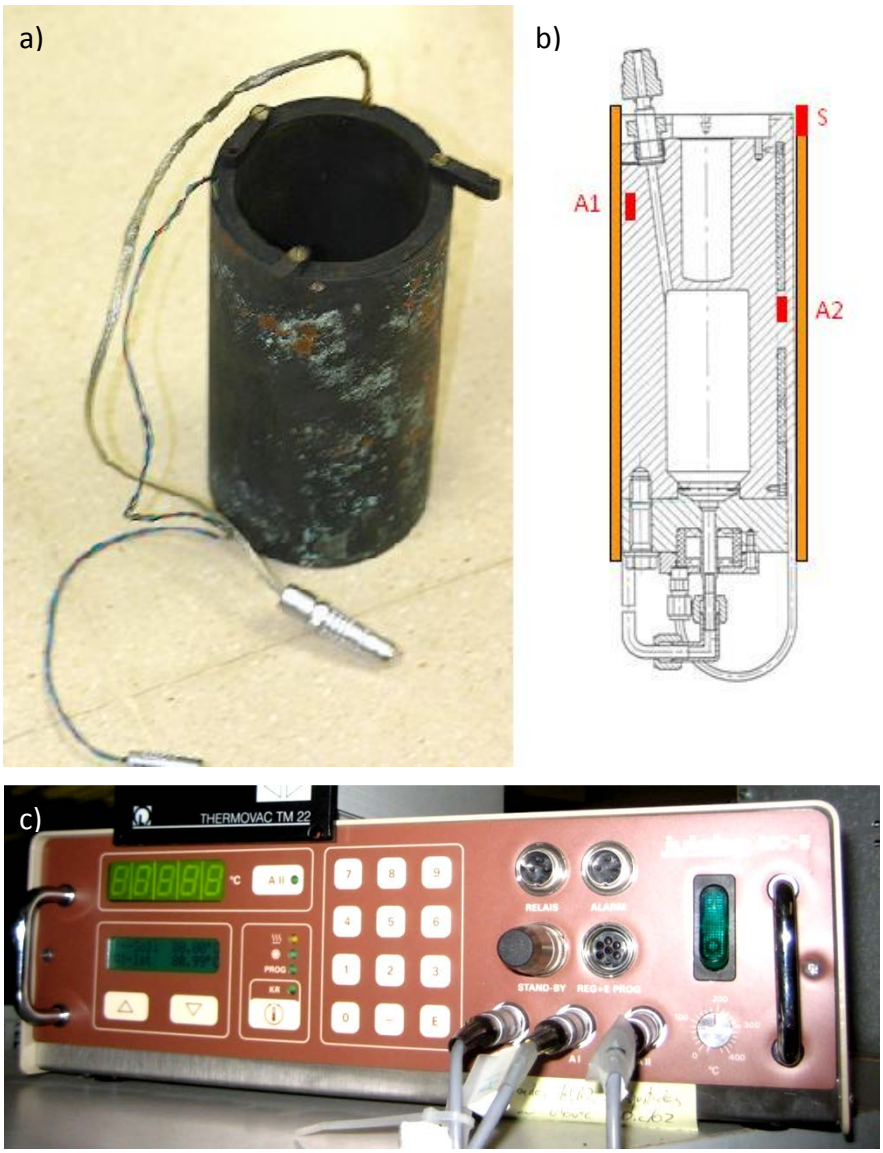

Figure 2.10. a) Electrical resistance controlled by the electronic temperature regulator during the assembly of the densimeter b) Schema showing the position of the electrical resistance with respect to the measuring cell and the PRT-100 probes S, A1 and A2. c) Electronic temperature controller Julabo MC-E.

Insulation of the measuring cell

The measuring cell was insulated with a cell silicone foam (250 $kg \cdot m^{-3}$) for a working range (213 – 473) K. Finally a casing with a synthetic rubber made of polyethylene (Armaflex) for the temperature range (203 – 383) K was disposed.

A study about the stability of the temperature inside the cell, based on a previous study (11), was performed over the whole temperature working range of the densimeter (250 – 400) K to compare the two stage thermostat system with the use of only the secondary system thermostat. Results yielded that the deviations in the

temperature of the cell were lower when the two stage system was used than when only the electrical heating system was used.

Laboratory room temperature

The single sinker densimeter is located in a 18 m^2 room where the temperature is controlled by an air conditioning system which is set to a temperature between 20 ºC and 22 ºC. Since the room temperature could affect to the pressure transducers operation its value was also measured during the measurement procedure.

2.2.3. Mass measurement

Mass measurements in the densimeter are made by means of the accurate analytical microbalance (Mettler Toledo model AT261 DeltaRange) showed in Figure 2.11. Main technical characteristics of the balance are summarized in Table 2.2.

Table 2.2. Technical characteristics of the microbalance Mettler Toledo AT261 Deltarange.

Characteristic	Typical value
Resolution	0.01 mg
Maximal capacity	205 g
Repeatability	0.015mg
Linearity	±0.08 mg
Linearity below 10g	±0.03 mg
Stabilization time	8-12 seg
Temperature drift	±1.5 ppm/ºC

The high accuracy balance is connected to the control PC by means of a data bus so that it can be completely operated from the control program. It can be also operated manually. The balance is assembled above the measuring cell and rests over a firm and vibration-free aluminium structure.

The analytical microbalance was in situ calibrated, following the procedure described in the Guidelines on the calibration of non-automatic weighing instruments of Euramet (12), after the modifications were carried out and before the beginning of the measurements presented in this thesis to estimate its calibration uncertainty. Instead of the recommended weights to be used as standards for the calibration, the titanium and tantalum masses were utilized.

Figure 2.11. Microbalance Mettler Toledo AT261 assembled in the densimeter installation.

The operation of the balance in the whole setup has two particularities. The first one is the existence of a magnetic coupling between the balance hook and the sinker inside the measuring cell. The second one is an automatic calibrated masses changing device, by which compensating weights are placed over the balance plate. The reason of the use of the magnetic coupling, as mentioned previously at the beginning of the Chapter, is the contactless transmission of the weighting force from the sinker inside the measuring cell to the balance hook, which allows high pressures and extreme temperatures to be reached without affection of the microbalance. The operation and particularities of this magnetic coupling is described in detail later. The masses changing device is used to force the balance to operate in the low weight range, so that the non-linearity effects of the balance can be neglected, and to perform a calibration of the balance not affected by the air buoyancy effect. This device is described in the following subsection. Both particularities determine the mass measurement procedure which is explained now.

Weight changing device

Any electronic balance presents, independently of its quality, the so called 'nonlinearity effect'. This effect due to the non-ideal character of all balances, can be defined as a deviation of the balance's real curve, which represents the balance indication as a function of the real load measured, from a straight line. This effect, which is represented in Figure 2.12. means that the balance indication can differ from the real value of the load, even when the balance has been calibrated in several calibration points over its whole working range. Thus, if the balance is calibrated taking points A and B as weight calibration points, the balance indication for a weight between these two calibrations points can differ from the real value of the load. However, if the weighting point is close to one of the calibrating weights A or B, the difference between the indication of the balance and the real value of the load becomes almost imperceptible.

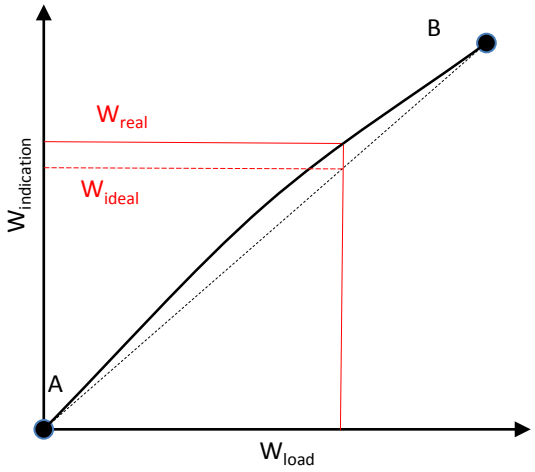

Figure 2.12. Nonlinearity effect (—) of the real curve of a balance between two calibrating points A and B. Here W_{load} refers to the load weight while $W_{indication}$ indicates the balance reading for that load.

Since the calibration weights used are always affected by an uncertainty value which can produce a distortion of the real weight of the loads, the best range for a correct operation of the balance avoiding the nonlinearity effect is that next to the zero weight.

In order to work as closa as possible to this range, the weight change device was incorporated to the balance. As it can be seen in Table 2.1., the maximal capacity of our microbalance is 205 g. The sinker mass is m_S≈60 g and the variations of its weight

due to the buoyancy force produced by the gas can be up to 10 g for fluid densities of 400 kg·m^{-3}. Thus, if the balance is tared with a calibrated mass of approximately m_{cal}≈60 g, which is placed directly on the balance plate, the mass measurements would move away from the zero point up to 10 g, so that the nonlinearity effect would be lower than if it was working at 60 g. However, the introduction of this calibrated mass would induce an additional term in the load weight due to the buoyancy force of the air acting on this mass. Since this term cannot be accurately evaluated, a good way to cancel it is by measuring the sinker mass with another additional calibrated mass with the same volume of the first one, and thus, the same buoyancy force acting on it. Therefore, a weight changing device is located in the balance so that it can place the two calibrated masses on the balance plate by means of two electronic engines, as represented in Figure 2.13.

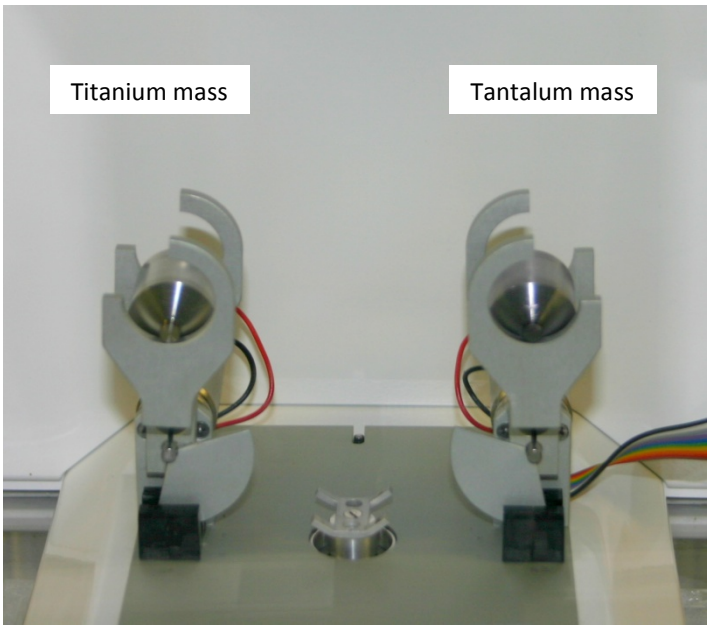

Figure 2.13. Weight changing device with the calibrated masses.

The masses are made of Tantalum (ρ ≈ 16670 kg·m^{-3}) and Titanium (ρ ≈ 4507 kg·m^{-3}) with the same volume of approximately V_{Ta} ≈ V_{Ti} ≈ 4.9 cm^3, so that the difference in weight between both of them is similar to the sinker mass (m_{S} ≈ 60 g). The two masses were provided by Rubotherm and their mass and volume were calibrated at the Mass Division of the Spanish Institut of Standards (Centro Español de Metrología, CEM). Results from the calibration are shown in Table 2.3.

Table 2.3. Results from the mass and volume calibration of the weights of Tantalum and Titanium used in the changing device.

Magnitude	**Tantalum calibrated mass**	**Titanium calibrated mass**
Real mass	82 g + 88.343 mg ± 0.100 mg	22 g + 399.677 mg ± 0.070 mg
Conventional mass	82 g + 94.748 mg ± 0.100 mg	22 g + 397.072 mg ± 0.070 mg
Volume (cm^3)	4.9240 ± 0.0007	4.9706 ± 0.0007
Density ($kg \cdot m^{-3}$)	16670.9 ± 2.5	4506.5 ± 0.6

The mass calibration was carried out by using a mass comparator with mass standards Type MP5, under controlled room temperature, pressure and humidity. The volume was calibrated with a volume comparator with volume standards Type MP14 and MP12.

The weights changing device can be operated both manually and from the control PC by means of a controller, provided by Rubotherm and shown in Figure 2.14.

Besides the correction of the nonlinearity effect of the balance by means of the calibrated masses and the weights changing device, a calibration factor is also determined so that the valid mass value for the measurements can be obtained as expressed in Eq.2.2.

$$m = CF \cdot m_{indication} \qquad \text{Eq.2.2.}$$

The determination of the calibration factor (CF) is performed by comparing the difference in weight of the two calibrated masses (W_{Ta}-W_{Ti}) measured by the balance with the difference calculated from the calibration certificates of both masses (m_{Ta}-m_{Ti}). Thus, the calibration factor can be expressed as indicated in Eq.2.3.

$$CF = \frac{m_{Ta} - m_{Ti}}{W_{Ta} - W_{Ti}} \qquad \text{Eq.2.3.}$$

Figure 2.14. Weights changing device controller. a) Switch on/off. b)

Magnetic suspension coupling

As mentioned in the beginning of this Chapter, the most innovative part of the single sinker densimeter is the magnetic suspension coupling. This coupling consists of an electromagnet hanging from the balance hook and a permanent magnet allocated in the sinker support. The sinker support sustains the sinker as shown in Figure 2.15. Thanks to this contactless coupling between the balance hook and the electromagnet of the sinker support, the fluid inside the measuring cell can work in a wide range of temperatures and up to high pressures. The measurement procedure, by which the zero point balance reading (ZP) is subtracted from the measuring point balance reading (MP), allows the influence of the permanent magnet and the sinker support to be avoided.

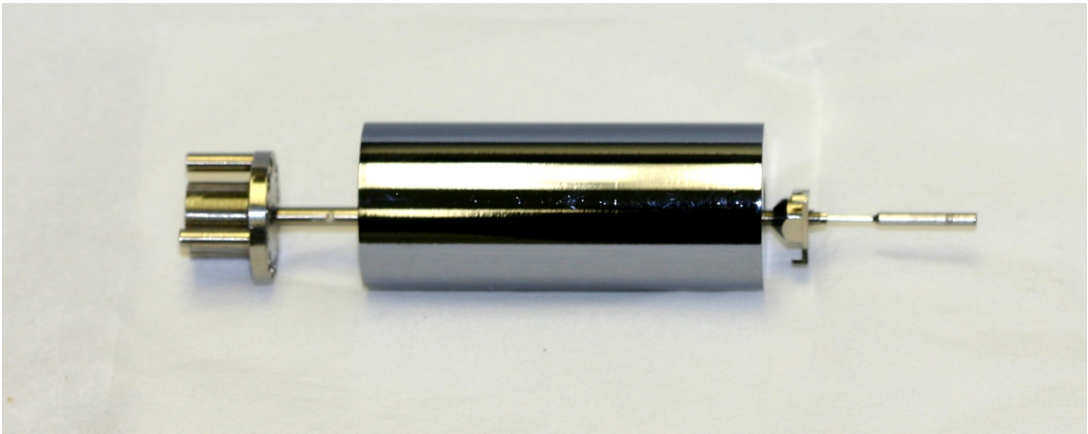

Figure 2.15. Silicon sinker with the sinker support, during the assembly of the densimeter.

The magnetic suspension coupling can be manually and remotely controlled by means of the Couplings controller provided by Rubotherm and shown in Figure 2.16.

Figure 2.16. Magnetic suspension coupling controller. a) Switch on/off. b)

With this controller the distance between the permanent magnet and the electromagnet can be controlled so that the position of the sinker support and the sinker can be determined. The magnetic suspension coupling has three different positions shown in Figure 2.17. and explained below.

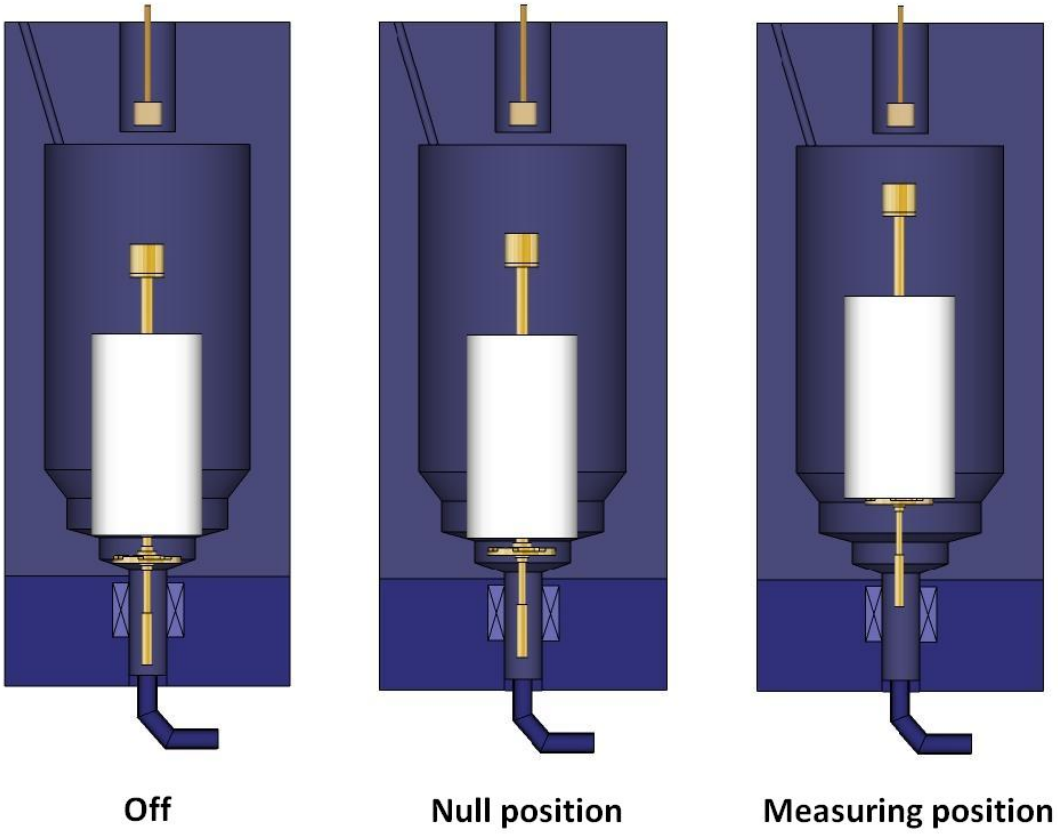

Figure 2.17. Magnetic suspension coupling positions.

- **Off Position (OFF):** The magnetic coupling is switched off and both the sinker support and the sinker rest at the bottom of the measuring cell. The balance load is the sum of the electromagnet hanging on the balance hook and the balance hook.

- **Null Position (NP):** The magnetic coupling is switched on and the sinker support levitates without lifting the sinker, which rests at the bottom of the measuring cell. The balance load is the sum of the electromagnet hanging on the balance hook, the balance hook and the sinker support.
- **Measuring Position (MP):** The magnetic coupling is switched on and, in this case, the sinker support levitates together with the sinker without contacting the top of the measuring cell. In this position the balance load is the sum of the electromagnet hanging on the balance hook, the balance hook, the sinker support and the sinker, affected or not by the buoyancy force.

The mass measurement procedure is carried out by combining the magnetic coupling positions described above with the calibrated masses mentioned in the previous subsection. This procedure will be explained in detail in the next subsection 'Mass measurement procedure'.

The force transmission error (FTE)

Despite the mentioned advantages of the magnetic suspension coupling, its presence is not completely neutral, since the force transmitted between the electromagnet of the sinker support and the permanent magnet connected to the balance can be influenced by external magnetic fields, but also by the magnetic properties of the sinker itself, the measuring cell and the measuring fluid. This phenomenon, the so called force transmission error (FTE), was described in detail by M.O. McLinden, R. Kleinrahm and W. Wagner at the Sixteenth Symposium on Thermophysical Properties (13). In that work, the authors described how this error affected to two different equipments, the single sinker densimeter and the two sinker densimeter, and proposed for each case the method to evaluate and compensate this error.

In a single sinker densimeter, the force transmission error can be separated into two terms, as indicated in Eq. 2.4.

$$\frac{\Delta\rho}{\rho_f} = \underbrace{(1-\phi_0)\frac{\rho_S-\rho_f}{\rho_f}}_{Apparatus} - \underbrace{\varepsilon_\rho \frac{\chi_f}{\chi_{f0}}\left(\frac{\rho_s}{\rho_0}-\frac{\rho_f}{\rho_0}\right)}_{Fluid} \qquad \text{Eq.2.4.}$$

Here, ρ_f and ρ_s are the densities of the fluid and the sinker, respectively, ϕ_0 is the so called coupling factor and χ_f is the magnetic susceptibility of the fluid. ρ_0 =1000 kg·m^{-3} and χ_{f0} = 10^{-8}m^3·kg^{-1} are reducing constants. The first term of Eq. 2.2. represents the relative effect in density produced by the force transmission error induced by the apparatus. The second term refers to the relative effect in density produced by the force transmission error induced by the measuring fluid and depends on its magnetic susceptibility. These two contributions to the force transmission error are discussed below together with the methods used to compensate or evaluate them.

Force transmission error induced by the apparatus

The force transmission error due to the magnetic behavior of the apparatus itself (including the measuring cell, the sinker,…) can be determined when the measuring cell is completely evacuated and no fluid effect affects to the force transmission of the weight. In this case, the mass indication given by the balance subtracted from the real mass of the sinker would give the influence of the apparatus to the force transmission error, as expressed in Eq.2.5.

$$W_{S0} = m_{S0} + FTE \qquad \text{Eq. 2.5.}$$

The apparatus term of the force transmission error changes with temperature but also after the leveling of the balance, the centering of the rod of the electromagnet. Thus, it was decided to measure the sinker mass in a vacuum for each isotherm measured in this work.

Figure 2.18. depicts the (1- ϕ_0)·10^6 values obtained in this work for all the isotherms of the *(p, ρ, T)* data when the measuring cell is evacuated, versus temperature. It can be observed that the sinker mass in a vacuum varied during the measurements, independently of the date in which they were carried out.

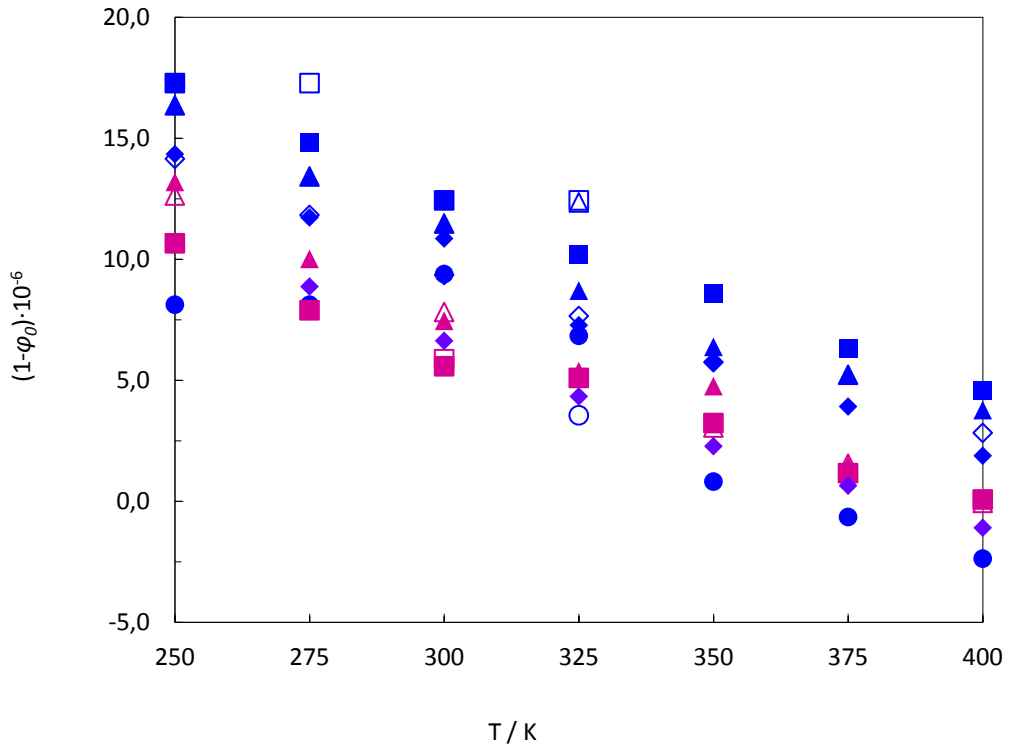

Figure 2.18. (1- ϕ_0)·10^6 values of all weightings in the evacuated measuring cell measured during this work, versus temperature. The mixtures are specified here CO_2 + N_2 mixtures: ▲ x_{CO_2} = 0.10; △ x_{CO_2} = 0.10 repeated; ■ x_{CO_2} = 0.15; □ x_{CO_2} = 0.15 repeated; ◆ x_{CO_2} = 0.20; ◇ x_{CO_2} = 0.20 repeated; ● x_{CO_2} = 0.50; ○ x_{CO_2} = 0.50 repeated; CO + N_2 mixtures: ■ x_{CO} = 0.05; □ x_{CO} = 0.05 repeated; ▲ x_{CO} = 0.10; △ x_{CO} = 0.10 repeated; CH_4 + CO_2 mixtures: ◆ x_{CO_2} = 0.20.

The maximum difference for each temperature between the values depicted in Figure 2.18. rose up to 10 ppm, which corresponds to a difference in mass of less than 0.001 g. Since this difference in mass affects significantly to the density value and these variations were already observed during the first test measurements with nitrogen, it was decided to measure the sinker mass in a vacuum after each singular isotherm performed with the densimeter (instead of using a fitted equation for the sinker mass in vacuum), so that the apparatus term of the FTE is cancelled.

Force transmission error induced by the fluid

The force transmission error due to the magnetic behavior of the measuring fluid depends, as it can be seen in Eq.2.2., on the magnetic susceptibility of the fluid χ_S, the difference between the fluid density and the sinker density (ρ_f-ρ_S), and the apparatus specific constant ε_ρ

The *magnetic susceptibility of the fluid* χ_S, affects proportionally to the fluid specific effect contribution. Thus, those fluids with a strong paramagnetic or diamagnetic behavior, such as oxygen and water, respectively, are expected to affect significantly to the transmission of the weight by the magnetic coupling.

As for the *difference between the fluid density and the sinker density*, the more different these densities are the bigger the specific fluid effect of the force transmission error will be. This means that the fluid specific effect affects more at low fluid densities than at high fluid densities.

Finally, the third magnitude affecting to the fluid specific effect, the so called *apparatus specific constant* ε_ρ, depends on each apparatus configuration. McLinden et al. (13) described a methodology for the determination of this apparatus specific constant, which consisted in the comparison of measurements at identical pressure and temperature conditions of the same gas, performed with different sinkers in the same densimeter. Thus, the value of ε_ρ can be obtained by comparing the deviation of the experimental density value from the equation of state caused by 'fluid term' of the force transmission error indicated in Eq.2.6. and Eq.2.7., assuming that the density of the fluid calculated from the equation of state is the same in both cases ($\rho_{EoS,1}=\rho_{Eos,2}$), as expressed in Eq. 2.8.

$$\frac{\rho_{S1}-\rho_{Eos,1}}{\rho_{Eos,1}} = -\varepsilon_\rho \frac{\chi_S}{\chi_{S0}}\left(\frac{\rho_{S1}}{\rho_0}-\frac{\rho_{Eos,1}}{\rho_0}\right) \qquad \text{Eq.2.6.}$$

$$\frac{\rho_{S2}-\rho_{Eos,2}}{\rho_{Eos,2}} = -\varepsilon_\rho \frac{\chi_S}{\chi_{S0}}\left(\frac{\rho_{S2}}{\rho_0}-\frac{\rho_{Eos,2}}{\rho_0}\right) \qquad \text{Eq.2.7.}$$

$$\varepsilon_\rho = \frac{\chi_{S0}}{\chi_S}\left(\frac{\rho_0}{\rho_{S2}-\rho_{S1}}\right)\left(\frac{\rho_1-\rho_2}{\rho_{EoS}}\right) \qquad \text{Eq.2.8.}$$

In this work the fluid specific effect of the force transmission error was not thoroughly evaluated since the literature suggested that this effect was negligible for the gas mixtures reported. However a preliminary study of this effect was performed by comparing the density data of nitrogen performed before and after the change of the

sinker commented in Chapter 3, in order to confirm whether this influence could be omitted. Therefore, density data measured with the titanium sinker in a previous work were compared with the density data of nitrogen measured during this work. Table 2.2. gives the *(p, ρ, T)* values of the measuring points compared. The calculated values of ε_ρ for each pair of measuring points are plotted versus density in Figure 2.19.

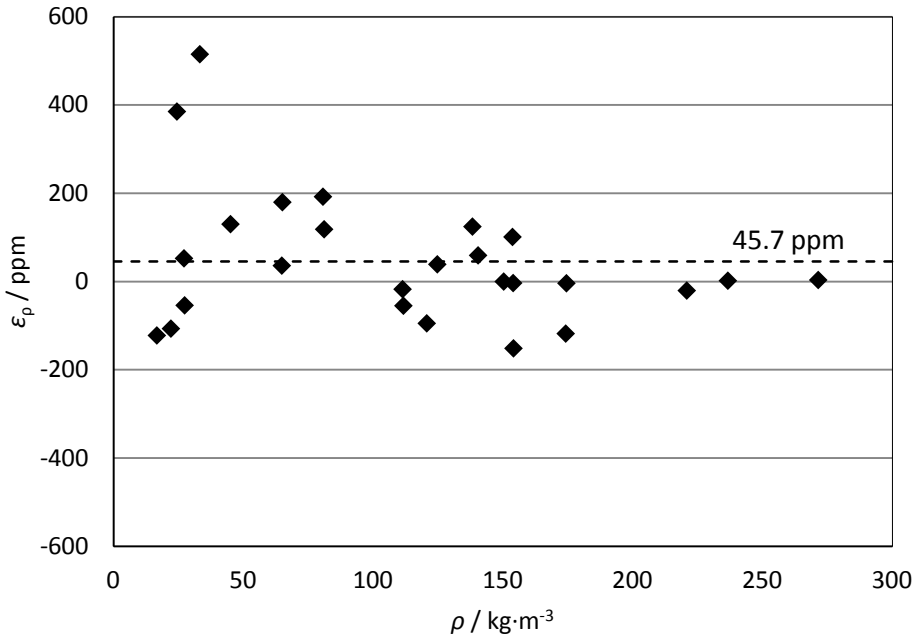

Figure 2.19. Specific apparatus constant calculated from nitrogen densities measured at the same temperature and pressure conditions with the titanium sinker and the new silicon sinker.

As it can be observed the scatter of the ε_ρ values is significantly high at low densities and is reduced at high densities. Values of the apparatus specific constant yielded an average value of 45.7 ppm, which is close to the values of ε_ρ given by several authors: ε_ρ = 189 ppm Cristancho et al. (14), ε_ρ = 36 ppm, Klimeck et al. (9). Since this value of the apparatus specific constant of our densimeter has been evaluated with very few data, it cannot be reliably used for the correction of the experimental data reported in this work. Nevertheless, this value of ε_ρ = 45.7 ppm, which corresponds to a correction of up to 0.005% in density (ρ = 300 kg·m^{-3}), confirms that the omission of the fluid specific effect correction for the mixtures presented in this thesis does not means a loss of accuracy if compared with the uncertainty in density evaluated in Chapter 3.

In conclusion, the experimental data reported in this thesis were only corrected for the apparatus effect of the force transmission error and not for the fluid specific effect.

Mass measurement procedure

The mass measurement procedure to determine the sinker mass both under a vacuum and in the pressurized measuring cell is performed in such a way that the nonlinearity of the balance is reduced as much as possible and the additional loads such as the sinker support and the electromagnet are cancelled. Therefore, two measuring points are here defined:

- **Zero Point (ZP):** The magnetic coupling is in the Null Position (NP) and the Tantalum mass is placed on the balance plate. The load of the balance is expressed in Eq. 2.9.

$$m_{ZP} = m_{Ta} + m_{em} + m_{pm} \qquad \text{Eq.2.9.}$$

- **Measuring Point (MP):** The magnetic coupling is in the Measuring Position (MP) and the Titanium mass is placed on the balance plate. The load of the balance is expressed in Eq. 2.10.

$$m_{MP} = m_{Ti} + m_{em} + m_{pm} + m_{Sf} \qquad \text{Eq.2.10.}$$

The steps of the mass measurement procedure are enumerated as follows:

1. Before measuring each mass point the magnetic coupling is switched on in the Null position and both calibrated masses are away from the balance plate.
2. In the first place, the calibration factor is determined. The Tantalum calibrated mass is placed on the balance plate while the magnetic coupling is in the Null position. After a stabilization period of approximately 25 seconds the balance is tared. Afterwards, the Tantalum mass is replaced by the Titanium mass while the magnetic coupling keeps in the Null position and the load mass is measured. The difference between the two values is collected and the calibration factor (FC) is calculated afterwards as indicated in Eq.2.5.
3. In the second place, the sinker mass is determined. First the Tantalum mass is placed on the balance plate while the magnetic coupling is in the Null position and the balance is tared again when the indication is stable. After that, the

Tantalum mass is replaced by the Titanium mass and the magnetic coupling changes into the measuring position. After the stabilization period, the sinker mass is measured and collected.

4. Finally the magnetic coupling and the calibrated masses are returned to their initial positions.

This process is followed when the measuring cell is evacuated and also when it is pressurized. The compensation of unknown weights (electromagnet and permanent magnet) in both cases is indicated below in expressions Eq.2.11. and Eq.2.12.

$$(MP-ZP)(T,p)=(m_{Ti}-m_{Ta})+m_{Sf} \qquad \text{Eq.2.11.}$$

$$(MP-ZP)(T,0)=(m_{Ti}-m_{Ta})+m_{S0} \qquad \text{Eq.2.12.}$$

The air buoyancy force acting on the titanium and tantalum weights is compensated for by subtracting the MP and ZP balance indications. With this methodology the possible adsorption of the gas on the sinker is the only effect which is not compensated for.

The density of the fluid is finally obtained by subtracting the expressions in Eq.2.11. and Eq.2.12. as shown in Eq.2.13.

$$\rho(T,p)=\frac{(MP-ZP)(T,0)-(MP-ZP)(T,p)}{V_S(T,p)}=\frac{m_{S0}-m_{Sf}}{V_S(T,p)} \qquad \text{Eq.2.13.}$$

The volume of the sinker changes influenced by the pressure and temperature of the measuring fluid. Therefore, the volume of the sinker to be used in Eq.2.10. must be determined for each measurement point, from the fluid temperature and pressure, and the volume calibration value. This calculus is later thoroughly described in Chapter 3.

2.3. PARTIAL AUTOMATION OF THE MEASURING PROCESS AND PROGRAM FOR THE CONTROL AND DATA ACQUISTION

Initially the single sinker densimeter measurement process was controlled by a Visual Basic-based program created and delivered by Rubotherm. This program operated by measuring continuously the three state point magnitudes at determined pressure and temperature conditions, which were established manually. When the user detected that the measurements were stable enough, the save button of the program was activated and the measuring point values were saved in a text file. However, due to the updating of the operative system of the control computer together with the need of automating the complete data acquisition process, the development of a new control program became necessary.

An Intel® desktop computer with a Pentium® 4 processor was used for the data acquisition and measurement procedure control. The magnetic controller coupling, the changing device controller and the automatic valve were all connected to the control computer by means of a Data acquisition digital I/O Counter module ECON Series model DT9810. The balance, both pressure transducers and the AC resistance bridge are directly connected to serial ports of the computer. It must be pointed out that all the equipment concerning the densimeter operation, except for the thermostatic bath, where connected to a UPS (Uninterruptible Power Supply) to avoid problems coming from a temporal failure of the input power source.

The new instrument control program was developed on the Agilent VEE Pro 7.0. virtual engineering software. Agilent VEE Pro 7.0. is a Windows® based instrumentation software developed by Hewlett Packard which is optimized for building and measurement applications. It is an easy-to-use graphical programming environment which makes easier and faster the development, modification and improvement of measurement, control and data acquisition applications.

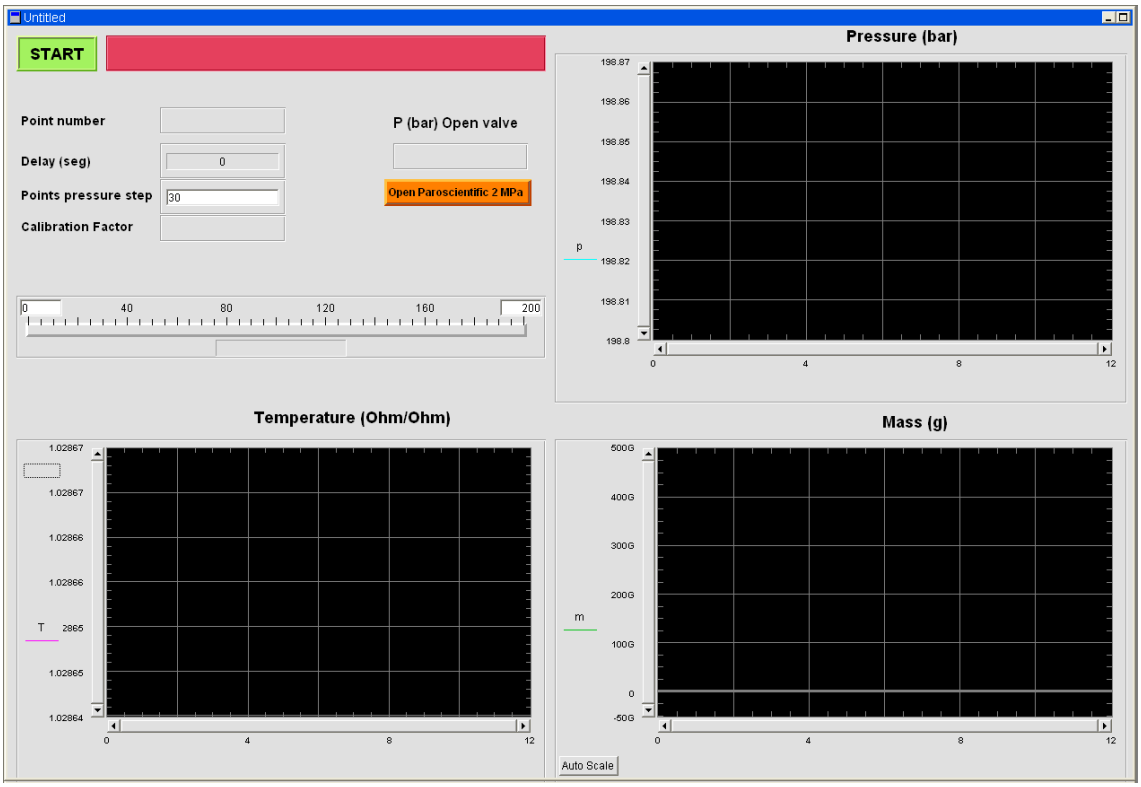

Figure 2.20. Screenshot of the control and data acquisition program during the measurement procedure.

The main aim of the new developed control program was to automate the isotherm measurement procedure, making it as easy as possible. Thus, it was decided to create a visual control panel with few options changeable by the user by predetermining many of the variable values. Figure 2.20. shows a screen shoot of the control panel during the measurement procedure.

As it can be observed the control panel is divided into two main parts: the graphical area and the user's area. The graphical area consists of the graphics representing the indications related with the three state point magnitudes and a progress bar which indicates the current pressure over the whole isotherm range. These graphics, which are detailed below, are auto-scaled depending on the indication values and are of great importance for the visual control of the stability of the state point magnitudes.

- **Pressure x-y plot:** in this graphic the indication of the pressure transducer which works up to 20 MPa is depicted, without being corrected with the calibration constants, versus the measurement point number. This graphic is reset for each pressure step.

- Temperature x-y plot: in this graphic the resistance ratio measured by the AC resistance bridge for the Minco 713 PRT-25 probe is plotted versus the measurement point number. This graphic is not reseted during the measurement of the whole isotherm so that the stability of the temperature over the whole isotherm can be observed.

- Corrected mass x-y plot: in this graphic the balance indication in the measuring point (MP) corrected with the calibration factor (CF) (the balance is tared in the zero point, ZP) is depicted against the measurement point number. This graphic is also reseted for each pressure step.

- **Pressure progress bar:** this progress bar indicates the pressure step which is being measured with respect to all the pressure steps which conforms the isotherm.

The user's area contains action buttons, information for the user of some of the magnitudes measured during the process and data input boxes, which are described below.

- **Start button:** when the start button is pressed an input window asks the user for a filename of the excel sheet where all data will be saved. Next, the measurement procedure begins. The label shows the filename.

- User's information: the user can see the current measurement point number and calibration factor.

- User's option: the user can decide the number of measurement points for each pressure step and an initial delay of the measurement procedure thanks to two dialog boxes. A value of 30 measurement points and 0 second of delay are predefined.

- Pressure step box: in this box the pressure transducer indication is measured while the piston air operated valve is open during the pressure step change. When the pressure of the fluid reaches a value of 2 MPa the control program is stopped to allow the valve of the 2 MPa pressure transducer to be manually opened. The button below resumes the measurement process when pressed.

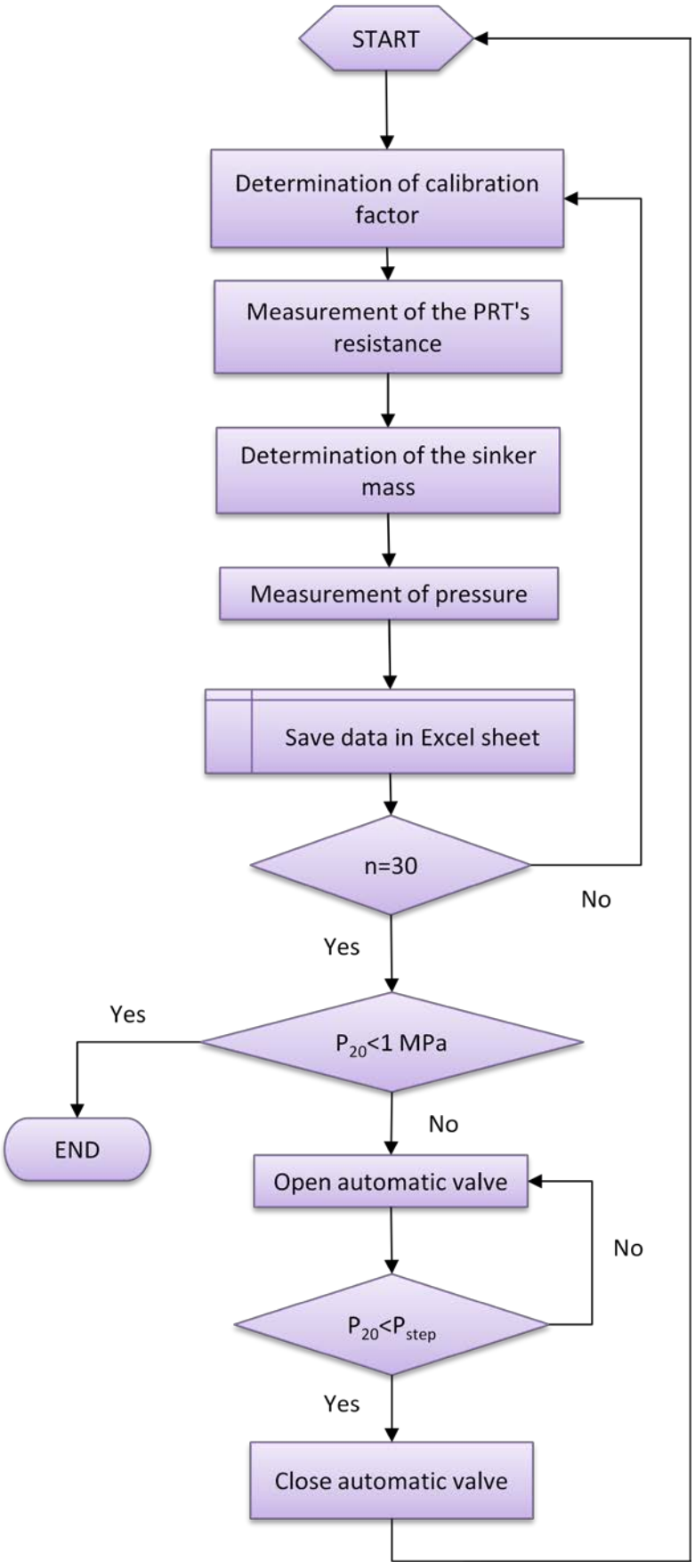

Figure 2.21. Flow diagram of the control and data acquisition program.

Despite the few possibilities to act in the program configuration from the user's panel, the ease of access and modification of the VEE Agilent environment allows continuous improvements to be easily performed.

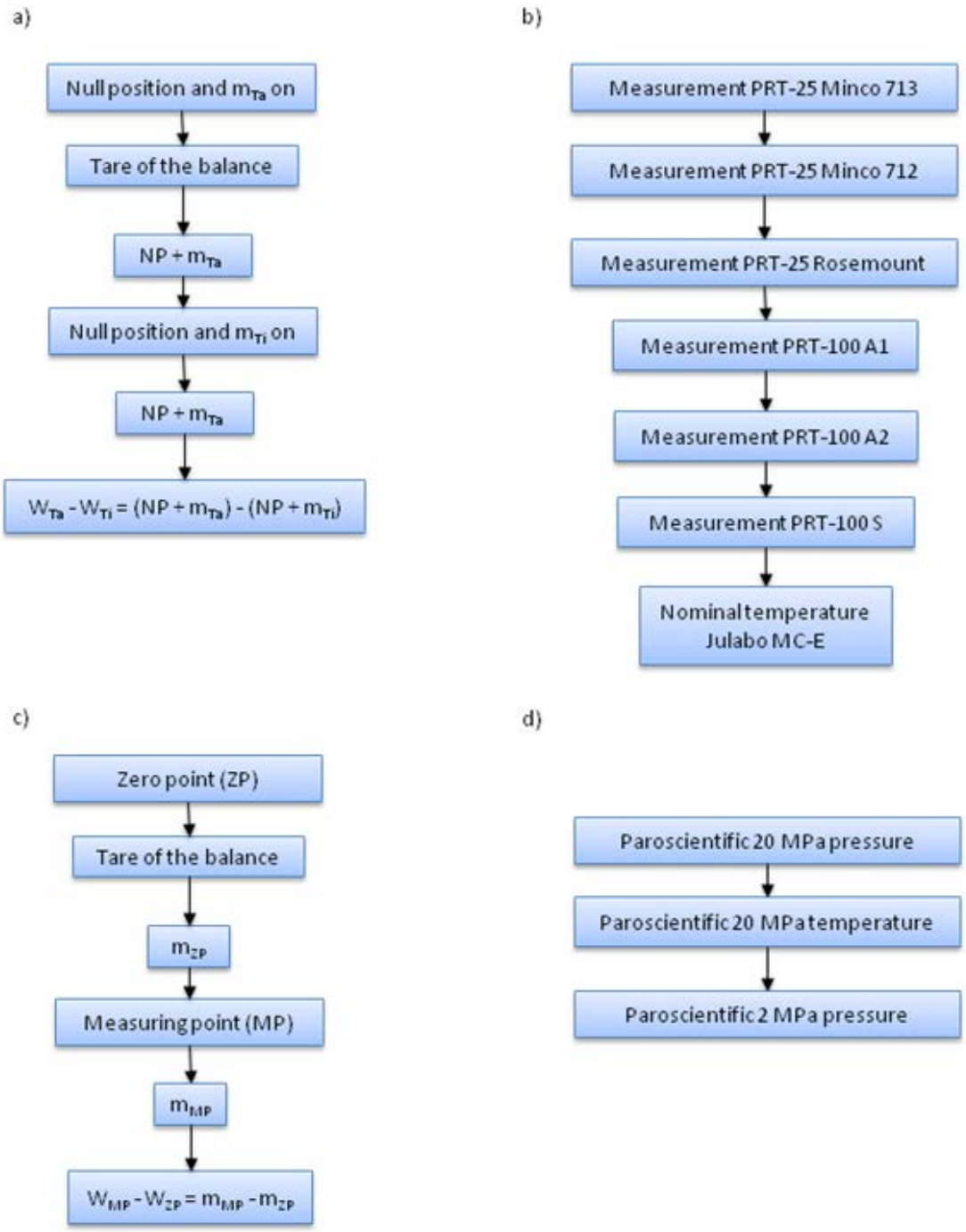

Figure 2.22. Flow diagram of each measurement block. a) Determination of calibration factor block; b) Measurement of the PRT's resistance; c) Determination of the sinker mass; d) Measurement of pressure.

The flow diagram of the control and data acquisition program is shown in Figure 2.21., where P_{20} refers to the pressure measured by the 20 MPa pressure transducer and P_{step} indicates the pressure value of the next pressure step. The flow diagram of each measurement block depicted in Figure 2.21. is shown in Figure 2.22.

As indicated earlier, the measurement procedure begins after pressing the 'Start' button and inserting the excel sheet filename. The calibration factor, which is determined as indicated in Eq.2.5., is the first magnitude to be calculated.

Next the resistance ratios of each PRT-25 probe connected to the AC resistance bridge are measured successively by using the Multichannel Switchbox.

The apparent mass of the sinker is measured afterwards by taring the balance when the magnetic coupling is in the null position and the tantalum weight is on (Zero Point), and immediately measuring the mass of the sinker and the titanium mass on (Measuring Point). The mass value is calculated by subtracting both indications.

Moreover, the temperature of the three PRT-100 probes connected to the electronic temperature regulator (Julabo MCE) and the pressure indicated by both pressure transducers are collected.

	A	B	C	D	E	F	G	H	I	J	K	L	M	N
1	Time	Minco 713	Minco 712	Rosement	Tara	Masa	FC	A1	A2	S	Nom	P200	P20	T_Parosc
2	03/02/2011 20:39	1,527408	1,524747	1,528423	0	-4,10301	59,52914	126,92	126,84	126,62	126,85	199,7922	16,4057	22,751
3	03/02/2011 20:41	1,527393	1,524722	1,528397	0	-4,10277	59,52915	127,01	126,84	126,62	126,85	199,7856	16,40668	22,748
4	03/02/2011 20:44	1,527413	1,524744	1,528419	0	-4,10253	59,52914	126,92	126,84	126,62	126,85	199,7763	16,40634	22,759
5	03/02/2011 20:47	1,527407	1,524745	1,528418	0	-4,10219	59,52911	127	126,84	126,62	126,85	199,7652	16,40598	22,762
6	03/02/2011 20:49	1,527418	1,52475	1,528425	0	-4,10195	59,52914	126,95	126,85	126,63	126,85	199,7592	16,40659	22,765
7	03/02/2011 20:52	1,52741	1,524739	1,528415	0	-4,10162	59,5291	126,92	126,85	126,63	126,85	199,7462	16,40573	22,757
8	03/02/2011 20:55	1,52741	1,524744	1,528423	0	-4,10141	59,52909	126,94	126,84	126,63	126,85	199,74	16,40692	22,754
9	03/02/2011 20:58	1,527405	1,524727	1,528399	0	-4,10123	59,52906	126,95	126,84	126,62	126,85	199,7318	16,40772	22,762
10	03/02/2011 21:00	1,527402	1,524746	1,528425	0	-4,1011	59,52908	126,99	126,85	126,62	126,85	199,7279	16,40945	22,806
11	03/02/2011 21:03	1,527414	1,52474	1,528414	0	-4,10086	59,52906	127,03	126,84	126,62	126,85	199,7205	16,40994	22,803
12	03/02/2011 21:06	1,527413	1,524745	1,528424	0	-4,10072	59,52907	126,95	126,85	126,63	126,85	199,7137	16,41082	22,803
13	03/02/2011 21:08	1,527407	1,524734	1,528412	0	-4,10046	59,52905	126,96	126,84	126,62	126,85	199,7059	16,40979	22,806
14	03/02/2011 21:11	1,527404	1,524739	1,528414	0	-4,10024	59,52906	126,91	126,84	126,62	126,85	199,6971	16,41023	22,819
15	03/02/2011 21:14	1,527391	1,524727	1,5284	0	-4,10009	59,52907	126,92	126,84	126,62	126,85	199,6911	16,41088	22,817
16	03/02/2011 21:16	1,527404	1,524752	1,528431	0	-4,09985	59,52907	126,93	126,85	126,62	126,85	199,6849	16,41079	22,822
17	03/02/2011 21:19	1,527411	1,524746	1,528416	0	-4,09966	59,52904	127	126,84	126,62	126,85	199,6783	16,41099	22,825
18	03/02/2011 21:22	1,527413	1,524754	1,528431	0	-4,09944	59,52903	126,91	126,85	126,62	126,85	199,6684	16,41113	22,819
19	03/02/2011 21:24	1,527403	1,52475	1,528428	0	-4,09926	59,52904	127,04	126,85	126,62	126,85	199,666	16,41283	22,825
20	03/02/2011 21:27	1,527424	1,524755	1,528432	0	-4,09904	59,52903	126,96	126,85	126,63	126,85	199,659	16,4129	22,855
21	03/02/2011 21:30	1,527418	1,52475	1,528422	0	-4,0989	59,529	126,91	126,85	126,62	126,85	199,6532	16,41426	22,855
22	03/02/2011 21:33	1,527392	1,524729	1,528412	0	-4,09869	59,529	126,94	126,84	126,62	126,85	199,6442	16,41398	22,855
23	03/02/2011 21:35	1,527399	1,524732	1,528401	0	-4,09854	59,52901	126,97	126,84	126,62	126,85	199,6386	16,41482	22,860
24	03/02/2011 21:38	1,527389	1,524726	1,528406	0	-4,09834	59,52899	126,97	126,85	126,62	126,85	199,6308	16,41394	22,860
25	03/02/2011 21:41	1,527411	1,524745	1,528429	0	-4,09805	59,52901	126,92	126,85	126,62	126,85	199,6238	16,41427	22,868
26	03/02/2011 21:43	1,527409	1,524746	1,528426	0	-4,09782	59,529	126,92	126,85	126,63	126,85	199,6129	16,41316	22,871
27	03/02/2011 21:46	1,527419	1,524748	1,528424	0	-4,09762	59,52899	126,92	126,85	126,62	126,85	199,6072	16,4141	22,868
28	03/02/2011 21:49	1,527408	1,524733	1,528403	0	-4,09752	59,52897	126,93	126,84	126,62	126,85	199,6022	16,41445	22,877
29	03/02/2011 21:51	1,527395	1,524728	1,528404	0	-4,0973	59,52898	127	126,84	126,62	126,85	199,5967	16,41506	22,879
30	03/02/2011 21:54	1,527415	1,524751	1,528426	0	-4,09708	59,52898	126,98	126,84	126,62	126,85	199,5878	16,41523	22,923
31	03/02/2011 21:57	1,527403	1,524741	1,528418	0	-4,09697	59,52896	126,95	126,85	126,62	126,85	199,5856	16,4163	22,917
32	03/02/2011 23:30	1,5274	1,524745	1,528435	0	-3,5228	59,52888	126,91	126,85	126,63	126,85	179,9988	16,42341	22,920

Figure 2.23. Data acquisition excel sheet.

Finally, all the data mentioned above, together with the current date and the room temperature of each measurement point are saved in an excel sheet for the

subsequent data treatment, as shown in Figure 2.23. The room temperature is taken from the temperature measurement of the Paroscientific pressure transducer for 20 MPa. After the data treatment, density is compared with the reference equation of state by using REFPROP (National Institute of Standards and Technology, 2009) as an add-in in the Microsoft Excel environment. The visual basic code of the add-in was modified to allow the use of different equations of state for the estimation of density values (GERG-2004, GERG 2008) equations of state, AGA8-DC92 equation of state and REFPROP model).

REFERENCES

1. MAJER, V. et al. *Measurement of the Thermodynamic Properties of Single Phases*, 2003. pp. 149-168.

2. WAGNER, W. and KLEINRAHM, R. Densimeters for very Accurate Density Measurements of Fluids Over Large Ranges of Temperature, Pressure, and Density. *Metrologia*, 2004, vol. 41, no. 2. pp. S24-S39.

3. KLEINRAHM, R. and WAGNER, W. Measurement and Correlation of the Equilibrium Liquid and Vapor Densities and the Vapor-Pressure along the Coexistence Curve of Methane. *Journal of Chemical Thermodynamics*, AUG, 1986, vol. 18, no. 8. pp. 739-760. ISSN 0021-9614.

4. GAST, Th. and BEHRNDT, K.H. Vacuum Microbalance Techniques, 1963, vol. 3. pp. 45-54.

5. LÖSCH, H.W. *Entwicklung Und Aufbau Von Neuen Magnetschwebewaagen Zur Beruhrungsfreien Messung Vertikaler Kräfte*, 1987.

6. LÖSCH, H.W.; KLEINRAHM, R. and WAGNER, W. Neue Magnetschwebewaagen Für Gravimetrische Messungen in Der Verfahrenstechnik. *Chem.Ing.Tech.*, 1994, vol. 66, no. 8. pp. 1055-1058.

7. BRACHTHÄUSER, K. et al. *Entwicklung Eines Neuen Dichtemeßverfahrens Und Aufbau Einer Hochtemperatur-Hochdruck-Dichtemeßanlage,* 1993.

8. WAGNER, W. et al. A New, Accurate Single-Sinker Densitometer for Temperatures from 233 to 523 K at Pressures Up to 30 MPa. *International Journal of Thermophysics*, 1995, vol. 16, no. 2. pp. 399-411.

9. KLIMECK, J. *Weiterentwicklung Einer Ein-Senkkörper- Dichtemessanlage Und Präzisionsmessungen Der Thermischen Zustandsgrößen Von Kohlendioxid, Argon, Stickstoff Und Methan*, 1997.

10. CHAMORRO, C.R. et al. Measurement of the (Pressure, Density, Temperature) Relation of Two (Methane Plus Nitrogen) Gas Mixtures at Temperatures between 240 and 400 K and Pressures Up to 20 MPa using an Accurate Single-Sinker Densimeter. *Journal of Chemical Thermodynamics*, 2006, vol. 38, no. 7. pp. 916-922. ISSN 0021-9614.

11. MONDÉJAR, M.E. Homogeneidad y Estabilidad De La Temperatura En La Celda De Medida De Un Densímetro De Flotador Con Acoplamiento Magnético Para Gases. *Trabajo Fin De Master*, 2009.

12. EURAMET (European Association of National Metrology Institutes). Guidelines on the Calibration of Non-Automatic Weighing Instruments, 2007, vol. cg-18 / v.02.

13. MCLINDEN, M.O.; KLEINRAHM, R. and WAGNER, W. Force Transmission Errors in Magnetic Suspension Densimeters. *International Journal of Thermophysics*, 2007, vol. 28, no. 2. pp. 429-448.

14. CRISTANCHO, D.E. et al. Force Transmission Error Analysis for a High-Pressure Single-Sinker Magnetic Suspension Densimeter. *International Journal of Thermophysics*, 2010, vol. 31, no. 4-5. pp. 698-709.

CHAPTER 3

DENSIMETER IMPROVEMENT BASED ON A STATE POINT UNCERTAINTY ANALYSIS

3.1. INTRODUCTION

The uncertainty in measurement, as defined in (1), is a “non negative parameter characterizing the dispersion of the quantity values being attributed to a measurand, based on the information used”. The importance of the uncertainty in measurement resides in the fact that it indicates quantitatively the quality of the measurement result. Therefore, to express correctly the value of a measurand, it must be accompanied by its uncertainty so that it can be compared and used with assessed reliability.

The uncertainty of a measurement result comes from many different sources comprising from an incorrect definition of the measurand to effects coming from the performance of measurement instruments and environmental conditions. According to the Recommendation INC-1 of the Working Group on the Statement of Uncertainties (2), these contributions to the measurement uncertainty are grouped by their evaluation method in two categories, ‘type A’ and ‘type B’. ‘Type A’ uncertainties are estimated through statistical methods as standard deviations of the mean of a series of independent observations of a measurand. ‘Type B’ uncertainties are obtained from an assumed probability density function (PDF) based on the available knowledge of a measurand and can be obtained from manufacturers’ specifications, calibration reports, handbooks, previous data sets and scientific experience.

Though several methods are available for the estimation of the measurement uncertainty, the most extended framework for assessing uncertainty is the law of propagation of uncertainties described in the Guide to the Expression of Uncertainty in Measurement (GUM)(3). However, this method has some limitations when being applied to non-linear models or when the probability density function of the output quantity departs significantly from a Gaussian distribution. In these cases, a Monte Carlo method, which is based on a propagation of distributions by performing repeated random sampling from probability distributions, can be used as an alternative to the GUM uncertainty framework.

3.2. UNCERTAINTY ANALYSIS AND IMPROVEMENTS PROPOSAL

As mentioned in Chapter 1, one of the scopes of this thesis was the reduction of the measurement uncertainty of the experimental data obtained with the single sinker densimeter with magnetic suspension coupling. This improvement process was considered since no significant modifications had been carried out on the densimeter since its final assembly in the laboratory.

To optimize the improvement of the measurement uncertainty, a method for the reduction of the uncertainty was established. First of all, the uncertainty of the three state point magnitudes (pressure, density and temperature) was thoroughly evaluated following the GUM. In the second place, the uncertainty sources with a major contribution to the measurement uncertainty of each magnitude were selected. Based on these uncertainty sources, several improvements on the setup configuration were proposed. After carrying out all the modifications, an uncertainty analysis was again performed in order to determine the reductions in uncertainty achieved for each magnitude.

3.2.1. Uncertainty analysis of each state point magnitude with the GUM approach

The uncertainties of the three state point magnitudes (pressure, density and temperature) were estimated, both before and after the improvement process, following the law of propagation of uncertainties (GUM). In this methodology, the measurand is defined as an output quantity Y which is expressed as a model function f of several input quantities X_i (i = 1, 2, … N), which represents the measurement procedure and the evaluation method. Therefore, the output estimation y is calculated from the estimates x_i of each input quantity as shown in Eq. 3.1. and its combined uncertainty $u(y)$ is calculated by using Eq.3.2.

$$y = f(x_1, x_2, ..., x_N) \qquad \text{Eq.3.1.}$$

$$u^2(y) = \sum_{i=1}^{N}\left(\frac{\partial f}{\partial x_i}u(x_i)\right)^2 + 2\sum_{i=1}^{N-1}\sum_{k=i+1}^{N}\left(\frac{\partial f}{\partial x_i}u(x_i)\right)\left(\frac{\partial f}{\partial x_k}u(x_k)\right)r(x_i, x_k) \qquad \text{Eq.3.2.}$$

Here, $u(x_i)$ and $u(x_k)$ are the standard uncertainties of the input estimates and $r(x_i,x_k)$ is the correlation coefficient, which is zero for independent input quantities and varies between -1 and 1 for correlated input quantities.

$$r(x_i, x_k) = \frac{s(x_i, x_k)}{s(x_i)s(x_k)} \qquad \text{Eq.3.3.}$$

The correlation coefficient, defined by Eq.3.3., depends on the standard deviations of the input estimates $s(x_i)$ and $s(x_k)$ and the covariance associated with them, $s(x_i, x_k)$.

Finally, the expanded uncertainty associated to the output estimate $U(y)$ is calculated by multiplying the combined uncertainty of the output estimate $u(y)$ by the coverage factor k: $U(y) = k \cdot u(y)$. The value of the coverage factor is chosen on the basis of the level of confidence required of the uncertainty interval and depends directly on the effective degrees of freedom v_{eff} of the output quantity. When v_{eff}>50, a coverage factor k=2 yields a coverage probability of the expanded uncertainty of 95.45%. The number of effective degrees of freedom of the output quantity can be calculated with Eq.3.4., the Welch-Satterhwaite formula (4, 4), and determine the reliability of the standard uncertainty assigned to an output estimate.

$$v_{eff} = \frac{u^4(y)}{\sum_{i=1}^{N} \frac{u_i^4(y)}{v_i}} \qquad \text{Eq.3.4.}$$

Here v_i is the number of degrees of freedom of each input quantity standard uncertainty. In the case of magnitudes estimated as the arithmetic mean of a series of n independent observations, v_i is calculated as $(n-1)$.

Though the combined uncertainty of an output quantity is defined as the root square of the sum of all squared uncertainty contributions, it is a common practice (5) to approximate it by grouping the standard uncertainty terms in several squared roots when they are proportional to the output quantity itself. This approximation yields an uncertainty value slightly higher than the combined uncertainty value obtained from Eq. 3.2. so that it does not reduce the real value of the uncertainty. This approximation is applied to the presentation of pressure and density uncertainty results.

Temperature uncertainty analysis

Before the single sinker densimeter with magnetic coupling was modified, the temperature inside the cell was determined with a single PRT-25 probe (Rosemount 162D) which was placed in the middle height of the measuring cell. The resistance of the probe was measured with an AC comparator resistance bridge (Automatic Systems Laboratory model F700) through a Multichannel Switchbox (Automatic Systems Laboratory model SB148/01). The probe was calibrated at our own calibration facility (accredited by ENAC, member of EA) for different temperature fixed points to determinate its calibration uncertainty and the PRT-25 drift. The calibration uncertainty of the probe in K is given in Table 3.1. for each calibration fixed point, together with the drift value.

Table 3.1. Calibration uncertainty and drift of the Rosemount PRT-25 probe.

Probe	Calibration expanded uncertainty (k=2) (K)				Drift (K)
	505.077 K	429.748 K	302.913 K	234.317 K	
Rosemount	$6\cdot10^{-3}$	$6\cdot10^{-3}$	$6\cdot10^{-3}$	$4\cdot10^{-3}$	$2\cdot10^{-3}$

Table 3.2. Uncertainty budget for temperature measurement with the Rosemount PRT-25 probe.

Uncertainty component	Units	Estimation	u(xi)	Distribution	Type	Sensitivity coefficient	Divisor	$u_i(y)^2$
PRT calibration uncertainty	K	0	$3.0\cdot10^{-3}$	Gaussian	B	1	1	$3.0\cdot10^{-3}$
Temperature reading	Ω	0	$7.2\cdot10^{-5}$	Gaussian	B	10.5	1	$7.6\ 10^{-4}$
Repeatability	K	0	$9.5\cdot10^{-4}$	Gaussian	A	1	1	$9.5\cdot10^{-4}$
Uniformity	K	0	$4.0\cdot10^{-3}$	Uniform	B	1	$2\sqrt{3}$	$1.2\cdot10^{-3}$
Drift	K	0	$1.0\cdot10^{-3}$	Uniform	B	1	$\sqrt{3}$	$5.8\cdot10^{-4}$
						Standard uncertainty (K)		$3.5\cdot10^{-3}$
						Expanded uncertainty (K) (k=2)		$7.0\cdot10^{-3}$

The calibration uncertainty of the probe was taken as the maximum value of that presented in Table 3.1. for the temperature working range of the apparatus.

Table 3.2. presents the uncertainty budget resulting from the temperature uncertainty analysis. It could be observed that main contributions to the uncertainty in temperature came from the calibration uncertainty of the probe and from the uniformity of the temperature.

Pressure uncertainty analysis

Initially, the pressure of the fluid contained in the measuring cell was determined by an absolute pressure transducer (Paroscientific 43KR-HHT-101) for the range 0-20 MPa. This pressure transducer was annually calibrated against a relative dead gauge at our own calibration facility (accredited by ENAC, member of EA). Table 3.3. shows the uncertainty budget for the 20 MPa pressure transducer, where it can be noticed that the most important contribution to the uncertainty come from the transducer calibration term. Repeatability was estimated as the standard deviation of the mean of the ten pressure values used to calculate each state point pressure. The drift was estimated from two consecutive calibrations.

Table 3.3. Uncertainty budget of the 20 MPa pressure transducer.

Uncertainty sources	Units	Estimation	Standard uncertainty	Distribution	Type	Sensitivity coefficient	Divisor	Contribution MPa
Transducer calibration	MPa	0	$38\cdot10^{-6}p + 1.74\cdot10^{-3}$	Gaussian	B	1	1	$38\cdot10^{-6}p + 1.74\cdot10^{-3}$
Resolution	MPa	0	$1.0\cdot10^{-5}$	Uniform	B	1	$2\sqrt{3}$	$2.89\cdot10^{-6}$
Repeatability	MPa	0	$2.6\cdot10^{-4}$	Gaussian	A	1	1	$2.6\cdot10^{-4}$
Drift	MPa	0	$1.4\cdot10^{-6}$	Gaussian	B	1	$\sqrt{3}$	$8.1\cdot10^{-7}$
						Standard uncertainty (MPa)		$38\cdot10^{-6}p + 1.76\cdot10^{-3}$
						Expanded uncertainty (k=2) (MPa)		$75\cdot10^{-6}p + 3.52\cdot10^{-3}$

Mass uncertainty analysis

As mentioned in Chapter 2, the mass of the sinker at different pressure and temperature conditions was determined with a high accuracy balance (Mettler Toledo AT261) with a resolution of 0.01 mg. The balance reading uncertainty was determined for two different conditions: with the measuring cell filled with gas and pressurized and with the measuring cell in a vacuum. The main contributions to the balance reading uncertainty are shown in Table 3.4. and Table 3.5., with the cell filled and evacuated respectively, were it can be observed that the main source of uncertainty was the balance calibration, followed by the drift and the repeatability term. This last term was different for the two cases studied and was estimated as the standard

deviation of the mean of the last ten mass values of each pressure step of test measurements with nitrogen.

Table 3.4. Uncertainty budget for the mass reading when the measuring cell is filled with gas.

Uncertainty sources	Units	Estimation	Standard uncertainty	Distribution	Type	Sensitivity coefficient	Divisor	Contribution
Balance calibration	kg	0	$2.0\cdot10^{-7}$	Gaussian	B	1	1	$2.0\cdot10^{-7}$
Balance resolution	kg	0	$1.0\cdot10^{-8}$	Uniform	B	1	$2\sqrt{3}$	$2.9\cdot10^{-9}$
Repeatability	kg	0	$9.5\cdot10^{-8}$	Gaussian	A	1	1	$9.5\cdot10^{-8}$
Drift	kg	0	$1.0\cdot10^{-7}$	Gaussian	B	1	$\sqrt{3}$	$5.8\cdot10^{-8}$
					Standard uncertainty (kg)			$2.3\cdot10^{-7}$
					Expanded uncertainty (k=2) (kg)			$4.6\cdot10^{-7}$

Table 3.5. Uncertainty budget for the mass reading when the measuring cell is evacuated.

Uncertainty sources	Units	Estimation	Standard uncertainty	Distribution	Type	Sensitivity coefficient	Divisor	Contribution
Balance calibration	kg	0	$2.0\cdot10^{-7}$	Gaussian	B	1	1	$2.0\cdot10^{-7}$
Balance resolution	kg	0	$1.0\cdot10^{-8}$	Uniform	B	1	$2\sqrt{3}$	$2.9\cdot10^{-9}$
Repeatability	kg	0	$5.1\cdot10^{-8}$	Gaussian	A	1	1	$5.1\cdot10^{-8}$
Drift	kg	0	$1.0\cdot10^{-7}$	Gaussian	B	1	$\sqrt{3}$	$5.8\cdot10^{-8}$
					Standard uncertainty (kg)			$2.1\cdot10^{-7}$
					Expanded uncertainty (k=2) (kg)			$4.3\cdot10^{-7}$

Density uncertainty budget

The density uncertainty depends on the balance reading and the sinker volume uncertainties as expressed in Eq.3.6. This expression results from taking Eq.2.1., repeated here as Eq.3.5. for clarity reasons, as the mathematical model for the implementation of the law of propagation of uncertainties (GUM) (3).

$$\rho(T,p)=\frac{m_{S0}-m_{Sf}}{V_S(T,p)} \qquad \text{Eq.3.5.}$$

$$u(\rho)=\frac{1}{V_S}\sqrt{u^2(m_{S0})+u^2(m_{Sf})+\rho^2\cdot u^2(V_S)} \qquad \text{Eq.3.6.}$$

According to the simplification commented in the subsection 3.2.1. of this Chapter, this expression was modified by separating the terms which were proportional to the density and the independent terms, as indicated in Eq.3.7. Therefore the uncertainty in density could be compared with the uncertainties estimated by other authors for similar apparatus.

$$u(\rho) \approx \frac{1}{V_S}\left(\sqrt{u^2(m_{S0}) + u^2(m_{Sf})} + \rho \cdot u(V_S)\right) \qquad \text{Eq.3.7.}$$

The uncertainty in density depends directly on the mass reading and sinker volume uncertainties. The correlation term between the two mass input quantities is not taken into account since the sinker mass in the fluid and in a vacuum are determined in independent experiments and can be considered as no correlated variables. To confirm this assumption, the correlation coefficient was calculated as indicated in Eq.3.3. and was $r(m_{S0}, m_{Sf}) = -3 \cdot 10^{-5}$. The balance calibration uncertainty was evaluated after its in situ calibration using the two reference masses of tantalum and titanium which take part in the measurement procedure. Their mass was calibrated in the CEM resulting in m_{Ta} = 82.09475 ± 0.00010 g and m_{Ti} = 22.0397072 ± 0.000070 g. However, the uncertainties of these calibrated weights do not affect the mass uncertainty value since the repeatability was taken as the standard deviation of the mean of balance readings.

The sinker volume uncertainty was taken from the calibration certificate of CEM. The titanium sinker volume calibration value, given in the CEM certificate was V_{S0} = 13.2648 ± 0.0010 cm^3 (coverage factor k=2). The sinker volume changes with temperature and pressure due to the titanium's thermal and mechanical properties. However, the influence of these magnitudes in the volume uncertainty is much lower than the main component, so the overall uncertainty in volume was taken as that given by the CEM.

The budget estimated for the density uncertainty is shown in Table 3.6.

Table 3.6. Budget estimated for the density uncertainty.

Uncertainty sources		Units	Estimation	Standard uncertainty	Sensitivity coefficient		Degrees of freedom	Contribution
$u(m_{S0})$	Mass vacuum	kg	$1.90 \cdot 10^{-3}$	$2.3 \cdot 10^{-7}$	$1/V_{S1}$	$7.5\ 10^{4}$	200	$1.7 \cdot 10^{-2}$
$u(m_{Sf})$	Mass fluid	kg	$-5.27 \cdot 10^{-3}$	$2.1 \cdot 10^{-7}$	$1/V_{S1}$	$7.5\ 10^{4}$	800	$1.6 \cdot 10^{-2}$
$u(V_S)$	Sinker volume	m^3	$1.33 \cdot 10^{-5}$	$5.0 \cdot 10^{-10}$	ρ/V_{S1}	$\rho \cdot 7.5 \cdot 10^{4}$	∞	$3.75 \cdot 10^{-5}\rho$
					Standard uncertainty ($kg \cdot m^{-3}$)			$2.4 \cdot 10^{-2} + 3.8 \cdot 10^{-5}\rho$
					Expanded uncertainty (k=2) ($kg \cdot m^{-3}$)			$4.7 \cdot 10^{-2} + 7.6 \cdot 10^{-5}\rho$

3.2.2. Improvements proposal

The modifications which were carried out on the single sinker densimeter were proposed based on the previous uncertainty analysis in order to act only on the most important sources of uncertainty for each magnitude.

As it can be observed in Figure 3.1. main uncertainty contributions to the temperature uncertainty came from the PRT calibration and the temperature uniformity.

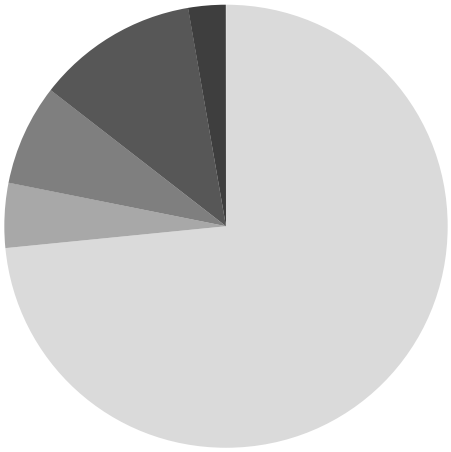

Figure 3.1. Individual contributions to the temperature uncertainty: Probe calibration; Temperature reading; Repeatability; Uniformity, Drift.

Therefore, it was proposed the addition of two Minco probes with lower calibration uncertainties, placed diametrically opposed at the middle height of the measuring cell while the existing Rosemount probe was relocated, to reduce these terms. The fluid temperature could be obtained as the average of the two Minco readings, reducing even more the temperature uncertainty.

Regarding the individual percentage contributions to the pressure uncertainty, Figure 3.2. depicts then the for three different pressures. It can be seen main uncertainty source arises from the transducer calibration, representing up to 97% of the total at low pressures.

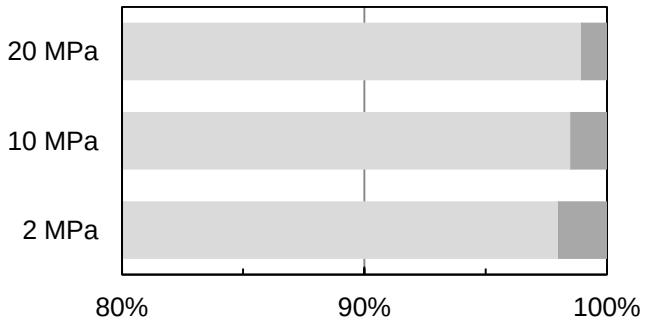

Figure 3.2. Individual contributions to the pressure uncertainty: Transducer calibration; Repeatability.

Both main terms could be reduced by replacing the pressure transducer by a more accurate one. However, even if a new transducer for the whole pressure range (up to 20 MPa) was installed, the accuracy of the pressure measurements would decrease at pressures below 2 MPa (10% of the whole apparatus range, as stated by the manufacturer). Therefore, it was decided to keep this instrument and add a new pressure transducer (Paroscientific 2300A-101) for the range 0 – 2 MPa. Thus, pressure in the range 2 – 20 MPa could be measured with the old transducer.

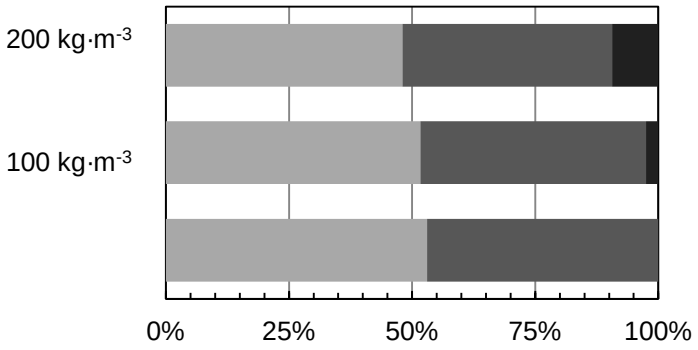

Figure 3.3. Individual contributions to the density uncertainty: Sinker mass in a vacuum; Sinker mass in the fluid; Sinker volume.

Finally, Figure 3.3. the percentage contribution of the uncertainty sources of density for three different density values. As presented, the main uncertainty source arose from the sinker mass reading in the fluid, followed by the sinker mass reading in a

vacuum. The sinker volume uncertainty is significant only at higher densities, accounting for less than 10% for a density value of ρ = 200 kg·m^{-3}.

These results suggested the importance of improving the balance reading uncertainty. The option of replacing the balance by a new one, with a higher resolution, was rejected because it also involved major changes in the whole setup, even in the measuring cell design. Therefore, the replacement of the sinker by a bigger one appeared to be a simpler solution with a similar effect to the increase in the balance resolution. With a new sinker, with double volume and equal mass, the accuracy of measurements at low densities is higher. This new sinker experiments a double buoyancy force under the same fluid pressure and temperature conditions and the change in the sinker mass due to the buoyancy effect can be measured by the balance more accurately, as if the balance resolution was higher. Moreover, this change affects directly the sensitivity coefficients of the density uncertainty budget which result in a decrease of all uncertainty contributions. Thus, the old titanium sinker (m_S ≈ 60 g, V_S ≈ 13 cm^3) was substituted by a new silicon sinker (m_S ≈ 60 g, V_S ≈ 26 cm^3) with double volume.

The proposed modifications are described in the following subsections.

3.3. REPLACEMENT OF THE SINKER

The old sinker of the densimeter was replaced by the silicon sinker due to the proportional relation between the buoyancy effect and the sinker volume. The selection of the sinker material and size depends on two factors: the maximum fluid density to be measured and the density range to work on.

In one side, the sinker density must be higher than the maximum fluid density value to be measured. Thus the buoyancy force exerted by the fluid compensates only for part of the sinker weight and the change in weight can be measured by the balance through the magnetic suspension. To this end, bigger sinker densities would be more appropriate for liquids or high pressurized gases measurements, and lower densities would enable more accurate measurements for gases at low pressures.

In the other side, the buoyancy force acting on the sinker is proportional to the sinker volume. As the resolution of the balance is limited, its reading would be more accurate for bigger values. Thus, the bigger the sinker volume is, the better the balance reading would be. Therefore a large sinker would permit to measure gases at low pressures with more accuracy.

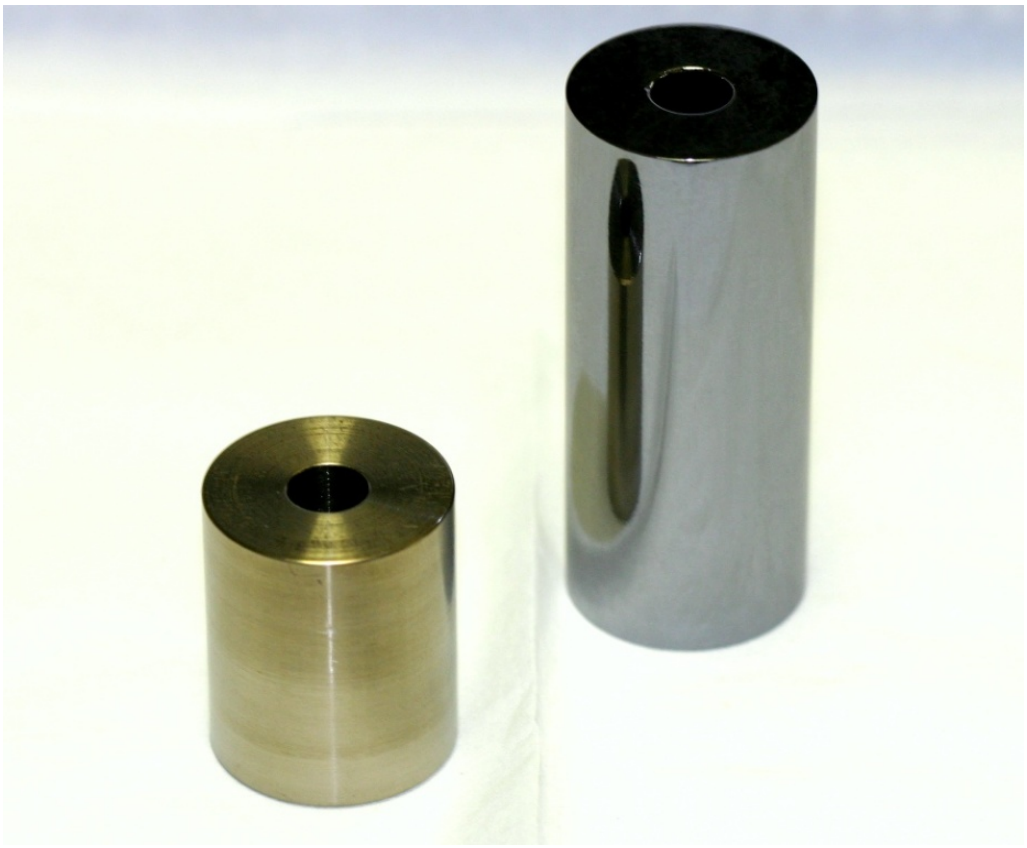

Figure 3.4. Titanium (left) and Silicon (right) sinkers for the measuring cell of the single sinker densimeter during the replacement.

As mentioned before, the single sinker densimeter was initially supplied with a titanium sinker in the measuring cell. As the aim of the project was measuring gaseous mixtures over a temperature range of (250 – 400) K up to 20 MPa, the most convenient sinker regarding the paragraphs above would be a low density and big volume one. Thus, the old titanium sinker was replaced by a new silicon sinker with a density of $\rho \approx 2300$ kg m^{-3} and a volume of 26 cm^3. Both sinkers can be seen for comparison in Fig. 3.4.

From the point of view of the force transmission error due to the specific fluid effect, described in Chapter 2, its effect is lower when the sinker density is next in value to the

fluid density. Therefore, the silicon sinker, with a lower density, reduces also the effect on the force transmission produced by the magnetic behavior of the fluid. The reduction of the term would become significant for measurements of gases strongly diamagnetic or paramagnetic.

3.3.1. Calibration of the sinker volume

The silicon sinker was built and provided by Rubotherm. The volume of the sinker was calibrated by both DKD (Deutscher Kalibrierdienst) and CEM (Centro Español de Metrología). Calibration results are shown in Table 3.7.

Table 3.7. Sinker volume calibration data

	DKD	CEM
Date	20/05/2009	17/09/2009
Volume (cm^3)	26.444 ± 0.015	26.444 ± 0.003
Real mass (g)	-	61.59181 ± 0.00016
Density (kg/m^3)	2329 ± 2	2329.12 ± 0.35
Calibration conditions		
Room temperature (ºC)	(19.9 – 20.3)	21.3 ± 0.15
Room pressure (mbar)	(1011.37 – 1011.77)	934.17 ± 0.03
Room humidity (%)	(49 – 54)	46.0 ± 0.5

Calculations for density were made taking into account the calibration results yielded by CEM due to the lower uncertainty in volume.

This sinker volume must be adjusted in function of temperature and pressure depending on the thermal and mechanical material properties. The volume variation of the sinker was approximated by the volume variation of a cube, expressed by Eq. 3.8.

$$V(T,p) = V_0(T_0,p_0)\left[1+\alpha(T)(T-T_0)-\frac{3(p-p_0)}{E(T)}(1-2\nu(T))\right] \qquad \text{Eq.3.8.}$$

This formula assumes that the material is isotropic and that the linear expansion coefficient, Young modulus and Poisson coefficient have the same value for the three directions of the cube.

Due to the anisotropy of silicon these material properties are dependent upon the direction of the silicon surface. Thus, a study on the last research for thermal and

mechanical properties for silicon was made in order to determine average values to be used in Eq. 3.8.

3.3.2. Temperature dependence of the volume

Thermal properties for silicon have been widely studied for the last few years due to the great importance of this material in the field of semiconductors and photovoltaic cells. The more accurate values for the thermal lineal expansion coefficient of silicon for the range (90 – 850) K are given by Eq. 3.9. (6).

$$\alpha(T) = a + A\frac{\left(\frac{\Theta_E}{T}\right)^2 e^{\frac{\Theta_E}{T}}}{\left(e^{\frac{\Theta_E}{T}} - 1\right)^2} + B\frac{\left(\frac{T}{\Phi_0} - 1\right)^2}{1 + b\frac{T}{\Phi_0}} \qquad \text{Eq.3.9.}$$

Parameters for Eq. 3.9. are given in Table 3.8. The uncertainty for the calculated thermal expansion values is approximately 10^{-8} K^{-1}.

Table 3.8. Parameters to be used in Eq.3.9.

Parameter	Value	Units
a	-0.687 10^{-6}	1/K
A	5.000 10^{-6}	1/K
Θ_E	685	K
B	0.22 10^{-6}	1/K
b	0.316	-
Φ_0	395	K

3.3.3. Pressure dependence of the volume

Variation in volume due to the change in the fluid pressure depends mainly on two material properties: the Young's Modulus *E* and the Poisson's coefficient ν. As mentioned above, owing to the anisotropy character of silicon these properties change their values depending on the direction of the crystal surface. As the surface direction of the sinker silicon is unknown, average values for both properties were used for the formulation.

Young's modulus and Poisson's coefficient values were obtained as functions of the second order elastic constants for silicon C_{11}, C_{12} and C_{44}, as shown in Eq.3.10. and

Eq.3.11., where $H = 2C_{44}+C_{12}-C_{11}$ is the anisotropy factor. The variation with temperature of the second order elastic constants and their average values at room temperature are shown in Table 3.9.

$$E = 2(C_{44} - H/5)(1+\nu) \qquad \text{Eq.3.10.}$$

$$\nu = \frac{C_{12} - H/5}{2(C_{12} + C_{44} - 2H/5)} \qquad \text{Eq.3.11.}$$

Table 3.9. Average values for second order elastic constants for Silicon.

C_{ij}	C_{ij}(298.15 K) (7)	$\left(\frac{1}{C_{ij}}\right)\frac{\partial C_{ij}}{\partial T}$
	MPa	K^{-1}
C_{11}	1.6564 10^5	-9.4 10^{-5}
C_{12}	0.6394 10^5	-9.8 10^{-5}
C_{44}	0.7951 10^5	-8.3 10^{-5}

Temperature dependent expressions calculated for E and ν where fitted to a linear regression for the working range of the single sinker densimeter (250 – 400) K. The fitting equations are shown in Eq. 3.12. and 3.13.

$$E = 1.6681\cdot10^5 - 1.4494\cdot10^2 T \qquad \text{Eq.3.12.}$$

$$\nu = 0.21788 - 2.3748\cdot10^{-5} T \qquad \text{Eq.3.13.}$$

3.4. IMPROVEMENT OF THE TEMPERATURE MEASUREMENT UNCERTAINTY

As mentioned at the beginning of this Chapter, temperature inside the measuring cell was initially measured by a single temperature probe (Rosemount 162D). With this configuration the temperature distribution in the cell was unknown so that it could not be concluded whether significant temperature gradients existed inside the cell.

In order to analyze the distribution of temperature inside the measuring cell, two more PRT-25 probes were added (Minco S1059PJ5X6). The probes, Minco 712 and Minco 713, were placed in the cell as shown in Figure 3.5. This disposition allowed the study of the homogeneity of temperature in both radial and axial directions by comparing the values given by the two Minco probes and the three probes, respectively.

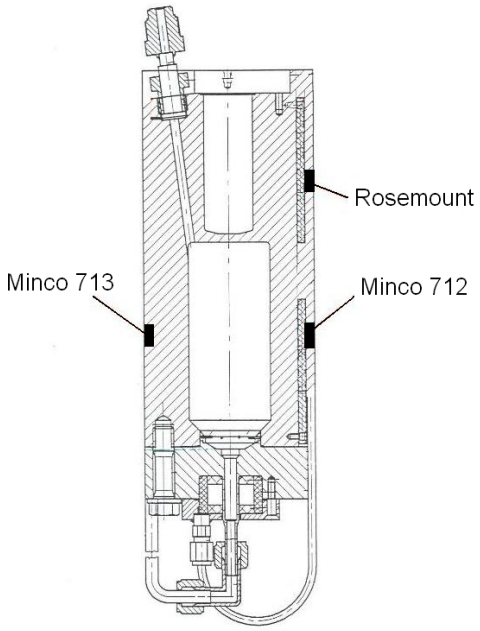

Figure 3.5. PRT-25 temperature probes location in the measuring cell.

Moreover the addition of the two PTR-25 probes permitted a more accurate determination of the temperature of the fluid, which was calculated as the average value of the two Minco probes readings.

3.4.1. Calibration of the PRT-25

The PRT-25 probes were calibrated at our own calibration facility (accredited by ENAC, member of EA) for the same temperature fixed points. The calibration uncertainties of both probes, together with the drift value, are given in K in Table 3.10. for each calibration fixed point.

Table 3.10. Calibration uncertainty and drift of the Minco PRT-25 probes.

Probe	Calibration expanded uncertainty (k=2) (K)				Drift (K)
	505.077 K	429.748 K	302.913 K	234.317 K	
Minco 712	$6 \cdot 10^{-3}$	$5 \cdot 10^{-3}$	$4 \cdot 10^{-3}$	$4 \cdot 10^{-3}$	$2 \cdot 10^{-3}$
Minco 713	$6 \cdot 10^{-3}$	$5 \cdot 10^{-3}$	$4 \cdot 10^{-3}$	$4 \cdot 10^{-3}$	$2 \cdot 10^{-3}$

The calibration uncertainty of each probe was taken as the maximum value observed in Table 3.10. in the temperature working range of the densimeter.

3.4.2. Study of the temperature homogeneity and stability

All density measurements performed on the densimeter contained simultaneously the temperature values of the three PTR-25 probes along the whole temperature range of the densimeter. This data collecting was carried out in order to study the temperature homogeneity and stability over time of the contained fluid for different nominal temperatures and pressures of the cell.

Thermal homogeneity study

Thermal homogeneity is defined as the maximum difference between the temperature values on two different points of an isothermal medium. Considering the measuring cell as the isothermal medium the temperature homogeneity was studied by calculating the maximum gradients between the temperature values measured by the PTR-25 probes. Thus, the temperature distribution in the radial direction was studied with the two Minco probes. Table 3.11. shows the maximum temperature gradients between the mentioned PTR-25 probes observed for each isotherm for several data sets.

Table 3.11. Results from the thermal homogeneity study.

Isotherm	$\triangle T_{\text{Mincos}}$ mK	$\triangle T_{\text{Minco-Ros}}$ mK
250 K	4	28
275 K	3	7
300 K	3	6
325 K	3	4
350 K	1	1
375 K	3	2
400 K	4	4

Thermal stability study

Thermal stability is defined as the maximum temperature variation during a period of time in an isothermal medium. Temperature inside the measuring cell, which was calculated as the average value between the two Minco temperature probes, was evaluated during a period of time slightly bigger than the measuring time for each point in order to study the stability of the temperature.

Table 3.12. Results from the thermal stability study.

Isotherm	$\triangle T_{max}$ mK	σ^2 mK^2
250 K	4	2
275 K	5	2
300 K	5	2
325 K	4	2
350 K	6	2
375 K	7	3
400 K	9	4

Results obtained after the study are shown in Table 3.12. The data yielded that the maximum difference between the initial and the last temperature value of the fluid during the measuring period was of 9 mK.

Conclusions

After analyzing the thermal homogeneity and stability, the following conclusions were drawn:

- The temperature of the fluid inside the measuring cell is homogeneous with a maximum temperature gradient between two faced points in the middle height of 4 mK.

- The maximum temperature gradient between the coupling house and the fluid reached a maximum of 28 mK at 250 K. This temperature gradient for the rest of the isotherms was always lower than 7 mK. The reason of this significant gradient resides in the fact that the magnet coupling house is not heated by the controlled electric resistance. However this difference in temperature did not affect the fluid temperature due to the Rosemount probe position.

- Uniformity inside the cell was estimated as the average of the collected homogeneity values, resulting in 2.5 mK.

Addition of an external resistor

The uncertainty of the resistance of the internal resistor of the AC resistance comparator bridge affected only the temperature reading term of the temperature uncertainty budget, which was the less significant contribution. Therefore, the

replacement of the internal resistor by an external calibrated resistor would not affect significantly the overall uncertainty in temperature.

Nevertheless, an external standard calibrated resistor (Tinsley model 5685A, 25 Ω) with a resistance value of R_{std} = 24.999800 ± 0.000075 Ω was connected to the AC resistance comparator bridge, so that the necessary periodical calibration of the internal resistor was avoided.

3.5. IMPROVEMENT OF PRESSURE MEASUREMENT UNCERTAINTY

Pressure inside the measuring cell was formerly measured by means of a Paroscientific absolute pressure transducer (Paroscientific 43KR-HHT-101) over the working range (0 – 20 MPa). According to the manufacturer indications, the accuracy of the pressure transducer at pressures below ten percent of its operating range decreases unacceptably. Therefore a new absolute pressure transducer (Paroscientific 2300A-101) for the range (0 – 2) MPa was added, in order to reduce the measurement uncertainty in the low pressure range.

Moreover, the addition of this new pressure transducer allowed the calibration curve of the old transducer to be corrected since the uncertainty in pressure of the 2 MPa transducer was lower than that the uncertainty of the calibration constants determined for the former one.

3.5.1. Calibration of the new pressure transducer

The new pressure transducer was calibrated against an absolute dead gauge at our own calibration facility (accredited by ENAC, member of EA) to determinate the transducer calibration uncertainty to be used in the uncertainty budget.

Once a year both pressure transducers were calibrated against respective dead weight gauges (traceable to international standards) at the calibration facility.

3.6. UNCERTAINTY ASSESMENT

The uncertainty of a measurement result quantifies its quality and reliability and allows comparing it with other reference values for the measurand. The two recognized

methods for uncertainty evaluation are the uncertainty propagation law, presented in the Guide to the Expression of Uncertainty in Measurement (GUM) and the Monte Carlo methodology. While the first method can be applied in all linear models and, to a lesser extent, in non-linear models, Monte Carlo simulation can be applied to any of the model. Therefore, Monte Carlo simulation is presented as an alternative to overcome the limitations of the uncertainty propagation law. Nonetheless, this second methodology can be also performed to validate a previous evaluation with the GUM or to discard secondary effects not taken into account.

In this work, the state point (p, ρ, T) measuring uncertainty of the modified single sinker densimeter was thoroughly evaluated following the uncertainty propagation law.

3.6.1. Mass uncertainty

The mass uncertainty budget was affected by the sinker replacement due to the change of the repeatability contribution, which was decreased, as it is indicated in Tables 3.13 and 3.14 for the evacuated and filled cell, respectively.

Table 3.13. Uncertainty budget for the mass reading when the measuring cell is evacuated.

Uncertainty sources	Units	Estimation	Standard uncertainty	Distribution	Type	Sensitivity coefficient	Divisor	Contribution
Balance calibration	kg	0	$2.0 \cdot 10^{-7}$	Gaussian	B	1	1	$2.0 \cdot 10^{-7}$
Balance resolution	kg	0	$1.0 \cdot 10^{-8}$	Uniform	B	1	$\frac{2}{\sqrt{3}}$	$2.9 \cdot 10^{-9}$
Repeatability	kg	0	$8.0 \cdot 10^{-8}$	Gaussian	A	1	1	$8.0 \cdot 10^{-8}$
Drift	kg	0	$1.0 \cdot 10^{-7}$	Gaussian	B	1	$\sqrt{3}$	$5.8 \cdot 10^{-8}$
					Standard uncertainty (kg)			$2.2 \cdot 10^{-7}$
					Expanded uncertainty (k=2) (kg)			$4.5 \cdot 10^{-7}$

The repeatability of the mass readings was again estimated as the maximum standard deviation of the mean of the last ten mass values of each pressure step of the test measurements. The mass repeatability was only dropped moderately which resulted in a slight reduction of the overall uncertainty in mass.

Table 3.14. Uncertainty budget for the mass reading when the measuring cell is filled with gas.

Uncertainty sources	Units	Estimation	Standard uncertainty	Distribution	Type	Sensitivity coefficient	Divisor	Contribution
Balance calibration	kg	0	$2.0 \cdot 10^{-7}$	Gaussian	B	1	1	$2.0 \cdot 10^{-7}$
Balance resolution	kg	0	$1.0 \cdot 10^{-8}$	Uniform	B	1	$2\sqrt{3}$	$2.9 \cdot 10^{-9}$
Repeatability	kg	0	$3.0 \cdot 10^{-8}$	Gaussian	A	1	1	$3.0 \cdot 10^{-8}$
Drift	kg	0	$1.0 \cdot 10^{-7}$	Gaussian	B	1	$\sqrt{3}$	$5.8 \cdot 10^{-8}$
						Standard uncertainty (kg)		$2.1 \cdot 10^{-7}$
						Expanded uncertainty (k=2) (kg)		$4.2 \cdot 10^{-7}$

3.6.2. Temperature uncertainty

The temperature uncertainty budget for the new layout of the PRT-25 probes in the measuring cell is given in Table 3.15.

Table 3.15. Temperature uncertainty budget.

Uncertainty component	Units	Estimation	u(xi)	Distribution	Type	Sensitivity coefficient	Divisor	$u_i(y)^2$
Minco 712 calibration uncertainty	K	0	$2.0 \cdot 10^{-3}$	Gaussian	B	0.5	1	$1.0 \cdot 10^{-3}$
Minco 712 calibration uncertainty	K	0	$2.0 \cdot 10^{-3}$	Gaussian	B	0.5	1	$1.0 \cdot 10^{-3}$
Temperature reading	Ω	0	$6.7 \cdot 10^{-5}$	Gaussian	B	10.5	1	$7.0\ 10^{-4}$
Repeatability	K	0	$6.3 \cdot 10^{-4}$	Gaussian	A	1	1	$6.3 \cdot 10^{-4}$
Uniformity	K	0	$2.5 \cdot 10^{-3}$	Uniform	B	1	$2\sqrt{3}$	$7.2 \cdot 10^{-4}$
Drift	K	0	$1.0 \cdot 10^{-3}$	Uniform	B	1	$\sqrt{3}$	$5.8 \cdot 10^{-4}$
						Standard uncertainty (K)		$1.9 \cdot 10^{-3}$
						Expanded uncertainty (K) (k=2)		$3.9 \cdot 10^{-3}$

The main observable reduction in the uncertainty comes from the PRT-25 probes calibration and the determination of the temperature as the average of their values. The repeatability and uniformity were also significantly reduced.

3.6.3. Pressure uncertainty

Table 3.16. shows the uncertainty budget for the 2 MPa pressure transducer, where it can be noticed that the most important contribution to the uncertainty come from the transducer calibration term. Repeatability was estimated as the standard deviation of

the mean of the ten pressure values used to calculate each state point pressure. The drift was estimated from two consecutive calibrations.

Table 3.16. Uncertainty budget of the 20 MPa pressure transducer.

Uncertainty sources	Units	Estimation	Standard uncertainty	Distribution	Type	Sensitivity coefficient	Divisor	Contribution
								MPa
Transducer calibration	MPa	0	$38\cdot10^{-6}p + 1.74\cdot10^{-3}$	Gaussian	B	1	1	$38\cdot10^{-6}p + 1.74\cdot10^{-3}$
Resolution	MPa	0	$1.0\cdot10^{-5}$	Uniform	B	1	$2\sqrt{3}$	$2.89\cdot10^{-6}$
Repeatability	MPa	0	$2.6\cdot10^{-4}$	Gaussian	A	1	1	$2.6\cdot10^{-4}$
Drift	MPa	0	$1.4\cdot10^{-6}$	Gaussian	B	1	$\sqrt{3}$	$8.1\cdot10^{-7}$
						Standard uncertainty (MPa)		$38\cdot10^{-6}p + 1.76\cdot10^{-3}$
						Expanded uncertainty (k=2) (MPa)		$75\cdot10^{-6}p + 3.52\cdot10^{-3}$

3.6.4. Uncertainty budget for density

Finally, the measurement uncertainty in density was calculated following Eq.3.7. with the new values of the magnitudes and uncertainties. The density uncertainty budget is given in Table 3.17.

Table 3.17. Budget estimated for the density uncertainty.

Uncertainty sources		Units	Estimation	Standard uncertainty	Sensitivity coefficient		Degrees freedom	Contribution
$u(m_{S0})$	Mass vacuum	kg	$1.90\cdot10^{-3}$	$2.2\cdot10^{-7}$	$1/V_{S2}$	$3.8\ 10^{4}$	500	$8.4\cdot10^{-3}$
$u(m_{Sf})$	Mass fluid	kg	$-5.27\cdot10^{-3}$	$2.1\cdot10^{-7}$	$1/V_{S2}$	$3.8\ 10^{4}$	1200	$8.0\cdot10^{-3}$
$u(V_S)$	Sinker volume	m^3	2.64·10-^{5}	$1.5\cdot10^{-9}$	ρ/V_{S2}	$3.8\ 10^{4}\rho$	∞	$5.7\ 10^{-5}\rho$
					Standard uncertainty ($kg\cdot m^{-3}$)			$1.2\cdot10^{-2} + 5.7\cdot10^{-5}\rho$
					Expanded uncertainty (k=2) ($kg\cdot m^{-3}$)			$2.3\cdot10^{-2} + 1.1\cdot10^{-4}\rho$

It was previously indicated that the reduction in the mass uncertainty achieved with the replacement of the sinker was not significantly high. However, it can be seen that the new sinker has a major influence in the density uncertainty since all the uncertainty contributions are divided by the sinker volume, which is double in value as the old titanium sinker volume. Therefore, the drop in the uncertainty in density is more significant than the reduction in mass uncertainty.

One disadvantage of the new sinker comes from its higher volume uncertainty. However, since this term is proportional to the density it would only affect high densities.

3.6.5. Analysis of the achieved improvements

Table 3.18. summarizes the results of both uncertainty analysis performed before and after the modifications were carried out. As it is shown, the temperature uncertainty was decreased by 44% from the initial value of $U(T)$ = $7.0 \cdot 10^{-3}$ K, thank to the determination of the temperature from the average of the two added PRT-25 probes and to the lower calibration uncertainty of these new probes.

Table 3.18. Summary of the state point expanded uncertainty before and after the modifications were carried out on the densimeter (k=2).

Magnitude		Units	Before	After
T	Temperature	K	$7.0 \cdot 10^{-3}$	$3.9 \cdot 10^{-3}$
p	Pressure 2 – 20 MPa	MPa	$3.52 \cdot 10^{-3} + 7.5 \cdot 10^{-5} p$	$3.52 \cdot 10^{-3} + 7.5 \cdot 10^{-5} p$
p	Pressure 0 – 2 MPa	MPa	$3.52 \cdot 10^{-3} + 7.5 \cdot 10^{-5} p$	$1.8 \cdot 10^{-4} + 6.0 \cdot 10^{-5} p$
ρ	Density	$kg \cdot m^{-3}$	$4.7 \cdot 10^{-2} + 7.6 \cdot 10^{-5} \rho$	$2.3 \cdot 10^{-2} + 1.1 \cdot 10^{-4} \rho$

Pressure in the range 0 – 2 MPa was also significantly reduced by more than 92% with the addition of the new pressure transducer. This reduction contributed to compensate for the higher mass uncertainty which occurs at low pressures. Moreover, with the new pressure transducer, the calibration curve of the initial pressure transducer for the range 2-20 MPa was corrected since the uncertainty of the calibration parameters was higher than the measurement uncertainty of the new transducer.

The measurement uncertainty in density was influenced by the replacement of the sinker in two ways. In the first place, the new silicon sinker with double volume increased the balance resolution so that the standard uncertainty of the balance reading decreased. In the second place, the volume affected directly the sensitivity coefficients of each uncertainty contribution reducing them to the half. Therefore, uncertainty in density was decreased by more than 22% over the whole apparatus working range, especially at low densities were the uncertainty in density was near 50% less the initial uncertainty value. Figure 3.3 shows the percentage contribution of

each density uncertainty component to the total uncertainty value, at different gas densities. It can be seen that, for a high density value above 200 kg·m^{-3} the contribution of the sinker volume uncertainty represents the half of the total uncertainty value. However, at low densities the contribution of the volume is negligible since the effect of the mass reading uncertainty is more significant. This means that a new calibration of the sinker volume would have influence only at high densities, as it can be observed in Figure 3.6.

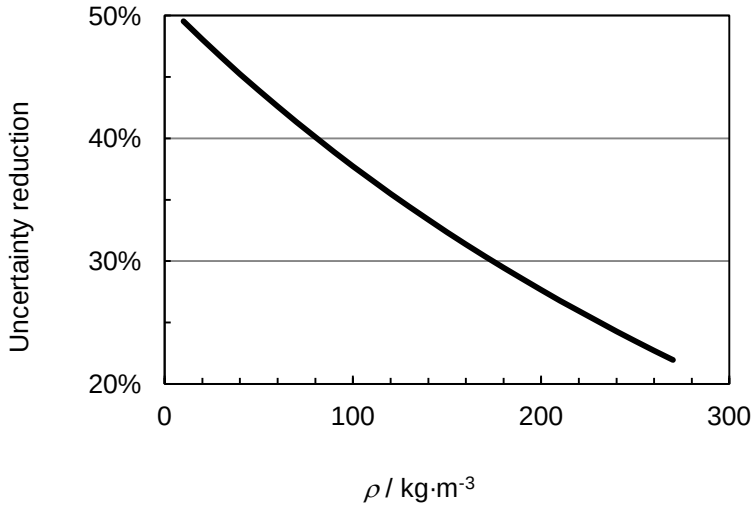

Figure 3.6. Percentage reduction of the density measurement uncertainty as a function of the density value.

Figure 3.7. shows the percentage contribution of each uncertainty source to the uncertainty in density. As compared to Figure 3.3, it can be seen that the percentage contribution of each term to the total uncertainty on density changed. For low densities the main contributions still come from the sinker mass reading in a vacuum and in the fluid. Nevertheless, at high densities the main input comes now from the sinker volume, accounting for 40% of the total uncertainty for a density value of ρ = 200 kg·m^{-3}. Based on this new distribution it can be concluded that the reduction of the sinker volume calibration uncertainty would affect only at high densities.

The total state point uncertainties for different densimeters based on a similar measurement technique are collected in Table 3.19 for comparison with those evaluated in this work. Uncertainties in density are given for a density range corresponding to that of nitrogen in the temperature and pressure working ranges of the apparatus described in this work.

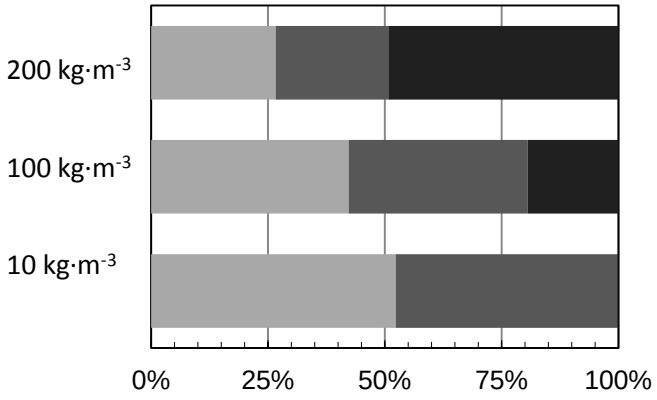

Figure 3.7. Percentage contribution of each state density uncertainty component. Sinker mass in a vacuum; Sinker mass when it is immersed in a fluid; Sinker volume.

The estimated uncertainty for each magnitude estimated in this uncertainty analysis resulted to be of the same order as those reported by other authors for similar apparatus. It can be observed, for some cases, that the wider the working apparatus range, the higher the uncertainties are. However, uncertainty in density reported by McLinden (8) keeps relatively low due to the fact that the two sinker densimeter is more accurate than single sinker densimeters, as stated in (9).

Table 3.19. Measuring expanded uncertainty for different densimeters (coverage factor k=2).

Reference	Year	Densimeter type	Working range T(K)	p(MPa)	U(T) K	U(p) MPa	U(ρ) kg·m^{-3}
This work	2011	SSMSD	250 – 400	0 - 20	$3.9\cdot10^{-3}$	0.007-0.015%	0.020-0.155%
D.E. Cristancho (10)	2010	SSMSD	265 - 400	0 - 200	$5.0\cdot10^{-3}$	0.010%	0.030-0.100%
Mark O MacLinden (8)	2006	TSMSD	90 - 520	0 - 40	$4.0\cdot10^{-3}$	0.005-0.050%	0.003-0.006%
Gunnar Schilling (11)	2006	SSMSD	233 - 476	0 - 30	$4.0\cdot10^{-3}$	0.006%	0.010-0.018%
J. Klimeck (12)	2001	SSMSD	240 - 520	0 - 30	$4.0\cdot10^{-3}$-$10.0\cdot10^{-3}$	0.016%	0.013-0.021%

It must be noted that the measurement uncertainties in density given in Table 3.18. do not take into account the influence of the temperature and pressure uncertainties. The overall uncertainty in density of the density measurements presented in this thesis must include therefore these two terms but also the term due to the uncertainty of the composition of the studied mixtures. The determination of this total uncertainty in density is explained in Chapter 4 and the final expression of the uncertainty is given before the analysis of the results of each mixture in Chapters 4 to 6.

3.7. EXPERIMENTAL VALIDATION OF THE MODIFIED APPARATUS

Finally, after all the improvements had been carried out, test measurements with pure nitrogen were performed to check the correct performance of the modified densimeter. The test measurements consisted of seven isotherms which cover the temperature range 250 K – 400 K at pressures up to 20 MPa and were carried out before the beginning of the study of the gas mixtures presented in this thesis. Results yielded relative deviations in density from the equation of state for nitrogen of Span et al.(13) within a 0.02% band. Figure 3.8. depicts the relative deviations in density of the experimental values measured during all the test measurements and Table 3.20 gives the magnitudes obtained from the statistical analysis of these data. The statistical magnitudes are defined later in Chapter 4.

Table 3.20. Statistical analysis of the density data measured during the test measurements with nitrogen.

n	AAD	Bias	SDV	RMS
217	0.01084	0.00298	0.01516	0.01541

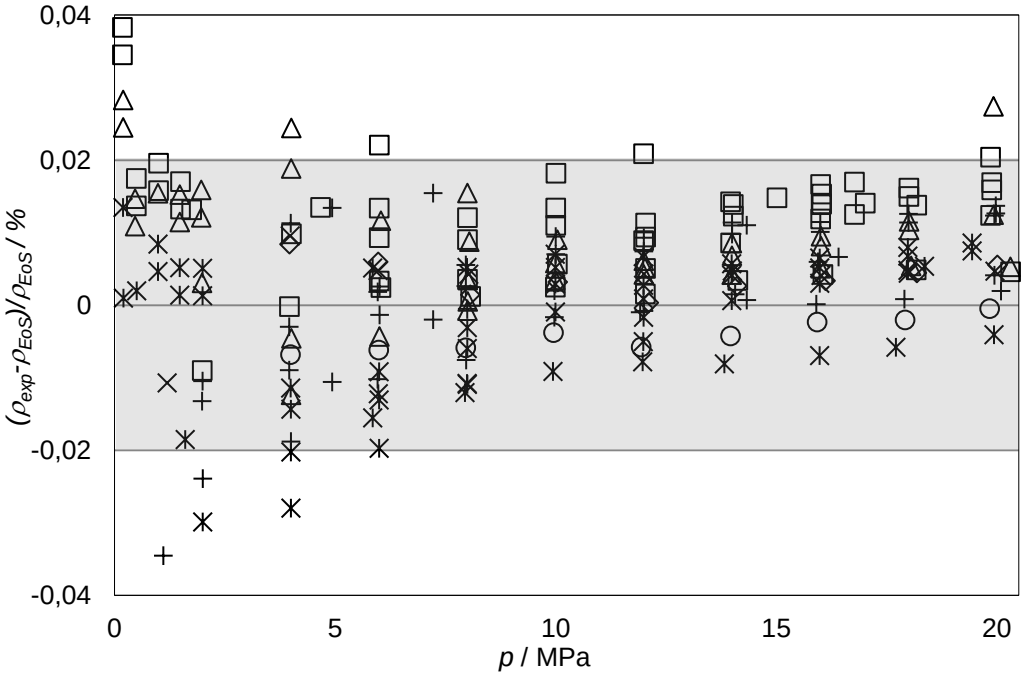

Figure 3.8. Relative deviations in density of experimental *(p, ρ, T)* data of the test measurements from the equation of state for nitrogen of Span et al. □ 250 K; ◇ 275 K; △ 300 K; × 325 K; + 350 K; ○ 375 K; ✳ 400 K.

Afterwards, before the measurement of each gas mixture, some isotherms on nitrogen were carried out again in order to discard a possible incorrect operation of the apparatus.

REFERENCES

1. BIPM, IEC, IFCC, ILAC, IUPAC, IUPAP, ISO and OOIML. International Vocabulary of Metrology-Basic and General Concepts and Associated Terms (VIM), 3rd Edn. *JCGM 200:2008*, 2008.

2. *Recommendation INC-1 - Working Group on the Statement of Uncertainties.* Sévres, France, 1980.

3. BIPM, IEC, IFCC, ISO, IUPAC, IUPAP and OIML. Guide to the Expression of Uncertainty in Measurement*. International Organization for Standarization*, 1995.

4. EA-4/02 - Expression of the Uncertainty of Measurement in Calibration, Appendix E*. Expression of the Uncertainty of Measurement in Calibration*, 1999.

5. EA-4/17 Calibration of Pressure Balances, Appendix B, 1997.

6. SWENSON, C.A. Recommended Values for the Thermal Expansivity of Silicon from 0 to 1000 K*. J. Phys. Chem. Ref. Data*, 1983, vol. 12, no. 2. pp. 179-182.

7. Landolt-Börnstein. *Elastic Constants of Second Order: Temperature Coefficients Tc*. Berlin, 2001*.*

8. MCLINDEN, M. O. -WILL, C. Apparatus for Wide-Ranging, High-Accuracy Fluid (p, ρ, T) Measurements Based on a Compact Two-Sinker Densimeter*. Journal of Chemical Thermodynamics*, 2007, vol. 39, no. 4. pp. 507-530.

9. WAGNER, W. and KLEINRAHM, R. Densimeters for very Accurate Density Measurements of Fluids Over Large Ranges of Temperature, Pressure, and Density. *Metrologia*, 2004, vol. 41, no. 2. pp. S24-S39.

10. CRISTANCHO, D.E. et al. Force Transmission Error Analysis for a High-Pressure Single-Sinker Magnetic Suspension Densimeter*. International Journal of Thermophysics*, 2010, vol. 31, no. 4-5. pp. 698-709.

11. SCHILLING, G.; KLEINRAHM, R. and WAGNER, W. Measurement and Correlation of the (p, ρ, T) Relation of Liquid n-Heptane, n-Nonane, 2,4-Dichlorotoluene, and Bromobenzene in the Temperature Range from (233.15 to 473.15) K at Pressures Up to 30 MPa for use as Density Reference Liquids. *Journal of Chemical Thermodynamics*, 2008, vol. 40, no. 7. pp. 1095-1105.

12. KLIMECK, J.; KLEINRAHM, R. and WAGNER, W. Measurements of the (p, ρ, T) Relation of Methane and Carbon Dioxide in the Temperature Range 240 K to 520 K at Pressures Up to 30 MPa using a New Accurate Single-Sinker Densimeter. *Journal of Chemical Thermodynamics*, 2001, vol. 33, no. 3. pp. 251-267.

13. SPAN, R. et al. A Reference Equation of State for the Thermodynamic Properties of Nitrogen for Temperatures from 63.151 to 1000 K and Pressures to 2200 MPa. *Journal of Physical and Chemical Reference Data*, 2000, vol. 29, no. 6. pp. 1361-1401.

CHAPTER 4

MEASUREMENTS OF MIXTURES OF NITROGEN AND CARBON DIOXIDE

4.1. INTRODUCTION

Substantial quantities of gaseous carbon dioxide and nitrogen are present mixed in many industrial schemes, including energetic exploitation of non conventional fuels, such as biogas or syngas, carbon capture and storage processes, exhaust gases from combustion reactions and the enhanced oil extraction with nitrogen or carbon dioxide injection. For this reason, thermodynamic data concerning binary mixtures of carbon dioxide with nitrogen have been reported by several authors and used to fit correlations.

According to the data base of thermodynamic data of gas mixtures listed in (1, 2) there are 2856 (p, ρ, T) data available in the temperature range (209 – 673) K and pressures up to 274 MPa, for molar fractions of carbon dioxide ranging from 0.10 to 0.98. Despite the number of data is in principle significant, the number of experimental density data used for the fitting of the mixture parameters of the GERG-2004 equation of state is comparatively low (only 823 (p, ρ, T) data, which represents less than 30% of the original data). This fact is due to the low accuracy and reliability of many of these data, since some of them were measured in the early 1940's when the equipments accuracy was still low. Therefore, it was decided to measure the density of four mixtures of carbon dioxide with nitrogen with different compositions.

In this Chapter a set of 347 density measurements for mixtures of nitrogen with carbon dioxide with molar compositions x_{CO_2} = (0.10, 0.15, 0.20, 0.50) in the gas phase at temperatures between (250 – 400) K and pressures up to 20 MPa are presented. The experimental density data are compared with the densities calculated from the GERG-2004 model (2). Second and third virial coefficients were also fitted for these mixtures, since these coefficients are important, not only because they represent the non ideal behavior of real gases, but also because many models of properties estimation use their values (i.e. it has been pointed out that third virial coefficients significantly affect calculations of heat capacities (3)).

4.2. GRAVIMETICAL PREPARATION OF THE MIXTURES

The four mixtures of nitrogen with carbon dioxide were prepared by the Reference Materials Laboratory of the Spanish national metrology institute (Centro Español de Metrología, CEM). The final composition of each mixture, which was supplied in a 10 dm^3 aluminum cylinder, was verified before its delivery by gas chromatography analysis. Table 4.1. gives the mixtures compositions with estimated uncertainties together with the purity of the component gases and the gas cylinder pressure at room temperature, for each mixture of carbon dioxide with nitrogen presented here.

Table 4.1. Carbon dioxide / nitrogen mixtures compositions.

Cylinder number	Composition (x_{CO_2})	Specified purity of N_2 (x_{N_2})	Specified purity of CO_2 (x_{CO_2})	Pressure (bar)
02435	0.10009 ± 0.001	0.999995	0.99995	70
92380	0.15045 ± 0.001	0.999995	0.99995	95
02452	0.20004 ± 0.001	0.999997	0.99995	110
92313	0.500985 ± 0.0027	0.999997	0.99995	85

The mixtures were synthesized according to the gravimetric method for the preparation of calibration gas mixtures (ISO 6142:2001) (4), which is briefly described in the next subsection.

4.2.1. Preparation of gas mixtures

The binary mixtures of carbon dioxide with nitrogen measured in this work were prepared by means of a quantitative transference of pure nitrogen and pure carbon dioxide of high purity (parent gases) from the supply cylinders to the sample cylinder.

In this method, the quantity of gas added to the receiver cylinder is determined as the difference in weight of the cylinder before and after the addition of the gas. The mass determination is made by comparing the mass of a reference cylinder and the receiver cylinder with a mass comparator

Initially, the room temperature, pressure and humidity conditions are determined and are proved to be within a certain range. Before the beginning of the preparation process some considerations are made:

- The final pressure of the gas mixture cylinder must be under a safe range from the vapor pressure at -10ºC, in order to avoid the condensation of any of the components during the storage or the transportation of the mixture.
- The minimum accessible difference in mass must be higher than 20 g. If it is necessary a lower addition of gas, gas dilutions must be used as parent gases.
- Any incompatibility between the mixture components such as potential chemical reactions or inflammability must be avoided.

Preparation of the receiver cylinder

In the first place, the receiver cylinder is connected to a forced extraction system, which can heat the cylinders up to 70 ºC by means of heating jackets, shown in Figure 4.1., to evacuate all the gas contained. Afterwards the cylinder is connected to the vacuum net until the pressure inside the cylinder is less than 10^{-5} mbar.

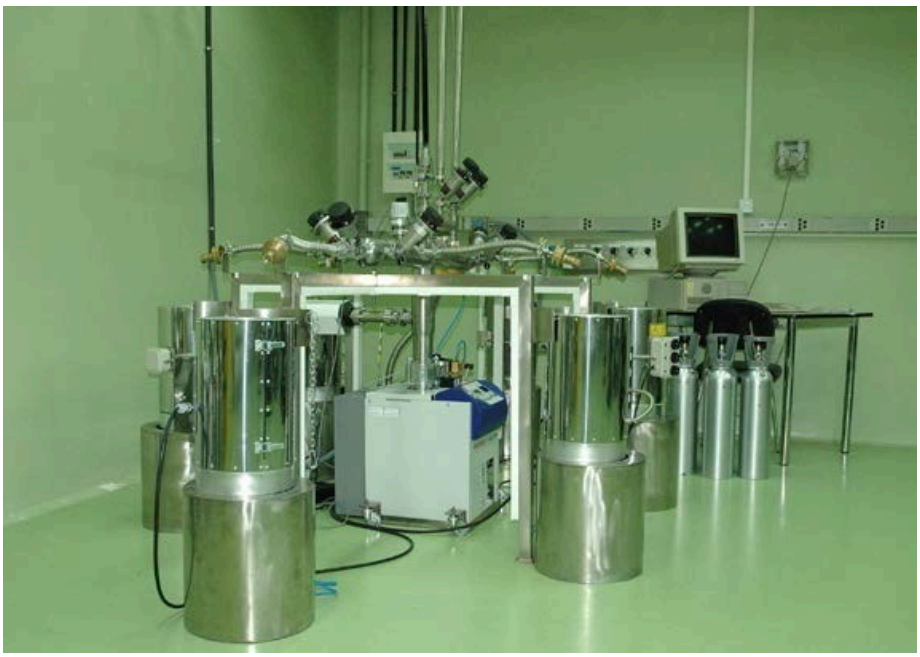

Figure 4.1. Vacuum system with heating jackets for seven cylinders at the Spanish national metrology institute (Centro Español de Metrología, CEM).

In the second place, the cylinder is filled with nitrogen in the circular filling ramp, where four additional cylinders can be filled simultaneously with the first one. All pipes of the installation are cleaned with nitrogen by filling them up to a pressure between

15 bar and 20 bar and evacuating them up to 10^{-2} mbar and repeating the process three times.

Figure 4.2. Circular filling ramp for five gas cylinders at the Spanish national metrology institute (Centro Español de Metrología, CEM).

Afterwards, the balance is tared and the cylinder is filled with nitrogen up to a pressure of 20 bar.

Injection of the mixture components in the cylinder

In a first step, the receiver cylinder is weighted with a mass comparator and type E calibration masses. The cylinder weight is compared against several calibrated masses until the measured difference in mass is within the range 1.000 g ± 0.005 g, so that the measurement is considered valid. After the weighting cycle the mass value is saved.

Next the filling pipelines are cleaned with the parent gas up to the cylinder connector by doing several fillings and evacuations in the circular filling ramp, depicted in Figure 4.2. The balance is tared again and the receiver cylinder, which must be placed in the balance, shown in Figure 4.3., is filled up to the required mass value is measured. The cylinder is closed and weighted again and all the filling pipelines are cleaned with nitrogen. For the addition of the rest of the mixture components the same process described in this paragraph is followed.

Figure 4.3. Accurate mass comparator used in the gravimetrical preparation of gas mixtures at the Spanish national metrology institute (Centro Español de Metrología, CEM), Madrid (Spain).

The mixture prepared contained in the cylinder is homogenized by placing it on a set of rollers, shown in Figure 4.4., and spinning it about the axis of the cylinder during 18 hours, with an inversion time of the cylinder of 300 seconds.

Figure 4.4. Homogenizer rollers for five cylinders at the Spanish national metrology institute (Centro Español de Metrología, CEM).

Finally the composition of the prepared mixture is checked by gas chromatography according to the ISO 6143:2001 (5) for gas analysis.

Gas stratification

The stratification of gases contained in the cylinder is a potential problem which can occur when working with gas mixtures. The stratification of the components of a gas mixture happens during the preparation of the mixture due to the difference in molar mass of each gas component or when the difference between the components densities is substantial (6). However, theoretically once a gas mixture is correctly homogenized, the stratification of the gas components can only take place when one or more components of the mixture partially condense when the partial pressure of the component reach its vapor pressure (7).

Nevertheless experience when working with gas mixtures proves that even when the gas mixture has been correctly homogenized after its preparation and no partial condensation has taken place, the mixture suffers significant stratification after a long period of time storage. Therefore, in order to avoid any deviation in the mixture composition from the calibration certificate of the mixture produced by the stratification of carbon dioxide, cylinders were again homogenized before their supply.

4.3. EXPERIMENTAL DATA AND COMPARISON WITH THE LITERATURE DATA

The number of isotherms performed for each mixture depended on the vapor pressure of each mixture in the temperature range (250 K – 400 K). All measurements were carried out in the gas phase of the mixture and far enough from saturation conditions to avoid the condensation of carbon dioxide in any of the colder parts of the densimeter or the pressure installation. Table 4.2. shows the isotherms measured for each of the mixtures presented in this Chapter.

Table 4.2. Isotherms measured for each of the mixtures of carbon dioxide with nitrogen.

Mixture	250 K	275 K	300 K	325 K	350 K	375 K	400 K
x_{CO_2} = 0.10							
x_{CO_2} = 0.15							
x_{CO_2} = 0.20							
x_{CO_2} = 0.50							

As mentioned in the Introduction Chapter of this thesis, the experimental density data concerning mixtures of carbon dioxide with nitrogen were compared with the densities calculated from the GERG-2004 equation of state (2), which is the current reference equation of state for natural gas and related mixtures.

The relative deviations of the experimental data reported in the Appendix from the densities calculated with the GERG-2004 equation of state were calculated as expressed in Eq. 4.1. as studied for all the isotherms performed as functions of pressure.

$$\Delta\rho = 10^2 \frac{\left(\rho_{\exp} - \rho_{EoS}\right)}{\rho_{EoS}} \qquad \text{Eq.4.1.}$$

Density experimental data of the (0.10 CO_2 + 0.90 N_2) mixture.

()Pressure, density and temperature experimental data measured for the mixture with carbon dioxide molar fraction x_{CO_2} = 0.10 are collected in Table A.1. (Appendix) together with their relative deviations from the densities calculated with the GERG-2004 equation of state. These relative deviations are depicted in Figure 4.5. for all isotherms versus pressure. The shaded area represents the estimated uncertainty of the equation of state (u_{EoS} = 0.10 %) when estimating densities of mixtures of nitrogen and carbon dioxide in the defined working range.

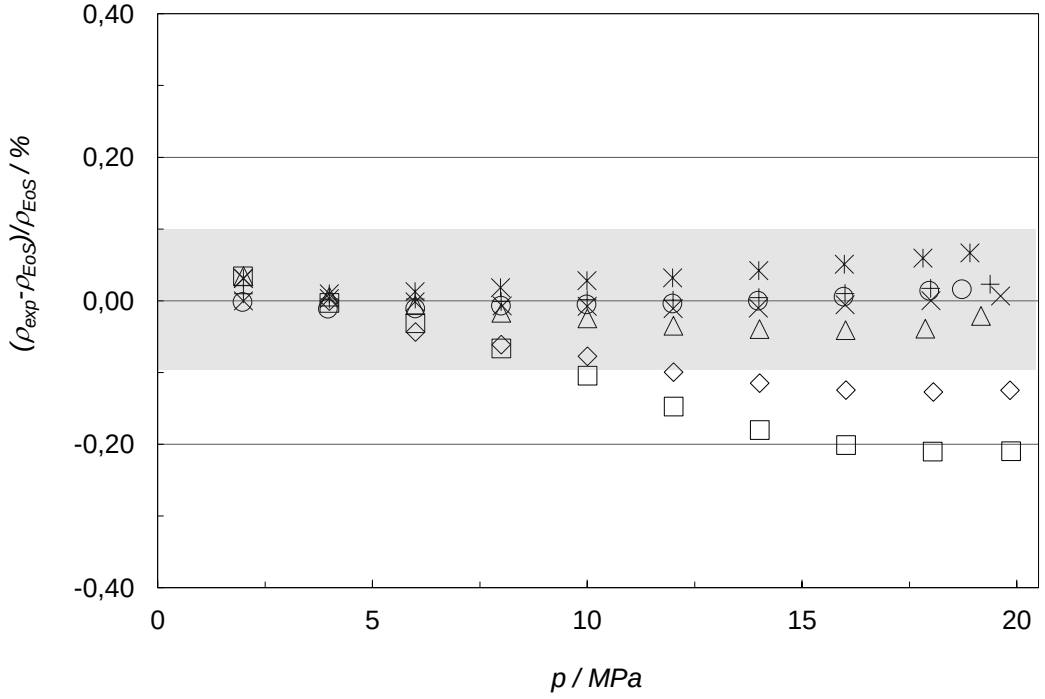

Figure 4.5. Relative deviations in density of experimental *(p, ρ, T)* data of the (0.10 CO_2 + 0.90 N_2) binary mixture from density values ρ_{EoS} calculated from the GERG-2004 equation of state (2) versus pressure: □ 250 K; ◇ 275 K; △ 300 K; × 325 K; + 350 K; ○ 375 K; ✳ 400 K.

As it can be observed, relative deviations for isotherms above 275 K are within the uncertainty percentage band of 0.1%, particularly at low pressures where relative deviations are lower than 0.05%. However, deviations reported for 250 K and 275 K exceed the expected uncertainty, reaching maximum negative deviations of 0.21% and 0.16%, respectively at 20 MPa.

Density experimental data of the (0.15 CO_2 + 0.85 N_2) mixture.

Experimental *(p, ρ, T)* data measured for the mixture with carbon dioxide molar fraction x_{CO_2} = 0.15 are collected in Table A.2. (Appendix) together with their relative deviations from the densities calculated with the GERG-2004 equation of state. Figure 4.6. shows the relative deviations of the experimental data versus pressure.

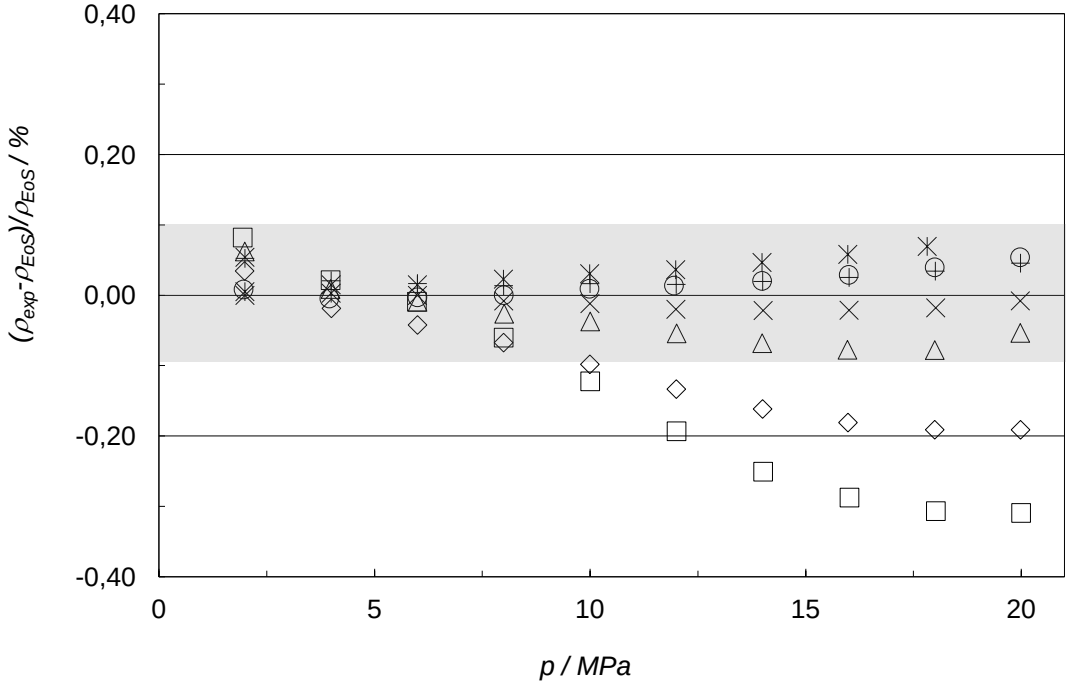

Figure 4.6. Relative deviations in density of experimental *(p, ρ, T)* data of the (0.15 CO_2 + 0.85 N_2) binary mixture from density values ρ_{EoS} calculated from the GERG-2004 equation of state (2) versus pressure: □ 250 K; ◇ 275 K; △ 300 K; × 325 K; + 350 K; ○ 375 K; ✳ 400 K.

Relative deviations in density plotted for the x_{CO_2} = 0.15 mixture show a similar behavior at high pressures and low temperatures to that observed for the first mixture. In this case, the relative deviations for the 250 K and 275 K isotherms reach negative values of 0.32% and 0.20% respectively. As it happened with the other mixture, the relative deviations at low pressures and also, at high pressures for temperatures above 275 K, are within the shaded area which represents the estimated uncertainty of the equation of state. While deviations in density at high temperatures were similar to the relative deviations obtained for the x_{CO_2} = 0.10 mixture, it can be seen that relative deviations at low temperatures, including at 300 K and 325 K, expanded to the negative direction.

Density experimental data of the (0.20 CO_2 + 0.80 N_2) mixture.

Table A.3. (Appendix) gives the experimental *(p, ρ, T)* data measured for the mixture with carbon dioxide molar fraction x_{CO_2} = 0.20 and the relative deviations in density from the values calculated with the GERG-2004 equation of state. Figure 4.7. shows these relative deviations of the experimental data versus pressure.

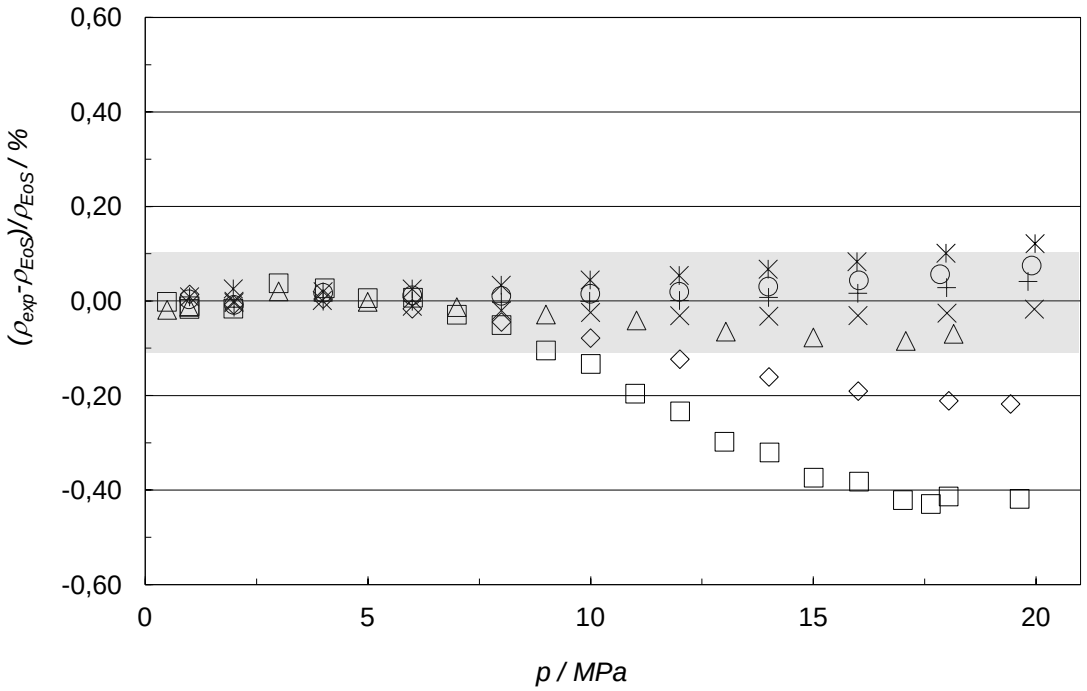

Figure 4.7. Percentage density deviations of experimental *(p, ρ, T)* data of {0.20 CO_2 + 0.80 N_2} binary mixture from density values ρ_{EoS} calculated from the GERG-2004 equation of state (2) versus pressure: □ 250 K; ◇ 275 K; △ 300 K; × 325 K; + 350 K; ○ 375 K; ✳ 400 K.

In this case, the relative deviations of the experimental data from the equation of state follow the same trend observed in the first mixtures. Deviations for the 250 K and 275 K isotherms reached negative values of 0.41% and 0.20%, respectively, at 20 Mpa. Only the experimental data below 10 MPa and the rest of the data at temperatures above 275 K agreed with the equation of state within a 0.1% band. As it was observed in the previous subsections, data at low pressures agree with the GERG model within less than 0.05% band.

Density experimental data of the (0.50 CO_2 + 0.50 N_2) mixture.

Experimental *(p, ρ, T)* data measured for the mixture with carbon dioxide molar fraction x_{CO_2} = 0.50 and their relative deviations from the densities calculated with the GERG-2004 equation of state are given in Table A.4. (Appendix). Figure 4.8. shows the relative deviations of the experimental data versus pressure.

As it was mentioned at the beginning of this Chapter, the 250 K isotherm was not carried out for this mixture in order to avoid the partial condensation of carbon dioxide in any of the parts of the single sinker densimeter.

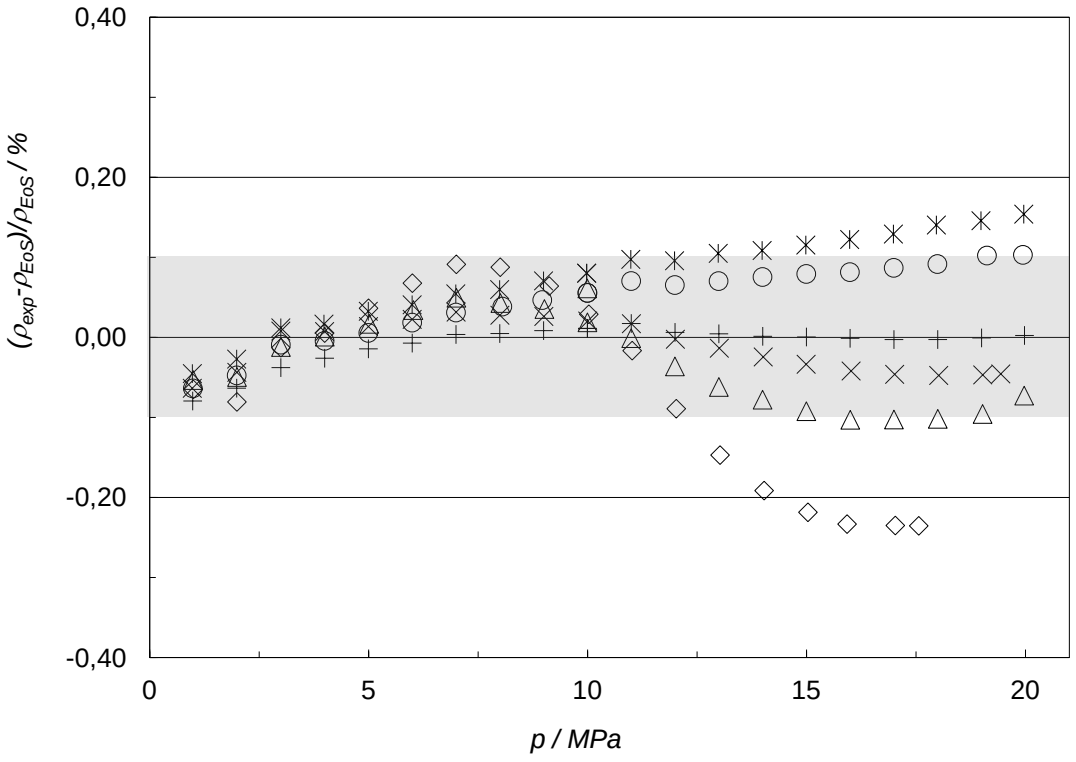

Figure 4.8. Percentage density deviations of experimental (p, ρ, T) data of {0.50 CO_2 + 0.50 N_2} binary mixture from density values ρ_{EoS} calculated from the GERG-2004 equation of state (2) versus pressure: ◇ 275 K; △ 300 K; × 325 K; + 350 K; ○ 375 K; ✳ 400 K.

Experimental densities are observed to deviate significantly at high pressures. In this case, isotherms at 275 K, 300 K and 400 K exceed the 0.1% band representing the uncertainty of the equation of state, at pressures above 13 MPa.

Despite experimental densities show here a more significant undulation with respect to the equation of state, the relative deviations at low pressures are still within the shaded area, concluding that the experimental data measured in this work agree the equation of state at pressures below 12 MPa.

Comparison of the experimental data with data from the literature

As indicated in the introduction of this Chapter, the thermophysical properties of binary mixtures of carbon dioxide with nitrogen have been studied by several authors during the 20th century.

In this subsection, the experimental density data reported in this thesis for mixtures of carbon dioxide with nitrogen are compared with experimental data reported by other authors for similar compositions in the same temperature and pressure range.

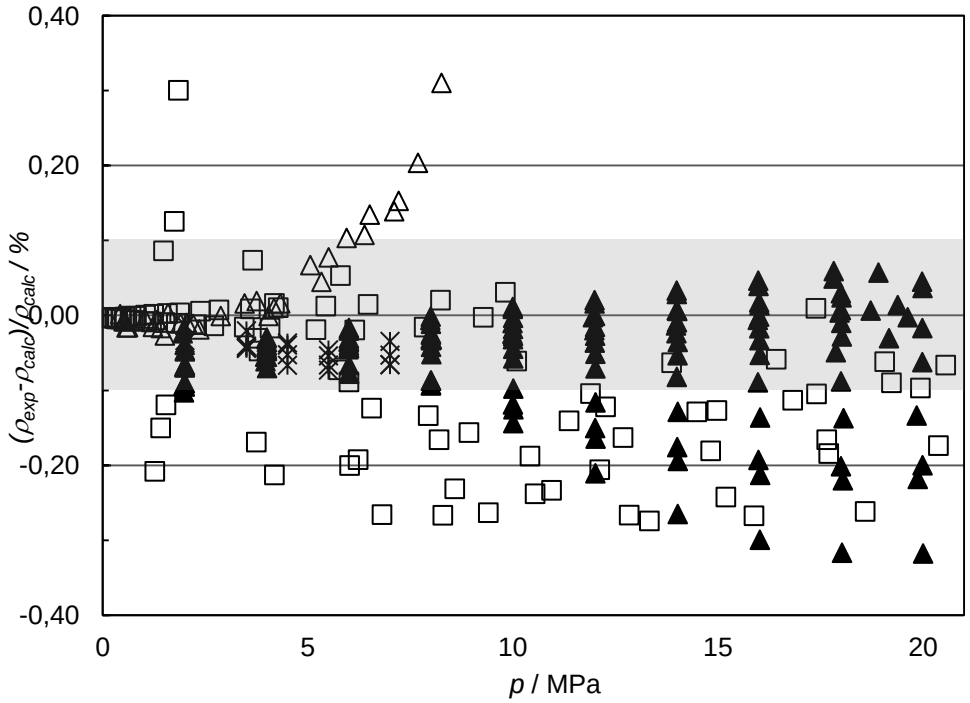

Figure 4.9. Percentage density deviations of experimental *(p, ρ, T)* data of CO_2 / N_2 binary mixtures from density values ρ_{EoS} calculated from the GERG-2004 equation of state (2) versus pressure, for CO_2 molar compositions between 0.10 and 0.18 in the temperature range (240 – 410) K and at pressures up to 20 MPa: ▲ this work; □ Brugge et al. (8, 9); △ Rivkin (10); ∗ Gaz de France (1).

Figure 4.9. shows the percentage deviations in density of experimental data from this work for x_{CO_2} = 0.10 and x_{CO_2} = 0.15 mixtures along with other density data sets with carbon dioxide molar composition in the range x_{CO_2} = (0.10 – 0.18), which were used to develop the binary departure functions for mixtures of carbon dioxide with nitrogen of the GERG equation of state.

It can be observed that the deviations reported in this thesis and represented here increase with the pressure and at low temperatures, reaching deviations in density higher than the estimated uncertainty of the equation of state. Densities measured by Brugge et al. (8) for a x_{CO_2} = 0.11 mixture show also negative relative deviations with values of the same order as those obtained in this work, except at low pressure where the scatter is also high. Experimental densities reported by Brugge et al. (9) (x_{CO_2} = 0.11), Gaz de France (1) (x_{CO_2} = 0.10) and Rivkin (10) (x_{CO_2} = 0.18) show a similar behavior to that observed in the data of this work at low pressures. However, the agreement of these data at pressures below 3 MPa is much better since the

uncertainty in density of the single sinker densimeter increases dramatically at very low pressures.

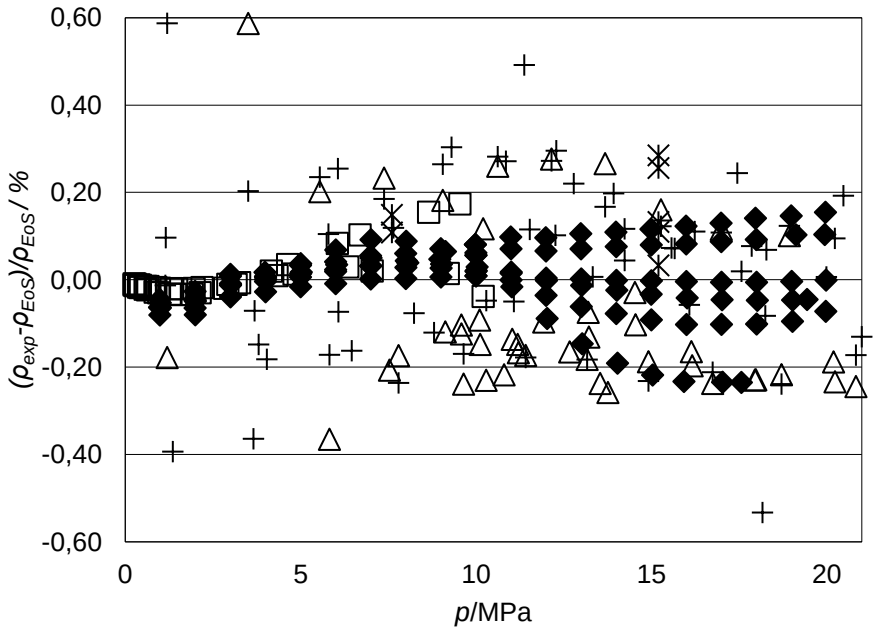

Figure 4.10. Percentage density deviations of experimental (p, ρ, T) data of CO_2 / N_2 binary mixtures from density values ρ_{EoS} calculated from the GERG-2004 equation of state versus pressure, for x_{CO_2} = 0.50 mixtures in the temperature range (250 – 400) K and at pressures up to 20 MPa: ◆ This work (x_{CO_2} = 0.50); ＋ Brugge *et al*. (8); □ Brugge *et al*. (9); △ Duarte-Garza *et al*. (11); ✳ Haney and Bliss (12)

Figure 4.10. depicts the relative deviations in density of the mixture x_{CO_2} = 0.50 mixture presented in this thesis, together with the deviations of the experimental data reported by other authors for the same composition (x_{CO_2} = 0.50) and in the same temperature and pressure range.

It can be noticed that there is a very good agreement between our data at low pressures and the density data measured by Brugge et al. (9), and also with the GERG model. However, at pressures between 5 MPa and 15 MPa the scatter of the data reported by Brugge et al. (8), Duarte-Garza et al. (11) and Haney and Bliss (12) is comparatively higher than that from our data. At high pressures all the data plotted in Figure 4.7. show significant deviations with the equation of state.

No comparison could be done for the x_{CO_2} = 0.20 mixture studied in this thesis since there are not available data for this composition in the temperature and pressure working range.

To complete this qualitative comparison, a statistical study was made to compare the data presented in this Chapter with that found in the references. Four statistical quantities, defined below, were calculated for each mixture dataset presented in this Chapter and for the datasets of the authors mentioned above.

Table 4.3. presents the results from the statistical analysis of the experimental data concerning the mixtures of carbon dioxide with nitrogen, were AAD is the average absolute deviations defined in Eq.4.2., Bias is the average deviation defined in Eq.4.3., RMS is the root mean squared defined in Eq.4.4. and MaxD refers to the maximum value of the relative deviations of the dataset. Here *n* is the number of density data of each dataset.

$$AAD = \frac{1}{n}\sum_{i=1}^{n}\left| 10^2 \frac{\rho_{i,\exp} - \rho_{i,EoS}}{\rho_{i,EoS}} \right| \qquad \text{Eq.4.2.}$$

$$Bias = \frac{1}{n}\sum_{i=1}^{n}\left(10^2 \frac{\rho_{i,\exp} - \rho_{i,EoS}}{\rho_{i,EoS}} \right) \qquad \text{Eq.4.3.}$$

$$RMS = \sqrt{\frac{1}{n}\sum_{i=1}^{n}\left(\frac{\rho_{i,\exp} - \rho_{i,EoS}}{\rho_{i,EoS}} \right)^2} \qquad \text{Eq.4.4.}$$

The same observations mentioned above can be here quantitatively seen.

Table 4.3. Statistical comparison of the density measurements of the experimental data plotted in Figure 3.

Source	Year	x_{CO_2}	*n*	10^2·AAD	10^2·Bias	10^2·RMS	10^2·MaxD
		x_{CO_2} = (0.10 – 0.18)					
This work	2011	0.10	69	0.0407	-0.0239	0.0670	0.2105
This work	2011	0.15	69	0.0601	-0.0310	0.0955	0.3102
Brugge et al. (9)	1989	0.11	38	0.0080	-0.0010	0.0100	0.0270
Brugge et al. (8)	1997	0.11	141	0.1550	-0.0060	0.1880	0.4620
Gaz de France (1)	1990	0.10	19	0.0460	-0.0460	0.0490	-0.0740
Rivkin (10)	1975	0.18	43	0.0610	0.0500	0.1040	0.3450
		x_{CO_2} = (0.50)					
This work	2011	0.50	122	0.056	0.003	0.076	-0.235
Brugge et al. (8)	1997	0.50	68	0.258	0.089	0.393	1.501
Brugge et al. (9)	1989	0.50	40	0.031	0.002	0.047	0.173
Duarte-Garza et al. (11)	1995	0.50	101	1.781	1.345	2.443	5.004
Haney and Bliss (12)	1944	0.50	11	0.931	2.039	1.137	1.694

Reproducibility and overall uncertainty of the experimental data

Before the measurement of each mixture studied in this Chapter, test measurements on nitrogen were carried out at selected temperatures and pressures covering the whole working range of the densimeter to ensure its correct operation. Results yielded by the test measurements showed always relative deviations in density of the experimental data from the reference equation of state for nitrogen of Span (13) were within a 0.02% percentage band, which is the estimated uncertainty of the equation for this temperature and pressure working range.

The measurement uncertainty of the density data presented in this thesis was evaluated in Chapter 3 for each state point magnitude (pressure, density and temperature). The overall uncertainty of the density data reported in this Chapter must include therefore the uncertainties of pressure and temperature, and also, the uncertainty of the mixtures compositions. Thus, the total uncertainty in density can be expressed as indicated in Eq.4.5.

$$u(\rho)=\left(u(\rho)^2+\left[\left(\frac{\partial\rho}{\partial p}\right)_{T,x}u(p)\right]^2+\left[\left(\frac{\partial\rho}{\partial T}\right)_{p,x}u(T)\right]^2+\left[\left(\frac{\partial\rho}{\partial x}\right)_{p,T}u(x)\right]^2\right)^{1/2} \quad \text{Eq.4.5.}$$

Eq.4.6. express the total uncertainty in density for the density data reported in this Chapter for mixtures of carbon dioxide with nitrogen, where the partial derivatives of Eq.4.5. were estimated with the GERG-2004 equation of state, uncertainties in pressure, density and temperature were taken from the uncertainty analysis in Chapter 3 and the uncertainty in composition was taken from Table 4.1.

$$u(\rho) = 10^{-4}\left(458 + 1.10\rho - 8.23p\right) \qquad \text{Eq.4.6.}$$

4.4. SECOND AND THIRD VIRIAL COEFFICIENTS

Experimental *(p, ρ, T)* data reported in this Chapter for mixtures of carbon dioxide with nitrogen were fitted to a second-order virial equation of state, with the form expressed in Eq.4.7.

$$\frac{Z-1}{\rho} = B_{mix} + C_{mix}\rho \qquad \text{Eq.4.7.}$$

Here, *Z* is the experimental compressibility factor, ρ is the experimental density, *B* and *C* are the second and third virial coefficients.

The fitted second and third virial coefficients B_{mix} and C_{mix} are listed in Table 4.4., together with the absolute deviations of each coefficient from the values calculated with the GERG-model. The uncertainties of both coefficients were calculated following the law of propagation of uncertainties (GUM) and the recommendation given by Higbie (14) for the calculus of the uncertainty of the slope of a linear regression. Uncertainties of the second virial coefficient were lower than 2.7 $cm^3 \cdot mol^{-1}$ and uncertainties of the third virial coefficient were lower than 45 $(m^3 \cdot mol^{-1})^2$.

Table 4.4. Second and third virial coefficients (B_{mix}, C_{mix}) fitted from experimental data and deviation of these values from the second virial coefficients from the GERG model, for mixtures of carbon dioxide with nitrogen.

T/K	B_{mix}/cm^3·mol^{-1}	C_{mix}/(cm^3·mol^{-1})^2	$\triangle B_{mix}$/cm^3·mol^{-1}	$\triangle C_{mix}$/(cm^3·mol^{-1})^2
		x_{CO_2} = 0.10		
250	-27,49	2036	-0,51	72
275	-19,25	1881	-0,44	141
300	-12,80	1774	-0,51	192
325	-7,44	1690	-0,50	223
350	-2,89	1604	-0,39	220
375	1,00	1523	-0,23	203
400	3,90	1531	-0,54	260
		x_{CO_2} = 0.15		
250	-33,43	2196	-0,61	-71
275	-24,11	1990	-0,36	23
300	-17,13	1886	-0,59	132
325	-11,25	1789	-0,61	189
350	-6,45	1720	-0,68	235
375	-1,96	1583	-0,30	184
400	1,53	1512	-0,31	179
		x_{CO_2} = 0.20		
250	-38,86	2272	0,11	-352
275	-29,03	2076	-0,12	-156
300	-20,69	1834	0,25	-122
325	-14,60	1786	-0,12	30
350	-9,25	1680	-0,12	72
375	-4,87	1615	-0,21	120
400	-1,31	1596	-0,48	188
		x_{CO_2} = 0.50		
275	-65,22	2994	1,64	-1695
300	-51,84	2629	1,12	-1219
325	-41,07	2337	0,91	-899
350	-32,10	2070	1,04	-713
375	-25,16	1916	0,70	-522
400	-19,38	1815	0,35	-354

Figure 4.11. and Figure 4.12. depict the absolute deviations of the second and third virial coefficients, respectively, from the values calculated with the GERG model. In both cases it can be observed that the virial coefficients of the x_{CO_2} = 0.50 mixture deviate significantly from the GERG model even at temperatures above 275 K. Major deviations occur at low temperatures.

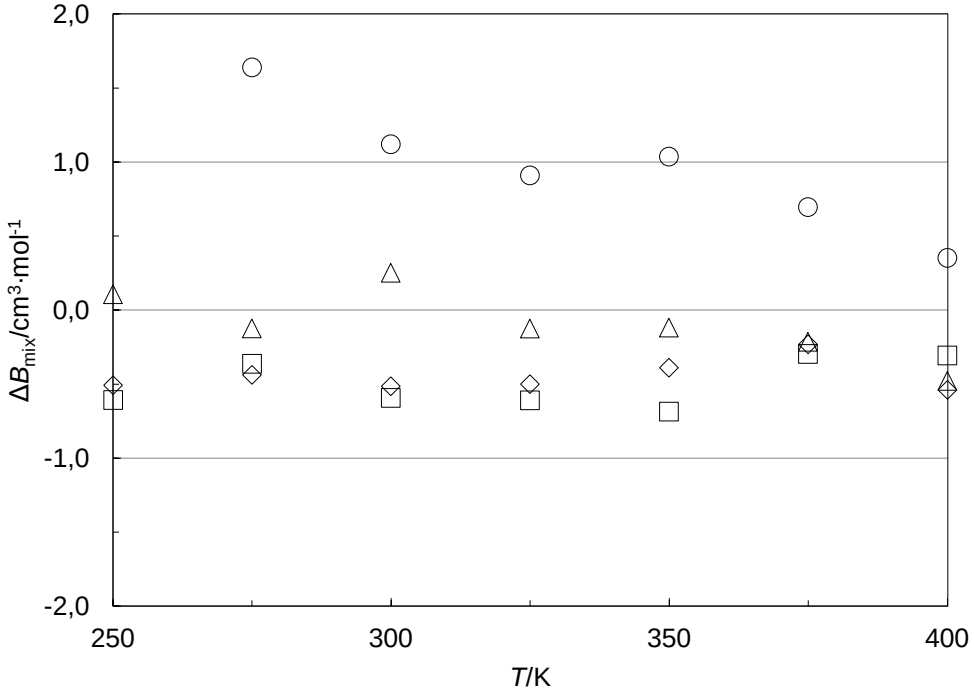

Figure 4.11. Deviations of the second virial coefficients (B_{mix}) from the values calculated with the GERG-2004 equation of state versus temperature: ◇ $x_{\mathrm{CO_2}}$ = 0.10; □ $x_{\mathrm{CO_2}}$ = 0.15; △ $x_{\mathrm{CO_2}}$ = 0.20; ○ $x_{\mathrm{CO_2}}$ = 0.50.

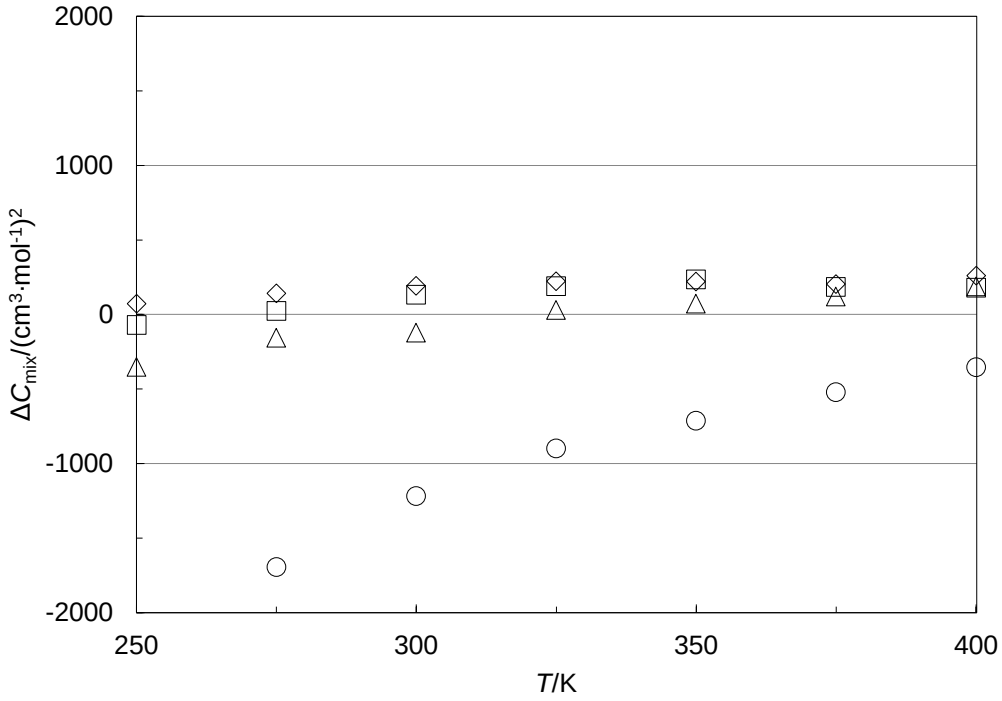

Figure 4.12. Deviations of the third virial coefficients (C_{mix}) from the values calculated with the GERG-2004 equation of state versus temperature: ◇ $x_{\mathrm{CO_2}}$ = 0.10; □ $x_{\mathrm{CO_2}}$ = 0.15; △ $x_{\mathrm{CO_2}}$ = 0.20; ○ $x_{\mathrm{CO_2}}$ = 0.50.

The second virial coefficient values for the x_{CO_2} = 0.50 mixture were compared with the values measured by Brugge et al. (9) and Cottrell et al. (15) and with the GERG-2004 equation of state in Figure 4.13. As can be observed, since the second virial coefficients for the x_{CO_2} = 0.50 mixture presented in this thesis show large deviations from the values calculated with the GERG model, they agree similar or better than that reported by the other authors represented in the figure.

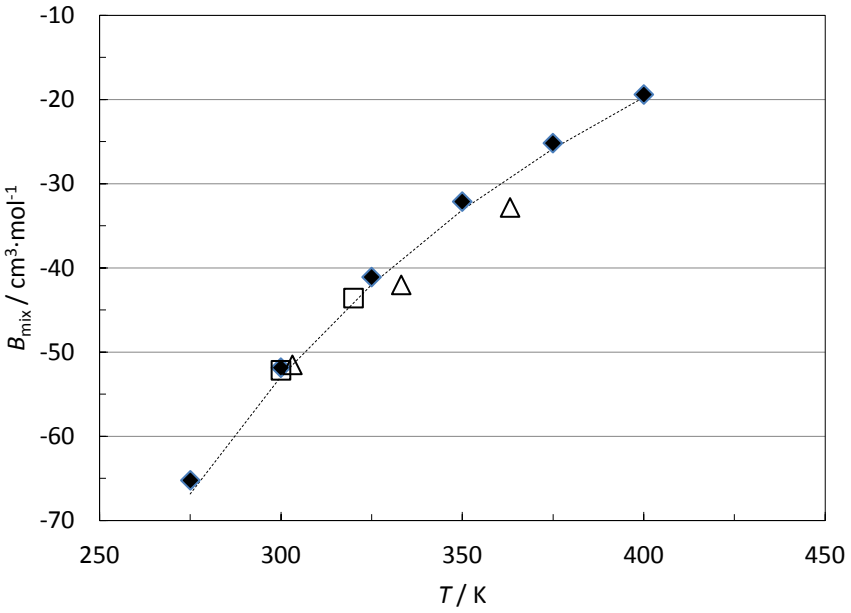

Figure 4.13. Second virial coefficients of a x_{CO_2} = (0.50) mixture. ◆ This work ; □ Brugge et al. ; △ Cottrell et al. ; --- GERG 2004 model.

4.5. DISCUSION ON DENSITY MEASUREMENT RESULTS

The new accurate *(p, ρ, T)* data for four mixtures of carbon dioxide with nitrogen with molar compositions x_{CO_2} = (0.10, 0.15, 0.20, 0.50) in the temperature range (250 – 400) K at pressures up to 20 MPa, presented in this Chapter, were compared with the reference equation of state GERG-2004 for natural gases and related mixtures, but also, with experimental data reported by other authors.

Relative deviations in density of the experimental data presented in this thesis from the equation of state showed an interesting behavior at low temperatures and high pressures. Since it was observed that the agreement of the density data at low pressures with the GERG model was within a 0.05% band (lower than the estimated

uncertainty of the equation for these mixtures in the working range), relative deviations at high pressures showed important and unexpected negative values for the 250 K and 275 K isotherms. These relative deviations were higher than the measurement uncertainty in density of the data, which implies that the observed deviations are significant enough to be taken into account.

When comparing the relative deviations plotted in Figures 4.3.-4.6. it is clear that the deviations of the experimental data increase in the negative y-axis direction with the carbon dioxide molar fraction. Moreover, it was observed that deviations of the experimental densities at 400 K for the mixture with highest molar composition of carbon dioxide were also higher than the estimated uncertainty of the equation.

These deviations from the equation of state at high pressures are not only observed in our data but also in the experimental densities reported by other authors. Thus, it can be concluded that the GERG-2004 equation of state shows slight deviations from the real behavior of mixtures of carbon dioxide with nitrogen in the estimation of densities.

Second and third virial coefficients fitted to the data presented here showed similar behaviors than that commented above. In the case of the x_{CO_2} = 0.50 mixture, the values of the virial coefficients differ significantly from that calculated with the GERG model.

REFERENCES

1. JAESCHKE, M. et al. *The GERG Databank of High Accuracy Compressibility Factor Measurements, GERG Technical Monograph*, 1997.

2. KUNZ, O. et al. The GERG-2004 Wide-Range Reference Equation of State for Natural Gases and Other Mixtures*. GERG Technical Monograph Fortschr*, 2007.

3. ICHIKURA, K.; KANO, Y. and SATO, H. Importance of Third Virial Coefficients for Representing the Gaseous Phase Based on Measuring PVT-Properties of 1,1,1-Trifluoroethane (R143a)*. International Journal of Thermophysics*, 2006, vol. 27, no. 1. pp. 23-38.

4. ISO 6142:2001, Gas Analysis-Preparation of Calibration Gas Mixtures-Gravimetric Methods*. Gas Analysis - Preparation of Calibration Gas Mixtures - Gravimetric Method*, 2001.

5. GUENTHER, F.R. and POSSOLO, A. Calibration and Uncertainty Assessment for Certified Reference Gas Mixtures*. Analytical and Bioanalytical Chemistry*, 2011, vol. 399, no. 1. pp. 489-500.

6. ISO 6142:2011 - *Preparation of Calibration Gas Mixtures - Gravimetric Method.* ISO draft.

7. SCORNAVACCA, F. and CARLUCCI, P. *Gas Mixtures - Facts and Fables - A Manual for the Gas Mixture User.* NJ (USA), 1978.

8. BRUGGE, H.B. et al. Densities of Carbon Dioxide + Nitrogen from 225 K to 450 K at Pressures Up to 70 MPa*. Journal of Chemical and Engineering Data*, 1997, vol. 42, no. 5. pp. 903-907.

9. BRUGGE, H.B. et al. Experimental Cross Virial Coefficients for Binary Mixtures of Carbon Dioxide with Nitrogen, Methane and Ethane at 300 and 320 K*. Physica A: Statistical Mechanics and its Applications*, 1989, vol. 156, no. 1. pp. 382-416.

10. Rivkin S.L. *Experimental Study of the Compressibility of Gases: Mixtures of Nitrogen and Carbon Dioxide*, 1975.

11. Duarte-Garza H. et al. Thermodynamic Properties of CO2 + N2 Mixtures. *Gas Processors Association / Gas Research Institute*, 1995.

12. HANEY, R.E.D. and BLISS, H. Compressibilities of Nitrogen - Carbon Dioxide Mixtures. *Ind. Eng. Chem.*, 1944, vol. 36, no. 11. pp. 985-989.

13. SPAN, R. et al. A Reference Equation of State for the Thermodynamic Properties of Nitrogen for Temperatures from 63.151 to 1000 K and Pressures to 2200 MPa. *Journal of Physical and Chemical Reference Data*, 2000, vol. 29, no. 6. pp. 1361-1401.

14. HIGBIE, J. Uncertainty in the Linear Regression Slope. *Am. J. Phys.*, 1991, vol. 59, no. 2. pp. 184-185.

15. COTTRELL, T.L.; HAMILTON, R.A. and TAUBINGER, R.P. The Second Virial Coefficients of Gases and Mixtures: Part 2. - Mixtures of Carbon Dioxide with Nitrogen, Oxygen, Carbon Monoxide, Argon and Hydrogen. *Transactions of the Faraday Society*, 1956, vol. 52. pp. 1310-1312.

CHAPTER 5

MEASUREMENTS OF MIXTURES OF NITROGEN AND CARBON MONOXIDE

5.1. INTRODUCTION

The importance of the study of mixtures containing nitrogen and carbon monoxide lies, not only in their relation with the exploitation of new gaseous biofuels, but also in the significant lack of (p, ρ, T) data for these binary mixtures.

Mixtures containing significant quantities of carbon monoxide and nitrogen are present whether as gaseous by-products in exhaust gases from coke ovens and blast furnaces as products from biomass pyrolysis and gasification. These fuel gases are currently under research by several projects, such as Marcogaz (1) and BONGO (2), since they are intended to be used independently or by injecting them into the existing natural gas networks, in order to contribute to the development of a more sustainable energy model. Another joint research project ENG01 GAS (3) is currently run for the characterization of energy gases with the aim of enabling the injection of alternative fuel gases into the natural gas-grids.

The extensive data base of thermodynamic properties of gas mixtures listed in (4, 5) has only 343 (p, ρ, T) data available concerning mixtures of carbon monoxide and nitrogen in the temperature range (273 – 353) K and pressures up to 30.1 MPa, for a single carbon monoxide molar fraction of x_{CO} = (0.03). These data were used for the fitting of the mixture parameters of the GERG-2004 equation of state for mixtures of carbon monoxide and nitrogen. This fact shows the important scarcity of density data, in contrast with the great importance and relevance of these binary mixtures. Thus, any contribution with new experimental data of thermophysical properties is of great importance, both for the improvement, if necessary, of the mixture parameters and for the test of the estimation capability of the equation of state.

In this Chapter a set of 223 density measurements for mixtures of nitrogen with carbon monoxide with molar compositions x_{CO} = (0.05, 0.10) in the gas phase at temperatures between (250 – 400) K and pressures up to 20 MPa are presented. Experimental density data are compared with the densities calculated from the GERG-2004 model (5). Second and third virial coefficients were also fitted for these mixtures, due to their interest for some properties estimation models.

5.2. GRAVIMETICAL PREPARATION OF THE MIXTURES

Mixtures of carbon monoxide with nitrogen were synthesized gravimetrically by the Reference Materials Laboratory of the Spanish national metrology institute (Centro Español de Metrología, CEM) following the same methodology used to prepare the mixtures of carbon dioxide with nitrogen, described in Chapter 4.

The final compositions of both mixtures were also verified by gas chromatography analysis. Each mixture was supplied in a 10 dm^3 aluminum cylinder. Mixture compositions and estimated uncertainties, together with the purity of the component gases and the gas cylinder pressure at room temperature, are given in Table 5.1.

Table 5.1. Carbon monoxide / nitrogen mixtures compositions.

Cylinder number	Composition (x_{CO})	Specified purity of N_2 (x_{N_2})	Specified purity of CO (x_{CO})	Pressure (bar)
92337	0.04999 ± 0.001	0.999995	0.999985	80
01163	0.10018 ± 0.002	0.999995	0.9997	90

All measurements were carried out in the gas phase of the mixture. Since there was no possibility of a partial condensation of carbon monoxide, the isotherms performed covered the whole temperature and pressure range of the apparatus.

Safety conditioning of the laboratory

Due to the high toxicity of carbon monoxide and to the high content of carbon monoxide of the mixtures studied as compared to the risk concentration, several modifications were performed in our laboratory to avoid any risk coming from accidental gas leaks from the densimeter or the gas cylinders.

1. In the first place an air ventilation system was installed. One ventilation grill was placed close to the floor for those gases with higher molar weight than the air and three ventilation grills were placed at the top of the room, for the gases with lower molar weight than the air. Exhaust gases were conducted to the roof of the building, far from any human presence. The extraction pump was proved against flammable gases.

2. In the second place, the gas exhaust from the measuring cell of the single sinker densimeter was directed by means of a flexible tube to the outside of the building, independently of the exit of the air extraction system.
3. Finally, a carbon monoxide personal detector was used during all the measurements with mixtures containing carbon monoxide.

5.3. EXPERIMENTAL DATA AND COMPARISON WITH THE LITERATURE DATA

Experimental density data concerning mixtures of carbon monoxide with nitrogen presented in this Chapter were also compared with the values calculated with the GERG-2004 equation of state (5). Relative deviations, calculated as indicated in Eq.4.1. were also reported for these mixtures and studied as functions of pressure.

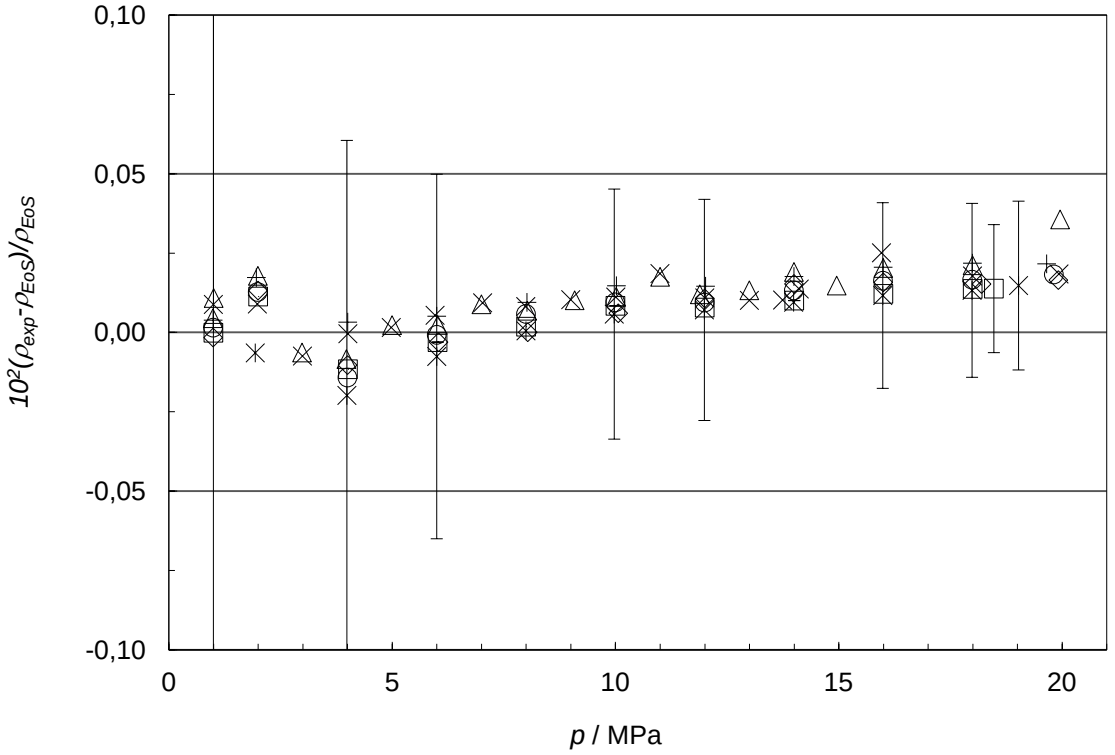

Figure 5.1. Percentage density deviations of experimental (p, ρ, T) data of (0.05 CO + 0.95 N_2) binary mixture from density values ρ_{EoS} calculated from the GERG-2004 equation of state (5) versus pressure: □ 250 K; ◇ 275 K; △ 300 K; × 325 K; + 350 K; ○ 375 K; ✳ 400 K. The error bars represent expanded uncertainties in density (k=2) of the experimental data.

Density experimental data of the (0.05 CO + 0.95 N_2) mixture.

Experimental *(p, ρ, T)* data measured for the mixture with carbon monoxide molar fraction x_{CO} = 0.05 are collected in Table B.1. (Appendix) together with their relative deviations from the densities calculated with the GERG-2004 equation of state. Figure 5.1. shows the relative deviations of the experimental data versus pressure.

The estimated uncertainty in density of the GERG equation of state for mixtures of carbon monoxide with nitrogen is 0.01%, which in this case agrees with the y-axis limits of Figure 5.1. It can be seen that all relative deviations in density of the experimental data agree the GERG model within less than a 0.05% band, since the maximum deviation of 0.036% occurs at 300 K and 20 MPa. Error bars represent the expanded uncertainty in density (*k*=2) of the experimental data.

Density experimental data of the (0.10 CO + 0.90 N_2) mixture.

Pressure, density and temperature experimental data measured for the x_{CO} = 0.10 mixture are collected in Table B.2. (Appendix) together with their relative deviations from the densities calculated with the GERG-2004 equation of state (5). These relative deviations are depicted in Figure 5.2. for all isotherms versus pressure.

Densities for this mixture show also a very good agreement with the equation of state since all relative deviations depicted in Figure 5.2. are within a 0.05% band, which is lower than the estimated uncertainty of the equation (0.1%). Almost all experimental densities show positive deviations with a maximum value of 0.04% at 375 K. Error bars represent the expanded uncertainty in density (*k*=2) of the experimental data.

Comparison of the experimental data with the data from the references

As mentioned in the introduction of this Chapter, the thermophysical properties of binary mixtures of carbon monoxide with nitrogen have been seldom studied. In fact, only Jaeschke et al. (4) reported density data for a mixture with a carbon monoxide molar fraction of x_{CO} = 0.03.

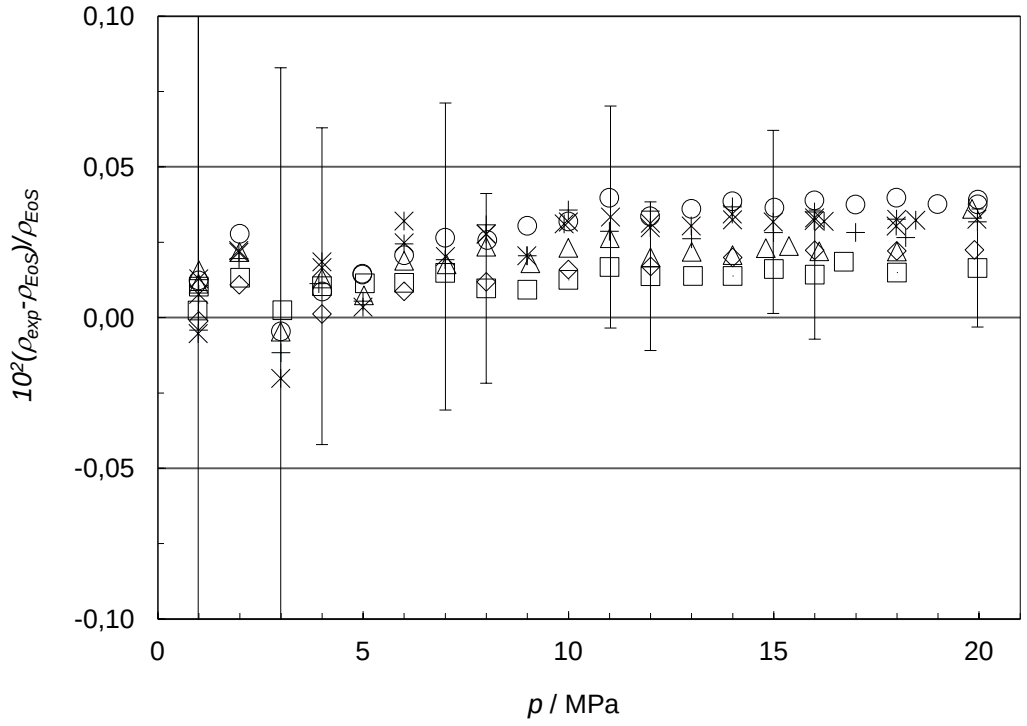

Figure 5.2. Percentage density deviations of experimental (p, ρ, T) data of (0.10 CO + 0.90 N_2) binary mixture from density values ρ_{EoS} calculated from the GERG-2004 equation of state (5) versus pressure: □ 250 K; ◇ 275 K; △ 300 K; × 325 K; + 350 K; ○ 375 K; ✳ 400 K. The error bars represent expanded uncertainties in density (k=2) of the experimental data.

Figure 5.3. depicts relative deviations from the GERG model of the experimental data presented in this Chapter and the experimental densities published by Jaeschke et al (4) measured with two different methodologies: a Burnett apparatus and an optical interferometer.

In this Figure the deviations of mixtures with different compositions are represented for comparison of the data as functions of the carbon monoxide molar fraction. While the data reported for the x_{CO} = (0.05, 0.10) mixtures and the data measured with the Burnett apparatus show positive deviations, data obtained with the optical interferometer show negative deviations from the equation of state. In principle a slight increase in the relative deviations at high pressures with the carbon monoxide content can be observed. However, since the uncertainty in density of the experimental values is much larger than these deviations, a relation between the agreement of the data with the equation and the mixture composition cannot be concluded.

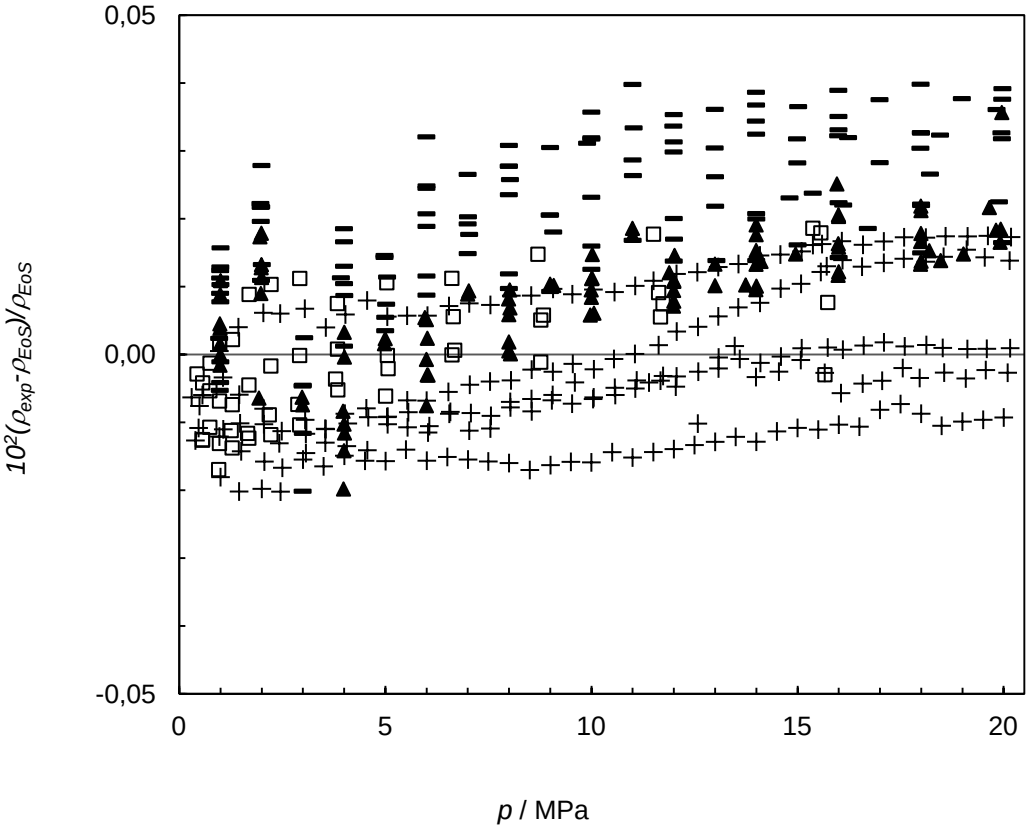

Figure 5.3. Percentage density deviations of experimental (p, ρ, T) data of CO / N_2 binary mixtures from density values ρ_{EoS} calculated from the GERG-2008 equation of state versus pressure, for CO molar compositions between 0.03 and 0.10 in the temperature range (250 – 400) K and pressures up to 20 MPa: ▲ This work (x_{CO} = 0.05); ▬ This work (x_{CO} = 0.10); □ Jaeschke *et al*. (Burnett apparatus) (4); + Jaeschke *et al*. (Optical interferometer) (4) (x_{CO} = 0.03).

Table 5.2. presents the results from the statistical analysis of the experimental data concerning mixtures of carbon monoxide with nitrogen depicted in Figure 5.3. Here AAD is the average absolute deviations defined in Eq.4.2., RMS is the root mean squared defined in Eq.4.4. and MaxD refers to the maximum value of the relative deviations of the dataset and n is the number of density data of each dataset.

Table 5.2. Statistical comparison of the experimental density measurements plotted in Figure 3 with respect to the GERG model.

Source	Year	Experimental technique	x_{CO}	n	10^2·AAD	10^2·RMS	10^2·MaxD
Jaeschke et al. (4)	1997	Burnett apparatus	0.03	56	0.009	0.012	-0.052
Jaeschke et al. (4)	1997	Optical interferometer	0.03	287	0.009	0.011	-0.023
This thesis	2011	Single sinker densimeter	0.05	99	0.011	0.014	0.036
This thesis	2011	Single sinker densimeter	0.10	125	0.022	0.024	0.040

Reproducibility and overall uncertainty of the experimental data

As mentioned in the previous Chapter, test density measurements with nitrogen were carried out before the measurement of each mixture of carbon monoxide with nitrogen. The test measurements consisted in the measurement of the two limit isotherms (250 K and 400 K) over the whole pressure range of the apparatus. Density results showed relative deviations from the densities calculated with the equation of state for nitrogen of Span (6) lower than the estimated uncertainty of this equation in the working temperature and pressure range.

The overall uncertainty of the data presented in this Chapter was also estimated by taking into account the contributions to the uncertainty in density coming from the uncertainties in temperature, pressure and composition, as indicated in Eq.4.5. The partial derivatives of Eq.4.5. were also estimated by using the GERG model for mixtures of carbon monoxide with nitrogen. Eq.5.1. gives the expression of the total uncertainty in density for the density data concerning mixtures of carbon monoxide with nitrogen.

$$u(\rho) = 10^{-4}\left(545 + 1.10\rho - 8.23p\right) \qquad \text{Eq.5.1.}$$

5.4. SECOND AND THIRD VIRIAL COEFFICIENTS

Second and third virial coefficients were fitted for both mixtures of carbon monoxide and nitrogen from the experimental density data reported in this Chapter, by using Eq.4.7.

Table 5.3. lists the fitted virial coefficients together with the absolute deviations of each coefficient from the values calculated with the GERG-model. Uncertainties of the fitted values were estimated following the law of propagation of uncertainties (GUM) and the recommendation given by Higbie (7) for the calculus of the uncertainty of the slope of a linear regression, resulting in $u(B_{\mathrm{mix}})$ < 0.30 $cm^3 \cdot mol^{-1}$ and $u(C_{\mathrm{mix}})$ < 91 $(cm^3 \cdot mol^{-1})^2$. The deviations of the fitted virial coefficients of both mixtures were plotted against temperature in Figure 5.4.

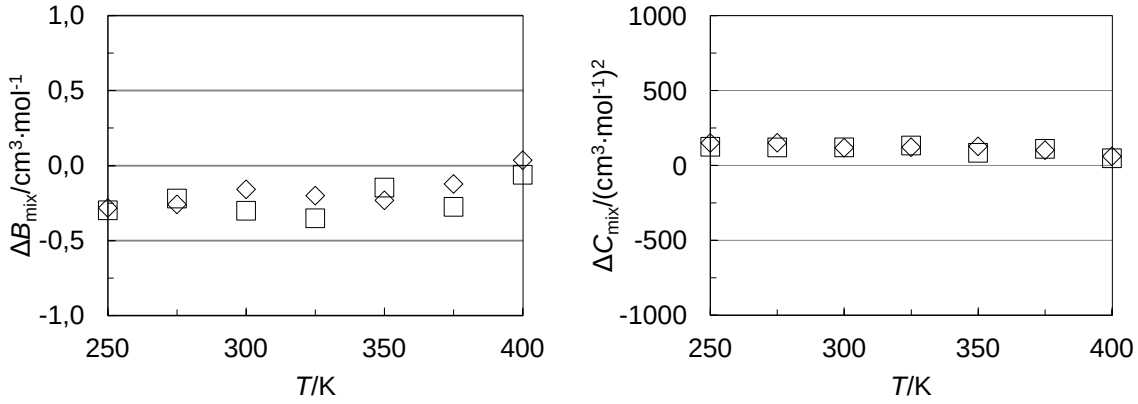

Figure 5.4. Percentage density deviations of experimental (p, ρ, T) data of CO / N_2 binary mixtures from density values ρ_{EoS} calculated from the GERG-2008 equation of state versus pressure, for CO molar compositions between 0.03 and 0.10 in the temperature range (250 – 400) K and pressures up to 20

Absolute deviations were found to be lower than 0.40 $cm^3 \cdot mol^{-1}$ for the second virial coefficient and less than 160 $(cm^3 \cdot mol^{-1})^2$ for the third virial coefficient, which confirmed the good agreement of the experimental data with the GERG model observed above.

Table 5.3. Second and third virial coefficients (B_{mix}, C_{mix}) fitted from experimental data and deviations of these values from the second and third virial coefficients from the GERG model, for mixtures of carbon monoxide with nitrogen.

T/K	B_{mix}/$cm^3 \cdot mol^{-1}$	C_{mix}/$(cm^3 \cdot mol^{-1})^2$	$\triangle B_{mix}$/$cm^3 \cdot mol^{-1}$	$\triangle C_{mix}$/$(cm^3 \cdot mol^{-1})^2$
		x_{CO} = 0.05		
250	-16.95	1763	-0.28	152
275	-10.30	1667	-0.26	153
300	-4.86	1564	-0.16	119
325	-0.52	1517	-0.20	123
350	3.10	1485	-0.23	129
375	6.29	1430	-0.12	103
400	9.08	1366	0.04	62
		x_{CO} = 0.10		
250	-17.19	1778	-0.30	126
275	-10.45	1673	-0.22	122
300	-5.16	1601	-0.30	122
325	-0.80	1559	-0.35	135
350	3.08	1469	-0.15	86
375	6.06	1464	-0.27	112
400	8.92	1375	-0.06	50

5.5. DISCUSION ON DENSITY MEASUREMENT RESULTS

As part of this thesis new accurate *(p, ρ, T)* data for two mixtures of carbon monoxide with nitrogen with molar compositions x_{CO} = (0.05, 0.10) in the temperature range (250 – 400) K at pressures up to 20 MPa were presented. The experimental density data were compared with the densities calculated from the GERG-2004 equation of state and also with the data reported by Jaeschke et al. (4) for a single mixture with molar composition of x_{CO} = 0.03.

The relative deviations in density of the experimental data measured for the two mixtures presented in this Chapter showed an exceptionally good agreement with the GERG-2004 equation of state. All deviations were within a 0.05% band while the estimated uncertainty of the GERG model for these mixtures is 0.10%. The uncertainty in density of the experimental data was estimated to be much higher than the deviations observed, so that the effectiveness of the GERG mixture model can be here concluded.

There was no available density data for comparison with the experimental data reported in this work, since the only *(p, ρ, T)* data for mixtures of carbon monoxide with nitrogen of the data bank were corresponded to a carbon monoxide molar fraction of x_{CO} = 0.03. However, all experimental data were compared together graphically and statistically, in order to analyze any relation between the relative deviations in density and the mixture composition, as observed before for the mixtures of carbon dioxide with nitrogen. Results yielded that the deviations seemed to increase with the carbon monoxide molar fraction. However, due to the high uncertainty of the data compared to the value of the deviations, no conclusion could be made.

Second and third virial coefficients fitted to the data presented showed also a good agreement with the coefficient values calculated from the GERG model.

REFERENCES

1. Marcogaz. *Final Recommendation - Injection of Gases from Non-Conventional Sources into Gas Networks*, 2006.

2. FLORRISSON, O. and PINCHBECK, D. *Biogas and Others in Natural Gas Operations (BONGO): A Project Under Development.* Burgel ed. 23 rd World Gas Conference, 2006.

3. HALOUA, F. et al. *Caloric Quantities and Density Measurement of Non-Conventional Gases,* 2011.

4. JAESCHKE, M. et al. *The GERG Databank of High Accuracy Compressibility Factor Measurements, GERG Technical Monograph*, 1997.

5. KUNZ, O. et al. The GERG-2004 Wide-Range Reference Equation of State for Natural Gases and Other Mixtures*. GERG Technical Monograph Fortschr*, 2007.

6. SPAN, R. et al. A Reference Equation of State for the Thermodynamic Properties of Nitrogen for Temperatures from 63.151 to 1000 K and Pressures to 2200 MPa*. Journal of Physical and Chemical Reference Data*, 2000, vol. 29, no. 6. pp. 1361-1401.

7. HIGBIE, J. Uncertainty in the Linear Regression Slope*. Am. J. Phys.*, 1991, vol. 59, no. 2. pp. 184-185.

CHAPTER 6

MEASUREMENT OF A MIXTURE OF METHANE AND CARBON DIOXIDE

6.1. INTRODUCTION

Mixtures containing methane and carbon dioxide are one of the gas binary mixtures of which most data of thermophysical properties are available, after mixtures of methane with nitrogen and ethane, due to their interest in the natural gas industry. Available (p, ρ, T) data for these mixtures, according to the GERG data bank (1), are of 3581 (about 7% of the total density data available for binary mixtures) of which less than a half were used in the fitting of the mixture parameters of the GERG equation of state for these mixtures. Therefore, despite the apparently extensive density data sets concerning mixtures of carbon dioxide with methane, the low use of the available data in the development of the GERG model reveals an important lack of reliability and accuracy of many of the measured data.

The used density data listed in (1, 2) concerning mixtures of carbon dioxide with methane cover a temperature range of (225 – 478) K and pressures up to 69.5 MPa, for carbon dioxide molar fraction in the range x_{CO_2} = (0.08 – 0.90). However, few data are available for mixtures with a carbon dioxide content of x_{CO_2} = 0.20.

In this Chapter a set of 138 density measurements for a mixture of methane with carbon dioxide with molar composition x_{CO_2} = (0.20) in the gas phase at temperatures between (250 and 400) K and pressures up to 20 MPa are presented. Experimental density data are compared with the densities calculated from the GERG-2004 model (2).

The density data measured here are part of the joint research project ENG01 GAS (3), supported by EURAMET and the European Commission, included in the program Energy (2009). This project includes the measurement of caloric quantities and density of non-conventional fuel gases for the characterization of energy gases which could be injected in the existing natural gas grids.

6.2. GRAVIMETICAL PREPARATION OF THE MIXTURE

The mixture of carbon dioxide with methane was prepared gravimetrically by the Reference Materials Laboratory of the Spanish national metrology institute (Centro

Español de Metrología, CEM) following the same methodology used to prepare the mixtures of carbon dioxide with nitrogen, described in Chapter 4.

The final composition of the mixture was verified by gas chromatography analysis. Each mixture was supplied in a 10 dm^3 aluminum cylinder. The composition of the mixture and its estimated uncertainty, together with the purity of the component gases and the gas cylinder pressure at room temperature, are given in Table 6.1.

Table 6.1. Carbon dioxide / methane mixture composition.

Cylinder number	Composition (x_{CO_2})	Specified purity of CH_4 (x_{CH_4})	Specified purity of CO_2 (x_{CO_2})	Pressure (bar)
92305	0.199778 ± 0.0025	0.999995	0.99995	100

All measurements were carried out in the gas phase. The presence of carbon dioxide implied the possibility of a partial condensation of this component in any of the parts of the densimeter or the pressure pipelines, at low temperatures and high pressures. However the saturation curve of the mixture, which was estimated with the GERG model, was far enough from the temperature and pressure working ranges. Therefore seven isotherms between (250 K and 400 K) were performed over the whole pressure range.

Safety conditioning of the laboratory

Although the presence of methane in the mixtures studied in this Chapter, makes them to be considered as inflammable mixtures, no additional precautions were taken apart from the air extraction system installed before carrying out measurements with carbon monoxide.

6.3. EXPERIMENTAL DATA AND COMPARISON WITH THE LITERATURE DATA

Experimental density data concerning the mixtures of carbon dioxide with methane presented in this Chapter were compared with the density values calculated with the GERG-2004 equation of state (2). Relative deviations, obtained as indicated in Eq.4.1. were also reported for these mixtures and studied as functions of pressure.

Density experimental data of the (0.20 CO_2 + 0.80 CH_4) mixture.

Experimental *(p, ρ, T)* data measured for the mixture with carbon dioxide molar fraction x_{CO_2} = 0.20 are collected in Table C.1. (Appendix) together with their relative deviations from the densities calculated with the GERG-2004 equation of state. The relative deviations of the experimental data versus pressure are depicted in Figure 6.1.

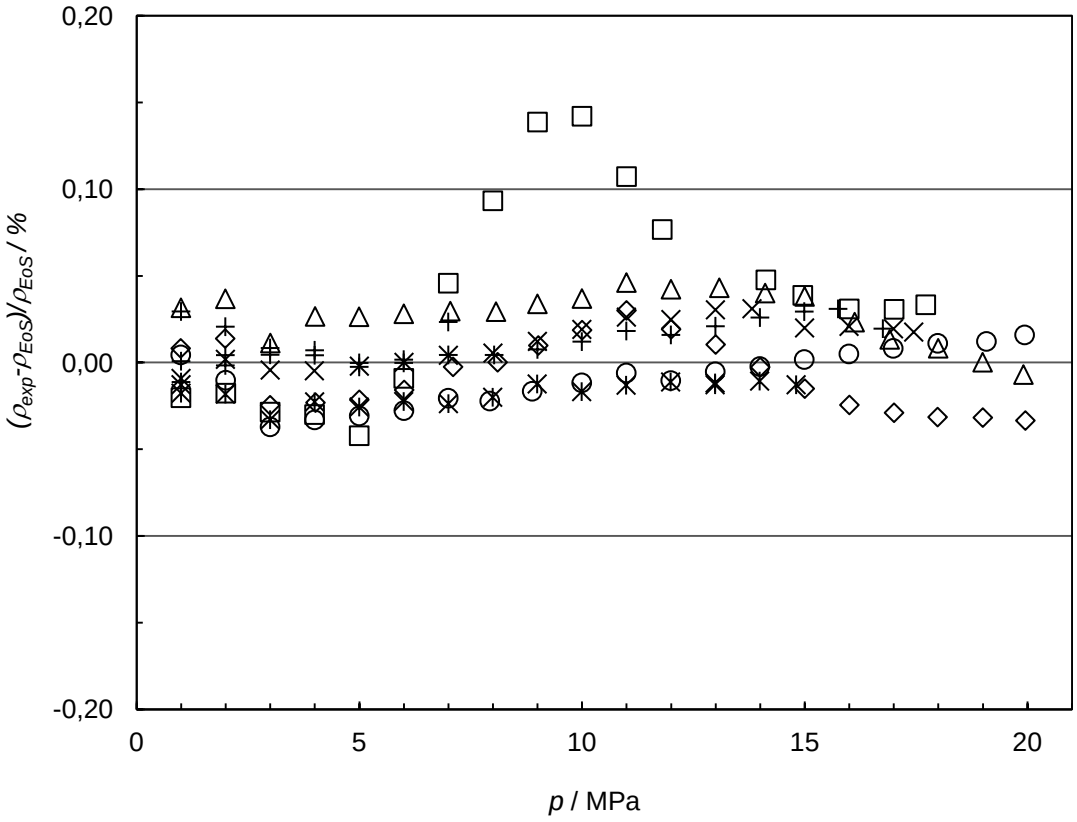

Figure 6.1. Percentage density deviations of experimental *(p, ρ, T)* data of (0.20 CO_2 + 0.80 CH_4) binary mixture from density values ρ_{EoS} calculated from the GERG-2004 equation of state (2) versus pressure: □ 250 K; ◇ 275 K; △ 300 K; × 325; + 350 K; ○ 375 K; ✳ 400 K.

The estimated uncertainty of the GERG equation of state for mixtures of carbon dioxide with methane is 0.1%. It can be observed in Figure 6.1. that all relative deviations in density of the experimental data presented in this Chapter agree the GERG model within less than a 0.05% band, except for the isotherm at 250 K in the medium pressure range (between (7 and 12) MPa. In this case, interesting high relative deviations are observed as they reach values up to 0.14%). The deviations in density for the rest of the isotherms presented show a wavy form which is, however, within

the percentage band representing the uncertainty of the GERG model. No relation between the relative deviations and the temperature could be concluded.

Comparison of the experimental data with the data from the references

As indicated at the beginning of this Chapter, the thermophysical properties concerning binary mixtures of carbon monoxide with methane have been widely studied. According to the data base provided by the GERG Technical Monograph 15 (2), many of the existing experimental data measured for these mixtures were not used in the fitting of the GERG 2004 equation of state because of their low reliability. Of all the used data, experimental densities of Hwang et al. (4) and Brugge et al. (5), which cover pressure and temperature ranges of (0.2 – 69.5) MPa and (225 - 350) K respectively, were compared with the data of this work.

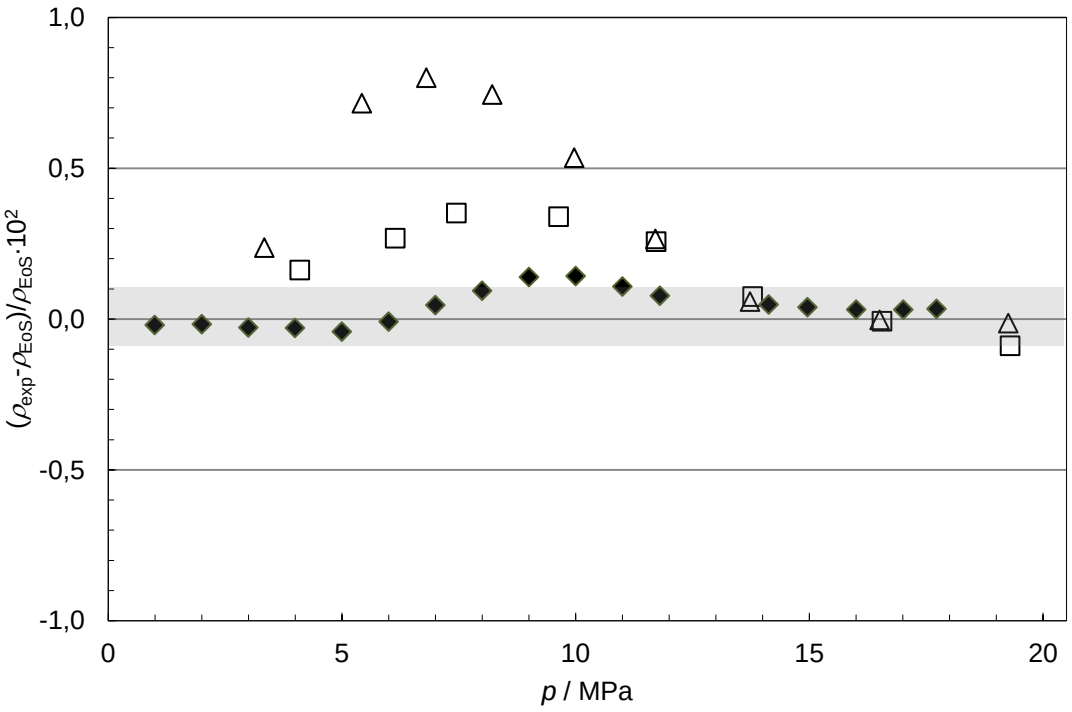

Figure 6.2. Percentage density deviations of experimental *(p, ρ, T)* data of CO_2 / CH_4 binary mixtures from density values ρ_{EoS} calculated from the GERG-2004 equation of state versus pressure, for CO_2 molar compositions (x_{CO_2} = 0.20, 0.29) at low temperatures and pressures up to 20 MPa: ◆ This work (x_{CO_2} = 0.20, *T* = 250 K); □ Hwang *et al*. (4) (x_{CO_2} = 0.29, *T* = 280 K); △ Hwang *et al*. (4) (x_{CO_2} = 0.29, *T* = 260 K). The shaded 0.1% band represents the estimated uncertainty of the equation of state for these mixtures.

Mixtures of carbon dioxide with methane studied by the mentioned authors did not include, however, a mixture with carbon dioxide molar fraction x_{CO_2} = 0.20, so that the data reported in this work could not be compared with them. However, data from the literature at low temperatures were used to confirm if the high deviation from the GERG model observed at 250 K and pressures between 7 and 12 MPa in Figure 6.2. was reliable. Figure 6.2. depicts the relative deviations from the GERG equation of state of the experimental data presented in this Chapter for the 250 K isotherm and the experimental densities published by Hwang et al. (4) at 260 K and 280 K, measured with a continuously-weighted pycnometer.

Apart from the fact that the composition of the mixture studied by Hwang et al. (4) and the mixture measured in this work are different, it can be observed that similar deviations to that mentioned previously are present at 260 K and 280 K for a x_{CO_2} = 0.29 mixture in the medium pressure range. In this case, relative deviations in density are higher at 260 K and for the highest carbon dioxide composition x_{CO_2} = 0.29. At high pressures, experimental data agree the equation of state within the 0.1% shaded band.

Reproducibility and overall uncertainty of the experimental data

The repeatability of the apparatus was tested before the beginning of the measurements presented in this Chapter by performing density measurements with nitrogen. The test measurements consisted in the measurement of the two limit isotherms (250 K and 400 K) over the whole pressure range of the apparatus. Density results showed an agreement of less than 0.02% between the relative deviations and the densities calculated with the equation of state for nitrogen of Span (6).

The overall uncertainty of the data presented in this Chapter was also estimated by taking into account the contributions to the uncertainty in density which come from the uncertainties in temperature, pressure and composition, as indicated in Eq.4.5. The partial derivatives of Eq.4.5. were also estimated by using the GERG model for mixtures of carbon monoxide with nitrogen. Eq.6.1. gives the expression of the total uncertainty in density for the density data concerning mixtures of carbon dioxide with methane.

$$u(\rho) = 10^{-4}\left(522 + 1.10\rho - 9.70p\right) \qquad \text{Eq.6.1.}$$

6.4. DISCUSION ON DENSITY MEASUREMENT RESULTS

In this thesis new accurate *(p, ρ, T)* data for one mixture of carbon dioxide with methane with molar composition x_{CO_2} = (0.20) in the temperature range (250 – 400) K at pressures up to 20 MPa were presented. The experimental density data were compared with the densities calculated from the GERG-2004 equation of state. Data were also compared with the data reported by Hwang et al. for mixtures of carbon dioxide with methane with different molar compositions.

The relative deviations in density of the experimental data presented in this Chapter showed a good agreement with the GERG-2004 equation of state. All deviations, except for that of the 250 K isotherm, were within a 0.05% band while the estimated uncertainty of the GERG model for these mixtures is 0.10%. Interesting high deviations were observed at 250 K and pressures between 7 and 12 MPa. These deviations were also observed in the data reported by other authors for similar mixtures, with even higher deviations.

REFERENCES

1. JAESCHKE, M. et al. *The GERG Databank of High Accuracy Compressibility Factor Measurements, GERG Technical Monograph*, 1997.

2. KUNZ, O. et al. The GERG-2004 Wide-Range Reference Equation of State for Natural Gases and Other Mixtures*. GERG Technical Monograph Fortschr*, 2007.

3. HALOUA, F. et al. *Caloric Quantities and Density Measurement of Non-Conventional Gases.* , 2011.

4. HWANG, C.A. et al. Densities of Carbon Dioxide + Methane Mixtures from 225 K to 350 K at Pressures Up to 35 MPa*. Journal of Chemical and Engineering Data*, 1997, vol. 42, no. 5. pp. 897-899.

5. BRUGGE, H.B. et al. Experimental Cross Virial Coefficients for Binary Mixtures of Carbon Dioxide with Nitrogen, Methane and Ethane at 300 and 320 K*. Physica A: Statistical Mechanics and its Applications*, 1989, vol. 156, no. 1. pp. 382-416.

6. SPAN, R. et al. A Reference Equation of State for the Thermodynamic Properties of Nitrogen for Temperatures from 63.151 to 1000 K and Pressures to 2200 MPa*. Journal of Physical and Chemical Reference Data*, 2000, vol. 29, no. 6. pp. 1361-1401.

CHAPTER 7

CONCLUSION AND FUTURE WORK

7.1. SUMMARY AND SCIENTIFIC CONTRIBUTIONS OF THIS THESIS

This thesis has contributed to the field of the determination of the thermodynamic properties of gases. In this final Chapter, the research contributions of this work are reviewed and some directions of future research are discussed and proposed. The main research contributions of this thesis are summarized as follows:

Improvement of the single sinker densimeter based on a state point uncertainty analysis.

As concluded from Chapter 3, the measurement uncertainties of the three state point magnitudes (pressure, density and temperature) were satisfactorily reduced thanks to the modifications performed on the setup. The uncertainty in temperature was significantly reduced over the whole temperature working range of the apparatus. Pressure uncertainty was decreased only in the low pressure range to compensate the lower accuracy at low densities due to the loss of accuracy of the balance. Finally, uncertainty in density was significantly reduced especially at low densities. The uncertainty analysis was confirmed as an excellent methodology for the detection of the densimeter's weaknesses and for the effective improvement of the accuracy of the single sinker densimeter. This analysis not only provided the directions for the improvements carried out on the densimeter, but also suggested new modifications for further reductions of the measurement uncertainty.

Automation of the operation of the single sinker densimeter.

The control and data acquisition program, developed prior to the beginning of the measurements presented in this thesis, optimized the time needed to measure each isotherm and increased the number of density data collected for each studied gas mixture. The user interface of the control program eases the execution of the measurement thanks to the graphical programming environment of VEE Agilent. Moreover the flexibility of the program allows modifications to be easily performed in order to adapt the control program to new operation conditions.

Contribution to the data base of binary mixtures of components present in biogases and other alternative fuel gases.

The new accurate density data reported in this thesis for binary mixtures containing carbon dioxide with nitrogen, carbon monoxide with nitrogen and methane with carbon dioxide contribute significantly to the existing data-base of experimental density data of binary gas mixtures.

The importance of the new data reported for the mixtures containing carbon dioxide lies in the high accuracy of the new data, which confirms the unexpected deviation of the experimental data from the equation of state observed at low temperatures and high pressures. It was also concluded that the mentioned deviations increased with the carbon dioxide content of the mixture.

On the other hand, the great interest of the new density data of the mixtures containing carbon monoxide and nitrogen was not only their low uncertainty but also the important lack of data for these mixtures. The new density data reported in this thesis extended the temperature range of the previous density data for these mixtures and were reported for two new compositions.

Finally, the experimental density data reported for one mixture of methane with carbon dioxide contributed to the data base with very high accuracies in density. These data showed good agreement with the densities calculated from the equation of state, except for the data at low temperatures and medium pressures, where high deviations were observed.

Test of the reference equation of state for natural gases and related mixtures

The GERG 2004 equation of state, whose departure functions and mixtures parameters were fitted on the basis of the up-to-date experimental data for the mixtures studied in this thesis, was tested in this work with new, accurate experimental data. As mentioned previously, though the equation of state showed a very good agreement of the experimental data for mixtures of carbon monoxide with nitrogen, the calculated densities for the other mixtures were observed to differ significantly from the

experimental data at low temperatures and high pressures. The comparisons established in this work can contribute to the improvement of the equation of state as well as to the updating of virial coefficient tables.

7.2. FUTURE RESEARCH DIRECTIONS

The work presented in this thesis provides a guide to future research, since it began as a continuation of the previous work carried out with the densimeter, but it also offers new working lines in the area of the determination of the density data of gas mixtures related with alternative biofuels. For instance, the working range can be extended and the accuracy of the densimeter can still be improved. Moreover, very few density data are available for many binary mixtures containing majority components of alternative fuel gases. The remainder of this section lays out some of the immediately accessible lines for future work.

Extend the working temperature range of the densimeter

The temperature working range of the single sinker densimeter ranges from 250 K to 400 K. The upper limit of this range is conditioned by the operating temperatures of the materials used in the measuring cell, its thermal insulating material and the connections of the PRT probes. Although the extent of the temperature range to higher temperatures would require minor changes in the setup, this is of little importance due to the relatively great availability of experimental data at high temperatures. However, the lower limitation in temperature of the densimeter comes mainly from the operation capacity of the thermostatic bath used as the primary stage thermostat of the measuring cell. Thus, the replacement of this thermostatic bath by another one with better technical characteristics would increase the temperature working range of the densimeter at low temperatures. This modification would be of great interest, since many of the experimental density data of gases are available for temperatures above 260 K, which means that there are still very few data at low temperatures. Under this modification of the temperature range, two important considerations should be taken into account: the availability of a fluid for the thermostatic bath capable of operating in the extended working range and the possibility of partial condensation for some gases at the lowest temperatures.

Reduction of the measurement uncertainty

One of the conclusions yielded by the uncertainty analysis performed for the densimeter was that the sinker volume was the most important source of uncertainty at high densities. The sinker volume, calibrated at the Spanish metrology institute (CEM), has a relatively high uncertainty. Several authors have reported lower uncertainty in the sinker volume by calibrating it following different methodologies. Thus, a re-calibration of the sinker volume would increase the accuracy of the experimental density data at high densities, which is of great interest if new mixtures with higher molar mass are measured.

The force transmission error induced by the specific fluid effect was rejected for all the measurements reported in this thesis since its value was negligible with respect to the uncertainty in density of the experimental data. However, if new mixtures containing components with high magnetic susceptibility are studied, or the uncertainty in density is reduced as proposed above, the term of the force transmission error due to the magnetic behavior of the fluid would put on weight. Therefore, in these cases the specific fluid effect should be evaluated to correct the experimental density data.

In situ preparation of gas mixtures

From the point of view of the availability of new binary and even ternary mixtures for density measurement, the development of a system for the in situ preparation of gas mixtures would be interesting. The pros and cons of this new system should be evaluated since, though the uncertainties in the composition of the final mixtures would probably be higher than that given for the mixtures studied in this work and the additional equipment would need a high initial investment, the system would allow mixtures of any composition to be prepared.

Measurement of new binary and ternary mixtures

As mentioned at the beginning of this section, the most important line of research is the contribution to the thermophysical properties database with new sets of accurate experimental density data of gaseous binary mixtures containing majority components

of alternative fuels. To this end, in Chapter 1 also mentioned the lack of data for mixtures containing carbon monoxide with carbon dioxide and mixtures containing oxygen.

An interesting research line would be the measurement of ternary mixtures containing components which are present in the alternative biofuels, but also in natural gas systems. In this case, special attention should be paid to the uncertainty in compositions of each mixture component, since this would be one of the main sources of uncertainty to the overall uncertainty in density.

Biogas like mixtures

Following the previous future research proposition, the number of components can be extended to multicomponent mixtures simulating the composition of real biogas and synthetic gas samples. The study of these mixtures has the main objective of testing the equation of state when it predicts properties of mixtures containing several components. The use of synthetic mixtures simulating real biogas or syngas compositions is owing to the fact that the impurities present in the real gas mixtures could affect the operation of the densimeter.

APPENDIX

APPENDIX A – DENSITY EXPERIMENTAL DATA OF THE MIXTURES OF CARBON DIOXIDE WITH NITROGEN

A.1. (0.10 CO_2 + 0.90 N_2) Mixture

A.2. (0.15 CO_2 + 0.85 N_2) Mixture

A.3. (0.20 CO_2 + 0.80 N_2) Mixture

A.4. (0.50 CO_2 + 0.50 N_2) Mixture

A.1. (0.10 CO_2 + 0.90 N_2) Mixture

Table A.1. Results of the (p, ρ, T) measurements for a {0.10 CO_2 + 0.90 N_2} binary mixture, where T is the temperature (ITS-90), p the pressure, ρ_{exp} the experimental density and ρ_{EoS} the density calculated from the GERG-2004 equation of state.

T/K	p/MPa	ρ_{exp}/(kg·m^{-3})	$10^2(\rho_{exp}-\rho_{EoS})/\rho_{EoS}$
		T = 250 K	
250.044	19.86622	302.682	-0.210
250.044	18.04077	278.626	-0.210
250.044	16.02422	250.228	-0.201
250.044	14.01532	220.196	-0.180
250.045	12.01104	188.824	-0.147
250.046	10.00715	156.529	-0.104
250.047	8.00002	123.810	-0.066
250.048	5.99883	91.410	-0.031
250.047	3.99732	59.733	-0.003
250.046	1.98511	29.000	0.034
		T = 275 K	
275.019	19.84087	262.442	-0.125
275.019	18.05655	241.448	-0.127
275.018	16.02186	216.330	-0.124
275.016	14.01343	190.433	-0.115
275.017	12.00866	163.678	-0.099
275.016	10.00450	136.290	-0.077
275.012	7.99787	108.505	-0.061
275.009	6.00199	80.825	-0.043
275.019	3.99710	53.276	0.000
		T = 300 K	
299.963	19.16513	226.098	-0.021
299.966	17.86924	212.244	-0.039
299.967	16.01378	191.829	-0.041
299.966	14.00977	169.025	-0.039
299.966	12.00591	145.550	-0.035
299.967	10.00204	121.553	-0.024
299.967	7.99970	97.214	-0.017
299.967	5.99638	72.692	-0.006
299.968	3.99646	48.220	0.006
299.967	1.99790	23.945	0.035

T/K	p/MPa	ρ_{exp}/(kg·m^{-3})	$10^2(\rho_{exp}-\rho_{EoS})/\rho_{EoS}$
		T = 325 K	
324.979	19.62110	208.360	0.007
324.980	18.00085	192.790	0.000
324.979	16.00130	172.971	-0.005
324.979	13.98251	152.335	-0.010
324.979	11.99919	131.525	-0.011
324.978	9.99890	110.087	-0.008
324.978	8.01923	88.521	-0.007
324.978	5.99183	66.201	-0.001
324.978	3.99616	44.111	0.003
324.980	1.99599	21.979	0.032
		T = 350 K	
349.967	19.37788	188.339	0.023
349.967	17.99350	176.127	0.017
349.966	15.99987	158.084	0.010
349.966	13.99498	139.425	0.005
349.966	11.99755	120.373	0.001
349.966	9.99755	100.892	0.002
349.966	7.99575	81.051	-0.001
349.965	5.99670	60.978	0.003
349.964	3.99656	40.709	0.003
349.964	1.99606	20.340	0.010
		T = 375 K	
374.975	18.71878	168.450	0.016
374.975	17.96004	162.237	0.014
374.974	15.96599	145.587	0.006
374.974	13.97204	128.504	0.000
374.974	11.98120	111.044	-0.004
374.973	9.98248	93.148	-0.005
374.973	7.98995	74.983	-0.007
374.973	5.99454	56.518	-0.011
374.970	3.96223	37.494	-0.011
374.969	1.97464	18.733	-0.001
		T = 400 K	
400.038	18.90806	158.136	0.067
400.037	17.81457	149.796	0.060
400.035	15.98414	135.572	0.051
400.036	13.99217	119.725	0.042
400.035	11.98674	103.403	0.032

T/K	p/MPa	ρ_{exp}/(kg·m^{-3})	$10^2(\rho_{exp}-\rho_{EoS})/\rho_{EoS}$
400.034	9.99291	86.844	0.028
400.035	7.98095	69.818	0.018
400.036	5.99205	52.720	0.013
400.034	3.99487	35.321	0.010
400.037	1.99589	17.722	0.031

A.2. (0.15 CO_2 + 0.85 N_2) Mixture

Table A.2. Results of the (p, ρ, T) measurements for a {0.15 CO_2 + 0.85 N_2} binary mixture, where T is the temperature (ITS-90), p the pressure, ρ_{exp} the experimental density and ρ_{EoS} the density calculated from the GERG-2004 equation of state.

T/K	p/MPa	ρ_{exp}/(kg·m^{-3})	$10^2(\rho_{exp}-\rho_{EoS})/\rho_{EoS}$
		T = 250 K	
250.059	19.99666	326.225	-0.309
250.063	18.01935	298.361	-0.307
250.064	16.01636	267.875	-0.287
250.066	14.01375	235.308	-0.251
250.066	12.00577	201.013	-0.193
250.066	10.00316	165.836	-0.122
250.064	7.99621	130.387	-0.060
250.064	5.98407	95.441	-0.009
250.061	3.98271	61.879	0.022
250.061	1.94406	29.337	0.082
		T = 275 K	
275.028	19.98318	280.214	-0.191
275.027	17.99374	255.193	-0.191
275.027	15.98143	228.492	-0.181
275.026	14.00115	201.020	-0.161
275.026	12.00000	172.315	-0.133
275.026	9.99554	142.952	-0.098
275.025	7.99430	113.405	-0.067
275.022	5.99802	84.088	-0.042
275.019	4.00063	55.255	-0.018
275.019	1.98846	26.992	0.035
		T = 300 K	
299.963	19.97735	247.119	-0.053
299.965	17.99426	224.784	-0.078
299.968	15.96936	201.068	-0.077
299.967	13.99130	177.090	-0.068
299.968	12.00779	152.379	-0.054
299.966	10.00322	126.921	-0.037
299.966	8.00779	101.300	-0.026
299.966	5.99919	75.467	-0.009
299.967	3.98234	49.692	0.009
299.969	1.99212	24.615	0.062
		T = 325 K	
324.980	19.97825	221.898	-0.008
324.980	18.01598	202.007	-0.018
324.981	16.00631	180.933	-0.021

T/K	p/MPa	ρ_{exp}/(kg·m^{-3})	$10^2(\rho_{exp}-\rho_{EoS})/\rho_{EoS}$
324.981	14.01385	159.405	-0.021
324.981	11.99115	137.002	-0.020
324.981	9.99694	114.495	-0.012
324.981	7.99759	91.632	-0.008
324.982	5.99660	68.599	0.000
324.982	3.99587	45.557	0.015
324.982	1.99613	22.645	0.054
		T = 350 K	
349.967	19.98296	202.168	0.046
349.967	18.00779	183.902	0.034
349.967	16.00783	164.842	0.026
349.967	14.00355	145.221	0.020
349.967	11.99797	125.127	0.016
349.967	9.99946	104.724	0.017
349.967	7.99535	83.959	0.014
349.967	5.99688	63.049	0.017
349.967	3.99534	41.993	0.021
349.967	1.99594	20.947	0.053
		T = 375 K	
374.956	19.97235	185.971	0.054
374.956	17.99229	169.101	0.040
374.956	15.99852	151.646	0.029
374.956	13.98957	133.615	0.021
374.955	11.94535	114.852	0.014
374.954	9.98626	96.527	0.009
374.954	7.99726	77.627	0.000
374.954	5.99557	58.378	-0.003
374.953	3.95365	38.571	-0.004
374.955	1.96362	19.172	0.008
		T = 400 K	
400.023	17.81821	155.538	0.070
400.022	15.97720	140.583	0.058
400.022	13.98802	124.054	0.047
400.020	11.98638	107.065	0.037
400.020	9.99083	89.804	0.031
400.021	7.99123	72.219	0.023
400.019	5.99535	54.424	0.015
400.020	3.99567	36.397	0.003
400.019	1.99535	18.223	0.005

A.3. (0.20 CO_2 + 0.80 N_2) Mixture

Table A.3. Results of the (p, ρ, T) measurements for the {0.20 CO_2 + 0.80 N_2} binary mixture, where T is the temperature (ITS-90), p the pressure, ρ_{exp} the experimental density and ρ_{EoS} the density calculated from the GERG-2004 equation of state.

T/K	p/MPa	ρ_{exp}/(kg·m^{-3})	$10^2(\rho_{exp}-\rho_{EoS})/\rho_{EoS}$
		T = 250 K	
250.020	19.6329	345.629	-0.418
250.020	18.0387	321.449	-0.413
250.047	17.6393	314.981	-0.429
250.046	17.0116	304.796	-0.421
250.019	16.0267	288.385	-0.382
250.047	15.0085	270.511	-0.374
250.020	14.0175	252.741	-0.320
250.046	13.0049	233.864	-0.298
250.020	12.0102	215.101	-0.233
250.049	11.0009	195.630	-0.196
250.020	10.0041	176.401	-0.133
250.046	8.99881	156.893	-0.104
250.020	8.00094	137.785	-0.051
250.048	6.99772	118.767	-0.029
250.019	6.01320	100.543	0.007
250.044	4.99748	82.144	0.006
250.018	4.03244	65.204	0.027
250.044	2.99627	47.559	0.038
250.018	1.97928	30.827	-0.016
250.046	0.997911	15.262	-0.011
250.015	0.994481	15.210	-0.017
250.046	0.488236	7.397	-0.002
		T = 275 K	
274.985	19.4297	290.888	-0.218
274.986	18.0431	272.044	-0.211
274.988	16.0091	243.011	-0.190
274.989	14.0057	213.010	-0.160
274.989	12.0048	182.017	-0.123
274.991	10.0003	150.404	-0.078
274.990	7.99888	118.772	-0.044
274.991	5.99721	87.563	-0.016
274.991	3.99564	57.180	0.004
274.989	1.98781	27.804	-0.008
274.987	0.998226	13.800	0.014
		T = 300 K	
299.954	18.1509	238.850	-0.069

T/K	p/MPa	ρ_{exp}/(kg·m^{-3})	$10^2(\rho_{exp}-\rho_{EoS})/\rho_{EoS}$
299.953	17.0768	225.549	-0.084
299.951	15.0017	199.149	-0.077
299.951	13.0369	173.362	-0.065
299.950	11.0322	146.500	-0.041
299.951	8.99761	118.906	-0.028
299.951	6.99712	91.756	-0.013
299.951	4.99627	64.833	-0.002
299.953	2.99620	38.386	0.021
299.956	0.984743	12.423	-0.012
299.957	0.492877	6.193	-0.019
		T = 325 K	
324.963	19.9638	232.536	-0.017
324.962	18.0020	211.461	-0.025
324.962	16.0036	189.249	-0.031
324.961	14.0015	166.343	-0.032
324.961	12.0013	142.924	-0.031
324.960	9.99931	119.106	-0.024
324.959	7.99747	95.062	-0.020
324.960	5.99710	70.986	-0.011
324.960	3.97658	46.775	0.001
324.960	1.99409	23.265	-0.003
324.959	1.99404	23.265	0.000
		T = 350 K	
349.948	19.8205	209.531	0.042
349.948	17.9934	191.695	0.029
349.948	15.9992	171.670	0.017
349.948	13.9952	151.019	0.008
349.948	11.9964	129.976	0.001
349.948	9.97881	108.381	0.000
349.949	7.99624	86.910	-0.002
349.947	5.99652	65.117	0.000
349.948	3.99594	43.283	0.000
349.949	1.99547	21.523	-0.013
		T = 375 K	
374.942	19.9027	192.989	0.075
374.941	17.8466	174.574	0.057
374.942	16.0234	157.817	0.044
374.940	13.9881	138.676	0.031
374.941	11.9900	119.489	0.020
374.942	9.99297	99.987	0.016
374.941	7.99534	80.217	0.011
374.941	5.99514	60.236	0.012

T/K	p/MPa	ρ_{exp}/(kg·m^{-3})	$10^2(\rho_{exp}-\rho_{EoS})/\rho_{EoS}$
374.940	3.99570	40.155	0.018
374.941	1.99240	19.995	-0.008
374.940	0.981916	9.845	0.004
		T = 400 K	
400.011	19.9790	179.326	0.121
400.012	17.9791	162.772	0.101
400.011	15.9812	145.821	0.083
400.012	13.9866	128.512	0.068
400.012	11.9899	110.835	0.054
400.012	9.99056	92.826	0.045
400.012	7.99379	74.576	0.034
400.012	5.99466	56.097	0.026
400.012	3.99403	37.452	0.020
400.010	1.97816	18.570	0.026
400.008	0.996681	9.356	0.009

A.4. (0.50 CO_2 + 0.50 N_2) Mixture

Table A.4. Results of the (p, ρ, T) measurements for the {0.50 CO_2 + 0.50 N_2} binary mixture, where T is the temperature (ITS-90), p the pressure, ρ_{exp} the experimental density and ρ_{EoS} the density calculated from the GERG-2004 equation of state.

T/K	p/MPa	ρ_{exp}/(kg·m^{-3})	$10^2(\rho_{exp}-\rho_{EoS})/\rho_{EoS}$
		T = 275 K	
275.039	17.5630	426.437	-0.235
275.037	17.0270	414.634	-0.235
275.029	15.9257	388.806	-0.233
275.027	15.0321	366.266	-0.218
275.027	14.0316	339.405	-0.191
275.025	13.0253	310.916	-0.147
275.025	12.0251	281.541	-0.089
275.024	11.0183	251.523	-0.016
275.023	10.0288	222.169	0.029
275.023	9.12550	196.081	0.064
275.023	8.00600	165.225	0.088
275.023	7.00335	139.278	0.091
275.023	5.99952	114.980	0.068
275.023	4.99873	92.411	0.037
275.024	3.99739	71.374	0.006
275.024	2.99662	51.754	-0.013
275.023	1.99331	33.323	-0.080
275.023	0.996577	16.162	-0.065
		T = 300 K	
299.971	19.9696	385.259	-0.073
299.969	19.0204	368.091	-0.095
299.969	17.9972	348.774	-0.102
299.971	16.9958	329.040	-0.102
299.965	15.9985	308.658	-0.103
299.968	14.9957	287.528	-0.092
299.968	13.9962	266.000	-0.078
299.966	12.9982	244.208	-0.062
299.968	11.9948	222.215	-0.036
299.969	10.9965	200.469	-0.001
299.973	9.99650	178.959	0.019
299.973	9.99330	178.967	0.061
299.970	9.01433	158.299	0.036
299.969	8.00905	137.740	0.043
299.969	7.00490	117.900	0.050
299.966	6.02374	99.216	0.034
299.967	5.01581	80.785	0.017

T/K	p/MPa	ρ_{exp}/(kg·m^{-3})	$10^2(\rho_{exp}-\rho_{EoS})/\rho_{EoS}$
299.966	4.00017	62.993	0.001
299.966	2.99882	46.195	-0.012
299.966	1.99512	30.061	-0.049
299.964	0.995865	14.686	-0.053
		T = 325 K	
324.980	19.4357	315.426	-0.045
324.980	19.0231	308.813	-0.047
324.980	18.0181	292.404	-0.047
324.980	17.0124	275.602	-0.046
324.981	16.0175	258.660	-0.042
324.981	14.9908	240.922	-0.033
324.981	14.0109	223.826	-0.024
324.982	13.0084	206.250	-0.013
324.981	12.0051	188.662	-0.002
324.980	11.0012	171.162	0.017
324.980	10.0036	153.908	0.021
324.981	9.00191	136.826	0.026
324.981	7.99825	120.002	0.028
324.981	6.99807	103.583	0.032
324.982	5.99509	87.485	0.023
324.982	4.99725	71.872	0.014
324.982	3.99531	56.615	0.008
324.983	2.99643	41.830	0.008
324.984	1.99147	27.367	-0.043
324.983	0.974072	13.176	-0.063
		T = 350 K	
349.961	19.9771	281.556	0.003
349.962	18.9973	267.945	0.000
349.961	17.9957	253.790	-0.002
349.961	16.9963	239.453	-0.003
349.962	15.9946	224.908	-0.001
349.962	14.9975	210.290	0.001
349.961	14.0001	195.573	0.002
349.961	12.9982	180.741	0.005
349.962	11.9972	165.911	0.006
349.961	10.9977	151.155	0.018
349.961	9.99633	136.421	0.011
349.961	9.99633	136.421	0.011
349.960	8.99622	121.830	0.009
349.960	7.99547	107.379	0.005
349.961	6.99592	93.129	0.004
349.961	5.99622	79.074	-0.007
349.962	4.99593	65.240	-0.014

349.962	3.99702	51.667	-0.026
349.961	2.99638	38.326	-0.038
349.962	1.98830	25.152	-0.063
349.962	0.983480	12.303	-0.079
		T = 375 K	
374.953	19.9408	250.440	0.103
374.951	19.1192	240.354	0.102
374.953	17.9878	226.253	0.092
374.953	16.9901	213.677	0.087
374.953	15.9896	200.942	0.082
374.953	14.9937	188.172	0.079
374.954	13.9947	175.285	0.076
374.954	12.9915	162.294	0.071
374.953	11.9925	149.335	0.066
374.954	10.9952	136.416	0.071
374.953	9.99586	123.471	0.056
374.953	9.99586	123.471	0.056
374.953	8.96527	110.186	0.047
374.954	8.05362	98.499	0.039
374.952	6.99503	85.031	0.031
374.953	5.99458	72.415	0.019
374.952	4.99326	59.918	0.006
374.952	3.99475	47.603	-0.004
374.953	2.99568	35.439	-0.009
374.951	1.98785	23.329	-0.047
374.954	0.987061	11.492	-0.064
		T = 400 K	
400.020	19.9603	227.147	0.154
400.018	18.9831	216.347	0.146
400.020	17.9647	204.970	0.141
400.018	16.9838	193.894	0.129
400.018	15.9850	182.526	0.123
400.019	14.9839	171.050	0.116
400.018	13.9859	159.545	0.109
400.019	12.9837	147.944	0.105
400.018	11.9864	136.359	0.096
400.019	10.9874	124.751	0.098
400.019	9.97978	113.018	0.080
400.019	9.97978	113.018	0.080
400.017	8.99459	101.571	0.071
400.018	7.99241	89.956	0.060
400.019	6.99141	78.405	0.055
400.020	5.99420	66.950	0.041
400.020	4.99316	55.527	0.033
400.019	3.98088	44.058	0.017

T/K	p/MPa	ρ_{exp}/(kg·m^{-3})	$10^2(\rho_{exp}-\rho_{EoS})/\rho_{EoS}$
400.018	2.99564	32.992	0.012
400.019	1.98761	21.767	-0.027
400.018	0.975887	10.626	-0.045

APPENDIX B – DENSITY EXPERIMENTAL DATA OF THE MIXTURES OF CARBON MONOXIDE WITH NITROGEN

B.1. (0.05 CO + 0.95 N_2) Mixture

B.2. (0.10 CO + 0.90 N_2) Mixture

B.1. (0.05 CO + 0.95 N_2) Mixture

Table B.1. Results of the (p, ρ, T) measurements for the (0.05 CO + 0.95 N_2) binary mixture, where T is the temperature (ITS-90), p the pressure, ρ_{exp} the experimental density and ρ_{EoS} the density calculated from the GERG-2004 equation of state.

T/K	p/MPa	ρ_{exp}/(kg·m^{-3})	$10^2(\rho_{exp}-\rho_{EoS})/\rho_{EoS}$
		T = 250 K	
250.049	18.4739	250.840	0.014
250.049	17.9994	245.259	0.014
250.045	15.9997	220.890	0.012
250.047	14.0036	195.251	0.010
250.049	11.9985	168.354	0.008
250.051	9.99983	140.653	0.008
250.047	7.99853	112.326	0.002
250.045	6.01694	84.044	-0.003
250.044	4.00994	55.503	-0.012
250.043	1.99903	27.340	0.011
250.041	0.996970	13.537	0.000
		T = 275 K	
275.023	19.9174	235.882	0.017
275.023	18.1977	218.123	0.015
275.021	15.9971	194.336	0.016
275.023	13.9973	171.740	0.015
275.023	11.9993	148.339	0.011
275.030	10.0622	124.995	0.006
275.029	8.03660	100.073	0.000
275.029	6.03862	75.170	-0.003
275.023	4.00007	49.643	-0.010
275.020	1.99595	24.643	0.013
275.020	0.990786	12.187	-0.002
		T = 300 K	
299.978	19.9569	212.314	0.036
299.977	17.9967	193.879	0.021
299.977	15.9967	174.350	0.020
299.957	14.9541	163.889	0.015
299.980	13.9973	154.113	0.019
299.962	12.9975	143.747	0.013
299.975	11.8888	132.063	0.012
299.962	10.9995	122.587	0.018
299.972	10.0171	111.971	0.011
299.962	9.08652	101.826	0.010
299.974	8.02482	90.132	0.007
299.962	6.99826	78.744	0.009

T/K	p/MPa	ρ_{exp}/(kg·m^{-3})	$10^2(\rho_{exp}-\rho_{EoS})/\rho_{EoS}$
299.972	6.02019	67.811	0.002
299.962	4.99795	56.340	0.002
299.972	3.97500	44.812	-0.008
299.961	2.98189	33.609	-0.006
299.971	1.99343	22.457	0.018
299.962	1.00376	11.294	0.011
299.971	0.986706	11.101	0.005
		T = 325 K	
324.983	19.9309	193.033	0.018
324.983	17.9952	176.379	0.018
324.982	15.9569	158.239	0.025
324.985	14.1156	141.303	0.014
324.974	13.7432	137.825	0.010
324.975	12.9991	130.817	0.010
324.984	12.0000	121.293	0.011
324.977	10.9966	111.619	0.019
324.983	10.0066	101.939	0.011
324.979	8.99869	91.988	0.010
324.984	7.99104	81.935	0.008
324.978	7.02577	72.228	0.009
324.983	5.96077	61.428	0.005
324.978	4.97996	51.417	0.002
324.984	4.00852	41.449	0.000
324.978	2.99127	30.967	-0.007
324.982	1.98129	20.531	0.009
324.984	0.996209	10.328	0.009
		T = 350 K	
349.969	19.6554	175.420	0.022
349.969	17.9925	162.172	0.022
349.970	15.9944	145.784	0.021
349.970	13.9972	128.911	0.018
349.970	12.0181	111.731	0.015
349.970	10.0220	93.976	0.015
349.969	8.01856	75.757	0.010
349.968	5.99817	57.037	0.005
349.971	4.00481	38.283	0.003
349.970	1.95895	18.808	0.017
349.970	0.991177	9.530	0.004
		T = 375 K	
374.959	19.8166	163.859	0.018
374.959	17.9875	150.312	0.017
374.959	15.9900	135.101	0.016
374.959	13.9946	119.477	0.013

T/K	p/MPa	ρ_{exp}/(kg·m^{-3})	$10^2(\rho_{exp}-\rho_{EoS})/\rho_{EoS}$
374.959	11.9955	103.411	0.009
374.958	9.99598	86.957	0.010
374.960	7.99654	70.138	0.006
374.958	5.99791	52.996	-0.001
374.959	3.99850	35.556	-0.014
374.959	1.98927	17.794	0.013
374.959	0.991138	8.887	0.002
		T = 400 K	
400.020	19.0266	147.507	0.015
400.019	17.9853	140.246	0.013
400.020	15.9860	126.014	0.012
400.019	13.9897	111.428	0.010
400.019	11.9915	96.459	0.007
400.019	9.97324	80.982	0.006
400.021	7.99662	65.491	0.001
400.019	5.99803	49.518	-0.008
400.020	3.98633	33.151	-0.020
400.020	1.93445	16.200	-0.006

B.2. (0.10 CO + 0.90 N_2) Mixture

Table B.2. Results of the (p, ρ, T) measurements for the (0.10 CO_2 + 0.90 N_2) binary mixture, where T is the temperature (ITS-90), p the pressure, ρ_{exp} the experimental density and ρ_{EoS} the density calculated from the GERG-2004 equation of state.

T/K	p/MPa	ρ_{exp}/(kg·m^{-3})	$10^2(\rho_{exp}-\rho_{EoS})/\rho_{EoS}$
		T = 250 K	
250.060	19.9624	268.002	0.016
250.060	17.9996	245.432	0.015
250.055	16.7064	229.835	0.019
250.059	15.9987	221.035	0.014
250.051	15.0030	208.407	0.016
250.061	13.9985	195.325	0.014
250.053	13.0333	182.506	0.014
250.063	11.9982	168.471	0.014
250.051	11.0009	154.742	0.017
250.056	9.99883	140.734	0.013
250.050	8.99903	126.622	0.009
250.055	7.99832	112.391	0.010
250.057	6.99906	98.128	0.015
250.056	5.99926	83.836	0.012
250.056	5.04318	70.198	0.011
250.054	3.99885	55.373	0.010
250.056	3.03294	41.760	0.002
250.053	2.00426	27.416	0.013
250.053	0.999785	13.577	0.010
250.051	0.969128	13.157	0.002
		T = 275 K	
275.024	19.8876	235.720	0.023
275.024	17.9971	216.135	0.022
275.024	15.9977	194.459	0.022
275.022	14.0007	171.880	0.020
275.019	12.0042	148.483	0.017
275.018	9.99954	124.305	0.016
275.015	7.99941	99.667	0.012
275.014	5.99890	74.708	0.009
275.012	3.99849	49.641	0.001
275.012	1.98443	24.502	0.011
275.011	0.997907	12.276	-0.001
		T = 300 K	
299.977	19.8296	211.228	0.036
299.976	17.9986	193.977	0.022
299.975	16.1086	175.535	0.022

T/K	p/MPa	ρ_{exp}/(kg·m^{-3})	$10^2(\rho_{exp}-\rho_{EoS})/\rho_{EoS}$
299.974	15.3704	168.159	0.024
299.973	14.8070	162.461	0.023
299.972	13.9972	154.176	0.021
299.972	13.0026	143.858	0.022
299.972	11.9990	133.290	0.020
299.972	11.0075	122.717	0.026
299.973	9.99714	111.800	0.023
299.969	9.07366	101.718	0.018
299.976	7.99752	89.866	0.024
299.971	7.03398	79.163	0.018
299.974	5.99923	67.600	0.019
299.969	5.02084	56.608	0.007
299.972	3.99843	45.092	0.013
299.969	2.99357	33.744	-0.005
299.972	1.98975	22.417	0.022
299.972	1.00194	11.274	0.016
299.971	0.992979	11.173	0.011
		T = 325 K	
324.978	19.9475	193.262	0.033
324.977	17.9956	176.463	0.033
324.978	15.9946	158.639	0.033
324.977	13.9961	140.254	0.032
324.977	11.9970	121.320	0.031
324.978	9.99872	101.905	0.032
324.976	7.99937	82.050	0.028
324.977	5.99998	61.847	0.025
324.976	3.99850	41.357	0.017
324.976	1.97022	20.421	0.022
324.977	0.997476	10.342	0.013
		T = 350 K	
349.966	19.9592	177.859	0.032
349.964	18.2140	164.000	0.027
349.966	17.9917	162.217	0.033
349.965	16.9943	154.090	0.028
349.968	15.9939	145.829	0.035
349.965	14.9956	137.446	0.028
349.968	13.9949	128.938	0.037
349.965	12.9990	120.335	0.026
349.968	11.9970	111.586	0.035
349.963	10.9983	102.742	0.029
349.969	9.99826	93.794	0.036
349.963	8.99760	84.725	0.021
349.968	7.99894	75.601	0.031

T/K	p/MPa	ρ_{exp}/(kg·m^{-3})	$10^2(\rho_{exp}-\rho_{EoS})/\rho_{EoS}$
349.963	6.99788	66.355	0.019
349.968	5.99772	57.048	0.024
349.962	4.99789	47.663	0.005
349.967	3.92247	37.508	0.011
349.964	2.99918	28.731	-0.012
349.967	1.97883	18.999	0.020
349.967	0.993387	9.551	-0.004
349.963	0.991956	9.538	0.009
		T = 375 K	
374.957	19.9713	165.047	0.039
374.954	19.9666	165.012	0.038
374.956	18.9875	157.820	0.038
374.956	17.9867	150.362	0.040
374.955	16.9904	142.823	0.038
374.957	15.9904	135.151	0.039
374.955	15.0159	127.569	0.037
374.957	13.9926	119.504	0.039
374.954	12.9938	111.524	0.036
374.957	11.9876	103.381	0.034
374.955	10.9952	95.265	0.040
374.957	9.99790	86.999	0.032
374.955	8.99739	78.624	0.031
374.956	8.02423	70.391	0.026
374.955	6.99762	61.627	0.027
374.958	5.99898	53.019	0.021
374.955	4.98094	44.170	0.014
374.956	4.00484	35.621	0.009
374.955	2.99823	26.743	-0.005
374.955	1.99501	17.848	0.028
374.957	0.993407	8.908	0.012
		T = 400 K	
400.031	18.4582	143.591	0.032
400.021	17.9819	140.257	0.030
400.020	16.2271	127.785	0.032
400.022	15.9860	126.048	0.032
400.020	14.9879	118.800	0.032
400.019	13.9901	111.464	0.034
400.019	12.9907	104.017	0.030
400.022	11.9942	96.505	0.030
400.019	11.0249	89.118	0.033
400.021	9.89549	80.402	0.031
400.018	8.98697	73.307	0.021
400.018	7.99464	65.495	0.028

T/K	p/MPa	ρ_{exp}/(kg·m^{-3})	$10^2(\rho_{exp}-\rho_{EoS})/\rho_{EoS}$
400.020	7.00550	57.622	0.020
400.017	5.99615	49.523	0.032
400.021	4.99706	41.415	0.004
400.019	3.99728	33.254	0.019
400.020	2.99426	24.985	-0.020
400.020	1.97547	16.545	0.022
400.017	0.997158	8.375	0.008
400.020	0.984405	8.268	-0.005

APPENDIX C – DENSITY EXPERIMENTAL DATA OF A MIXTURE OF CARBON DIOXIDE WITH METHANE

C.1. (0.20 CO_2 + 0.80 CH_4) Mixture

C.1. (0.20 CO_2 + 0.80 CH_4) Mixture

Table C.1. Results of the (p, ρ, T) measurements for the (0.20 CO_2 + 0.80 CH_4) binary mixture, where T is the temperature (ITS-90), p the pressure, ρ_{exp} the experimental density and ρ_{EoS} the density calculated from the GERG-2004 equation of state.

T/K	p/MPa	ρ_{exp}/(kg·m^{-3})	$10^2(\rho_{exp}-\rho_{EoS})/\rho_{EoS}$
		T = 250 K	
250.059	17.719615	317.764	0.033
250.061	17.009170	310.486	0.031
250.062	16.001278	298.981	0.031
250.061	14.958709	285.286	0.039
250.063	14.129468	272.744	0.048
250.040	11.802802	227.426	0.077
250.042	11.001107	207.851	0.107
250.044	10.000669	181.260	0.142
250.041	9.001713	154.043	0.139
250.039	7.999295	128.049	0.093
250.041	6.999025	104.637	0.046
250.039	5.999760	84.000	-0.009
250.036	4.998653	65.842	-0.042
250.046	3.996516	49.786	-0.030
250.053	2.998686	35.502	-0.029
250.053	2.003681	22.645	-0.018
250.053	0.996081	10.779	-0.020
		T = 275 K	
275.017	19.956462	276.100	-0.033
275.016	19.000711	266.217	-0.032
275.014	17.985723	254.779	-0.031
275.011	17.007502	242.757	-0.029
275.009	16.005184	229.349	-0.024
275.009	15.002908	214.815	-0.015
275.009	14.002698	199.243	-0.003
275.008	13.002227	182.762	0.010
275.009	12.001580	165.645	0.019
275.009	11.000405	148.263	0.030
275.009	10.003057	131.045	0.019
275.009	9.019965	114.534	0.010
275.009	8.106889	99.811	0.000
275.007	7.106305	84.505	-0.002
275.004	6.008265	68.753	-0.016
275.005	5.001371	55.279	-0.021
275.004	4.016804	42.954	-0.023
275.006	2.998524	31.022	-0.025

T/K	p/MPa	ρ_{exp}/(kg·m^{-3})	$10^2(\rho_{exp}-\rho_{EoS})/\rho_{EoS}$
275.004	1.989898	19.957	0.014
275.004	0.990945	9.645	0.008
		T = 300 K	
299.950	19.912948	227.409	-0.007
299.952	18.996495	217.937	0.000
299.957	17.998390	207.086	0.008
299.959	16.909924	194.645	0.013
299.958	16.123365	185.307	0.023
299.960	14.999014	171.496	0.038
299.959	14.113456	160.305	0.040
299.961	13.084183	147.072	0.043
299.964	11.998593	132.991	0.042
299.967	10.998937	120.061	0.046
299.968	9.999430	107.267	0.037
299.968	9.000257	94.735	0.034
299.967	8.070242	83.364	0.029
299.967	7.044695	71.216	0.030
299.968	5.999984	59.296	0.028
299.969	4.995167	48.286	0.026
299.969	4.008117	37.909	0.027
299.971	3.003224	27.780	0.011
299.969	1.993292	18.042	0.037
299.969	0.996182	8.825	0.032
		T = 325 K	
324.979	17.449202	169.541	0.018
324.979	16.995296	165.043	0.020
324.980	15.997051	154.988	0.021
324.980	14.998810	144.749	0.020
324.983	13.818159	132.486	0.031
324.981	12.996790	123.884	0.030
324.980	11.997049	113.390	0.025
324.982	10.997759	102.936	0.026
324.981	9.997562	92.547	0.019
324.981	8.999827	82.311	0.012
324.980	8.001563	72.237	0.006
324.979	7.001029	62.343	0.004
324.978	6.004387	52.708	0.000
324.979	5.001787	43.259	-0.002
324.980	3.991951	34.000	-0.005
324.980	2.999484	25.159	-0.004
324.980	1.994196	16.469	0.002
324.980	0.998171	8.115	-0.013
324.981	0.998037	8.114	-0.009

T/K	p/MPa	ρ_{exp}/(kg·m^{-3})	$10^2(\rho_{exp}-\rho_{EoS})/\rho_{EoS}$
		T = 350 K	
349.966	16.756538	142.049	0.020
349.965	15.750106	133.311	0.031
349.966	14.991423	126.643	0.029
349.967	13.995929	117.828	0.026
349.966	12.996658	108.933	0.021
349.967	11.996505	100.011	0.016
349.968	10.996080	91.104	0.018
349.966	9.997060	82.241	0.012
349.967	9.000391	73.462	0.008
349.966	8.028339	64.986	0.004
349.968	6.999333	56.125	0.004
349.968	6.997579	56.121	0.023
349.969	5.997824	47.627	0.002
349.969	5.997824	47.626	0.000
349.967	4.998483	39.289	0.000
349.967	4.998483	39.288	-0.002
349.970	3.997872	31.094	0.007
349.970	3.997872	31.093	0.004
349.970	2.998006	23.064	0.008
349.970	2.998006	23.063	0.005
349.970	1.992904	15.159	0.004
349.970	1.992904	15.158	-0.002
349.970	1.992584	15.159	0.021
349.970	0.998026	7.505	0.001
349.970	0.998026	7.504	-0.011
349.970	0.997743	7.505	0.030
		T = 375 K	
374.944	19.939071	150.707	0.016
374.945	19.081802	144.421	0.012
374.946	17.988131	136.285	0.011
374.943	16.988583	128.742	0.008
374.946	15.993395	121.141	0.005
374.947	14.991107	113.416	0.002
374.945	13.993319	105.670	-0.002
374.946	12.992618	97.863	-0.005
374.945	11.993831	90.049	-0.010
374.946	10.994470	82.233	-0.006
374.944	9.995028	74.421	-0.012
374.947	8.883363	65.767	-0.016
374.947	7.929903	58.389	-0.022
374.947	6.997277	51.228	-0.020
374.945	6.002124	43.652	-0.028

T/K	p/MPa	ρ_{exp}/(kg·m^{-3})	$10^2(\rho_{exp}-\rho_{EoS})/\rho_{EoS}$
374.945	4.999333	36.102	-0.031
374.945	3.997312	28.651	-0.033
374.947	2.997760	21.319	-0.037
374.950	1.999996	14.112	-0.010
374.949	0.991894	6.941	0.004
		T = 400 K	
400.014	14.808810	101.918	-0.013
400.015	13.989564	96.226	-0.011
400.015	12.989235	89.239	-0.013
400.015	11.990820	82.244	-0.011
400.016	10.991104	75.222	-0.013
400.015	9.993484	68.212	-0.017
400.014	8.994274	61.204	-0.012
400.015	12.989235	89.240	-0.012
400.016	7.995549	54.210	-0.020
400.018	7.001807	47.282	-0.024
400.016	5.997466	40.322	-0.022
400.015	4.998715	33.446	-0.026
400.015	3.997814	26.613	-0.023
400.018	2.997772	19.845	-0.033
400.016	1.994191	13.127	-0.018
400.017	0.998124	6.531	-0.018

APPENDIX D - PUBLICATIONS RELATED WITH THE THESIS

D.1. International Journals

[1] Improvement of the measurement uncertainty of a high accuracy single sinker densimeter via setup modifications based on a state point uncertainty analysis, Mondéjar, M. E., Segovia, J. J., and Chamorro, C. R. (2011), Measurement, 44 (9), 1768-1780.

[2] New (p, ρ, T) data for carbon dioxide - nitrogen mixtures from (250 to 400) K at pressures up to 20 MPa, Mondéjar, M. E., Martin, M. C., Span, R., and Chamorro, C. R. (2011), Journal of Chemical Thermodynamics, 43 (12), 1950-1953.

[3] Accurate (p, ρ, T) data for two new carbon dioxide - Nitrogen mixtures from (250 to 400) K at pressures up to 20 MPa, Mondéjar, M.E., Villamañán, R.M., Span, R. and Chamorro, C.R. Accepted for publication in the Journal of Chemical Thermodynamics.

[4] (p, ρ, T) behavior of two mixtures of carbon monoxide with nitrogen in the temperature range from 250 K to 40 K and pressures up to 20 MPa, Mondéjar, M.E., Villamañán, M.A., Span, R. and Chamorro, C.R. (2011), Journal of Chemical & Engineering Data, 56 (10), 3933-3939.

D.2. International Congresses and Seminars

Two oral communications and two posters where presented in international congresses with the content of this thesis.

1. **ECOS 2010:** 23rd International Conference on Efficiency, Cost, Optimization, Simulation and Environmental Impact of Energy Systems, June 14-17, 2010, Laussane (Switzerland).

   ECOS 2010 Volume I (Thermodynamics) - ISBN/EAN13: 1456303007 / 9781456303006.

   Oral communication: Improvement and Automation of a Single Sinker Densimeter for the Determination of (p, ρ, T) Properties of Mixtures of Gases

Related with Biogas, *María E. Mondéjar, José J. Segovia, Miguel A. Villamañán, Rosa M. Villamañán, M. Carmen Martín and César R. Chamorro*.

In this communication the modifications carried out on the single sinker densimeter together with the results of the test measurements with nitrogen were presented.

2. **ESAT 2011: 25th European Symposium on Applied Thermodynamics, June 24-**27, 2011, Saint Petersburg (Russia).

   Poster: Experimental (p, ρ, T) properties of binary mixtures of carbon dioxide with nitrogen, *M.E. Mondéjar, J.J. Segovia, R.M. Villamañán, M.C. Martín, M.A. Villamañán and C.R. Chamorro*.

   In this poster the results of the (p, ρ, T) behavior of the four mixtures of carbon dioxide with nitrogen were presented.

3. **RCCT 2011:** XVIII International Conference on Chemical Thermodynamics in Russia, October 3-7, 2011, Samara (Russia).

   ISBN 978-5-7964-1447-7

   Oral communication: Accurate density measurements of two gaseous mixtures of nitrogen with carbon monoxide via an improved single sinker Densimeter, *Mondéjar M.E., Segovia J.J., Villamañán R.M., Martín M.C., Villamañán M.A., Chamorro C.R.*

   In this poster the experimental density data for the two mixtures of carbon monoxide with nitrogen were presented.

4. **18th Symposium on Thermophysical Properties:**, June 24-29, 2012, Boulder, CO (USA).

   Poster: Experimental determination of (p, ρ, T) data for mixtures of carbon dioxide with methane for indirect calorific value determination of non-conventional energy gases, *Mondéjar M.E., Segovia J.J., Villamañán R.M.,*

Martín M.C., Villamañán M.A., Chamorro C.R, Fernández-Vicente T., del Campo D.

An abstract presenting the results from the measurements of the mixtures of methane with carbon dioxide has been submitted to the congress which will be held in June 2012.

D.3. Research projects related with the thesis

The development of this thesis was included in the research projects mentioned below:

Project name	Financing Institution and Ref. number	Period	Main researcher
Mejora de carburantes líquidos y gaseosos para el transporte, su almacenamiento y distribución: uso de combustibles renovables líquidos y de mezclas gaseosas con hidrógeno	Secretaría de Estado de Universidades e Investigación (Ministerio de Educación y Ciencia) ENE2006-13349/CON	2006-2010	Miguel Ángel Villamañán
GR152 – Infraestructuras – Investigación termodinámica de combustibles innovadores renovables procedentes de biomasa y de hidrógeno y de hidrógeno para su uso en automoción.	Junta de Castilla y León GR152	2008-2010	Miguel Ángel Villamañán
Caracterización termodinámica de nuevas mezclas combustibles derivadas del petróleo y de componentes renovables de interés medioambiental: medida y modelización.	Cooperación Mediterráneo	2009-2010	Miguel Ángel Villamañán
Combustibles ambientales sostenibles: caracterización termofísica de mezclas de biocombustibles líquidos y gaseosos con hidrocarburos de referencia convencionales.	Secretaría de Estado de Universidades e Investigación (Ministerio de Educación y Ciencia) ENE2009-14644-C02-01	2009-2012	José Juan Segovia
Characterization of Energy Gases	Unión Europea, European Metrology Research Programme EMRP ENG01 N 912/2009/EC	2010-2013	José Juan Segovia
El mix energético petróleo – gas natural + biocombustible/biogás: caracterización termodinámica sostenibilidad ambiental	International Cooperation Spanish Agency, C/033908/10	2011-2012	Miguel Ángel Villamañán

Measurement 44 (2011) 1768–1780

Contents lists available at ScienceDirect

Measurement

journal homepage: www.elsevier.com/locate/measurement

Improvement of the measurement uncertainty of a high accuracy single sinker densimeter via setup modifications based on a state point uncertainty analysis

M.E. Mondéjar, J.J. Segovia, C.R. Chamorro *

Research Group TERMOCAL, Dpto. Ingeniería Energética y Fluidomecánica, Universidad de Valladolid, Paseo del Cauce 59, E-47071 Valladolid, Spain

ARTICLE INFO

Article history:
Received 11 February 2011
Received in revised form 30 June 2011
Accepted 14 July 2011
Available online 23 July 2011

Keywords:
Density measurement
Uncertainty analysis
Single sinker densimeter
Monte Carlo method

ABSTRACT

The single sinker densimeter with magnetic suspension coupling is one of the state of the art methods for the accurate measurement of fluid densities. The uncertainties of experimental pressure, density and temperature data, measured with a single sinker densimeter, were thoroughly evaluated following the uncertainty propagation law. The main uncertainty sources of each magnitude were determined. Based on this statistical study, several modifications were performed to reduce the uncertainty associated to each magnitude. Firstly two new PTR-25 probes were added. Secondly a new pressure transducer for the low pressure range was added. Finally the sinker of the densimeter was replaced by a bigger one to improve the balance reading. After these modifications the uncertainty of each magnitude was evaluated and validated with a Monte Carlo simulation. Results yielded a significant reduction of 44% in temperature uncertainty, more than 92% on pressure below 2 MPa, and more than 22% on density.

1. Introduction

An accurate knowledge of the thermodynamic behavior of gases is of great importance in current industrial processes, such as storage and transport in the natural gas industry, but also in the scientific field, in the development of new fuels based on biogas or hydrogen. This thermodynamic behavior is estimated by using accurate equations of state.

The first developed equations of state, which had a theoretical foundation (e.g. virial equation of state), have been replaced by the current empirical multiparameter equations of state, which have demonstrated a better fit in the thermodynamic properties estimation [1]. To develop these empirical equations of state a huge amount of experimental data of different thermodynamic properties is needed, of which density is one of the most accessible properties.

While the database of density measurements for the most important industrial fluids is extensive and of high quality, few reliable and accurate density data have been reported for other fluids, such as new generation HFC refrigerant fluids, or mixtures. Therefore the contribution of new accurate experimental density data of different gases and mixtures in a wide range of temperatures and pressures is of great scientific interest.

The density measurement techniques which accomplish the highest accuracies in extensive working ranges of pressure and temperature are based on a combination of hydrostatic balances with magnetic suspension couplings, as stated in [2]. These methods are classified into the two sinker densimeter with magnetic suspension coupling and the single sinker densimeter with magnetic suspension coupling.

The two sinker densimeter, developed by Kleinrahm and Wagner [3] in the early 1980s, achieves the lowest uncertainties in density measurement in a wide density range. This high accuracy is obtained due to the contactless

* Corresponding author. Tel.: +34 983423756; fax: +34 983186462.
E-mail address: cescha@eis.uva.es (C.R. Chamorro).

0263-2241/$ - see front matter © 2011 Elsevier Ltd. All rights reserved.
doi:10.1016/j.measurement.2011.07.012

Nomenclature

CEM	Centro Español de Metrología (Spanish National Metrology Institute)
EA	European co-operation for Accreditation
ENAC	Entidad Nacional de Acreditación de España (Spanish Institution of Accreditation)
PDF	probability distribution function
PRT	platinum resistance thermometer
SSMSD	single sinker magnetic suspension densimeter
TSMSD	two sinker magnetic suspension densimeter
f	model function for the propagation of uncertainties law
k	coverage factor
K	compressibility modulus, MPa^{-1}
m	mass, kg
p	pressure, MPa
r	correlation coefficient
R	resistance, Ω
T	temperature, K
u	standard uncertainty
U	expanded uncertainty
V	volume, m^3
x	input quantity estimate
X	input quantity
y	output quantity estimate
Y	output quantity
W	resistance ratio, Ω/Ω
α	thermal expansion coefficient, K^{-1}
μ	mean
ρ	density, kg m^{-3}
v	degrees of freedom
σ	standard deviation

Subscripts and superscripts

1	titanium sinker
2	silicon sinker
eff	effective degrees of freedom
i,j	input quantity numbers
n	number of independent repeated observations
N	total number of input quantities
std	standard resistance
probe	temperature probe resistance
S	sinker
Sf	sinker immersed in fluid
S0	sinker under vacuum
0	sinker volume calibration reference state

magnetic coupling, developed by Gast [4] and improved by Lösch et al. [5,6], and to the application of Archimedes' principle as a differential method, which allows many of the disturbing side effects due to buoyant forces, surface-tension forces and gas adsorption to be avoided. The single sinker densimeter was developed by Brachthäuser et al. [7,8] in the early 1990s with the aim of simplifying the complex design of the two sinker densimeter. This new densimeter, with only one sinker, avoided the use of a sinker-changing device resulting in the reduction of the complexity of the measurement process. This simplified design led to slightly higher uncertainties in density measurement, especially at low densities, since side effects such as gas adsorption on the sinker surface were not compensated. However, the still high accuracy of this densimeter consolidates it, together with the two sinker densimeter, as state of the art methods in density measurement. A more detailed comparison between both densimeters is given by Wagner and Kleinrahm in [2].

The original version of the single sinker densimeter was improved by Klimeck [9] and Klimeck et al. [10]. Several compact versions of the single sinker densimeter, which unified the coupling housing and the measuring cell, were also developed. Following this last version of the densimeter, a compact version for gases was assembled at our laboratory in 1996 and is described by Chamorro et al. in [11].

In this paper, the improvement of the measurement uncertainty of our single sinker densimeter by performing several modifications based on the state point uncertainty analysis is presented.

In the first place the state point measurement uncertainty, consisting of the temperature, pressure and density measurement uncertainties, was evaluated over the whole temperature, pressure and density working ranges. Based on this estimation, several modifications were performed on the densimeter in order to reduce the main uncertainty sources of each state point magnitude and consequently improve their measurement uncertainties. The reduction in the uncertainty achieved on each magnitude was evaluated and the calculus was validated with a set of test density measurements on nitrogen.

2. Measurement principle

The single sinker densimeter with magnetic suspension coupling analyzed in this work was especially designed for density measurements of pure gases and gaseous mixtures. As mentioned above, it is based on Archimedes' Principle by which the buoyancy force acting on the sinker immersed in the fluid is proportional to the density of the fluid. Fig. 1 shows a simplified scheme of the measuring cell.

The cell thermostatization was achieved through two independent systems. Firstly, the oil from a thermostatic bath (Julabo MV FP50) flowed through a steal cylinder surroundings the cell. Secondly, for a more accurate temperature control, a temperature controller (Julabo MC-E) heated the fluid through an electric resistance in direct contact with the cell.

The main advantage of this densimeter is that the sinker mass is measured by means of the magnetic suspension coupling between the balance hook and the sinker support. Therefore, the cell where the gas is injected is separated from the balance, allowing very accurate measurements to be performed within a wide range of pressure and temperature. Our single sinker densimeter operates in the temperature range 250–400 K, pressures up to 20 MPa and densities up to 2000 kg m^{-3}.

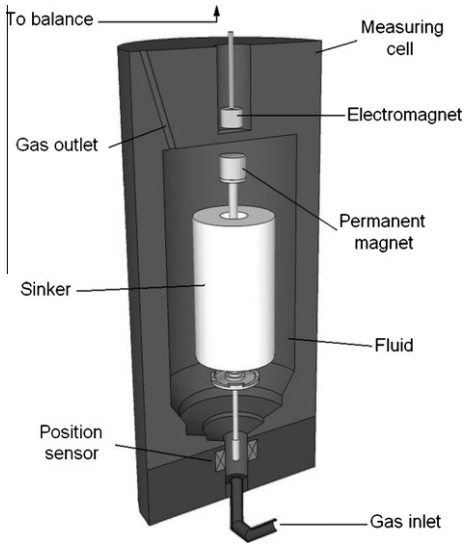

Fig. 1. Schematic view of the single sinker densimeter with magnetic suspension coupling measuring cell.

The density of the fluid surrounding the sinker is calculated with following equation

$$\rho = (m_{S0} - m_{Sf})/V_s(T, p), \tag{1}$$

where $(m_{s0} - m_{sf})$ refers to the buoyancy force, in kg, calculated as the difference between the sinker mass in a vacuum and the sinker mass in the fluid, and $V_S(T, p)$ refers to the sinker volume, in m^3, as a function of the fluid temperature and pressure. This density is associated to the corresponding measured temperature and pressure to define a (p, ρ, T) state point. Density measurements performed for this work were carried out by measuring isotherms, beginning with gas pressures of 20 MPa and reducing it through several pressure steps to 1 MPa. Each pressure step consisted of 30 (p, ρ, T) state point data. The sinker mass in a vacuum was measured with the evacuated measuring cell at the end of each isotherm. Thus the force transmission error of the magnetic coupling induced by the temperature is almost totally compensated for, as reported by McLinden, Kleinrahm and Wagner in [12].

As no significant modifications had been carried out on our single sinker densimeter since its final assembly at our laboratory, an improvement of the whole setup was considered. In order to avoid unnecessary modifications, the main uncertainty sources were determined. In this analysis, the individual contributions to the state point measurement uncertainty were carefully studied in order to act only on the main uncertainty sources. Thus, the improvement process of the setup was optimized, avoiding unnecessary changes or extra costs.

3. Uncertainty calculations

As the starting point of the uncertainty based optimization, the state point measurement uncertainty of the single sinker densimeter, consisting of the vector (p, ρ, T), was evaluated following the law of propagation of uncertainties (GUM) [13].

The uncertainty, as defined in [14], is a "non-negative parameter characterizing the dispersion of the quantity values being attributed to a measurand, based on the information used". The law of propagation of uncertainties (GUM) provides a framework for assessing uncertainty depending on the nature of the measurand and measurement.

The measurand is expressed as an output quantity Y which is expressed as a model function f of several input quantities X_i ($i = 1, 2, \ldots, N$). This model function f represents the measurement procedure and the evaluation method.

Thus, the output estimation y can be calculated by using estimates x_i for each input quantity as shown in following equation.

$$y = f(x_1, x_2, \ldots, x_N). \tag{2}$$

The standard measurement uncertainties of these input estimates are evaluated according to the "Type A" or "Type B" procedure. "Type A" uncertainties are evaluated through statistical methods as standard deviations of the mean of a series of independent observations. "Type B" uncertainties can be obtained from manufacturers' specifications, calibration reports, data taken from handbooks, previous measurement data and scientific experience and knowledge.

The combined uncertainty of the output estimate $u(y)$ is given by following equation.

$$u^2(y) = \sum_{i=1}^{N} \left(\frac{\partial f}{\partial x_i} u(x_i)\right)^2 + 2 \sum_{i=1}^{N-1} \times \sum_{k=i+1}^{N} \left(\frac{\partial f}{\partial x_i} u(x_i)\right)\left(\frac{\partial f}{\partial x_k} u(x_k)\right) r(x_i, x_k). \tag{3}$$

Here, $u(x_i)$ and $u(x_k)$ are the standard uncertainties of the input estimates and $r(x_i, x_k)$ is the correlation coefficient, which is zero for independent input quantities and varies between -1 and 1 for correlated input quantities. This correlation coefficient can be calculated by using following equation.

$$r(x_i, x_k) = \frac{s(x_i, x_k)}{s(x_i)s(x_k)}. \tag{4}$$

Here, $s(x_i)$ and $s(x_k)$ are standard deviations of estimates x_i and x_k, and $s(x_i, x_k)$ is the estimated covariance associated with x_i and x_k.

Finally, the expanded uncertainty of the output estimate $U(y)$ can be calculated by multiplying the coverage factor k by the combined uncertainty $u(y)$ of the output estimate: $U(y) = k \cdot u(y)$. The value of the coverage factor k depends directly on the effective degrees of freedom v_{eff}. When $v_{eff} > 50$ a value of $k = 2$ yields a coverage probability of the expanded uncertainty of 95.45%. The degrees of freedom, which determine the reliability of the standard uncertainty assigned to the output estimate, can be obtained based on the Welch-Satterhwaite formula [15] shown in following equation.

$$v_{eff} = \frac{u^4(y)}{\sum_{i=1}^{N} \frac{u_i^4(y)}{v_i}}. \tag{5}$$

Here, v_i refers to the degrees of freedom of each input quantity standard uncertainty and, in the case of magnitudes estimated as the arithmetic mean of a series of n independent observations, it is obtained as the number of independent observations minus 1, $n-1$.

It is a common practice [16], to make the presentation of the output function uncertainty easier, to sum the constant terms and the proportional terms separately when the standard uncertainties associated with some of the input quantities are proportional to the output quantity itself. The uncertainty value calculated with this approximation is always slightly higher than the combined uncertainty value so that the approximation does not reduce the real value of the uncertainty. This approximation was applied to the presentation of pressure and density uncertainty results.

To evaluate Type A uncertainty terms from statistical values, such as repeatability, test density measurements on nitrogen were performed on the densimeter. These test density measurements consisted of seven isotherms between 250 K and 400 K, pressures up to 20 MPa and densities up to 270 kg m^{-3}.

The International System of Units (SI) was followed in the whole uncertainty evaluation though pressure was expressed in MPa, for clarity.

3.1. Uncertainty on temperature measurements

The temperature of the cell was determined with a PRT-25 probe (Rosemount 162D) placed at the middle height of the measuring cell and an AC comparator resistance bridge (Automatic Systems Laboratory model F700) to which several temperature probes can be connected thanks to a Multichannel Switchbox (Automatic Systems Laboratory model SB148/01). The bridge measures the resistance ratio W, in Ω/Ω, between the PRT-25 probe and the standard resistor, as indicated in following equation.

$$W = R_{probe}/R_{std}. \tag{6}$$

The internal resistor of the bridge, with a value of R_{std} = 100.00312 ± 0.00030 Ω, was used as the standard resistor. Thus, temperature values of the probe could be obtained following the International Temperature Scale of 1990 [17] with the ratio W.

Calibration uncertainty of the Rosemount probe was determined at our own calibration facility (accredited by ENAC, a member of EA), for different temperature fixed points presented in Table 1, together with the PRT-25 drift.

Main uncertainty sources for the temperature measurement uncertainty came from the probe calibration, the resistance bridge, the uniformity and repeatability of the cell temperature, and the drift. The temperature uncertainty budget presented in Table 2 contains all the significant contributions to the overall uncertainty in temperature.

Each state point temperature was taken as the average of the last ten temperature values of each pressure step. The calibration uncertainty was taken as the maximum value of Table 1 in the working range 250–400 K. Repeatability, regarded as a Type A term, was estimated as the standard deviation of the mean of the used measurement values. Due to the impossibility of measuring the temperature in different points of the same cell in the initial state of the apparatus, temperature uniformity, regarded as Type B, was estimated as the maximum temperature gradient between the selected temperature values. The drift, also Type B, was taken from Table 1. The calibration uncertainty of the bridge was obtained, as expressed in Eq. (7), through the uncertainties propagation law, as expressed in Eq. (3), and taking Eq. (6) as the mathematical model.

$$u(R_{probe}) = R_{std} \cdot u(W) + W \cdot u(R_{std}). \tag{7}$$

The calibration uncertainty of the bridge $u(W)$, given by the manufacturer, was of 1×10^{-6} Ω/Ω and included the effect from the resolution and the noise.

The number of effective degrees of freedom of the temperature was determined to be 400, following Eq. (5).

3.2. Uncertainty on pressure measurements

In the initial state of the densimeter, pressure was measured by an absolute pressure transducer (Paroscientific 43KR-HHT-101) for the range 0–20 MPa, which was

Table 1
Rosemount PRT-25 probe calibration uncertainty and drift.

Probe	Calibration expanded uncertainty (K) (k = 2)				Drift (K)
	505.077 K	429.748 K	302.913 K	234.317 K	
Rosemount	6×10^{-3}	6×10^{-3}	6×10^{-3}	4×10^{-3}	2×10^{-3}

Table 2
Uncertainty budget for temperature measurement with the Rosemount PRT-25 probe, for a measuring cell temperature of 400 K.

Uncertainty component	Units	Estimation	Standard uncertainty	Distribution	Type	Sensitivity coefficient	Divisor	Contribution
PRT calibration uncertainty	K	0	3.0×10^{-3}	Gaussian	B	1	1	3.0×10^{-3}
Temperature reading	Ω	0	7.2×10^{-5}	Gaussian	B	10.5	1	7.6×10^{-4}
Repeatability	K	0	9.5×10^{-4}	Gaussian	A	1	1	9.5×10^{-4}
Uniformity	K	0	4.0×10^{-3}	Uniform	B	1	$2\sqrt{3}$	1.2×10^{-3}
Drift	K	0	1.0×10^{-3}	Uniform	B	1	$\sqrt{3}$	5.8×10^{-4}
					Standard uncertainty (K)			3.5×10^{-3}
					Expanded uncertainty (K) (k = 2)			7.0×10^{-3}

Table 3
Calibration uncertainty of the 20 MPa pressure transducer.

Uncertainty sources	Units	Estimation	Standard uncertainty	Distribution	Type	Sensitivity coefficient	Divisor	Contribution (MPa)
Calibration system	MPa	0	$7.5 \times 10^{-5}p$	Gaussian	A	1	2	$3.8 \times 10^{-5}p$
Repeatability	MPa	0	1.73×10^{-3}	Gaussian	A	1	1	1.73×10^{-3}
Stability	MPa	0	3.30×10^{-4}	Uniform	B	1	$\sqrt{3}$	1.91×10^{-4}
Resolution	MPa	0	1.0×10^{-4}	Uniform	B	1	$2\sqrt{3}$	2.9×10^{-5}
					Standard uncertainty (MPa)			$3.8 \times 10^{-5}p + 1.74 \times 10^{-3}$
					Expanded uncertainty ($k = 2$) (MPa)			$7.5 \times 10^{-5}p + 3.49 \times 10^{-3}$

Table 4
Uncertainty budget for the pressure transducer measurement.

Uncertainty sources	Units	Estimation	Standard uncertainty	Distribution	Type	Sensitivity coefficient	Divisor	Contribution (MPa)
Transducer calibration	MPa	0	$38 \times 10^{-6}p + 1.74 \times 10^{-3}$	Gaussian	B	1	1	$38 \times 10^{-6}p + 1.74 \times 10^{-3}$
Resolution	MPa	0	1.0×10^{-5}	Uniform	B	1	$2\sqrt{3}$	2.89×10^{-6}
Repeatability	MPa	0	2.6×10^{-4}	Gaussian	A	1	1	2.6×10^{-4}
Drift	MPa	0	1.4×10^{-6}	Gaussian	B	1	$\sqrt{3}$	8.1×10^{-7}
					Standard uncertainty (MPa)			$38 \times 10^{-6}p + 1.76 \times 10^{-3}$
					Expanded uncertainty ($k = 2$) (MPa)			$75 \times 10^{-6}p + 3.52 \times 10^{-3}$

annually calibrated against a dead weight gauge at our own calibration facility (accredited by ENAC, a member of EA). Calibration uncertainty for this transducer is given in Table 3.

The pressure uncertainty in the whole working range (0–20 MPa) was evaluated. The main uncertainty sources for the pressure uncertainty were the transducer calibration, the repeatability, the apparatus resolution and the drift. Each state point pressure was taken as the average of the last ten values of each pressure step. The uncertainty budget for the pressure transducer measurement is shown in Table 4.

Calibration uncertainty was taken from the calibration certificates. Moreover the equipment drift uncertainty, also Type B, was obtained by comparing the two last calibrations budgets for the transducer. Repeatability was calculated as the standard deviation of the mean of the ten pressure values used for each step pressure value, so it is regarded as a Type A component. The number of degrees of freedom of pressure was calculated following Eq. (5) and its value was greater than 20,000 within the whole pressure range.

3.3. Uncertainty on density measurements

The uncertainty on density was estimated by taking Eq. (1) as the mathematical model and following the uncertainty propagation law as expressed in Eq. (3). The resulting uncertainty is presented in following equation.

$$u(\rho) = \frac{1}{V_S}\sqrt{u^2(m_{S0}) + u^2(m_{Sf}) + \rho^2 \cdot u^2(V_S)}. \quad (8)$$

As indicated at the beginning of this section, Eq. (8) was simplified to Eq. (9) in order to give a more readable value of the density uncertainty and to facilitate its comparison with the density uncertainties reported by other authors.

$$u(\rho) \approx \frac{1}{V_S}\left(\sqrt{u^2(m_{S0}) + u^2(m_{Sf})} + \rho \cdot u(V_S)\right). \quad (9)$$

As can be seen, the uncertainty in density depends directly on the mass reading and sinker volume uncertainties. The correlation term between the two mass input quantities does not appear here since the sinker mass in the fluid and in a vacuum are determined in independent experiments. To ensure this assumption, the correlation coefficient was calculated using Eq. (4) and the result was $r(m_{S0}, m_{Sf}) = -3 \times 10^{-5}$. The balance (Mettler Toledo AT261) calibration uncertainty was evaluated after its *in situ* calibration using two reference masses. These two masses are made of tantalum and titanium and have the same volume to compensate and eliminate the air buoyancy effect. The masses were especially designed to perform the calibration of this balance. Their mass was calibrated in the CEM resulting in $m_{Ta} = 82.09475 \pm 0.00010$ g and $m_{Ti} = 22.0397072 \pm 0.000070$ g.

The uncertainty budget for the mass reading, under a vacuum and in the fluid, is presented in Tables 5 and 6, respectively.

The repeatability term was obtained as the standard deviation of the mean of the last mass values of each pressure step. The sinker volume uncertainty was given by its calibration certificate from the CEM. The titanium sinker volume calibration value, given in the CEM certificate was $V_{S0} = 13.2648 \pm 0.0010\ \text{cm}^3$ (coverage factor $k = 2$). The sinker volume changes with temperature and pressure due to the titanium's thermal and mechanical properties. However, the influence of these magnitudes in the volume uncertainty is much lower than the main component, so the overall uncertainty in volume was taken as that given by the CEM. The number of degrees of freedom of the mass reading, in a vacuum and in the fluid, was determined to be 200 and 800, respectively, by using Eq. (5).

Table 5
Uncertainty budget for the mass reading when the measuring cell is evacuated.

Uncertainty sources	Units	Estimation	Standard uncertainty	Distribution	Type	Sensitivity coefficient	Divisor	Contribution
Balance calibration	kg	0	2.0×10^{-7}	Gaussian	B	1	1	2.0×10^{-7}
Balance resolution	kg	0	1.0×10^{-8}	Uniform	B	1	$2\sqrt{3}$	2.9×10^{-9}
Repeatability	kg	0	9.5×10^{-8}	Gaussian	A	1	1	9.5×10^{-8}
Drift	kg	0	1.0×10^{-7}	Gaussian	B	1	$\sqrt{3}$	5.8×10^{-8}
					Standard uncertainty (kg)			2.3×10^{-7}
					Expanded uncertainty ($k = 2$) (kg)			4.6×10^{-7}

Table 6
Uncertainty budget for the mass reading when the measuring cell is filled with gas.

Uncertainty sources	Units	Estimation	Standard uncertainty	Distribution	Type	Sensitivity coefficient	Divisor	Contribution
Balance calibration	kg	0	2.0×10^{-7}	Gaussian	B	1	1	2.0×10^{-7}
Balance resolution	kg	0	1.0×10^{-8}	Uniform	B	1	$2\sqrt{3}$	2.9×10^{-9}
Repeatability	kg	0	5.1×10^{-8}	Gaussian	A	1	1	5.1×10^{-8}
Drift	kg	0	1.0×10^{-7}	Gaussian	B	1	$\sqrt{3}$	5.8×10^{-8}
					Standard uncertainty (kg)			2.1×10^{-7}
					Expanded uncertainty ($k = 2$) (kg)			4.3×10^{-7}

Table 7
Budget estimated for the density uncertainty ($\rho = 271.5$ kg m^{-3}).

Uncertainty sources		Units	Estimation	Standard uncertainty	Sensitivity coefficient		Degrees of freedom	Contribution
$u(m_{S0})$	Mass vacuum	kg	1.90×10^{-3}	2.3×10^{-7}	$1/V_{S1}$	7.5×10^{4}	200	1.7×10^{-2}
$u(m_{Sf})$	Mass fluid	kg	-5.274×10^{-3}	2.1×10^{-7}	$1/V_{S1}$	7.5×10^{4}	800	1.6×10^{-2}
$u(V_S)$	Sinker volume	m^3	1.33×10^{-5}	5.0×10^{-10}	ρ/V_{S1}	2.0×10^{7}	∞	1.0×10^{-2}
					Standard uncertainty (kg m^{-3})			2.6×10^{-2}
					Expanded uncertainty ($k = 2$) (kg m^{-3})			5.1×10^{-2}

Table 7 shows the budget estimated for the density uncertainty given in detail for one density $\rho = 271.5$ kg m^{-3}. The density expanded uncertainty ($k = 2$) as a function of the density was estimated to be $U(\rho) = 4.7 \times 10^{-2} + 7.6 \times 10^{-5}\rho$, with 2000 degrees of freedom.

4. Improvements proposal based on uncertainty analysis

Individual contributions to the measurement uncertainty of each state point magnitude were analyzed. Therefore, modifications on the setup could be focused to reduce the main uncertainty sources for each magnitude.

Regarding the temperature measurement uncertainty, Fig. 2 shows the percentage contributions of each term.

As can be seen, the most important sources for temperature are due to the probe calibration uncertainty and to the temperature repeatability and uniformity. To reduce these terms, it was proposed that the existing Rosemount probe should be relocated and that two Minco probes with lower calibration uncertainty, placed diametrically opposed at the middle height of the measuring cell, should be added. Thus, the fluid temperature could be obtained as the average of the two readings.

Fig. 3 shows the individual percentage contributions to the pressure uncertainty for three different pressures. The main uncertainty source arises from the transducer calibration, representing up to 97% of the total at low

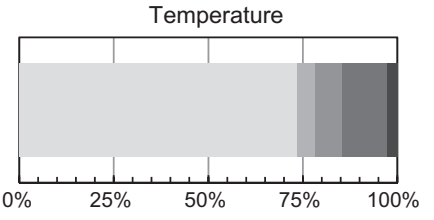

Fig. 2. Individual contributions to the temperature uncertainty: probe calibration; temperature reading; repeatability; uniformity, drift.

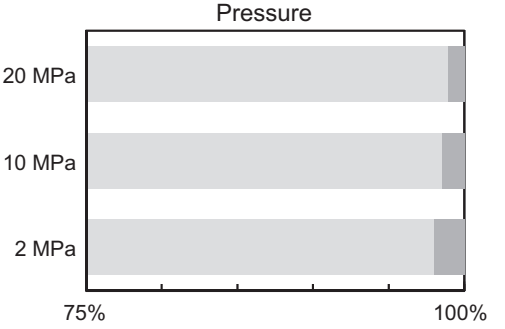

Fig. 3. Individual contributions to the pressure uncertainty: transducer calibration; repeatability.

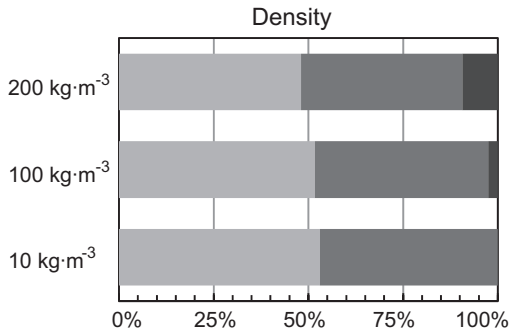

Fig. 4. Individual contributions to the density uncertainty: sinker mass in a vacuum; sinker mass in the fluid; sinker volume.

pressures. The second uncertainty source comes from the repeatability.

Both main terms could be reduced by replacing the pressure transducer by a more accurate one. However, even if a new transducer for the whole 20 MPa range was to be installed, the accuracy of the pressure measurements would decrease at pressures below 2 MPa (10% of the whole apparatus range, as stated by the manufacturer). Therefore, it was decided to keep this instrument and add a new pressure transducer (Paroscientific 2300A-101) for the range 0–2 MPa. Thus, pressure in the range 2–20 MPa could be measured with the old transducer.

Finally, Fig. 4 shows how the uncertainty sources of the density affected the uncertainty value for three different densities. As presented, the main uncertainty source arose from the sinker mass reading in a vacuum, followed by the sinker mass reading in the fluid, accounting for approximately 54% and 45% respectively for a density value of $\rho = 10$ kg m^{-3}. The sinker volume uncertainty is significant only at higher densities, accounting for less than 10% for a density value of $\rho = 200$ kg m^{-3}.

This distribution suggested the importance of improving the balance reading. The option of replacing the balance by a new one, with a higher resolution, was rejected because it also involved major changes in the whole setup, even in the measuring cell design. Therefore, the replacement of the sinker by a bigger one appeared to be a simpler solution with a similar effect to the increase in the balance resolution. Thus, the old titanium sinker ($m_s \approx 60$ g, $V_S \approx 13$ cm^3) could be substituted by a new silicon sinker ($m_s \approx 60$ g, $V_S \approx 26$ cm^3), as there was enough space for it inside the measuring cell. This silicon sinker, with double volume and equal mass, experiments a double buoyancy force under the same fluid pressure and temperature conditions. Thus, the change in the sinker mass due to the buoyancy effect can be measured by the balance more accurately, as if the balance resolution was higher. Moreover, this change affects directly the sensitivity coefficients of the density uncertainty budget which result in a decrease of all uncertainty contributions. With this new sinker the accuracy of measurements at low densities is higher.

To summarize, in order to improve the state point uncertainty, the following proposed modifications were performed on our single sinker densimeter.

- Two PRT-25 probes were added to improve the temperature measurement uncertainty.
- A new pressure transducer for the range 0–2 MPa was added to increase the accuracy of pressure measurement at low pressures.
- The titanium sinker was replaced by a silicon sinker to reduce the uncertainty of the balance reading and thus the uncertainty on density.

5. Results with the modified experimental setup

The proposed improvements were carried out. State measurement uncertainty was then evaluated following the uncertainties propagation law [13] and validated with a Monte Carlo simulation [18]. Results were compared with those obtained in the previous estimation in order to study the uncertainty reduction achieved.

5.1. Evaluation of the new state point expanded measurement uncertainty

5.1.1. Temperature measurement uncertainty

Two PRT-25 probes (Minco S1059PJ5X6) were placed diametrically opposed at the middle height of the measuring cell. Both probes were calibrated at our own calibration facility (accredited by ENAC, a member of EA) between 234.317 K and 505.077 K. Data from the calibration certificate, together with the PRT-25 drift, are shown in Table 8.

The original PRT-25 (Rosemount) probe was maintained, but relocated in the upper section of the measuring cell in order to study whether temperature gradients existed in the cell or not. The location of the three PRT-25 probes is shown in Fig. 5.

Moreover, the internal standard resistor of the bridge was replaced by an external standard calibrated resistor (Tinsley model 5685A, 25Ω) whose value was $R_{std} = 24.999800 \pm 0.000075\ \Omega$. This modification avoided the additional intermediate step consisting of calibrating the internal resistor by using the external resistor. The temperature uncertainty budget with the new layout is presented in Table 9. Each state point temperature was taken as the average between the two Minco probe values, in turn calculated as the average between the last ten temperature values of each pressure step. The calibration uncertainty was taken from Table 8as the value corresponding to the mentioned probes in the working range 250–400 K. The repeatability was estimated as the standard deviation of the mean of the measurement values and the temperature uniformity was taken as the maximum temperature gradient between the two probe values. The drift was taken from Table 8. The calibration uncertainty of the bridge was recalculated following Eq. (7) with the value of the new standard external resistor. The effective degrees of freedom of the temperature were determined to be 200 following Eq. (5).

5.1.2. Pressure measurement uncertainty

The new absolute pressure transducer for the range 0–2 MPa was added with the objective of increasing the accuracy in the low pressure range. It was calibrated against an

Table 8
Calibration uncertainty and drift of the new PRT-25 probes.

Probe	Calibration expanded uncertainty (K) ($k = 2$)				Drift (K)
	505.077 K	429.748 K	302.913 K	234.317 K	
Minco 712	6×10^{-3}	5×10^{-3}	4×10^{-3}	4×10^{-3}	2×10^{-3}
Minco 713	6×10^{-3}	5×10^{-3}	4×10^{-3}	4×10^{-3}	2×10^{-3}

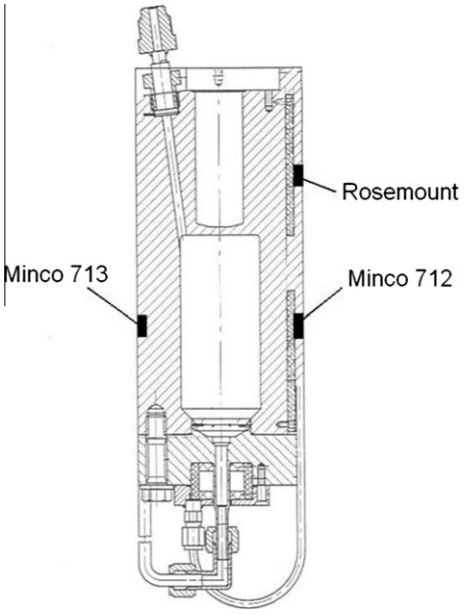

Fig. 5. Location of the PRT-25 probes in the cell.

absolute dead weight gauge and results from the certificate are shown in Table 10.

The uncertainty on pressure measurements in the working range (0–2 MPa) was evaluated and the uncertainty budget is shown in Table 11.

The main sources of pressure uncertainty came from the transducer calibration, the apparatus resolution, the repeatability and the device drift. Each state point pressure was taken as the average of the last ten values of each pressure step. Repeatability was obtained as the standard deviation of the mean of the last ten pressure values of each pressure step (Type A variable). Calibration uncertainty, from Table 10, and the resolution term were regarded as Type B terms. Drift, also Type B, was estimated from two consecutive calibrations. The number of degrees of freedom of pressure was calculated following Eq. (5) and its value was greater than 200 within the whole pressure range.

5.1.3. Density measurement uncertainty

The uncertainty on density was calculated following Eq. (8). The balance reading uncertainty, under a vacuum and in the fluid was again evaluated. The new silicon sinker volume, calibrated at CEM, was $V_{S0} = 26.444 \pm 0.003$ cm^3 ($k = 2$), at ambient conditions. This silicon sinker, with a

Table 9
Uncertainty budget for temperature measurement, for a measuring cell temperature of 400 K.

Uncertainty component	Units	Estimation	Standard uncertainty	Distribution	Type	Sensitivity coefficient	Divisor	Contribution
Minco 712 calibration uncertainty	K	0	2.0×10^{-3}	Gaussian	B	0.5	1	1.0×10^{-3}
Minco 713 calibration uncertainty	K	0	2.0×10^{-3}	Gaussian	B	0.5	1	1.0×10^{-3}
Temperature reading	Ω	0	6.7×10^{-5}	Gaussian	B	10.5	1	7.0×10^{-4}
Repeatability	K	0	6.3×10^{-4}	Gaussian	A	1	1	6.3×10^{-4}
Uniformity	K	0	2.5×10^{-3}	Uniform	B	1	$2\sqrt{3}$	7.2×10^{-4}
Drift	K	0	1.0×10^{-3}	Uniform	B	1	$\sqrt{3}$	5.8×10^{-4}
						Standard uncertainty (K)		1.9×10^{-3}
						Expanded uncertainty (K) ($k = 2$)		3.9×10^{-3}

Table 10
Calibration uncertainty for the 2 MPa pressure transducer.

Uncertainty sources	Units	Estimation	Standard uncertainty	Distribution	Type	Sensitivity coefficient	Divisor	Contribution (MPa)
Calibration system	MPa	0	$6.0 \times 10^{-5}p$	Gaussian	A	1	2	$3.0 \times 10^{-5}p$
Repeatability	MPa	0	4.9×10^{-5}	Gaussian	A	1	1	4.9×10^{-5}
Stability	MPa	0	3.6×10^{-5}	Uniform	B	1	$\sqrt{3}$	2.1×10^{-5}
Resolution	MPa	0	1.0×10^{-6}	Uniform	B	1	$2\sqrt{3}$	2.9×10^{-7}
						Standard uncertainty (MPa)		$3.0 \times 10^{-5}p + 5.32 \times 10^{-5}$
						Expanded uncertainty ($k = 2$) (MPa)		$6.0 \times 10^{-5}p + 1.06 \times 10^{-4}$

Table 11
Uncertainty budget for the 2 MPa pressure transducer measurement.

Uncertainty sources	Units	Estimation	Standard uncertainty	Distribution	Type	Sensitivity coefficient	Divisor	Contribution (MPa)
Transducer calibration	MPa	0	$3.0 \times 10^{-5}p + 5.32 \times 10^{-5}$	Gaussian	B	1	1	$3.0 \times 10^{-5}p + 5.32 \times 10^{-5}$
Resolution	MPa	0	1.0×10^{-6}	Uniform	B	1	$2\sqrt{3}$	2.89×10^{-7}
Repeatability	MPa	0	7.0×10^{-5}	Gaussian	A	1	1	7.0×10^{-5}
Drift	MPa	0	2.4×10^{-5}	Gaussian	B	1	$\sqrt{3}$	1.4×10^{-5}
					Standard uncertainty (MPa)			$3.0 \times 10^{-5}p + 8.9 \times 10^{-5}$
					Expanded uncertainty ($k = 2$) (MPa)			$6.0 \times 10^{-5}p + 1.8 \times 10^{-4}$

bigger volume, affected the repeatability term, which was obtained as the standard deviation of the mean of the last mass values of each pressure step, but also to the sensitivity coefficients. However the reduction in repeatability affected only slightly to the total mass uncertainty since repeatability was not a dominant contribution. The uncertainty budget for the mass reading, under a vacuum and in the fluid, is presented in Tables 12 and 13, respectively.

The number of degrees of freedom of the mass reading, in a vacuum and in the fluid, was determined to be 500 and 1200, respectively, by using Eq. (5).

Finally, Table 14 shows the new density uncertainty budget, given in detail for one density $\rho = 247.1\ \mathrm{kg\ m^{-3}}$. The density expanded uncertainty ($k = 2$) as a function of the density was estimated to be $U(\rho) = 2.3 \times 10^{-2} + 1.1 \times 10^{-4}\rho$, with 1600 degrees of freedom. As can be appreciated, the uncertainty of the new sinker volume is higher than the uncertainty of the old titanium sinker. However, since this value affects the term which is proportional to the density this increase would only be significant at very high densities.

5.2. Validation of the uncertainty estimation with the Monte Carlo method

In order to validate the previous density uncertainty evaluation, a Monte Carlo simulation for the determination of the density uncertainty after the modifications was performed. In this case, the sinker volume was calculated as a function of the fluid temperature and pressure to prove the previous hypothesis that fluid conditions did not significantly affect the volume uncertainty. The change in the sinker volume induced by the temperature and pressure of the surrounding fluid can be calculated through the equations of Lamé–Hooke, which characterize the behavior of linear elastic isotropic solids. Thus, the sinker volume can be determined by using following equation [19]

Table 12
Uncertainty budget for the mass reading when the measuring cell is evacuated.

Uncertainty sources	Units	Estimation	Standard uncertainty	Distribution	Type	Sensitivity coefficient	Divisor	Contribution
Balance calibration	kg	0	2.0×10^{-7}	Gaussian	B	1	1	2.0×10^{-7}
Balance resolution	kg	0	1.0×10^{-8}	Uniform	B	1	$2\sqrt{3}$	2.9×10^{-9}
Repeatability	kg	0	8.0×10^{-8}	Gaussian	A	1	1	8.0×10^{-8}
Drift	kg	0	1.0×10^{-7}	Gaussian	B	1	$\sqrt{3}$	5.8×10^{-8}
					Standard uncertainty (kg)			2.2×10^{-7}
					Expanded uncertainty ($k = 2$) (kg)			4.5×10^{-7}

Table 13
Uncertainty budget for the mass reading when the measuring cell is filled with gas.

Uncertainty sources	Units	Estimation	Standard uncertainty	Distribution	Type	Sensitivity coefficient	Divisor	Contribution
Balance calibration	kg	0	2.0×10^{-7}	Gaussian	B	1	1	2.0×10^{-7}
Balance resolution	kg	0	1.0×10^{-8}	Uniform	B	1	$2\sqrt{3}$	2.9×10^{-9}
Repeatability	kg	0	3.0×10^{-8}	Gaussian	A	1	1	3.0×10^{-8}
Drift	kg	0	1.0×10^{-7}	Gaussian	B	1	$\sqrt{3}$	5.8×10^{-8}
					Standard uncertainty (kg)			2.1×10^{-7}
					Expanded uncertainty ($k = 2$) (kg)			4.2×10^{-7}

Table 14
Budget estimated for the density uncertainty ($\rho = 247.1\ \mathrm{kg\ m^{-3}}$).

Uncertainty sources		Units	Estimation	Standard uncertainty	Sensitivity coefficient		Degrees freedom	Contribution
$u(m_{S0})$	Mass vacuum	kg	1.90×10^{-3}	2.2×10^{-7}	$1/V_{S2}$	3.8×10^{4}	500	8.4×10^{-3}
$u(m_{Sf})$	Mass fluid	kg	-5.27×10^{-3}	2.1×10^{-7}	$1/V_{S2}$	3.8×10^{4}	1200	8.0×10^{-3}
$u(V_S)$	Sinker volume	$\mathrm{m^3}$	2.64×10^{-5}	1.5×10^{-9}	ρ/V_{S2}	9.4×10^{6}	∞	1.4×10^{-2}
					Standard uncertainty ($\mathrm{kg\ m^{-3}}$)			1.8×10^{-2}
					Expanded uncertainty ($k = 2$) ($\mathrm{kg\ m^{-3}}$)			3.6×10^{-2}

Table 15
Assigned probability density functions for input variables in the simulation model.

X_i	Variable	Units	PDF	Parameters	
				Estimation	Standard uncertainty
m_0	Sinker mass in vacuum	kg	Gaussian	$\mu_{m0}(T)$	$u(m_0)$
m_{Sf}	Sinker mass immersed	kg	Gaussian	$\mu_{mf}(T, p)$	$u(m_f)$
V_{S0}	Sinker calibration volume	m^3	Gaussian	26.444×10^{-6}	1.5×10^{-9}
$\alpha(T)$	Silicon thermal expansion coefficient	K^{-1}	Uniform	$\mu_\alpha(T)$	±0.5% [21,22]
T	Fluid temperature	K	Gaussian	$\mu_T(T)$	$u(T)$
T_0	Reference state temperature	K	Uniform	294.45	0.15
p	Fluid pressure	MPa	Gaussian	$\mu_p(p)$	$u(p)$
p_0	Reference state pressure	MPa	Uniform	0.093417	3×10^{-6}
$K(T)$	Silicon compressibility modulus	MPa^{-1}	Uniform	$\mu_K(T)$	±0.02% [20]

$$V_S(T,p) = V_{S0}\left(1 + 3\alpha(T)(T - T_0) - \frac{p - p_0}{K(T)}\right). \quad (10)$$

Here, V_{S0} is the sinker volume calibration value in m^3, $\alpha(T)$ the thermal expansion coefficient as a function of temperature in K^{-1}, $K(T)$ the compressibility modulus as a function of temperature in MPa^{-1} and T_0 and p_0 the reference state temperature and pressure in K and MPa. Since silicon is an anisotropic mechanical material, the compressibility modulus was calculated from average elastic constants reported by Landolt-Börnstein [20].

Assignment of probability density functions (PDF) to the input quantities are given in Table 15, where the description of all variables which appear in Eq. (10) is given. Estimations of the sinker mass, in a vacuum and in the fluid, were taken as the average values for each temperature and pressure of the test measurements. Silicon properties, $\alpha(T)$ and $K(T)$, were calculated for each temperature value and sinker volume V_{S0} and the reference state temperature and pressure were taken from the calibration certificate. Standard deviations for each magnitude were taken both from calibration certificates, from the literature and from our own uncertainty evaluation.

The Monte Carlo model was run for 50,000 steps for three different isotherms (250, 325 and 400 K) and three pressure values (2, 10, 20 MPa) for nitrogen, resulting in 450,000 simulated observations. It was clear from obtained data that the maximum relative difference between the lower expanded uncertainty limit, calculated with the GUM and the Monte Carlo simulation, occurred at 400 K and 2 MPa and was of 0.01%. Table 16 shows the comparison of the two evaluation methods for density at 400 K and 2 MPa. Results for the other simulations showed an even better agreement. The coverage factor was chosen for a 95.45% coverage probability of the expanded uncertainty. The output PDF for density, determined by Monte Carlo simulation at 400 K and 2 MPa, is illustrated in Fig. 6.

Table 16
Comparison of the results for nitrogen density using GUM and Monte Carlo simulation at 400 K and 2 MPa.

	GUM	Monte Carlo
Mean ($kg\,m^{-3}$)	16.7002	16.6997
Combined uncertainty ($kg\,m^{-3}$)	0.0110	0.0126
Expanded uncertainty ($kg\,m^{-3}$)	0.0220	0.0242
Coverage factor (k)	2.00	2.00

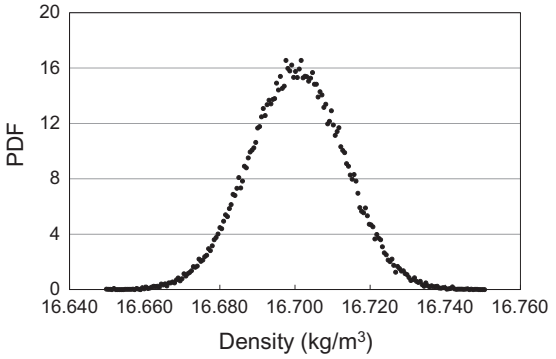

Fig. 6. Output PDF for density at 400 K and 2 MPa.

Thus, two conclusions are extracted from this analysis. In the first place, it is demonstrated that fluid temperature and pressure do not affect the overall sinker volume uncertainty. Secondly, the Monte Carlo simulation validates the application of the GUM methodology and tests the previous uncertainty estimation.

5.3. Experimental testing of the modified technique

Finally, a set of density measurements on nitrogen was performed in the range 250 K–400 K and pressures up to 20 MPa in order to validate the modified technique. Fig. 7

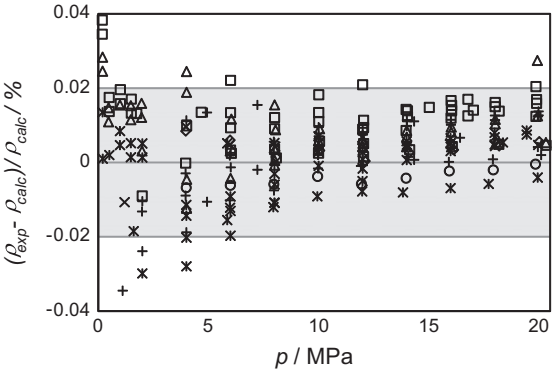

Fig. 7. Relative density deviations of experimental (p, ρ, T) data, between 250 K and 400 K, from the equation of state for nitrogen of Span et al. [23,24]: □ 250 K; ◇ 275 K; Δ 300 K; × 325 K; + 350 K; ○ 375 K; ∗ 400 K.

illustrates the relative deviation in density of the experimental values from the reference equation of state for nitrogen of Span et al. [23,24].

As can be seen, experimental density data shows a good agreement with the calculated values within the uncertainties claimed for the equation of state for nitrogen below 20 MPa.

6. Discussion

Results extracted from the uncertainty evaluation for the single sinker densimeter operation following the ISO approach, before and after the modifications on the setup were carried out, are summarized in Table 17.

Temperature measurement uncertainty dramatically decreased by 44 % from an initial value of $U(T) = 7.0 \times 10^{-3}$ K. This reduction was mainly due to two facts: the calculation of temperature as the average from the measured values of two probes and the lower calibration uncertainty of these two new probes.

Pressure in the low pressure range was also significantly reduced by more than 92%. On this basis the uncertainty of pressure at 2 MPa before the modifications was of 3.7×10^{-3} MPa and now it is of 2.4×10^{-4} MPa. The great importance of this reduction was that it also contributed to compensating for the bigger mass uncertainty for low gas densities. The addition of the new low pressure transducer also contributed to correcting the calibration curve of the 20 MPa transducer for a more accurate measurement.

Fig. 8 shows the reduction in percentage of density uncertainty from the starting point of this work as a function of measured density.

Density measurement uncertainty was reduced by more than 22% due to the change of the cell sinker. This reduction is near 50% at low densities. According to this calculation, the initial uncertainty of density of 0.048 kg m^{-3}, for a density value of 10 kg m^{-3}, was reduced to a value of 0.025 kg m^{-3} for the same density value after the modifications. This change directly affected the sensitivity coefficient of the volume and mass components. Moreover, the change of the sinker indirectly affects the mass components through the mass reading repeatability term.

Regarding the density uncertainty components, Fig. 9 shows the contribution in percentage of each term to the uncertainty in density for three different densities within the working range.

As compared to Fig. 4, it can be seen that, once the improvements were executed, the percentage contribution of each term to the total uncertainty on density changed. For low densities the main contributions still come from the sinker mass in a vacuum and in the fluid. Nevertheless, at high densities the main input now comes from the sinker volume, accounting for 40% of the total uncertainty. Based on this new distribution the reduction of the sinker volume calibration uncertainty would affect only at high densities.

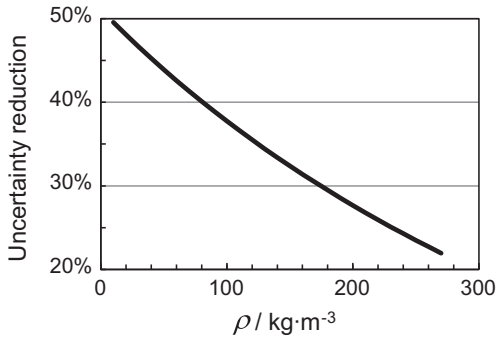

Fig. 8. Percentage reduction of density uncertainty as a function of fluid density.

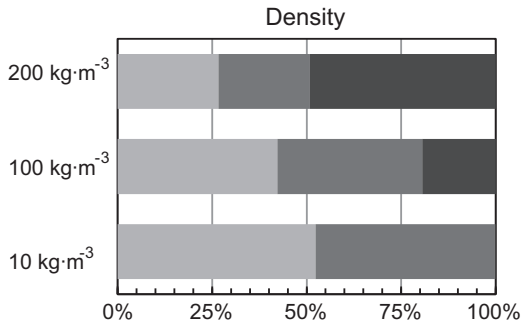

Fig. 9. Percentage contribution of each state density uncertainty component. Sinker mass in a vacuum; sinker mass when it is immersed in a fluid; sinker volume.

The total state point uncertainties for different densimeters based on a similar measurement technique are collected in Table 18 for comparison with those evaluated in this work. Uncertainties in density are given for a density range corresponding to that of nitrogen in the temperature and pressure working ranges of the apparatus described in this work.

As expected, the estimated uncertainty for each magnitude is of the same order as those reported by other authors for similar apparatus. It can be observed, for some cases, that the wider the working apparatus range, the higher the uncertainties are. However, uncertainty in density reported by McLinden [25] keeps relatively low due to the fact that the two sinker densimeter is more accurate than single sinker densimeters, as stated in [2].

Table 17
Summary of the state point expanded measurement uncertainty before and after the modifications were carried out ($k = 2$).

Magnitude		Units	Before	After
T	Temperature	K	7.0×10^{-3}	3.9×10^{-3}
p	Pressure 2–20 MPa	MPa	$3.52 \times 10^{-3} + 7.5 \times 10^{-5} p$	$3.52 \times 10^{-3} + 7.5 \times 10^{-5} p$
p	Pressure 0–2 MPa	MPa	$3.52 \times 10^{-3} + 7.5 \times 10^{-5} p$	$1.8 \times 10^{-4} + 6.0 \times 10^{-5} p$
ρ	Density	kg m^{-3}	$4.7 \times 10^{-2} + 7.6 \times 10^{-5} \rho$	$2.3 \times 10^{-2} + 1.1 \times 10^{-4} \rho$

Table 18
Measuring expanded uncertainty for different densimeters (coverage factor $k = 2$).

Reference	Year	Densimeter type	Working range		$U(T)$ (K)	$U(p)$ (MPa)	$U(\rho)$ (kg m^{-3})
			T (K)	p (MPa)			
This work	2011	SSMSD	250–400	0–20	3.9×10^{-3}	0.007–0.015%	0.020–0.155%
Cristancho and coworkers [26]	2010	SSMSD	265–400	0–200	5.0×10^{-3}	0.010%	0.030–0.100%
McLinden et al. [25]	2006	TSMSD	90–520	0–40	4.0×10^{-3}	0.005–0.050%	0.003–0.006%
Schilling et al. [27]	2006	SSMSD	233–476	0–30	4.0×10^{-3}	0.006%	0.010–0.018%
Klimeck et al. [28]	2001	SSMSD	240–520	0–30	4.0×10^{-3}–10.0×10^{-3}	0.016%	0.013–0.021%

It must be noticed that, despite the measurement uncertainties being of the same order for similar densimeters, it is very important to evaluate them for each single apparatus, since many of the main uncertainty sources depend on the particular densimeter setup.

7. Conclusion

The measurement uncertainty of the state point magnitudes was evaluated for our single sinker densimeter with magnetic suspension coupling. Based on the analysis of the main individual contributions of each uncertainty source to the total uncertainty value, several modifications on the setup were proposed.

An improvement of the temperature and pressure measurement procedures was carried out. Moreover, the titanium sinker was replaced by a silicon one in order to reduce the mass reading term of the density uncertainty and the sensitivity coefficients of each input quantity.

In order to quantify the degree of improvement achieved with this work, the measurement uncertainty of the densimeter state point (p, ρ, T) was once again evaluated following the uncertainty propagation law. Furthermore, a Monte Carlo simulation was performed to validate the actual uncertainty estimation and discard secondary effects.

Results showed that the state point uncertainty was significantly reduced. Temperature uncertainty decreased by 44% for the whole working range, while pressure uncertainty dropped by more than 92% below 2 MPa. Density uncertainty also decreased by more than 22%, and even more than 40%, at low densities. A set of test measurements on nitrogen validated the performance of the modified apparatus.

Thus, a method for the improvement of the uncertainty of measurement apparatus has been presented and proved in our particular case. The method consists of a thorough evaluation of the measurement uncertainty to determine the main uncertainty sources, so as to act directly on them. After that, modifications to reduce the classified terms are proposed and performed. Finally, the uncertainty can be estimated again to quantify the reduction obtained with the modifications in order to decide whether new modifications on the setup should be executed or not.

Acknowledgments

Support for this work came from the Programa Nacional de Formación de Profesorado Universitario (FPU) of The Spanish Ministry of Science and Innovation, Project Ref.: ENE2009-14644-C02-01 of the Spanish Ministry of Science and Innovation and from the Junta de Castilla y León reference GR 152.

References

[1] R. Span, Multiparameter Equations of State – An Accurate Source of Thermodynamic Property Data, Springer, Berlin, 2000.
[2] W. Wagner, R. Kleinrahm, Densimeters for very accurate density measurements of fluids over large ranges of temperature, pressure, and density, Metrologia 41 (2004) 24–39.
[3] R. Kleinrahm, W. Wagner, Measurement and correlation of the equilibrium liquid and vapor densities and the vapor pressure along the coexistence curve of methane, J. Chem. Thermodynam. 18 (1986) 739–760.
[4] T. Gast, Vacuum Microbalance Techniques, vol. 3, K.H. Behrndt, New York, 45–54.
[5] H.W. Lösch, Entwicklung und Aufbau von neuen Magnetschwebewaagen zur berührunsfreien Messung vertikaler Kräfte, VDI-Verlag: Fortschr. -Ber. VDI, vol. 3, Düsseldorf, 1987.
[6] H.W. Lösch, R. Kleinrahm, W. Wagner, Neue Magnetschwebewaagen für gravimetrische Messungen in der Verfahrenstechnik, Chem. Ing. Technol. 66 (1994) 1055–1058.
[7] K. Brachthäuser, R. Kleinrahm, H.W. Lösch, W. Wagner, Entwicklung eines neues Dichtemessverfahrens und Aufbau einer Hochtemperatur-Hochdruck-Dichtemessanlage, VDI-Verlag: Fortschr.-Ber. VDI, vol. 8, Düsseldorf, 1993.
[8] W. Wagner, K. Brachthäuser, R. Kleinrahm, H.W. Lösch, A new, accurate single-sinker densitometer for temperatures from 233 to 523 K at pressures up to 30 MPa, Int. J. Thermophys. 16 (1995) 399–411.
[9] J. Klimeck, Dissertation, Ruhr Universität Bochum, 1997.
[10] J. Klimeck, R. Kleinrahm, W. Wagner, An accurate single-sinker densimeter and measurements of the (p, ρ, T) relation of argon and nitrogen in the temperature range from (235 to 520) K at pressures up to 30 MPa, J. Chem. Thermodynam. 30 (1998) 1571–1588.
[11] C.R. Chamorro, J.J. Segovia, M.C. Martín, M.A. Villamañán, J.F. Estela-Uribe, J.P.M. Trusler, Measurement of the (pressure, density, temperature) relation of two (methan+nitrogen) gas mixtures at temperatures between 240 and 400 K and pressures up to 20 MPa using an accurate single-sinker densimeter, J. Chem. Thermodynam. 38 (7) (2006) 916–922.
[12] M.O. McLinden, R. Kleinrahm, W. Wagner, Force transmission errors in magnetic suspension densimeters, Int. J. Thermophys. 28 (2) (2007) 429–448.
[13] BIPM, IEC, IFCC, ISO, IUPAC, IUPAP, OIML, Guide to the Expression of Uncertainty in Measurement, International Organization for Standarization, Genève, 1995.
[14] BIPM, IEC, IFCC, ILAC, IUPAC, IUPAP, ISO, OIML, International Vocabulary of Metrology – Basic and General Concepts and Associated Terms (VIM), 3rd ed. JCGM 200:2008, 2008.
[15] EA-4/02, Expression of the Uncertainty of Measurement in Calibration, Appendix E, 1999.
[16] EA-4/17, Calibration of Pressure Balances, Appendix B, 1997.
[17] H. Preston-Thomas, The international temperature Scale of 1990 (ITS-90), Metrologia 27 (1) (1990) 3–10.
[18] BIPM, Evaluation of Measurement Data – Supplement 1 to the "Guide to the Expression of Uncertainty in Measurement" – Propagation of Distributions Using a Monte Carlo Method, JCGM-101, vol. 101, 2008.
[19] S.M.A. Kazimi, Solid Mechanics, Tata McGraw-Hill Education, 2001.
[20] Landolt-Börnstein, Elastic Constants of Second Order: Temperature Coefficients Tc, III/29a 1.2.2., vol. 225, Springer Verlag, Berlin, 2001.

[21] Y. Okada, Y. Tokumaru, Precise determination of lattice parameter and thermal expansion coefficient of silicon between 300 and 1500 K, J. Appl. Phys. 56 (2) (1984) 314–320.
[22] H. Watanabe, N. Yamada, M. Okaji, Linear thermal expansion coefficient of silicon from 293 to 1000 K, Int. J. Thermophys. 25 (1) (2004) 221–236.
[23] R. Span, E.W. Lemmon, R.T. Jacobsen, W. Wagner, A reference quality equation of state for nitrogen, Int. J. Thermophys. 19 (1998) 1121–1132.
[24] R. Span, E.W. Lemmon, R.T. Jacobsen, W. Wagner, A.J. Yokozeki, A reference equation of state for the thermodynamic properties of nitrogen for temperatures from 63.151 to 1000 K and pressures to 2200 MPa, Phys. Chem. Ref. Data 29 (2000) 1361–1401.
[25] M.O. McLinden, C. Losch-Will, Apparatus for wide-ranging, high-accuracy fluid (p, ρ, T) measurements based on a compact two-sinker densimeter, J. Chem. Therm. 39 (2007) 507–530.
[26] I.D. Mantilla, D.E. Cristancho, S. Ejaz, K.R. Hall, M. Atilhan, G.A. Iglesias-Silva, New P-ρ-T data for nitrogen at temperatures from (265 to 400) K at pressures up to 150 MPa, J. Chem. Eng. Data 55 (2010) 4227–4230.
[27] G. Schilling, R. Kleinrahm, W. Wagner, Measurement and correlation of the (p, ρ, T) relation of liquid n-heptane, n-nonane, 2,4-dichlorotoluene, and bromobenzene in the temperature range from (233.15 to 473.15) K at pressures up to 30 MPa for use as density reference liquids, J. Chem. Thermodynam. 40 (7) (2008) 1095–1105.
[28] J. Klimeck, R. Kleinrahm, W. Wagner, Measurements of the (p, ρ, T) relation of methane and carbon dioxide in the temperature range 240 K to 520 K at pressures up to 30 MPa using a new accurate single-sinker densimeter, J. Chem. Therm. 33 (2001) 251–267.

J. Chem. Thermodynamics 43 (2011) 1950–1953

Contents lists available at ScienceDirect

J. Chem. Thermodynamics

journal homepage: www.elsevier.com/locate/jct

New (p, ρ, T) data for carbon dioxide – Nitrogen mixtures from (250 to 400) K at pressures up to 20 MPa

M.E. Mondéjar [a], M.C. Martín [a], R. Span [b], C.R. Chamorro [a,*]

[a] Grupo de Termodinámica y Calibración (TERMOCAL), Dpto. Ingeniería Energética y Fluidomecánica, Escuela de Ingenierías Industriales, Universidad de Valladolid, Paseo del Cauce, 59, E-47011 Valladolid, Spain
[b] Lehrstuhl für Thermodynamik, Fakultät für Maschinenbau Gebäude IB, Ebene 5, Ruhr-Universität Bochum, Universitätsstr. 150, 44780 Bochum, Germany

ARTICLE INFO

Article history:
Received 2 March 2011
Received in revised form 30 June 2011
Accepted 6 July 2011
Available online 19 July 2011

Keywords:
Density measurements
CO_2/N_2 mixtures
Single sinker densimeter
GERG equation of state

ABSTRACT

Comprehensive (p, ρ, T) measurements on two binary mixtures (0.10 CO_2 + 0.90 N_2 and 0.15 CO_2 + 0.85 N_2) were carried out in the gas phase at seven isotherms between (250 and 400) K and pressures up to 20 MPa using a single sinker densimeter with magnetic suspension coupling. A total of 69 (p, ρ, T) data for the first mixture and 69 (p, ρ, T) data for the second are presented in this article. The uncertainty in density was estimated to be (0.02 to 0.15)%, while the uncertainty in temperature was 3.9 mK and the uncertainty in pressure was less than 0.015% (coverage factor k = 2). Experimental results were compared with densities calculated from the GERG equation of state and with data reported by other authors for similar mixtures. Results yielded that, while deviations between experimental data and values calculated from the GERG equation were lower than 0.05% in density for low pressures, the relative error at high pressures and low temperatures increased to about (0.2 to 0.3)%. The main aim of this work was to contribute to an accurate density data base for CO_2/N_2 mixtures and to check or improve equations of state existing for these binary mixtures.

1. Introduction

Gaseous mixtures containing substantial quantities of carbon dioxide and nitrogen are present in several industrial schemes, from energetic exploitation of biogases, through carbon capture and storage processes, to enhanced oil extraction with nitrogen or carbon dioxide injection. An accurate knowledge of the thermodynamic behavior of these gaseous mixtures is of great importance for the development and optimization of the mentioned processes.

Equations of state developed for thermodynamic properties of natural gases are also used to predict the behavior of different natural gas components mixtures. The AGA8-DC92 equation of state [1], which was commonly used for the prediction of CO_2/N_2 mixture properties, was replaced by the GERG-2004 wide range equation of state for natural gas and other mixtures [2], which overcame many of the limitations of the AGA8-DC92. Departure functions and mixing parameters of the GERG-2004 equation of state for CO_2/N_2 mixtures are highly dependent on the experimental data used for fitting. In this context, density measurements are of great importance. Therefore, more reliable and consistent studies on densities for CO_2/N_2 mixtures would lead to a better description of these mixtures.

Several authors have previously studied carbon dioxide/nitrogen mixtures in the gas and liquid phases as well as in the supercritical region and at (vapor + liquid) equilibrium. All density measurements on these mixtures performed before 2004 were collected in the GERG data base of compressibility factors [3] and many of them were used to establish the GERG-2004 equation of state for natural gas and other mixtures [2]. However, due to the low reliability and accuracy of some of the experimental data for mixtures, only less than 30% of the collected experimental density data for CO_2/N_2 mixtures were used to fit the GERG-2004 – though many data sets were published for this mixture, there still is a need for accurate density data in certain temperature, pressure and composition ranges.

In order to contribute to the existing data base for binary mixtures properties, new accurate measurements for two mixtures of carbon dioxide with nitrogen (x_{CO_2} = 0.10, 0.15) from (250 to 400) K and pressures up to 20 MPa were performed in a single sinker densimeter with magnetic suspension coupling.

Density data for these compositions could already be found in the bibliography. Brugge et al. [4,5] reported cross virial coefficients for a CO_2/N_2 mixture with a CO_2 molar fraction of x_{CO_2} = 0.11 using the Burnett technique between (300 and 320) K. Gaz de France measured compressibility factors of a CO_2/N_2 mixture with x_{CO_2} = 0.10 in the range (279 to 308) K up to 7 MPa, which are collected in [3]. Rivkin [6] presented compressibility data for a mixture with x_{CO_2} = 0.18 between (273 and 473) K and

* Corresponding author. Tel.: +34 983423756; fax: +34 983186462.
E-mail address: cescha@eis.uva.es (C.R. Chamorro).

0021-9614/$ - see front matter © 2011 Elsevier Ltd. All rights reserved.
doi:10.1016/j.jct.2011.07.006

pressures up to 10 MPa. Most recent *pvT* properties were reported by Brugge et al. [7] for x_{CO_2} = 0.11 between (225 and 450) K at pressures up to 70 MPa using a continuously-weighed pycnometer.

Experimental densities reported in this work and by the authors mentioned above were compared with densities calculated using the GERG-2004 equation of state to test its performance for the studied mixtures.

2. Experimental

Density measurements were carried out with a single sinker densimeter with magnetic suspension coupling. This densimeter, which was originally developed by Brachthäuser et al. [8], applies one of the state of the art techniques for density determination [9,10] and is based on the Archimedes' principle by which the buoyancy force acting on a sinker immersed in a fluid is proportional to the density of the fluid. The sinker inside a pressurized cell is coupled contactless to a very accurate balance by means of a magnetic suspension coupling. Therefore the densimeter works in a wide range of temperatures and pressures. Our single sinker densimeter covers the gas phase in the range (250 to 400) K and at pressures up to 20 MPa. The temperature inside the cell is measured with an expanded uncertainty of 3.9 mK while the expanded uncertainty in pressure measurement is 75 ppm + 0.0035 MPa at pressures above 2 MPa and 60 ppm + 0.00018 MPa at pressures below 2 MPa (coverage factor, $k = 2$). The overall density measuring uncertainty of measured densities was estimated to be less than $0.023 + 0.00011\rho$ (kg · m^{-3}) [11].

The experimental density data reported in this work were measured on seven isotherms at (250, 275, 300, 325, 350, 375 and 400) K at 10 pressure steps between 2 and 20 MPa. Before and after measuring each mixture, test measurements on nitrogen were carried out in the whole range of the apparatus to validate it by comparing the results with densities calculated from the reference equation of state for nitrogen by Span et al. [12]. The force transmission error induced by the measured fluid discussed in detail by McLinden et al. [13] was ignored since the magnetic susceptibilities of the components of the studied mixtures are relatively low, resulting in a negligible influence of the magnetic coupling.

Both carbon dioxide/nitrogen mixtures used for performing the density measurements presented in this work were prepared gravimetrically in the spanish national metrology institute (Centro Español de Metrología, CEM) and supplied in 10 dm^3 aluminum cylinders filled to a pressure of approximately 6 MPa at room temperature. Mixtures compositions with estimated uncertainties are given in table 1. Nitrogen and carbon dioxide used during the preparation of the mixtures had specified minimum molar fraction purities of, respectively, 0.999995 and 0.99995. Nitrogen used for test measurements was supplied by Alphagaz (Air Liquid) with a certified mole fraction purity of 0.999999.

3. Results

Tables 2 and 3, respectively, contain the isothermal density data for the (0.10 CO_2 + 0.90 N_2) and (0.15 CO_2 + 0.85 N_2) mixtures together with the percentage relative deviation in density from values calculated by the GERG-2004 equation of state (2). Each (p, ρ, T) point was obtained as the average of the last ten values measured for each pressure step. Each isotherm was measured at least twice to check the repeatability of the measurements.

TABLE 1
Carbon dioxide/nitrogen mixtures compositions.

Cylinder number	Composition (x_{CO_2})
02435	0.10009 ± 0.001
92380	0.15045 ± 0.001

TABLE 2
Results of the (p, ρ, T) measurements for a (0.10 CO_2 + 0.90 N_2) binary mixture, where T is the temperature (ITS-90), p the pressure, ρ_{exp} the experimental density and ρ_{EoS} the density calculated from the GERG-2004 (2) equation of state.

T/K	p/MPa	ρ_{exp}/(kg · m^{-3})	$10^2(\rho_{exp} - \rho_{EoS})/\rho_{EoS}$
250.044	19.86622	302.682	−0.210
250.044	18.04077	278.626	−0.210
250.044	16.02422	250.228	−0.201
250.044	14.01532	220.196	−0.180
250.045	12.01104	188.824	−0.147
250.046	10.00715	156.529	−0.104
250.047	8.00002	123.810	−0.066
250.048	5.99883	91.410	−0.031
250.047	3.99732	59.733	−0.003
250.046	1.98511	29.000	0.034
275.019	19.84087	262.442	−0.125
275.019	18.05655	241.448	−0.127
275.018	16.02186	216.330	−0.124
275.016	14.01343	190.433	−0.115
275.017	12.00866	163.678	−0.099
275.016	10.00450	136.290	−0.077
275.012	7.99787	108.505	−0.061
275.009	6.00199	80.825	−0.043
275.019	3.99710	53.276	0.000
299.963	19.16513	226.098	−0.021
299.966	17.86924	212.244	−0.039
299.967	16.01378	191.829	−0.041
299.966	14.00977	169.025	−0.039
299.966	12.00591	145.550	−0.035
299.967	10.00204	121.553	−0.024
299.967	7.99970	97.214	−0.017
299.967	5.99638	72.692	−0.006
299.968	3.99646	48.220	0.006
299.967	1.99790	23.945	0.035
324.979	19.62110	208.360	0.007
324.980	18.00085	192.790	0.000
324.979	16.00130	172.971	−0.005
324.979	13.98251	152.335	−0.010
324.979	11.99919	131.525	−0.011
324.978	9.99890	110.087	−0.008
324.978	8.01923	88.521	−0.007
324.978	5.99183	66.201	−0.001
324.978	3.99616	44.111	0.003
324.980	1.99599	21.979	0.032
349.967	19.37788	188.339	0.023
349.967	17.99350	176.127	0.017
349.966	15.99987	158.084	0.010
349.966	13.99498	139.425	0.005
349.966	11.99755	120.373	0.001
349.966	9.99755	100.892	0.002
349.966	7.99575	81.051	−0.001
349.965	5.99670	60.978	0.003
349.964	3.99656	40.709	0.003
349.964	1.99606	20.340	0.010
374.975	18.71878	168.450	0.016
374.975	17.96004	162.237	0.014
374.974	15.96599	145.587	0.006
374.974	13.97204	128.504	0.000
374.974	11.98120	111.044	−0.004
374.973	9.98248	93.148	−0.005
374.973	7.98995	74.983	−0.007
374.973	5.99454	56.518	−0.011
374.970	3.96223	37.494	−0.011
374.969	1.97464	18.733	−0.001
400.038	18.90806	158.136	0.067
400.037	17.81457	149.796	0.060
400.035	15.98414	135.572	0.051
400.036	13.99217	119.725	0.042
400.035	11.98674	103.403	0.032
400.034	9.99291	86.844	0.028
400.035	7.98095	69.818	0.018
400.036	5.99205	52.720	0.013
400.034	3.99487	35.321	0.010
400.037	1.99589	17.722	0.031

TABLE 3
Results of the (p, ρ, T) measurements for a (0.15 CO_2 + 0.85 N_2) binary mixture, where T is the temperature (ITS-90), p the pressure, ρ_{exp} the experimental density and ρ_{EoS} the density calculated from the GERG-2004 (2) equation of state.

T/K	p/MPa	ρ_{exp}/(kg · m^{-3})	$10^2(\rho_{exp} - \rho_{EoS})/\rho_{EoS}$
250.059	19.99666	326.225	−0.309
250.063	18.01935	298.361	−0.307
250.064	16.01636	267.875	−0.287
250.066	14.01375	235.308	−0.251
250.066	12.00577	201.013	−0.193
250.066	10.00316	165.836	−0.122
250.064	7.99621	130.387	−0.060
250.064	5.98407	95.441	−0.009
250.061	3.98271	61.879	0.022
250.061	1.94406	29.337	0.082
275.028	19.98318	280.214	−0.191
275.027	17.99374	255.193	−0.191
275.027	15.98143	228.492	−0.181
275.026	14.00115	201.020	−0.161
275.026	12.00000	172.315	−0.133
275.026	9.99554	142.952	−0.098
275.025	7.99430	113.405	−0.067
275.022	5.99802	84.088	−0.042
275.019	4.00063	55.255	−0.018
275.019	1.98846	26.992	0.035
299.963	19.97735	247.119	−0.053
299.965	17.99426	224.784	−0.078
299.968	15.96936	201.068	−0.077
299.967	13.99130	177.090	−0.068
299.968	12.00779	152.379	−0.054
299.966	10.00322	126.921	−0.037
299.966	8.00779	101.300	−0.026
299.966	5.99919	75.467	−0.009
299.967	3.98234	49.692	0.009
299.969	1.99212	24.615	0.062
324.980	19.97825	221.898	−0.008
324.980	18.01598	202.007	−0.018
324.981	16.00631	180.933	−0.021
324.981	14.01385	159.405	−0.021
324.981	11.99115	137.002	−0.020
324.981	9.99694	114.495	−0.012
324.981	7.99759	91.632	−0.008
324.982	5.99660	68.599	0.000
324.982	3.99587	45.557	0.015
324.982	1.99613	22.645	0.054
349.967	19.98296	202.168	0.046
349.967	18.00779	183.902	0.034
349.967	16.00783	164.842	0.026
349.967	14.00355	145.221	0.020
349.967	11.99797	125.127	0.016
349.967	9.99946	104.724	0.017
349.967	7.99535	83.959	0.014
349.967	5.99688	63.049	0.017
349.967	3.99534	41.993	0.021
349.967	1.99594	20.947	0.053
374.956	19.97235	185.971	0.054
374.956	17.99229	169.101	0.040
374.956	15.99852	151.646	0.029
374.956	13.98957	133.615	0.021
374.955	11.94535	114.852	0.014
374.954	9.98626	96.527	0.009
374.954	7.99726	77.627	0.000
374.954	5.99557	58.378	−0.003
374.953	3.95365	38.571	−0.004
374.955	1.96362	19.172	0.008
400.023	17.81821	155.538	0.070
400.022	15.97720	140.583	0.058
400.022	13.98802	124.054	0.047
400.020	11.98638	107.065	0.037
400.020	9.99083	89.804	0.031
400.021	7.99123	72.219	0.023
400.019	5.99535	54.424	0.015
400.020	3.99567	36.397	0.003
400.019	1.99535	18.223	0.005

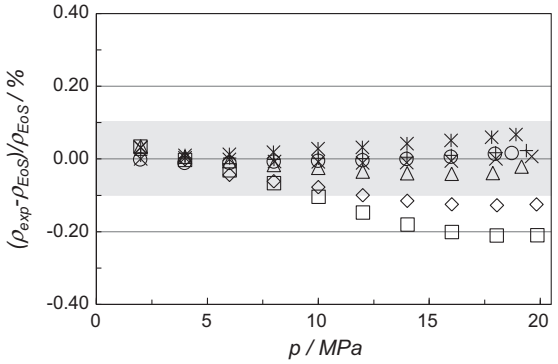

FIGURE 1. Percentage density deviations of experimental (p, ρ, T) data of (0.10 CO_2 + 0.90 N_2) binary mixture from density values ρ_{EoS} calculated from the GERG-2004 equation of state (2) *versus* pressure: □ 250 K; ◇ 275 K; Δ 300 K; × 325 K; +350 K; ○ 375 K; ⁎ 400 K.

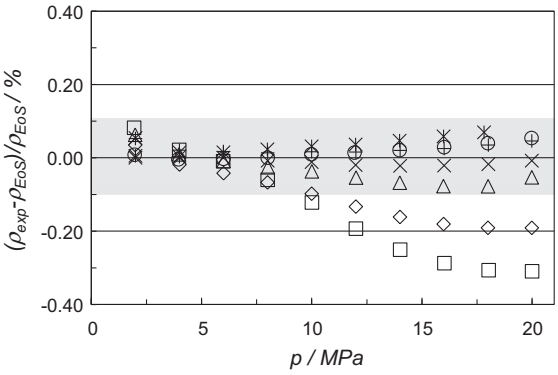

FIGURE 2. Percentage density deviations of experimental (p, ρ, T) data of (0.15 CO_2 + 0.85 N_2) binary mixture from density values ρ_{EoS} calculated from the GERG-2004 equation of state (2) *versus* pressure: □ 250 K; ◇ 275 K; Δ 300 K; × 325 K; + 350 K; ○ 375 K; ⁎ 400 K.

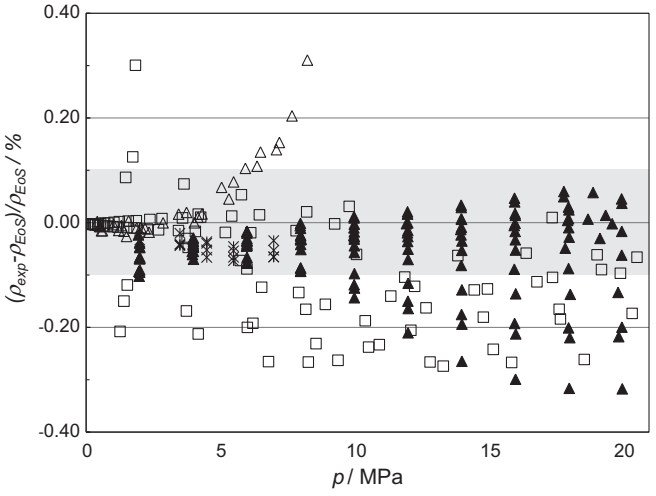

FIGURE 3. Percentage density deviations of experimental (p, ρ, T) data of CO_2/N_2 binary mixtures from density values ρ_{EoS} calculated from the GERG-2004 equation of state (2) *versus* pressure, for CO_2 molar compositions between 0.10 and 0.18 in the temperature range (240 to 410) K and at pressures up to 20 MPa: Δ this work; □ Brugge et al. [4,7]; ▲ Rivkin [6]; ⁎ Gaz de France [3].

Relative deviations for each isotherm reported in the last column of tables 2 and 3 are represented *versus* pressure in figures 1 and 2, respectively.

The shaded areas in figures 1 and 2 depict the estimated uncertainty in density of the equation of state when predicting densities of CO_2/N_2 mixtures, which is around 0.1%. As can be seen, relative

TABLE 4
Statistical comparison of the density measurements of the experimental data plotted in figure 3.

Source	Year	x_{CO_2}	n	$10^2 \cdot$ AAD	$10^2 \cdot$ Bias	$10^2 \cdot$ RMS	$10^2 \cdot$ MaxD
This work	2011	0.10	69	0.0407	−0.0239	0.0670	0.2105
This work	2011	0.15	69	0.0601	−0.0310	0.0955	0.3102
Brugge et al. [4]	1989	0.11	38	0.0080	−0.0010	0.0100	0.0270
Brugge et al. [7]	1997	0.11	141	0.1550	−0.0060	0.1880	0.4620
Gaz de France [3]	1990	0.10	19	0.0460	−0.0460	0.0490	−0.0740
Rivkin [6]	1975	0.18	43	0.0610	0.0500	0.1040	0.3450

deviations for isotherms above 300 K are within the uncertainty limits, particularly at low pressures where relative deviations are lower than 0.05%. However, deviations reported for 250 K and 275 K exceed the expected uncertainty, reaching maximums of 0.2% and 0.3%, respectively for compositions x_{CO_2} = (0.10, 0.15). When experimental density values are compared with calculated density data from an equation of state the composition of the mixtures must be taken into account since the uncertainty in composition may alter the reference density. In this case, the uncertainty in composition of the two mixtures could produce a maximum difference of 0.003% on the relative deviation in density for the x_{CO_2} = 0.15 mixture at 250 K and 20 MPa.

Figure 3 shows the percentage deviations in density of experimental data from this work along with other data sets used to develop the binary departure functions for CO_2/N_2 mixtures of the GERG equation of state. Experimental data reported in this work are compared with those presented by other authors for similar compositions in the same temperature and pressure range. It can be observed that deviations between measured and calculated densities increase at high pressures.

A statistical comparison of the plotted experimental data is given in table 4. Here n is the number of data points, AAD is the average absolute deviation, Bias is the average deviation, RMS refers to the root mean squared and MaxD indicates the maximum relative deviation in a data set.

4. Discussion

New density measurements for two binary mixtures of carbon dioxide and nitrogen with molar compositions x_{CO_2} = (0.10, 0.15) were performed in a single sinker densimeter with magnetic suspension coupling in the temperature range between (250 and 400) K and at pressures up to 20 MPa.

Experimental results were compared with densities calculated from the GERG-2004 equation of state and with data previously reported by other authors for similar mixtures in the same temperature and pressure range. Reported data showed good agreement with the equation of state particularly at low pressures, accounting for less than 0.05% at pressures up to 14 MPa in the x_{CO_2} = 0.10 mixture and up to 12 MPa in the x_{CO_2} = 0.15 mixture at temperatures above 300 K. However on isotherms below 300 K large deviations between measured and calculated values became obvious.

Further mixtures with higher CO_2 concentration will be investigated in order to check whether the deviation at high pressures and low temperatures increases or not.

Acknowledgments

Support for this work came from the Programa Nacional de Formación de Profesorado Universitario (FPU), Project ENE2009-14644-C02-01 of the Spanish Ministry of Science and Innovation and from the Junta de Castilla y León reference GR 152. We thank the Spanish national metrology institute (Centro Español de Metrología, CEM) for the preparation of the two binary mixtures studied in this work.

References

[1] K.E. Starling, J.L. Savidge, Compressibility Factors of Natural Gas and Other Related Hydrocarbon Gases – AGA Transmission Measurement Committee Report 8, American Gas Association, 1992.
[2] O. Kunz, R. Klimeck, W. Wagner, M. Jaeschke, The GERG-2004 Wide-Range Equation of State for Natural Gases and Other Mixtures, VDI Verlag GmbH, Düsseldorf, 2007.
[3] M. Jaeschke, A.E. Humphreys, The GERG Data Bank of High Accuracy Compressibility Factor Measurements, vol. 6, VDI Verlag , Düsseldorf, 1991.
[4] H.B. Brugge, C.A. Hwang, W.J. Rogers, J.C. Holste, K.R. Hall, W. Lemming, G.J. Esper, K.N. Marsh, B.E. Gammon, Physica A 156 (1989) 382–416.
[5] H. Duarte-Garza, H.B. Brugge, C.A. Hwang, P.T. Eubank, J.C. Holste, K.R. Hall, B.E. Gammon , K.N. Marsh, Thermodynamic Properties of (CO_2 + N_2) Mixtures, Gas Processors Association/Gas Research Institute, 1995.
[6] S.L. Rivkin, Teplofiz 8 (1975) 190–208.
[7] H.B. Brugge, J.C. Holste, K.R. Hall, B.E. Gammon, K.N. March, J. Chem. Eng. Data 42 (1997) 903–907.
[8] K. Brachthäuser, R. Kleinrahm, H.W. Lösch, W. Wagner, Entwicklung eines neues Dichtemessverfahrens und Aufbau einer Hochtemperatur-Hochdruck-Dichtemessanlage, vol. 8, VDI-Verlag: Fortschr.-Ber. VDI, Düsseldorf, 1993.
[9] W. Kleinrahm, R. Wagner, Metrologia 41 (2004) 24–39.
[10] W. Wagner, R. Kleinrahm, H.W. Lösch, J.T.R. Watson, Measur. Thermodyn. Properties Single Phases VI (2003) 127–149.
[11] M.E. Mondéjar, J.J. Segovia, C.R. Chamorro, Measurement (2011).
[12] R. Span, E.W. Lemmon, R.T. Jacobsen, W. Wagner, A.J. Yokozeki, J. Phys. Chem. Ref. Data 29 (2000) 1361–1433.
[13] M.O. McLinden, R. Kleinrahm, W. Wagner, Int. J. Thermophys. (2007) 429–448.

JOURNAL OF CHEMICAL & ENGINEERING DATA

ARTICLE

pubs.acs.org/jced

(p, ρ, T) Behavior of Two Mixtures of Carbon Monoxide with Nitrogen in the Temperature Range from (250 to 400) K and Pressures up to 20 MPa

María E. Mondéjar,[†] Miguel A. Villamañán,[†] Roland Span,[‡] and César R. Chamorro*[,†]

[†]Universidad de Valladolid, Paseo del Cauce, 59, E-47011-Valladolid, Spain

[‡]Ruhr-Universität Bochum, Universitätsstr. 150, D-44780-Bochum, Germany

ABSTRACT: The development of the current reference equation of state for natural gas and other related mixtures (GERG 2008) was based on a wide up-to-date database of experimental thermodynamic properties. This extensive data bank showed, however, a significant lack of data for many of the possible binary mixtures of natural gas components. In fact, density data for carbon monoxide−nitrogen mixtures were only available for one single composition (0.03 CO + 0.97 N_2) and in a limited temperature range, (273 to 353) K. In this paper density data are presented for two new binary mixtures, (0.05 CO + 0.95 N_2) and (0.10 CO + 0.90 N_2), along seven isotherms between (250 and 400) K and pressures up to 20 MPa. These data allow the predictive capacity of the GERG model to be tested and, if necessary, to contribute to an improvement in its mixture parameters. The measurements were carried out using an accurate single sinker densimeter with magnetic suspension coupling to achieve the highest accuracy. Results showed very good agreement with the GERG model, since relative deviations in density between experimental and estimated values are within a 0.05 % band. Interaction second virial coefficients were fitted and reported.

1. INTRODUCTION

Gaseous mixtures containing significant amounts of nitrogen and carbon monoxide are present in several industrial processes, whether as a combustion byproduct in exhaust gases from coke ovens and blast furnaces or as a product of biomass pyrolysis and gasification. These mixtures are currently of great interest due to their potential use as alternative or renewable fuels. Thus, several projects, such as Marcogaz[1] and BONGO,[2] are currently analyzing the viability and feasibility of the injection of these fuel gases into the existing natural gas networks to contribute to the development of a more sustainable energy model. Accurate knowledge of the thermodynamic and chemical properties of these gases is essential to ensure the quality requirements of the final delivered gas.

The AGA8-DC92 equation of state is the current industry standard for natural gas mixtures[3] in the homogeneous gas region. However, new equations of state have been developed in the past few years to extend the range of application of the AGA8-DC92 and improve its accuracy. Thus, the GERG-2004 wide-range equation of state[4] was developed as an international reference equation of state for natural gases and similar mixtures consisting of up to 18 components.[5] A new version of this equation of state (GERG-2008)[6] has recently been developed as an extension of the first version, since it incorporates three new components (*n*-nonane, *n*-decane, and hydrogen sulfide). This new GERG-2008 equation of state is currently the most comprehensive and widely used model for the estimation of thermodynamic properties of natural gas mixtures and is under consideration to be adopted as an ISO Standard (ISO 20765-2 and ISO 20765-3). In this work we compare our experimental data with the GERG-2008 model, which is equivalent to the GERG-2004 model for the gas mixtures studied here, since they do not contain any of the additional components covered by the GERG-2008 model.

The mentioned equations of state have an empirical basis and have been fitted to an extensive number of data sets of different thermodynamic properties and substances. Nevertheless, there is still a lack of reliable and accurate experimental data of thermodynamic properties for many of these substances, especially mixtures. To extend the scope of these correlations and to include the above-mentioned fuel gases as well as their mixtures with natural gas, accurate experimental measurements of mixtures containing their components are indispensable.

Despite the mentioned importance of carbon monoxide with nitrogen mixtures in these new alternative fuels, the study of their thermodynamic properties is comparatively poor. In fact, only density data for a single composition (0.03 CO + 0.97 N_2) for a limited temperature range, (273 to 353) K, and pressures up to 30.1 MPa were reported by Jaeschke et al.[7] in 1997. These measurements were carried out using both Burnett apparatus and optical interferometry apparatus, with reported accuracies of 0.07 % and 0.08 %, respectively.

In view of the potential exploitation of the mentioned new gaseous fuels, which contain significant amounts of nitrogen and carbon monoxide, the study of the (p, ρ, T) behavior of binary mixtures containing these components is of great interest. Thus, a 98 (p, ρ, T) data set of a (0.05 CO + 0.95 N_2) mixture and a 125 (p, ρ, T) data set of a (0.10 CO + 0.90 N_2) mixture in the temperature range (250 to 400) K and pressures up to 20 MPa are presented in this work. Measurements were carried out with

Received: July 22, 2011
Accepted: September 15, 2011
Published: September 28, 2011

Table 1. Molar Composition of the Gas Mixtures and Purity of Component Gases

composition (x_{CO})	specified purity of nitrogen (x_{N_2})	specified purity of carbon monoxide (x_{CO})
0.04999 ± 0.00001	0.999995	0.999985
0.10018 ± 0.00002	0.999995	0.999700

an accurate single sinker densimeter with magnetic suspension coupling to achieve the lowest uncertainties.

The experimental data reported here were compared with the densities calculated using the GERG-2008 equation of state to test its performance for these mixtures. Relative deviations in density of experimental data were listed and plotted for comparison with the literature data. Interaction second virial coefficients for binary mixtures of carbon monoxide and nitrogen were fitted with our experimental data and compared with the values reported by other authors.

2. EXPERIMENTAL SECTION

As mentioned above, measurements were carried out in a single sinker magnetic suspension densimeter. The apparatus, which was previously described by Chamorro et al.,[8] is based on the Archimedes' principle and yields high accuracy (p, ρ, T) data in the temperature range (250 to 400) K and pressures up to 20 MPa. The density of the fluid is determined with the following equation

$$\rho = (m_{S0} - m_{Sf})/V_s(T,p) \quad (1)$$

where ($m_{S0} - m_{Sf}$) refers to the buoyancy force, in kilograms, measured by a sinker immersed in the fluid, which is calculated as the difference between the sinker mass in a vacuum and the sinker mass in the pressurized fluid, while $V_s(T,p)$ refers to the sinker volume, in m^3, as a function of the fluid temperature and pressure. The densimeter has recently been modified[9] to improve its measurement uncertainty. The uncertainty in density has been estimated to be less than 0.12 %, while uncertainties in temperature and pressure were evaluated to be less than 4 mK and 0.015 %, respectively (k = 2). The pressure measurement instruments are two Digiquartz transducers (Paroscientific models 2300A-101 and 43KR-HHT-101) which cover pressure ranges up to (2 and 20) MPa, respectively. The temperature of the fluid is determined as the average of the measurements of two platinum resistance thermometers (PRTs) (model Minco S1059PJ5X6).

The experimental data presented in this work were collected along seven isotherms at (250, 275, 300, 325, 350, 375, and 400) K at 11 pressure steps between (1 and 20) MPa. Several isotherms were measured twice at different pressure steps to analyze the repeatability of the apparatus. Furthermore, test measurements on nitrogen were carried out along five isotherms, in the whole range of the apparatus, before measuring each mixture to check the correct operation of the densimeter. Relative deviations of experimental densities of nitrogen from the densities calculated with the reference equation of state of Span et al.[10] were within a 0.02 % band. The force transmission error due to the magnetic characteristics of the apparatus is compensated for by using an appropriate measurement procedure, as described by Chamorro et al.[8] The minor contribution produced by the fluid specific effect, described by McLinden et al.[11] and calculated by Cristancho et al.[12] and Kano et al.,[13] was omitted, since the deviation which could be induced by the magnetic behavior of the fluid was estimated to be in the order of

Table 2. Results of the (p, ρ, T) Measurements for the (0.05 CO + 0.95 N_2) Binary Mixture, Where T Is the Temperature (ITS-90), p the Pressure, ρ_{exp} the Experimental Density, and ρ_{EoS} the Density Calculated from the GERG-2008 Equation of State

T / K	p / MPa	ρ_{exp} / kg·m^{-3}	$10^2(\rho_{exp} - \rho_{EoS})/\rho_{EoS}$
250.049	18.4739	250.840	0.014
250.049	17.9994	245.259	0.014
250.045	15.9997	220.890	0.012
250.047	14.0036	195.251	0.010
250.049	11.9985	168.354	0.008
250.051	9.99983	140.653	0.008
250.047	7.99853	112.326	0.002
250.045	6.01694	84.044	−0.003
250.044	4.00994	55.503	−0.012
250.043	1.99903	27.340	0.011
250.041	0.996970	13.537	0.000
275.023	19.9174	235.882	0.017
275.023	18.1977	218.123	0.015
275.021	15.9971	194.336	0.016
275.023	13.9973	171.740	0.015
275.023	11.9993	148.339	0.011
275.030	10.0622	124.995	0.006
275.029	8.03660	100.073	0.000
275.029	6.03862	75.170	−0.003
275.023	4.00007	49.643	−0.010
275.020	1.99595	24.643	0.013
275.020	0.990786	12.187	−0.002
299.978	19.9569	212.314	0.036
299.977	17.9967	193.879	0.021
299.977	15.9967	174.350	0.020
299.957	14.9541	163.889	0.015
299.980	13.9973	154.113	0.019
299.962	12.9975	143.747	0.013
299.975	11.8888	132.063	0.012
299.962	10.9995	122.587	0.018
299.972	10.0171	111.971	0.011
299.962	9.08652	101.826	0.010
299.974	8.02482	90.132	0.007
299.962	6.99826	78.744	0.009
299.972	6.02019	67.811	0.002
299.962	4.99795	56.340	0.002
299.972	3.97500	44.812	−0.008
299.961	2.98189	33.609	−0.006
299.971	1.99343	22.457	0.018
299.962	1.00376	11.294	0.011
299.971	0.986706	11.101	0.005
324.983	19.9309	193.033	0.018
324.983	17.9952	176.379	0.018
324.982	15.9569	158.239	0.025
324.985	14.1156	141.303	0.014
324.974	13.7432	137.825	0.010
324.975	12.9991	130.817	0.010
324.984	12.0000	121.293	0.011

dx.doi.org/10.1021/je2007764 |J. Chem. Eng. Data 2011, 56, 3933–3939

Table 2. Continued

T	p	ρ_{exp}	
K	MPa	kg·m^{-3}	$10^2(\rho_{exp} - \rho_{EoS})/\rho_{EoS}$
324.977	10.9966	111.619	0.019
324.983	10.0066	101.939	0.011
324.979	8.99869	91.988	0.010
324.984	7.99104	81.935	0.008
324.978	7.02577	72.228	0.009
324.983	5.96077	61.428	0.005
324.978	4.97996	51.417	0.002
324.984	4.00852	41.449	0.000
324.978	2.99127	30.967	−0.007
324.982	1.98129	20.531	0.009
324.984	0.996209	10.328	0.009
349.969	19.6554	175.420	0.022
349.969	17.9925	162.172	0.022
349.970	15.9944	145.784	0.021
349.970	13.9972	128.911	0.018
349.970	12.0181	111.731	0.015
349.970	10.0220	93.976	0.015
349.969	8.01856	75.757	0.010
349.968	5.99817	57.037	0.005
349.971	4.00481	38.283	0.003
349.970	1.95895	18.808	0.017
349.970	0.991177	9.530	0.004
374.959	19.8166	163.859	0.018
374.959	17.9875	150.312	0.017
374.959	15.9900	135.101	0.016
374.959	13.9946	119.477	0.013
374.959	11.9955	103.411	0.009
374.958	9.99598	86.957	0.010
374.960	7.99654	70.138	0.006
374.958	5.99791	52.996	−0.001
374.959	3.99850	35.556	−0.014
374.959	1.98927	17.794	0.013
374.959	0.991138	8.887	0.002
400.020	19.0266	147.507	0.015
400.019	17.9853	140.246	0.013
400.020	15.9860	126.014	0.012
400.019	13.9897	111.428	0.010
400.019	11.9915	96.459	0.007
400.019	9.97324	80.982	0.006
400.021	7.99662	65.491	0.001
400.019	5.99803	49.518	−0.008
400.020	3.98633	33.151	−0.020
400.020	1.93445	16.200	−0.006

0.006 %, which is much lower than the estimated uncertainty in density for the measurements reported in this work.

The two mixtures studied in this work were prepared gravimetrically in the Spanish National Metrology Institute (Centro Español de Metrología, CEM) and supplied in 10 dm^3 aluminum cylinders filled to a pressure of 7 MPa at room temperature. Mixture compositions and estimated uncertainties, together with the purities of the component gases, are given in Table 1.

Table 3. Results of the (p, ρ, T) Measurements for the (0.10 CO_2 + 0.90 N_2) Binary Mixture, Where T Is the Temperature (ITS-90), p the Pressure, ρ_{exp} the Experimental Density, and ρ_{EoS} the Density Calculated from the GERG-2008 Equation of State

T	p	ρ_{exp}	
K	MPa	kg·m^{-3}	$10^2(\rho_{exp} - \rho_{EoS})/\rho_{EoS}$
250.060	19.9624	268.002	0.016
250.060	17.9996	245.432	0.015
250.055	16.7064	229.835	0.019
250.059	15.9987	221.035	0.014
250.051	15.0030	208.407	0.016
250.061	13.9985	195.325	0.014
250.053	13.0333	182.506	0.014
250.063	11.9982	168.471	0.014
250.051	11.0009	154.742	0.017
250.056	9.99883	140.734	0.013
250.050	8.99903	126.622	0.009
250.055	7.99832	112.391	0.010
250.057	6.99906	98.128	0.015
250.056	5.99926	83.836	0.012
250.056	5.04318	70.198	0.011
250.054	3.99885	55.373	0.010
250.056	3.03294	41.760	0.002
250.053	2.00426	27.416	0.013
250.053	0.999785	13.577	0.010
250.051	0.969128	13.157	0.002
275.024	19.8876	235.720	0.023
275.024	17.9971	216.135	0.022
275.024	15.9977	194.459	0.022
275.022	14.0007	171.880	0.020
275.019	12.0042	148.483	0.017
275.018	9.99954	124.305	0.016
275.015	7.99941	99.667	0.012
275.014	5.99890	74.708	0.009
275.012	3.99849	49.641	0.001
275.012	1.98443	24.502	0.011
275.011	0.997907	12.276	−0.001
299.977	19.8296	211.228	0.036
299.976	17.9986	193.977	0.022
299.975	16.1086	175.535	0.022
299.974	15.3704	168.159	0.024
299.973	14.8070	162.461	0.023
299.972	13.9972	154.176	0.021
299.972	13.0026	143.858	0.022
299.972	11.9990	133.290	0.020
299.972	11.0075	122.717	0.026
299.973	9.99714	111.800	0.023
299.969	9.07366	101.718	0.018
299.976	7.99752	89.866	0.024
299.971	7.03398	79.163	0.018
299.974	5.99923	67.600	0.019
299.969	5.02084	56.608	0.007
299.972	3.99843	45.092	0.013
299.969	2.99357	33.744	−0.005

dx.doi.org/10.1021/je2007764 |J. Chem. Eng. Data 2011, 56, 3933–3939

Table 3. Continued

T	p	ρ_{exp}	
K	MPa	kg·m^{-3}	$10^2(\rho_{exp} - \rho_{EoS})/\rho_{EoS}$
299.972	1.98975	22.417	0.022
299.972	1.00194	11.274	0.016
299.971	0.992979	11.173	0.011
324.978	19.9475	193.262	0.033
324.977	17.9956	176.463	0.033
324.978	15.9946	158.639	0.033
324.977	13.9961	140.254	0.032
324.977	11.9970	121.320	0.031
324.978	9.99872	101.905	0.032
324.976	7.99937	82.050	0.028
324.977	5.99998	61.847	0.025
324.976	3.99850	41.357	0.017
324.976	1.97022	20.421	0.022
324.977	0.997476	10.342	0.013
349.966	19.9592	177.859	0.032
349.964	18.2140	164.000	0.027
349.966	17.9917	162.217	0.033
349.965	16.9943	154.090	0.028
349.968	15.9939	145.829	0.035
349.965	14.9956	137.446	0.028
349.968	13.9949	128.938	0.037
349.965	12.9990	120.335	0.026
349.968	11.9970	111.586	0.035
349.963	10.9983	102.742	0.029
349.969	9.99826	93.794	0.036
349.963	8.99760	84.725	0.021
349.968	7.99894	75.601	0.031
349.963	6.99788	66.355	0.019
349.968	5.99772	57.048	0.024
349.962	4.99789	47.663	0.005
349.967	3.92247	37.508	0.011
349.964	2.99918	28.731	−0.012
349.967	1.97883	18.999	0.020
349.967	0.993387	9.551	−0.004
349.963	0.991956	9.538	0.009
374.957	19.9713	165.047	0.039
374.954	19.9666	165.012	0.038
374.956	18.9875	157.820	0.038
374.956	17.9867	150.362	0.040
374.955	16.9904	142.823	0.038
374.957	15.9904	135.151	0.039
374.955	15.0159	127.569	0.037
374.957	13.9926	119.504	0.039
374.954	12.9938	111.524	0.036
374.957	11.9876	103.381	0.034
374.955	10.9952	95.265	0.040
374.957	9.99790	86.999	0.032
374.955	8.99739	78.624	0.031
374.956	8.02423	70.391	0.026
374.955	6.99762	61.627	0.027
374.958	5.99898	53.019	0.021
374.955	4.98094	44.170	0.014

Table 3. Continued

T	p	ρ_{exp}	
K	MPa	kg·m^{-3}	$10^2(\rho_{exp} - \rho_{EoS})/\rho_{EoS}$
374.956	4.00484	35.621	0.009
374.955	2.99823	26.743	−0.005
374.955	1.99501	17.848	0.028
374.957	0.993407	8.908	0.012
400.031	18.4582	143.591	0.032
400.021	17.9819	140.257	0.030
400.020	16.2271	127.785	0.032
400.022	15.9860	126.048	0.032
400.020	14.9879	118.800	0.032
400.019	13.9901	111.464	0.034
400.019	12.9907	104.017	0.030
400.022	11.9942	96.505	0.030
400.019	11.0249	89.118	0.033
400.021	9.89549	80.402	0.031
400.018	8.98697	73.307	0.021
400.018	7.99464	65.495	0.028
400.020	7.00550	57.622	0.020
400.017	5.99615	49.523	0.032
400.021	4.99706	41.415	0.004
400.019	3.99728	33.254	0.019
400.020	2.99426	24.985	−0.020
400.020	1.97547	16.545	0.022
400.017	0.997158	8.375	0.008
400.020	0.984405	8.268	−0.005

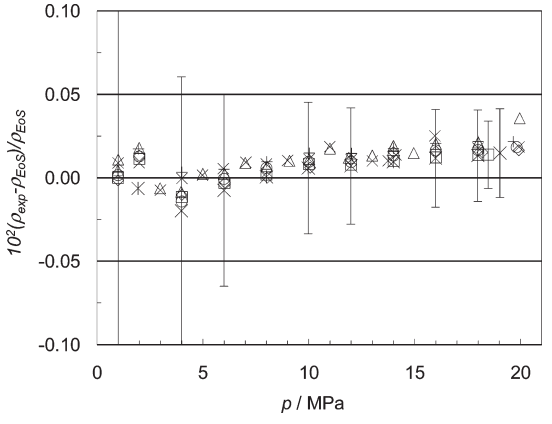

Figure 1. Percentage density deviations of experimental (p, ρ, T) data of the (0.05 CO + 0.95 N_2) binary mixture from density values ρ_{EoS} calculated from the GERG-2008 equation of state versus pressure: □, 250 K; ◇, 275 K; △, 300 K; ×, 325 K; +, 350 K; ○, 375 K; ∗, 400 K. The error bars represent expanded uncertainties in density (k = 2) of the experimental data.

Nitrogen used for test measurements was supplied by Alphagaz (Air Liquid) with a certified mole fraction purity of 0.999999.

3. RESULTS AND DISCUSSION

Experimental (p, ρ, T) data, together with their relative deviations in density from the GERG-2008 equation of state,

are presented in Tables 2 and 3 for the $x_{CO} = 0.05$ and $x_{CO} = 0.10$ mixtures, respectively. Each magnitude value was obtained as the average of the last 10 values of the 30 replicate measurements of each pressure step.

Figures 1 and 2 represent the relative deviations in density of the experimental data from the GERG-2008 equation of state versus pressure. As can be observed, both mixtures show very good agreement with the density values predicted by the equation of state, since the relative deviations in density are within a 0.05 % band and the estimated uncertainty of the equation is 0.1 %. The error bars, which represent the expanded uncertainties ($k = 2$) in density of the experimental values, were plotted only for some data points of the (250 and 400) K isotherms to show the uncertainty as a function of the density value.

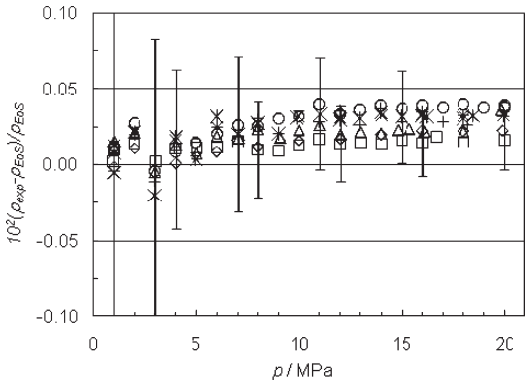

Figure 2. Percentage density deviations of experimental (p, ρ, T) data of the (0.10 CO + 0.90 N_2) binary mixture from density values ρ_{EoS} calculated from the GERG-2008 equation of state versus pressure: □, 250 K; ◇, 275 K; △, 300 K; ×, 325 K; +, 350 K; ○, 375 K; ∗, 400 K. The error bars represent expanded uncertainties in density ($k = 2$) of the experimental data.

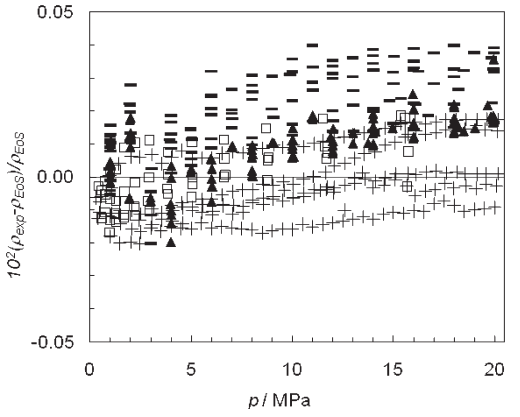

Figure 3. Percentage density deviations of experimental (p, ρ, T) data of CO/N_2 binary mixtures from density values ρ_{EoS} calculated from the GERG-2008 equation of state versus pressure, for CO molar compositions between 0.03 and 0.10 in the temperature range (250 to 400) K and pressures up to 20 MPa: ▲, this work ($x_{CO} = 0.05$); −, this work ($x_{CO} = 0.10$); □, Jaeschke et al. (Burnett apparatus); +, Jaeschke et al. (optical interferometer).

The percentage deviations of the experimental data reported in this work from the equation of state, together with the data reported by Jaeschke et al.[7] for a $x_{CO} = 0.03$ mixture, are shown in Figure 3. It can be seen that relative deviations are slightly larger for the mixtures with a higher carbon monoxide molar fraction. However, since these observed differences are much lower than the estimated uncertainty of the density data, it is not possible to confirm whether this can mean a worse agreement of the experimental data with the GERG-2008 equation of state for mixtures with a high carbon monoxide molar composition. This trend is also found in the statistical comparison given in Table 4, where n is the number of data points, AAD is the average absolute deviation defined in eq 2, RMS refers to the root mean squared defined in eq 3, and MaxD represents the maximum relative deviation in the considered data set

$$\mathrm{AAD} = \frac{1}{n}\sum_{i=1}^{n}\left|10^2\frac{\rho_{i,\mathrm{exp}} - \rho_{i,\mathrm{EoS}}}{\rho_{i,\mathrm{EoS}}}\right| \quad (2)$$

$$\mathrm{RMS} = \sqrt{\frac{1}{n}\sum_{i=1}^{n}\left(\frac{\rho_{i,\mathrm{exp}} - \rho_{i,\mathrm{EoS}}}{\rho_{i,\mathrm{EoS}}}\right)^2} \quad (3)$$

To determine the interaction second virial coefficient B_{12} for mixtures of carbon monoxide and nitrogen, the experimental data of the two mixtures measured in this work were fitted to a second-order virial equation of state, as indicated in eq 4.

$$\frac{Z-1}{\rho} = B + C\rho = (B_{11}x_1^2 + B_{22}x_2^2 + 2B_{12}x_1x_2) + C\rho \quad (4)$$

Here, Z is the experimental compressibility factor, ρ is the experimental density, B and C are the second and third virial coefficients, x_1 and x_2 are the molar fraction of nitrogen and carbon monoxide, and B_{11} and B_{22} are the pure-component virial coefficients of nitrogen and carbon monoxide, which were calculated from the equations of state of Span et al.[10] and Lemmon and Span,[14] respectively.

The fitted interaction second virial coefficients B_{12} are listed in Table 5, together with the B_{12} values and pure component second virial coefficients B_{11} and B_{22}, calculated from the GERG model. The uncertainty of the fitted B_{12} coefficients was calculated following the law of propagation of uncertainties (GUM)[15] and is estimated to be less than 2.7 $cm^3 \cdot mol^{-1}$. These values were compared with the measured values of McElroy and Buchanan[16] and with the GERG-2008 equation of state in Figure 4. As can be observed, there is a good agreement between

Table 4. Statistical Comparison of the Experimental Density Measurements Plotted in Figure 3 Respect to the GERG Model

source	year	experimental technique	x_{CO}	n	10^2 AAD	10^2 RMS	10^2 MaxD
Jaeschke et al.[5]	1997	Burnett apparatus	0.03	56	0.009	0.012	−0.052
Jaeschke et al.[5]	1997	optical interferometer	0.03	287	0.009	0.011	−0.023
this work	2011	single sinker densimeter	0.05	99	0.011	0.014	0.036
this work	2011	single sinker densimeter	0.10	125	0.022	0.024	0.040

dx.doi.org/10.1021/je2007764 |J. Chem. Eng. Data 2011, 56, 3933–3939

Table 5. Interaction (B_{12}) Second Virial Coefficients Obtained from Experimental Data Together with the Interaction and Pure Component ($B_{12\text{-GERG}}$, $B_{11\text{-GERG}}$, $B_{22\text{-GERG}}$) Second Virial Coefficients from the GERG Model for Mixtures of Carbon Monoxide with Nitrogen

T	B_{12}	$B_{12\text{-GERG}}$	$B_{11\text{-GERG}}$	$B_{22\text{-GERG}}$
K	$cm^3 \cdot mol^{-1}$	$cm^3 \cdot mol^{-1}$	$cm^3 \cdot mol^{-1}$	$cm^3 \cdot mol^{-1}$
250	−21.21	−18.67	−16.44	−21.91
275	−13.90	−11.68	−9.86	−14.48
300	−8.02	−6.03	−4.55	−8.47
325	−3.80	−1.39	−0.20	−3.52
350	1.08	2.49	3.43	0.63
375	4.12	5.76	6.49	4.13
400	8.11	8.55	9.10	7.13

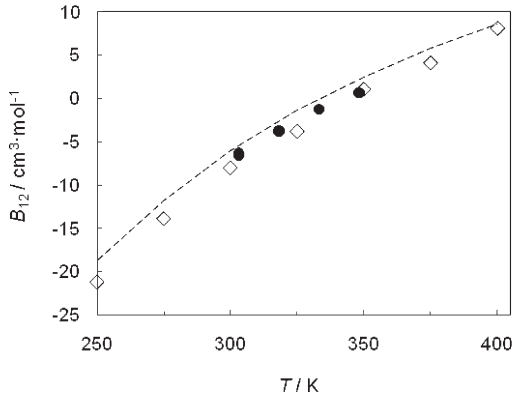

Figure 4. Interaction second virial coefficients of carbon monoxide with nitrogen mixtures. ◇, this work; ●, McElroy and Buchanan; - - -, GERG 2008 equation of state.

the fitted coefficients and the coefficients calculated from the equation of state. Major deviations occur at low temperatures, where the difference between the fitted and calculated coefficients reaches 2.5 $cm^3 \cdot mol^{-1}$.

4. CONCLUSION

Density data for two binary mixtures of carbon monoxide and nitrogen with molar compositions x_{CO} = (0.05, 0.10) in the temperature range (250 to 400) K and pressures up to 20 MPa are reported in this paper. The measurements were carried out using a single sinker densimeter with magnetic suspension coupling to achieve high accuracy determinations.

Experimental densities where compared with those calculated from the GERG-2008 equation of state showing a very good agreement within a 0.05 % deviation band, which is less than the 0.10 % estimated uncertainty of the equation of state for these mixtures. Plots for each mixture revealed deviations where independent from the temperature. Though the deviations showed a slight increase with the carbon monoxide molar fraction, a relation between the agreement of the equation of state and the carbon monoxide composition cannot be concluded, due to the uncertainty in density of the experimental values.

These new, accurate (p, ρ, T) data for carbon monoxide with nitrogen mixtures are a contribution to the few previously existing data, as they cover two additional compositions and a wider temperature range.

AUTHOR INFORMATION

Corresponding Author

*E-mail: cescha@eis.uva.es.

Funding Sources

Support for this work came from the Programa Nacional de Formación de Profesorado Universitario (FPU), project ENE2009-14644-C02-01 of the Spanish Ministry of Science and Innovation and from the Junta de Castilla y León reference GR 152.

ACKNOWLEDGMENT

We thank the Spanish National Metrology Institute (Centro Español de Metrología, CEM) for the preparation of the two binary mixtures studied in this work.

REFERENCES

(1) Marcogaz Final Recommendation. *Injection of Gases from Non-Conventional Sources into Gas Networks*, 2006. http://www.marcogaz.org/membernet/show.asp?wat=WG-Biogas-06-18%20D497%20Final%20Recommendationm.pdf.

(2) Florrisson, O.; Pinchbeck, D. In *Biogas and others in natural gas operations (BONGO): a project under development*; 23rd World Gas Conference, Amsterdam, The Netherlands, June 5−9, 2006.

(3) Starling K. E.; Savidge J. L. *Compressibility factors of natural gas and other related hydrocarbon gases*; AGA Transmission Measurement Committee Report 8; American Gas Association (AGA): Washington, DC, 1992.

(4) Kunz, O.; Klimeck, R.; Wagner, W.; Jaeschke, M. The GERG-2004 Wide-Range Reference Equation of State for Natural Gases and Other Mixtures. *GERG Tech. Monogr. Fortsch. 15*; VDI-Verlag: Düsseldorf, Germany, 2007.

(5) Jaeschke, M.; Benito, A.; Fredheim, A.; Henault, J.-M.; Sangalli, M.; Wesenbeeck, P. V.; Klimeck, R.; Kunz, O.; Span, R.; Wagner, W. In *GERG project: Wide-range reference equation of state for natural gases*; International Gas Research Conference Proceedings, Amsterdam, November 2001; p 11.

(6) Kunz, O.; Wagner, W. The GERG-2008 Wide-Range Equation of State for Natural Gases and Other Mixtures: An Expansion of GERG-2004. *J. Chem. Eng. Data*, to be submitted.

(7) Jaeschke, M.; Humphreys, A. E.; Van Caneghem, P.; Fauveau, M.; Janssen-van Rosmalen, R.; Pellei, Q. *The GERG Databank of High Accuracy Compressibility Factor Measurements*, GERG Technical Monograph, 1997; Vol. 4.

(8) Chamorro, C. R.; Segovia, J. J.; Martin, M. C.; Villamanan, M. A.; Estela-Uribe, J. F.; Trusler, J. P. M. Measurement of the (pressure, density, temperature) relation of two (methane plus nitrogen) gas mixtures at temperatures between 240 and 400 K and pressures up to 20 MPa using an accurate single-sinker densimeter. *J. Chem. Thermodyn.* **2006**, *7*, 916–922.

(9) Mondéjar, M. E.; Segovia, J. J.; Chamorro, C. R. Improvement of the measurement uncertainty of a high accuracy single sinker densimeter via setup modifications based on a state point uncertainty analysis. *Measurement* **2011**, *44*, 1768−1780.

(10) Span, R.; Lemmon, E. W.; Jacobsen, R. T.; Wagner, W.; Yokozeki, A. A reference equation of state for the thermodynamic properties of nitrogen for temperatures from 63.151 to 1000 K and pressures to 2200 MPa. *J. Phys. Chem. Ref. Data* **2000**, *6*, 1361–1401.

(11) McLinden, M. O.; Kleinrahm, R.; Wagner, W. Force transmission errors in magnetic suspension densimeters. *Int. J. Thermophys.* **2007**, *2*, 429–448.

(12) Cristancho, D. E.; Mantilla, I. D.; Ejaz, S.; Hall, K. R.; Iglesias-Silva, G. A.; Atilhan, M. Force transmission error analysis for a high-pressure single-sinker magnetic suspension densimeter. *Int. J. Thermophys.* **2010**, *4*−*5*, 698–709.

(13) Kano, Y.; Kayukawa, Y.; Fujii, K.; Sato, H. A new method for correcting a force transmission error due to magnetic effects in a magnetic levitation densimeter. *Meas. Sci. Technol.* **2007**, *3*, 659–666.

(14) Lemmon, E. W.; Span, R. Short fundamental equations of state for 20 industrial fluids. *J. Chem. Eng. Data* **2006**, *3*, 785–850.

(15) *BIPM, IEC, IFCC, ISO, IUPAC, IUPAP and OIML Guide to the Expression of Uncertainty in Measurement*; International Organization for Standarization: Geneva, Switzerland, 1995.

(16) Mcelroy, P. J.; Buchanan, S. Second virial coefficients of fuel-gas components: (carbon monoxide + nitrogen) and (carbon monoxide + ethene). *J. Chem. Thermodyn.* **1995**, *7*, 755–761.

APPENDIX E – RESEARCH STAY CERTIFICATE

As mentioned in the conclusions section of Chapter 7, this thesis included not only the experimental determination of densities of binary mixtures related with alternative fuels, but also the improvement of the measurement uncertainty of the single sinker densimeter with magnetic suspension coupling used to perform the measurements. A complete control and data acquisition program was developed to automate the measurement procedure.

The experimental work of this thesis was carried out entirely at the TERMOCAL group laboratory located in the Escuela de Ingenierías Industriales of the University of Valladolid (Spain).

However the data treatment, the literature data collection and the analysis and comparison of the experimental density data with the literature data was carried out both at the University of Valladolid and the Ruhr Universität Bochum (Germany), during a four month research sojourn.

The research sojourn was done, as the requirement to obtain the European Doctorate Mention, with the main objective of complementing the work developed in the home institution. This research stay, whose certificate is attached next, contributed to the deepening on the experimental techniques based on the magnetic suspension coupling and also to the collection of the literature data regarding the binary mixtures studied in this work.

THERMODYNAMIK

RUHR UNIVERSITÄT BOCHUM RUB

RUHR-UNIVERSITÄT BOCHUM | 44780 | GERMANY

FAKÜLTÄT FÜR MASCHINENBAU

Institut für Thermo- und Fluiddynamik
Lehrstuhl für Thermodynamik
Gebäude IB 5/27
Universitätsstr. 150, 44870 Bochum

PROF. DR.-ING. ROLAND SPAN
Fon +49 (0)234 32-23033
Fax +49 (0)234 32-14163
roland.span@thermo.rub.de
www.rub.de/thermo

To Whom it Concerns

October 14, 2010

Certificate for María Engracia Mondéjar Montagud

Mrs. Maria Engracia Mondéjar Montagud worked at my institute at Ruhr-Universität Bochum, Faculty Mechanical Engineering, from Tuesday, June 1, 2010 to Friday, October 1, 2010. Her stay was financed by a stipend granted by the Spanish government.

At her home university she is preparing a Ph.D. thesis working on highly accurate density measurements with a magnetic suspension balance based densitometer. This technique is internationally considered the most accurate method for density measurements over broad temperature and density ranges and was developed at my institute in the 1980s under the lead of my predecessor, Prof. Dr.-Ing. Wolfgang Wagner. Mrs. Mondéjar utilized her stay at Ruhr-Universität in three ways:

- She made use of the opportunity to talk directly to colleagues who have been involved in density measurements with magnetic suspension balances for many years, namely with Dr.-Ing. Reiner Kleinrahm, one of the inventors of this experimental technique. During these discussions she improved her fundamental understanding of possibilities and limitations of this advanced experimental technique, but also on requirements regarding peripheral measuring devices such as accurate pressure transducers and thermometers.
- With colleagues working on equations of state, namely with Dipl.-Ing. Johannes Gernert, and with myself she intensively discussed the data situation for the mixtures she is interested in. These discussions resulted in a deeper understanding on requirements on the data sets she is attempting to measure at her home university. In general my impression is that she selected fluids and mixtures, where additional accurate data are highly appreciated for the development of thermodynamic property models required for example for application in energy processes with carbon capture and sequestration.
- In the research team led by Dr.-Ing. Tobias she worked experimentally in a cooperative international project on combined sorption and density measurements. During this experimental work she established know-how on a completely different, but also magnetic-suspension bal-

RUHR UNIVERSITÄT BOCHUM RUB

ance based measurement system. Without any doubt this experience will help her to see her own thesis directed work in a broader context.

I already knew Mrs. Mondéjar from a stay at the University of Valladolid in March 2010. However, working with her on an actual scientific project I got a much deeper impression of her. I consider her a very intelligible young scientist. When being confronted with new and challenging tasks, she is able to get into the corresponding subjects within very short time. Though she is (professionally speaking) still very young, she is an experienced experimentalist and works very reliably. She has a very positive personality, making it easy to work with her. Her German has greatly improved during her stay. Towards the end of her stay she was even able to follow complex technical discussions in German. The colleagues who worked with her all share my point of view – the feedback I got was very positive.

I am convinced that Mrs. Mondéjar has all the skills required to become a successful engineering scientist, be it in an academic position or in industrial R&D. She is always welcome at my institute and I am looking forward to becoming one of the reviewers for her Ph.D.

Prof. Dr.-Ing. Roland Span

Universidad de Valladolid

ESCUELA DE INGENIERÍAS INDUSTRIALES

DPTO. INGENIERÍA ENERGÉTICA Y FLUIDOMECÁNICA

TESIS DOCTORAL:

CONTRIBUCIÓN AL DESARROLLO E INTRODUCCIÓN DE COMBUSTIBLES GASEOSOS RENOVABLES MEDIANTE LA CARACTERIZACIÓN TERMODINÁMICA DE MEZCLAS DE SUS COMPONENTES UTILIZANDO UN DENSÍMETRO DE FLOTADOR DE SUSPENSIÓN MAGNÉTICA OPTIMIZADO

Presentada por

MARÍA ENGRACIA MONDÉJAR MONTAGUD

para optar al grado de doctora por la Universidad de Valladolid

Dirigida por:
DR. CÉSAR R. CHAMORRO CAMAZÓN
DR. ROLAND SPAN

AGRADECIMIENTOS

Esta tesis cierra mi etapa como estudiante de doctorado, llena de horas de trabajo y aprendizaje, pero también de diversión, a la vez que abre la puerta a una nueva etapa, que espero sea igual o mejor que ésta. Sin la ayuda y apoyo que he recibido durante todo este tiempo esta tesis se abría hecho, sin duda, mucho más larga y difícil, y por ello quiero expresar mis más sinceros agradecimientos:

Al Dr. César R. Chamorro, en especial, por toda la ayuda que me ha prestado desde el comienzo de mi doctorado. Por la dirección de este trabajo, por su apoyo, por su gran dedicación, por su gran paciencia y por sus consejos, mil gracias.

Al Dr. Roland Span por la ayuda que me prestó, tanto durante mi estancia en la Ruhr Universität Bochum como en la dirección de esta tesis, *Danke schön!*

También, por supuesto, a todos los compañeros del grupo TERMOCAL que me han ayudado con mi trabajo y apoyado cuando lo necesitaba. Por los buenos momentos que hemos tenido en el laboratorio, gracias.

También, a los compañeros del Lehrstuhl für Thermodynamik de la Ruhr Universität Bochum, por acogerme desde el principio como una compañera más. Por los buenos momentos pasados en Bochum, a todos ellos, *Danke schön auch!*

Y por supuesto, a mi familia y amigos, gracias por apoyarme en los días más duros de toda esta etapa y por ayudarme a sonreír. Por los buenos momentos, gracias de nuevo.

Por último, estos agradecimientos no pueden finalizar sin mencionar al Programa Nacional de Formación de Profesorado Universitario (FPU) del Ministerio de Ciencia e Innovación de España, gracias al cual tuve la financiación para el desarrollo de esta tesis.

¡Gracias a todos los que me habéis apoyado!

RESUMEN

En esta tesis se trata la caracterización termodinámica de mezclas gaseosas binarias relacionadas con los combustibles alternativos a través de la medida de gran precisión de la densidad mediante un densímetro de flotador sencillo con acoplamiento magnético.

Previamente a las medidas se realizaron una serie de modificaciones del equipo con el fin de reducir las principales fuentes de incertidumbre de cada magnitud medida. Una vez realizadas las mejoras se procedió a una detallada estimación de la incertidumbre de medida.

Las medidas de densidad se llevaron a cabo en el rango de temperatura (250 – 400) K a presiones de hasta 20 MPa en las mezclas binarias dióxido de carbono + nitrógeno, monóxido de carbono + nitrógeno, y dióxido de carbono + metano.

Los datos experimentales se compararon con las densidades calculadas con la ecuación de estado de referencia para gases naturales y mezclas relacionadas, GERG-2004.

ÍNDICE

NOMENCLATURA

SÍMBOLOS

B	fuerza de empuje, N segundo coeficiente del virial, $cm^3 \cdot mol^{-1}$
C	constant elastic de segundo orden tercer coeficiente del virial, $(cm^3 \cdot mol^{-1})^2$
E	Módulo de Young, Pa^{-1}
f	función modelo para la ley de propagación de las incertidumbres
g	aceleración de la gravedad, $m \cdot s^{-2}$
k	factor de cobertura
K	módulo de compresibilidad, MPa^{-1}
m	masa, kg
N	número de componentes de una mezcla
p	presión, MPa
r	coeficiente de correlación
R	resistencia, Ω
s	desviación estándar
T	temperatura, K
u	incertidumbre estándar
U	incertidumbre expandida
V	volumen, m^3

W	ratio de resistencias, Ω/Ω
	lectura de la balanza, g
x	estimación de la magnitud de entrada
X	magnitud de entrada
y	estimación de la magnitud de salida
Y	magnitud de salida
Z	factor de compresibilidad

SÍMBOLOS GRIEGOS

α	energía libre de Helmholtz reducida
	coeficiente de expansión térmica, K^{-1}
δ	densidad reducida
ε_ρ	constante específica del aparato
ϕ_0	factor de acoplamiento
μ	media
ν	grados de libertad
ρ	densidad, $kg \cdot m^{-3}$
τ	temperatura reducida
χ	susceptibilidad magnética, $m^3 \cdot kg^{-1}$

SUBÍNDICES

0	estado de referencia de la calibración del volumen del flotador
1	flotador de titanio
2	flotador de silicio
eff	número efectivo de grados de libertad
em	electroimán
exp	dato experimental
EoS	calculado con la ecuación de estado
i, j	índices de las magnitudes de entrada
MP	punto de medida
n	número de observaciones independientes repetidas
N	número total de magnitudes de entrada
oi	componente i de una mezcla
pm	imán permanente
probe	resistencia de la sonda de tempertura
std	resistencia estándar
S	flotador
S0	flotador en el vacío
Sf	flotador inmerso en el fluido
Ti	masa calibrada de titanio
Ta	masa calibrada de Tántalo

ZP	punto cero

SUPERINDICES

r	comportamiento residual
0	comportamiento de gas ideal

ABREVIATURAS

AAD	desviación media absoluta
Bias	desviación media
CEM	Centro Español de Metrología
CF	Factor de calibración
EA	Agencia Europea de Acreditación
ENAC	Entidad Nacional de Acreditación de España
EU	Unión Europea
EURAMET	Asociación Europea de Institutos Nacionales de Metrología
FTE	Error en la transmisión de la fuerza
GERG	Grupo Europeo de Investigación del Gas
GUM	Guía para la expresión de la incertidumbre de medida
IUPAC	International Union of Pure and Applied Chemistry (Unión Internacional de Química Pura y Aplicada)
MaxD	máxima desviación relativa
MP	Punto de medida

NP	posición nula
PC	Ordenador personal
PRT	Termómetro de resistencia de platino
RMS	media cuadrática
SSMSD	Densímetro de flotador sencillo con acoplamiento magnético
TSMSD	Densímetro de dos flotadores con acoplamiento magnético
ZP	Punto cero

SÍMBOLOS QUÍMICOS

CH_4	Metano
CO	Monóxido de carbono
CO_2	Dióxido de carbono
N_2	Nitrógeno
O_2	Oxígeno
Si	Silicio
Ta	Tántalo
Ti	Titanio

CAPÍTULO 1

INTRODUCCIÓN Y JUSTIFICACIÓN

1.1. JUSTIFICACIÓN

La investigación presentada en esta tesis se justifica en los siguientes apartados.

Situación actual: crisis energética y medioambiental

A comienzos del siglo XXI el mundo se enfrenta a dos importantes amenazas: la profunda crisis del actual modelo energético debido al agotamiento de las reservas de petróleo y gas natural, y el incremento del calentamiento global provocado por el efecto invernadero. Estos dos problemas, lejos de ser independientes son, en realidad, las dos caras de una misma moneda: la economía de los combustibles fósiles.

A pesar de que los combustibles fósiles han sido utilizados por la humanidad desde mucho antes de la Edad Moderna, fue durante la Revolución Industrial cuando el consumo de éstos comenzó a crecer rápidamente. Desde entonces, los combustibles fósiles han encontrado multitud de aplicaciones, sobre todo el petróleo y el gas natural, cuyas reservas se están viendo gravemente reducidas. El aumento de los precios de los combustibles, sumado a la gran dependencia energética de Europa del exterior, cuestionan cada vez más la actual economía basada en los combustibles fósiles.

El cambio frente a la actual economía de los combustibles fósiles

La solución a esta situación requiere del cambio de nuestro modelo energético, lo cual, lejos de ser utópico, es un hecho que ya se ha dado con anterioridad en distintos momentos de la historia.

Puesto que el agotamiento de las reservas y el calentamiento global provocado por las altas emisiones de dióxido de carbono son hechos indiscutibles, nuestra prioridad es la investigación en nuevas fuentes de energía que reemplacen a los actuales combustibles fósiles cumpliendo unos requerimientos tanto energéticos como medioambientales.

Estrategias hacia un futuro sostenible

Las estrategias para el cambio hacia un modelo energético más sostenible se apoyan en tres pilares principales:

- El uso de las energías renovables, que además de reducir las emisiones de dióxido de carbono, reducirían notablemente la dependencia energética del exterior.
- La captura y secuestro del dióxido de carbono presente en las emisiones de los actuales sistemas de generación eléctrica.
- El ahorro y la eficiencia energética, con el fin de evitar pérdidas innecesarias de energía.

Combustibles gaseosos alternativos como parte de la nueva economía sostenible

Los combustibles gaseosos alternativos, entre los que se encuentran los producidos a partir de distintas fuentes de biomasa y aquellos procedentes de subproductos de procesos industriales como los que tienen lugar en los hornos de coque, pueden jugar un papel muy importante en el nuevo modelo energético sostenible.

Actualmente existen proyectos a nivel Europeo, como Marcogaz (1) y Bongo (2), para la integración de estos combustibles gaseosos alternativos en la red de gaseoductos de gas natural existente. Un proyecto de investigación de EURAMET (3) estudia, además, la caracterización energética de estos gases.

El papel de la termodinámica en el desarrollo y la explotación de los combustibles gaseosos alternativos

El conocimiento preciso del comportamiento termodinámico de los combustibles es imprescindible para su desarrollo y para la optimización de su explotación, transporte y almacenamiento. La descripción de las propiedades termodinámicas del combustible puede venir dada por diversas correlaciones, o de forma más extensa, por una ecuación de estado.

Actualmente el conocimiento del comportamiento termodinámico del gas natural es de una gran precisión gracias a toda la investigación previa que culminó con la creación de una ecuación de estado de referencia para gases naturales, GERG-2004 (4).

Esta ecuación, que viene dada de forma explícita en la energía libre de Helmholtz, está formulada, de forma resumida, como la suma de ecuaciones fundamentales de cada componente puro de la mezcla más funciones que representan el comportamiento de mezcla.

Como la energía libre de Helmholtz no es accesible desde el punto de vista experimental, el ajuste de la ecuación se realiza de forma simultánea con datos experimentales de distintas propiedades termodinámicas, a través de las cuales se ajustan los parámetros.

La importancia de los datos experimentales de densidad para el desarrollo de ecuaciones de estado

De entre todas las propiedades termodinámicas que participan en el desarrollo de una ecuación de estado, la densidad es de gran importancia por dos razones: su accesibilidad mediante técnicas experimentales de gran precisión y su comportamiento 'lineal' en relación al problema de optimización de parámetros de la ecuación. Por estas dos razones, la disponibilidad de datos experimentales de densidad es de gran interés para el desarrollo de ecuaciones de estado. Además, los datos experimentales de densidad son también utilizados en el cálculo indirecto de otras propiedades termodinámicas, como el índice de Woobe, o para el ajuste de los coeficientes de la ecuación del virial.

La actual ecuación de estado de referencia para gases naturales y mezclas relacionadas

El gran interés del gas natural, y por extensión, de otros combustibles gaseosos no convencionales, hizo necesario la caracterización precisa de su comportamiento termodinámico en un amplio rango de condiciones y composiciones. Para ello, la ecuación de estado AGA8-DC92 de Starling y Savidge (5) surgió como un modelo para

la predicción de las propiedades del gas natural y otras mezclas de sus componentes en la fase gas. Con la creciente exigencia en cuanto a la precisión de las estimaciones, esta ecuación comenzó a mostrar limitaciones, sobre todo a bajas temperaturas y para mezclas con composiciones notablemente diferentes de las del gas natural. Con el fin de superar estas limitaciones y, además, extender el rango de validez de la ecuación a toda la fase fluida, la nueva ecuación de estado de referencia para gases naturales y otras mezclas, GERG-2004 (4), fue desarrollada. Sin embargo, la ecuación de estado AGA8-DC92 se utiliza todavía como el actual estándar en la industria gasista.

Recientemente se ha desarrollado una nueva versión del modelo GERG, la ecuación de estado GERG-2008 (6), que amplía el original número de sustancias cubiertas por la ecuación GERG-2004 (18 componentes) a 21 componentes. Los nuevos componentes son el n-nonano, n-decano y el ácido sulfhídrico. Como estos componentes no forman parte de las mezclas estudiadas en este trabajo, los datos de densidad publicados en esta tesis son siempre comparados con densidades calculadas con la ecuación de estado GERG-2004.

Esta nueva ecuación de estado GERG-2008 está, además, bajo consideración para ser adoptada como un estándar ISO (ISO 20765-2 e ISO 20765-3).

El modelo GERG fue desarrollado principalmente para la estimación de propiedades de gases naturales o mezclas relacionadas. Por ello es apreciable una falta de datos para mezclas que contengan componentes minoritarios del gas natural, pero posiblemente mayoritarios en el caso de combustibles no convencionales como el biogás o el gas de síntesis. Por ello, cualquier mezcla que contenga estas sustancias resultará de gran interés para el estudio de sus propiedades termodinámicas, ya que éstas podrán ser utilizadas en la mejora de los actuales modelos de estimación y ecuaciones de estado.

1.2. OBJETO

Los principales objetivos de la presente tesis doctoral se enumeran a continuación:

Mejora de la incertidumbre de medida del densímetro de flotador sencillo

El primer objetivo de esta tesis era la reducción de la incertidumbre de medida del densímetro de flotador sencillo con acoplamiento magnético con el fin de obtener resultados experimentales de la mayor precisión posible.

Para reducir la incertidumbre de medida de las tres magnitudes del punto de medida (p, ρ, T), del modo más efectivo posible, se realizó un análisis de las principales fuentes de incertidumbre de cada magnitud, con el fin de reducir sólo las principales contribuciones. Las modificaciones que se llevaron a cabo en el densímetro fueron propuestas en base a este análisis con el objetivo de actuar solamente en los puntos realmente necesarios.

Desarrollo de un programa de control y adquisición de datos

La optimización del tiempo de adquisición de datos experimentales requería del desarrollo de un programa para el control y la adquisición de datos. El nuevo software debía de cumplir los requerimientos de facilidad de uso y flexibilidad para modificaciones.

Medida de datos experimentales (p, ρ, T) de mezclas binarias de componentes de combustibles no convencionales

El objetivo principal de esta tesis es la caracterización precisa del comportamiento (p, ρ, T) de distintas mezclas binarias compuestas de componentes mayoritarios de combustibles gaseosos alternativos, en un amplio rango de temperatura y presión. Este objetivo se lleva a cabo mediante la medida experimental de la densidad de las mezclas utilizando un densímetro de flotador sencillo con acoplamiento magnético. Este objetivo está directamente relacionado con la importancia del conocimiento preciso del comportamiento termodinámico de combustibles alternativos, que ya ha sido comentada anteriormente. Por esta razón, en esta tesis se han estudiado mezclas

binarias que contienen nitrógeno, dióxido de carbono, monóxido de carbono y metano.

Chequeo de la actual ecuación de estado de referencia para gases naturales

Otro de los objetivos de esta tesis es el chequeo de la capacidad de la actual ecuación de estado de referencia para gases naturales y otras mezclas relacionadas en la estimación de la densidad de mezclas binarias que contengan componentes de combustibles gaseosos. De esta forma, los datos experimentales medidos durante el desarrollo de esta tesis serán usados para comprobar la ecuación de estado GERG-2004.

Contribución a la actual base de datos experimentales de densidad para la mejora de los parámetros de mezcla de la ecuación de estado de referencia para gases naturales

La aportación de nuevos datos experimentales de densidad de gran precisión es de gran importancia dado el continuo proceso de mejora que afecta al desarrollo de una ecuación de estado. Por ello, los datos presentados en esta tesis no sólo sirven para evaluar la capacidad de la actual ecuación de estado para gases naturales, sino que también contribuyen a la futura mejora de la misma.

1.3. ESTRUCTURA DE LA TESIS

En esta tesis se presentan datos experimentales de densidad de mezclas binarias de dióxido de carbono con nitrógeno, monóxido de carbono con nitrógeno y dióxido de carbono con metano, obtenidas mediante un densímetro de flotador sencillo con acoplamiento magnético de gran precisión.

Esta tesis está estructurada en siete capítulos y un apéndice cuyo contenido se detalla a continuación:

En el **capítulo primero**, se ha expuesto la justificación y los objetivos de la investigación presentada y se detalla la estructura del presente documento.

En el **capítulo segundo**, se describe el principio de medida del densímetro de flotador sencillo con acoplamiento magnético, tras enumerar brevemente las actuales metodologías para la medida de la densidad de fluidos. Se describen los equipos auxiliares para la medida de cada magnitud y el desarrollo del programa de control y adquisición de datos.

En el **capítulo tercero**, se describen las modificaciones llevadas a cabo en el densímetro para la mejora de su incertidumbre de medida. Así mismo se detalla el cálculo de la incertidumbre de medida de cada magnitud del punto de estado y se analizan las mejoras obtenidas con respecto a su valor antes de realizar las modificaciones.

En el **capítulo cuarto**, se presentan los datos experimentales de densidad de cuatro mezclas de dióxido de carbono con nitrógeno, con fracciones molares de dióxido de carbono de 0.10, 0.15, 0.20 y 0.50. Además, se comparan estos datos con las densidades calculadas con la ecuación de estado para gases naturales GERG-2004 y con los datos experimentales de la bibliografía. Se proporcionan también los coeficientes segundo y tercero del virial ajustados con los datos experimentales.

En el **capítulo quinto**, se presentan los datos experimentales de densidad de dos mezclas de monóxido de carbono con nitrógeno, con fracciones molares de monóxido de carbono de 0.05 y 0.10. Los datos son comparados con las densidades calculadas con la ecuación de estado GERG-2004 y con los datos experimentales de la bibliografía. Se presentan, además, los coeficientes segundo y tercero del virial para estas mezclas.

En el **capítulo sexto**, se presentan los datos experimentales de densidad de una mezcla de dióxido de carbono con metano con una fracción molar de dióxido de carbono de 0.20. Los datos experimentales son comparados con las densidades calculadas con la ecuación de estado GERG-2004 y con datos experimentales de la bibliografía.

Finalmente, en el **capítulo séptimo**, se enumeran las conclusiones obtenidas tras la realización de esta tesis y se proponen diversas líneas de continuación del trabajo presentado.

En los **Apéndices** se recogen tabulados todos los datos experimentales de densidad medidos durante la realización de este trabajo y se enumeran las publicaciones en revistas internacionales y congresos enmarcados en esta tesis. Se recoge, además, el certificado de estancia para la obtención de la Mención de Doctorado Europeo.

BIBLIOGRAFÍA

1. Marcogaz. *Final Recommendation - Injection of Gases from Non-Conventional Sources into Gas Networks*, 2006.

2. FLORRISSON, O. and PINCHBECK, D. *Biogas and Others in Natural Gas Operations (BONGO): A Project Under Development.* Burgel ed. 23 rd World Gas Conference, 2006.

3. HALOUA, F. et al. *Caloric Quantities and Density Measurement of Non-Conventional Gases*, 2011.

4. KUNZ, O. et al. The GERG-2004 Wide-Range Reference Equation of State for Natural Gases and Other Mixtures*. GERG Technical Monograph Fortschr*, 2007.

5. STARLING, K.E.; and SAVIDGE, J.L. *Compressibility Factors of Natural Gas and Other Related Hydrocarbon Gases - AGA Transmission Measurement Committee Report 8*, 1992.

6. KUNZ, O. and WAGNER, W. The GERG-2008 Wide-Range Equation of State for Natural Gases and Other Mixtures: An Expansion of GERG-2004*. To be Submitted to J. Chem. Eng. Data*, 2011.

CAPÍTULO 2

EL DENSÍMETRO DE FLOTADOR SENCILLO CON ACOPLAMIENTO MAGNÉTICO

2.1. ESTADO DEL ARTE DE LOS MÉTODOS DE MEDIDA DE LA DENSIDAD

Entre todos los métodos de determinación de la densidad de fluidos, la IUPAC (International Union of Pure and Applied Chemistry) (1) reconoce los enumerados a continuación como los más precisos:

- Cuerpos vibrantes: que relacionan la frecuencia de vibración de un cuerpo con la densidad del fluido que lo rodea.

- Flotación: en los cuales se aplica el Principio de Arquímedes para relacionar la fuerza de empuje de un fluido actuante sobre un cuerpo con la densidad de dicho fluido.

- Piezómetros: en los que se determina la densidad del fluido a partir la cantidad de fluido contenido

- Densímetros volumétricos de fuelle: en los que la compresión del fluido presurizado se determina a través del desplazamiento sufrido por el fuelle.

- Métodos isocóricos: en los que la densidad del fluido a determinada presión se determina gracias al volumen conocido de la celda que lo contiene.

A pesar de que muchos de estos métodos han sido ampliamente desarrollados, existen limitaciones significantes tanto por rango de trabajo como por falta de precisión en algunos de ellos. Las metodologías más utilizadas en los últimos años para la medida de la densidad de fluidos son las basadas en hilo vibrante y tubo vibrante, de las que existen equipos comerciales en el mercado. Sin embargo, Wagner y Kleinrahm (2) concluyeron que la técnica que más requerimientos aúna, en cuanto a amplios rangos de trabajo y bajas incertidumbres de medida, son los densímetros hidrostáticos con acoplamiento magnético, de los que hay dos tipos principales: el densímetro de dos flotadores y el densímetro de flotador sencillo. Ambos densímetros son capaces de trabajar en amplios rangos de temperatura y presión gracias al acoplamiento magnético entre el flotador y la balanza, que permite que el fluido medido no entre en contacto con la balanza, evitando así posibles daños.

2.2. PRINCIPIO DE MEDIDA DEL DENSÍMETRO DE FLOTADOR SENCILLO CON ACOPLAMIENTO MAGNÉTICO

El densímetro de flotador sencillo con acoplamiento magnético fue originalmente desarrollado por Brachthäuser et al. (3), a principios de los añoso 90, con el objetivo de simplificar el complejo diseño del densímetro de dos flotadores. El densímetro fue posteriormente mejorado por Klimeck (4) y a partir de éste, se crearon distintas versiones compactas.

La versión compacta del densímetro de flotador sencillo con acoplamiento magnético utilizada y modificada en este trabajo, que fue fabricada por Rubotherm Präzisionsmesstechnik GmbH, trabaja a temperaturas entre 250 K y 400 K y a presiones de hasta 20 MPa. El equipo fue inicialmente descrito por Chamorro et al. (5) y ha sido modificado durante el desarrollo de esta tesis para reducir su incertidumbre de medida.

La densidad del fluido contenido en la celda de medida se determina mediante la Ec.2.1., en la que se relaciona la fuerza de empuje experimentada por el flotador al estar inmerso en el fluido con la densidad del mismo.

$$\rho(T,p)=\frac{B}{g\cdot V(T,p)}=\frac{m_{S0}-m_{Sf}}{V_S(T,p)} \qquad \text{Ec.2.1.}$$

En esta expresión, B es la fuerza de empuje del fluido, obtenida como la diferencia en masa del flotador en el vacío y del flotador inmerso en el fluido, m_{S0}-m_{Sf}, g es la aceleración de la gravedad y $V_S(T,p)$ es el volumen del flotador como función de la temperatura y presión del fluido.

En la Figura 2.1. se muestra un esquema de la celda de medida del densímetro de flotador sencillo. En ella se puede ver cómo el flotador es un cilindro con un taladro pasante a través del cual se encuentra el soporte con el imán permanente. Este imán permanente es atraído por el electroimán conectado a la balanza y la posición del acoplamiento es detectada mediante el sensor de posición situado en la parte inferior de la celda. En las siguientes secciones se describen los equipos auxiliares para la medida de cada magnitud del punto de estado.

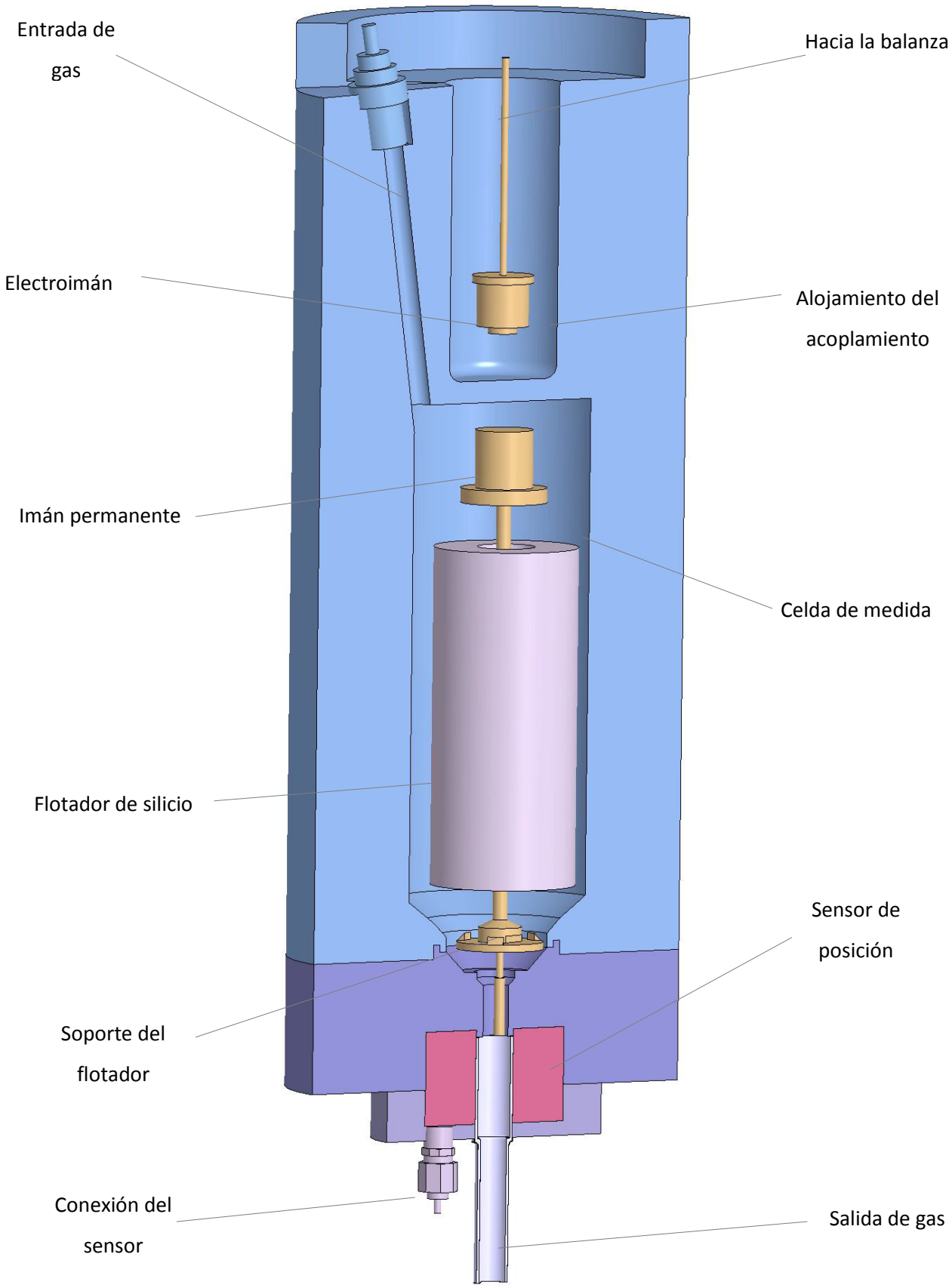

Figura 2.1. Esquema 3D de la celda de medida.

2.2.1. Medida de la presión

La presión del fluido contenido en la celda se mide utilizando dos transductores de presión Paroscientific, modelos 43KR-HHT-101 y 2300A-101, que trabajan en los rangos de 2 – 20 MPa y de 0 – 2 MPa, respectivamente. Éste último está separado del resto de la línea de presión mediante una válvula manual, para evitar su exposición a sobrepresiones.

La red de presión está formada por conductos de 1/4" de diámetro interior en la línea de vacío, 1/8" en la conexión de la celda de medida y de 1/16" en el resto. Las válvulas y juntas fueron suministradas por HIP (High Pressure Equipment Company) para presiones de hasta 15000 psi. Una bomba manual, del mismo proveedor, se utiliza para alcanzar las presiones requeridas en el interior de la celda cuando la botella que contiene el gas tiene une presión menor a la requerida.

El proceso de llenado y presurizado de la celda se lleva a cabo de forma manual y haciendo uso, en caso necesario, de la bomba manual. La evacuación de la celda puede realizarse de forma manual o de forma automática mediante una válvula accionada por un pistón neumático.

El vacío en la celda se alcanza mediante una bomba de vacío Leybold modelo Trivac D88. Una trampa de zeolitas y una trampa criogénica instaladas en la línea de vacío, evitan el paso de impurezas hacia la celda o el daño de la bomba provocado por los gases de medida.

2.2.2. Medida de la temperatura

La temperatura del fluido de la celda de medida se determina mediante dos sondas PRT-25, situadas diametralmente opuestas, a una altura media de la celda de medida. Estas sondas están a su vez conectadas a un puente comparador de resistencias Automatic Systems Laboratory F700 mediante un multicanal Switchbox ASL SB 148/01.

La termostatización de la celda se realiza en dos etapas. El sistema primario consiste en un cilindro de acero de doble pared que rodea a la celda y al sistema de termostatización secundario, a través del cual circula el fluido de un baño termostático Julabo MV FP50. El sistema secundario consiste en una resistencia eléctrica,

directamente en contacto con la celda de medida, que es controlada por un controlador electrónico de temperatura Julabo MC-E.

La celda de medida está aislada térmicamente con espuma de silicona y una carcasa de goma sintética de polietileno (Armaflex). La temperatura de la habitación fue controlada entre 20ºC y 22ºC para evitar que ésta afectara a la medida de los transductores de presión.

2.2.3. Medida de la masa

La masa del flotador es determinada mediante una balanza analítica de alta precisión Mettler Toledo AT261 Deltarange, con una resolución de 0.01mg. El funcionamiento de la balanza tiene dos particularidades: la existencia del acoplamiento magnético entre la balanza y el soporte del flotador, y el sistema de cambio de masas calibradas sobre el plato de la balanza.

El acoplamiento magnético tiene tres posibles posiciones (apagado, posición nula y posición de medida) según éste está desactivado, activado sin soportar en peso del flotador o activado soportando el peso del flotador.

El sistema de cambio de masas calibradas se utiliza para compensar el efecto de 'no linealidad' de la balanza. Colocando estas dos masas (de Titanio y de Tántalo, del mismo volumen) sobre el plato de la balanza, se procede de tal forma que la masa medida por ésta sea siempre lo más cercana posible al cero, para así evitar la 'no linealidad'. Además, midiendo la diferencia entre estas dos masas calibradas y comparando el valor con el de su certificado de calibración se calcula un factor de calibración con el que se corrige toda medida de la balanza.

Merece especial atención el error en la transmisión de la fuerza que tiene lugar en el acoplamiento magnético. Este error tiene dos contribuciones: la debida a las características magnéticas de la propia celda de medida y el equipo, y la inducida por el comportamiento magnético del fluido contenido en la celda. La primera puede ser fácilmente compensada midiendo la masa del flotador en el vacío para cada temperatura. La segunda contribución puede determinarse mediante un método descrito por McLinden et al. (6), que consiste en la determinación experimental de una

constante específica del aparato realizando medidas de densidad con diferentes flotadores. En este trabajo sólo se corrigieron los datos de densidad para compensar la contribución debida al propio equipo ya que la susceptibilidad magnética de los gases estudiados aquí era prácticamente despreciable.

Finalmente la determinación de la masa del flotador, tanto en vacío como con la celda presurizada, se lleva a cabo midiendo ésta en dos puntos:

- En el Punto Cero (ZP) el acoplamiento magnético está en la posición nula de modo que está activado y tan sólo sujeta el soporte del flotador. La masa de Tántalo está apoyada sobre el plato de la balanza.

- En el Punto de Medida (MP) el acoplamiento magnético esta activado y sostiene tanto el soporte del flotador como el flotador mismo. La masa de titanio está apoyada sobre el plato de la balanza.

Al hacer la diferencia entre estos dos puntos, se anulan las masas del soporte del flotador y del imán permanente. Cuando se hace la diferencia entre la medida en el vacío y la medida con la celda presurizada, como se indica en la Ec.2.1., se eliminan los efectos de las masas calibradas de Titanio y Tántalo. Finalmente, la densidad del fluido se obtiene dividiendo este valor entre el del volumen del flotador.

2.3. AUTOMATIZACIÓN PARCIAL DEL PROCESO DE MEDIDA Y PROGRAMA PARA EL CONTROL Y ADQUISICIÓN DE DATOS

El programa de control y adquisición de datos original del densímetro precisó ser sustituido por razones de actualización del software. Este nuevo programa fue desarrollado, como parte de este trabajo, en el entorno Agilent VEE Pro 7.0. Los principales objetivos del nuevo programa fueron la facilidad de uso y su flexibilidad de cara a futuras modificaciones.

El panel de control del nuevo programa muestra tres gráficas con las medidas de presión, masa y temperatura del set de datos de cada presión, el factor de calibración, el número de medidas por presión y la actual medida. Antes del cambio de presión todos los datos medidos son almacenados en una hoja Excel para su posterior tratamiento.

BIBLIOGRAFÍA

1. MAJER, V. et al. *Measurement of the Thermodynamic Properties of Single Phases*, 2003. pp. 149-168.

2. WAGNER, W. and KLEINRAHM, R. Densimeters for very Accurate Density Measurements of Fluids Over Large Ranges of Temperature, Pressure, and Density. *Metrologia*, 2004, vol. 41, no. 2. pp. S24-S39.

3. BRACHTHÄUSER, K. et al. *Entwicklung Eines Neuen Dichtemeßverfahrens Und Aufbau Einer Hochtemperatur-Hochdruck-Dichtemeßanlage*, 1993.

4. KLIMECK, J.; KLEINRAHM, R. and WAGNER, W. An Accurate Single-Sinker Densimeter and Measurements of the (p, ρ, T) Relation of Argon and Nitrogen in the Temperature Range from (235 to 520) K at Pressures Up to 30 MPa. *Journal of Chemical Thermodynamics*, 1998, vol. 30, no. 12. pp. 1571-1588.

5. CHAMORRO, C.R. et al. Measurement of the (Pressure, Density, Temperature) Relation of Two (Methane + Nitrogen) Gas Mixtures at Temperatures between 240 and 400 K and Pressures Up to 20 MPa using an Accurate Single-Sinker Densimeter. *Journal of Chemical Thermodynamics*, 2006, vol. 38, no. 7. pp. 916-922.

6. MCLINDEN, M.O.; KLEINRAHM, R. and WAGNER, W. Force Transmission Errors in Magnetic Suspension Densimeters. *International Journal of Thermophysics*, 2007, vol. 28, no. 2. pp. 429-448.

CAPÍTULO 3

MEJORA DEL DENSÍMETRO A PARTIR DE UN ANÁLISIS DE LA INCERTIDUMBRE

3.1. INTRODUCCIÓN

La incertidumbre de medida de un dato experimental es una magnitud cuyo valor es imprescindible evaluar puesto que cuantifica la calidad del dato experimental y permite, con ello, la comparación de dicho dato con otros existentes.

El método más extendido para la estimación de la incertidumbre de medida de una magnitud es la ley de propagación de la incertidumbre, descrita en la Guía para la expresión de la Incertidumbre de Medida (GUM) (1) y que fue utilizada para determinar la incertidumbre de las magnitudes del punto de estado en este capítulo. Como alternativa a ésta, el método de Monte Carlo permite estimar la incertidumbre de medida en aquellos casos donde la ley de propagación de la incertidumbre no es aplicable, además de servir para comprobar el resultado obtenido con la primera.

3.2. ANÁLISIS DE LA INCERTIDUMBRE Y PROPUESTA DE MODIFICACIONES

Para mejorar la incertidumbre de medida del densímetro de flotador sencillo de la forma más optimizada posible, se decidió evaluar la incertidumbre de medida de cada magnitud así como las principales fuentes de incertidumbre, con el fin de actuar sólo en las más importantes.

3.2.1. Incertidumbre de medida de cada magnitud del punto de estado

La incertidumbre de medida de la temperatura, la presión y la densidad fue evaluada aplicando la ley de propagación de la incertidumbre. Las Tablas 3.1., 3.2. y 3.3. muestran los resúmenes de los cálculos de incertidumbre de cada magnitud.

En el caso de la *temperatura* la mayor contribución a la incertidumbre venía de la incertidumbre de calibración de la propia sonda. Por ello, el uso de una sonda PRT-25 con menor incertidumbre de calibración reduciría la incertidumbre total en temperatura. Además, si se utilizaran dos sondas para la determinación de la temperatura como media de los dos valores, se reduciría igualmente la incertidumbre total en temperatura.

Tabla 3.1. Resumen del cálculo de incertidumbre de la temperatura medida con la sonda PRT-25 Rosemount.

Componente de incertidumbre	Unidad	Estimación	u(xi)	Distribución	Tipo	Coeficiente de sensibilidad	Divisor	$u_i(y)^2$
Incertidumbre de calibración	K	0	$3.0\cdot10^{-3}$	Gausiana	B	1	1	$3.0\cdot10^{-3}$
Lectura	Ω	0	$7.2\cdot10^{-5}$	Gausiana	B	10.5	1	$7.6\ 10^{-4}$
Repetibilidad	K	0	$9.5\cdot10^{-4}$	Gausiana	A	1	1	$9.5\cdot10^{-4}$
Uniformidad	K	0	$4.0\cdot10^{-3}$	Uniforme	B	1	$2\sqrt{3}$	$1.2\cdot10^{-3}$
Deriva	K	0	$1.0\cdot10^{-3}$	Uniforme	B	1	$\sqrt{3}$	$5.8\cdot10^{-4}$
						Incertidumbre estándar (K)		$3.5\cdot10^{-3}$
						Incertidumbre expandida (K) (k=2)		$7.0\cdot10^{-3}$

Tabla 3.2. Resumen del cálculo de incertidumbre de la presión medida con el Paroscientific de rango 20 MPa.

Componente de incertidumbre	Unidad	Estimación	u(xi)	Distribución	Tipo	Coeficiente de sensibilidad	Divisor	Contribución
								MPa
Calibración	MPa	0	$38\cdot10^{-6}p + 1.74\cdot10^{-3}$	Gausiana	B	1	1	$38\cdot10^{-6}p + 1.74\cdot10^{-3}$
Resolución	MPa	0	$1.0\cdot10^{-5}$	Uniforme	B	1	$2\sqrt{3}$	$2.89\cdot10^{-6}$
Repetibilidad	MPa	0	$2.6\cdot10^{-4}$	Gausiana	A	1	1	$2.6\cdot10^{-4}$
Deriva	MPa	0	$1.4\cdot10^{-6}$	Gausiana	B	1	$\sqrt{3}$	$8.1\cdot10^{-7}$
						Incertidumbre estándar (MPa)		$38\cdot10^{-6}p + 1.76\cdot10^{-3}$
						Incertidumbre expandida (k=2) (MPa)		$75\cdot10^{-6}p + 3.52\cdot10^{-3}$

Tabla 3.3. Resumen del cálculo de incertidumbre de la densidad.

Fuente de incertidumbre		Unidad	Estimación	Incertidumbre estándar	Coeficiente de sensibilidad		Grados de libertad	Contribución
$u(m_{S0})$	Masa en vacío	kg	$1.90\cdot10^{-3}$	$2.3\cdot10^{-7}$	$1/V_{S1}$	$7.5\ 10^{4}$	200	$1.7\cdot10^{-2}$
$u(m_{Sf})$	Masa	kg	$-5.27\cdot10^{-3}$	$2.1\cdot10^{-7}$	$1/V_{S1}$	$7.5\ 10^{4}$	800	$1.6\cdot10^{-2}$
$u(V_S)$	Volumen del flotador	m^3	$1.33\cdot10^{-5}$	$5.0\cdot10^{-10}$	ρ/V_{S1}	$\rho\cdot7.5\cdot10^{4}$	∞	$3.75\cdot10^{-5}\rho$
						Incertidumbre estándar ($kg\cdot m^{-3}$)		$2.4\cdot10^{-2} + 3.8\cdot10^{-5}\rho$
						Incertidumbre expandida (k=2) ($kg\cdot m^{-3}$)		$4.7\cdot10^{-2} + 7.6\cdot10^{-5}\rho$

En el caso de la *presión*, la principal contribución a la incertidumbre procedía también de la incertidumbre de calibración del propio transductor. Sin embargo, en este caso, incluso si el transductor de presión se sustituyera por uno nuevo con menor incertidumbre de calibración, la precisión de la lectura a presiones bajas sería muy mala. Por esto se decidió añadir un nuevo transductor que trabajara sólo en el rango

de bajas presiones (0 – 2 MPa), con el fin de mejorar la incertidumbre de las medidas a bajas presiones y, además, corregir la curva de calibración del otro transductor.

Finalmente, en el caso de la *densidad*, las fuentes de incertidumbre procedían de la lectura de la masa del flotador y de la incertidumbre de su volumen. La sustitución de la balanza por una de menor resolución fue descartada desde el principio puesto que la mejora conseguida no justificaba todos los cambios necesarios para adaptar la nueva balanza. Como propuesta se sugirió la sustitución del flotador de titanio por uno de silicio, con igual masa y doble volumen. Al tener éste doble volumen, experimenta una fuerza de empuje del fluido doble, lo cual equivale a un 'aumento de la resolución de la balanza'. Además, con este nuevo flotador los coeficientes de sensibilidad que afectan a cada término de la Tabla 3.3. se verían reducidos a la mitad, con la consecuente reducción de la incertidumbre total de la densidad.

3.2.2. Sustitución del flotador

Como ya se ha mencionado, el flotador de titanio fue sustituido por un nuevo flotador de silicio de igual masa y volumen doble. El volumen y la masa del nuevo flotador fueron calibrados en el Centro Español de Metrología (CEM) y la dependencia del primero con la presión y la temperatura fue determinada en base a las propiedades mecánicas y térmicas del silicio.

3.2.3. Mejora de la incertidumbre de medida de la temperatura

Dos nuevas sondas PRT-25 fueron colocadas diametralmente opuestas en torno a la celda de medida para poder determinar la temperatura del fluido como la media de las dos indicaciones. La sonda PRT-25 Rosemount fue situada a la altura del alojamiento del electroimán, con el fin de estudiar si existían gradientes de temperatura en el eje vertical de la celda.

Se realizó un estudio de la homogeneidad y estabilidad de la temperatura dentro de la celda comparando las indicaciones de cada sonda en todo el rango de temperaturas del densímetro y se determinó la uniformidad de la temperatura dentro de la celda.

Además, se instaló una resistencia externa calibrada de referencia para sustituir a la resistencia interna del puente de resistencias.

3.2.4. Mejora de la incertidumbre de medida de la presión

Se instaló un nuevo transductor de presión para el rango de presiones (0 – 2) MPa, que fue calibrado con una balanza de pesos muertos en el laboratorio de calibración.

3.3. EVALUACIÓN DE LA INCERTIDUMBRE

Tras realizar las mejoras descritas anteriormente se evaluó, de nuevo, la incertidumbre de medida de cada una de las magnitudes del punto de estado con el fin de analizar la reducción alcanzada. La Tabla 3.4. muestra las incertidumbres de cada magnitud antes y después de realizar las modificaciones en el equipo, para su comparación.

Tabla 3.4. Resumen de los resultados del cálculo de la incertidumbre de cada magnitud, antes y después de las modificaciones (k=2).

Magnitud		Unidades	Antes	Después
T	Temperatura	K	$7.0\cdot10^{-3}$	$3.9\cdot10^{-3}$
p	Presión 2 – 20 MPa	MPa	$3.52\cdot10^{-3} + 7.5\cdot10^{-5}p$	$3.52\cdot10^{-3} + 7.5\cdot10^{-5}p$
p	Presión 0 – 2 MPa	MPa	$3.52\cdot10^{-3} + 7.5\cdot10^{-5}p$	$1.8\cdot10^{-4} + 6.0\cdot10^{-5}p$
ρ	Densidad	kg·m^{-3}	$4.7\cdot10^{-2}+7.6\cdot10^{-5}\rho$	$2.3\cdot10^{-2}+1.1\cdot10^{-4}\rho$

Como se puede observar en la tabla, la incertidumbre de medida de la temperatura fue reducida en un 44% gracias a la instalación de las dos nuevas sondas PRT-25.

La incertidumbre de la presión fue reducida en el rango de bajas presiones (0 – 2) MPa en más de un 92%.

Finalmente, la incertidumbre de la densidad fue reducida en más de un 22%, sobre todo a bajas densidades, donde la reducción de la incertidumbre alcanzó casi el 50%.

Los resultados de la evaluación de la incertidumbre de medida fueron comparados con los valores dados por otros autores para similares densímetros con acoplamiento magnético, comprobándose que eran del mismo orden de magnitud.

3.4. VALIDACIÓN EXPERIMENTAL DEL EQUIPO MODIFICADO

Finalmente, previo a la medida de las mezclas binarias objeto de este trabajo, se realizaron medidas de densidad con nitrógeno puro con el fin de comprobar el buen funcionamiento y la precisión del densímetro modificado. La Figura 3.1. muestra las

desviaciones relativas de los datos experimentales con respecto a las densidades calculadas con la ecuación de estado de referencia del nitrógeno de Span et al. (2) , cuya incertidumbre en el rango de temperaturas y presiones tratado es de 0.02%.

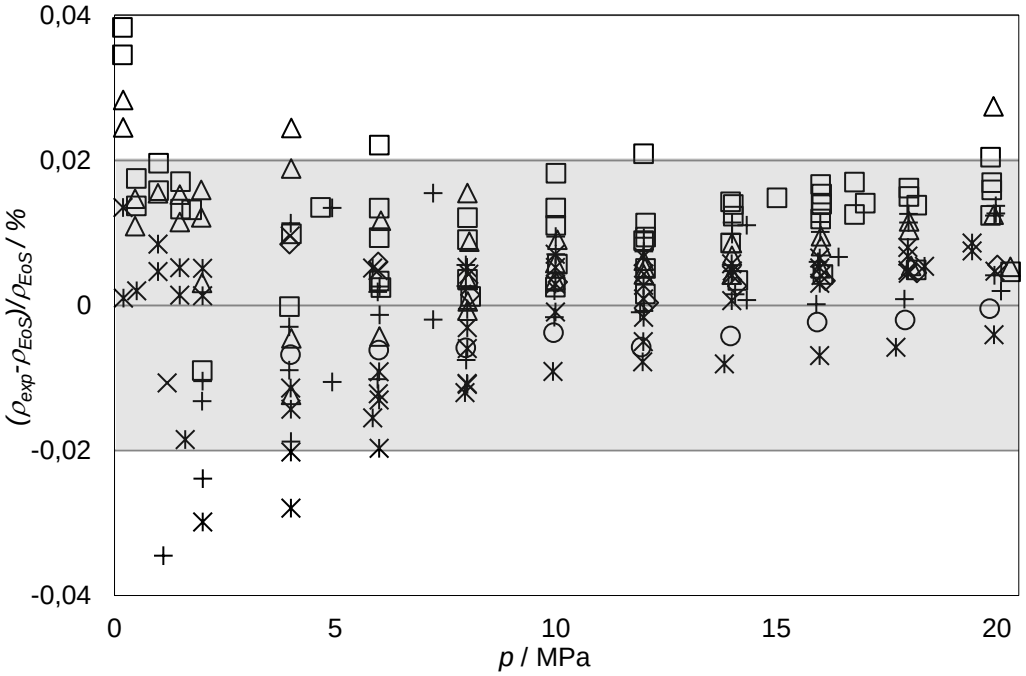

Figura 3.1. Desviaciones relativas de los datos experimentales (p, ρ, T) de las medidas de nitrógeno respecto de la ecuación de estado de referencia del nitrógeno, de Span et al. □ 250 K; ◇ 275 K; △ 300 K; × 325 K; + 350 K; ○ 375 K; ✳ 400 K.

BIBLIOGRAFÍA

1. BIPM, IEC, IFCC, ISO, IUPAC, IUPAP and OIML. Guide to the Expression of Uncertainty in Measurement*. International Organization for Standarization*, 1995.

2. SPAN, R. et al. A Reference Equation of State for the Thermodynamic Properties of Nitrogen for Temperatures from 63.151 to 1000 K and Pressures to 2200 MPa*. Journal of Physical and Chemical Reference Data*, 2000, vol. 29, no. 6. pp. 1361-1401.

CAPÍTULO 4

MEDIDAS DE MEZCLAS DE NITRÓGENO Y DIÓXIDO DE CARBONO

4.1. INTRODUCCIÓN

Las mezclas gaseosas compuestas de nitrógeno y dióxido de carbono han sido ampliamente estudiadas debido a su presencia en diversos procesos industriales, abarcando desde el desarrollo de nuevos combustibles hasta la extracción forzada de petróleo. Sin embargo, de todos los datos de densidad disponibles para mezclas binarias de nitrógeno y dióxido de carbono, alrededor del 70% no fueron utilizados durante el desarrollo de la ecuación de estado GERG-2004 dada su poca fiabilidad o precisión.

En este capítulo se presentan datos experimentales (p, ρ, T) de alta precisión de cuatro mezclas de nitrógeno y dióxido de carbono con composiciones x_{CO_2} = (0.10, 0.15, 0.20, 0.50) a temperaturas entre (250 – 400) K y presiones de hasta 20 MPa. Los datos experimentales fueron comparados con las densidades calculadas con la ecuación de estado GERG-2004 (1) y con los datos publicados por otros autores para mezclas similares. Se presentan también los coeficientes de la ecuación del virial de segundo orden, que fueron ajustados con los datos experimentales presentados.

Las mezclas gaseosas fueron preparadas en el Laboratorio de Materiales de Referencia del Centro Español de Metrología (CEM) mediante el método gravimétrico para la preparación de mezclas de calibración (ISO 6142:2001) (2), a partir de gases de alta pureza. Tras su preparación las mezclas fueron homogeneizadas y sus composiciones fueron comprobadas mediante cromatografía.

4.2. DATOS EXPERIMENTALES Y COMPARACIÓN CON LOS DATOS DE LA LITERATURA

Los datos experimentales de densidad presentados en esta tesis para mezclas de nitrógeno y dióxido de carbono se encuentran en el Apéndice A y las desviaciones relativas de éstos con respecto a la ecuación de estado GERG-2004 se representan en las Figuras 4.1, 4.2., 4.3. y 4.4.

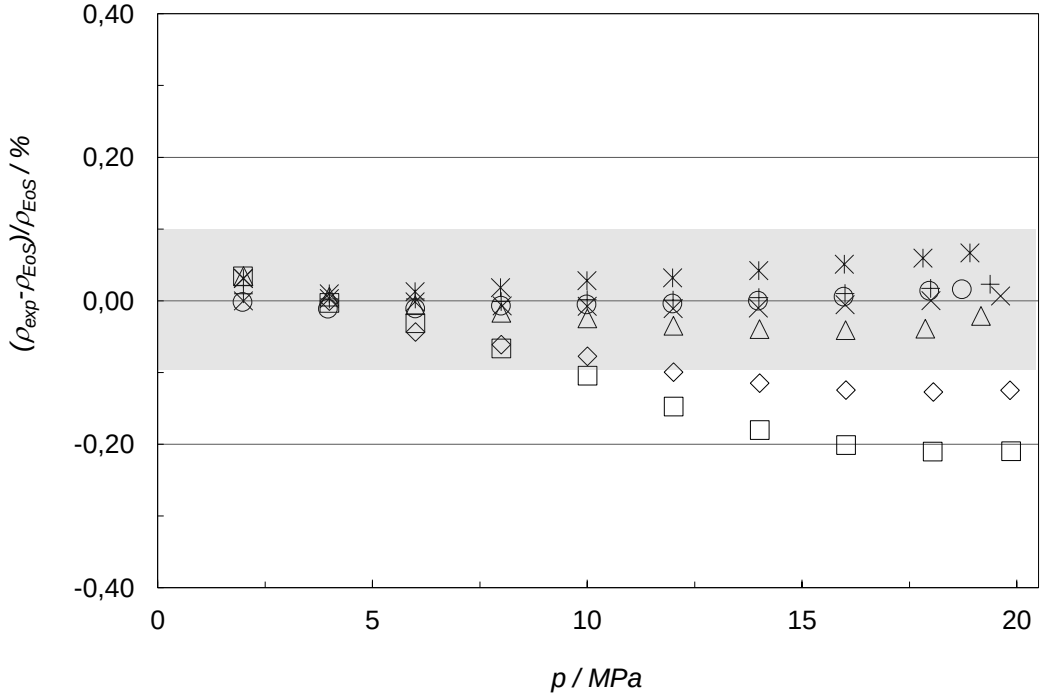

Figura 4.1. Desviaciones relativas porcentuales de los datos experimentales (p, ρ, T) para la mezcla (0.10 CO_2 + 0.90 N_2) respecto de las densidades ρ_{EoS} calculadas con la ecuación de estado GERG-2004, frente a la presión: □ 250 K; ◇ 275 K; △ 300 K; × 325 K; + 350 K; ○ 375 K; ✳ 400 K.

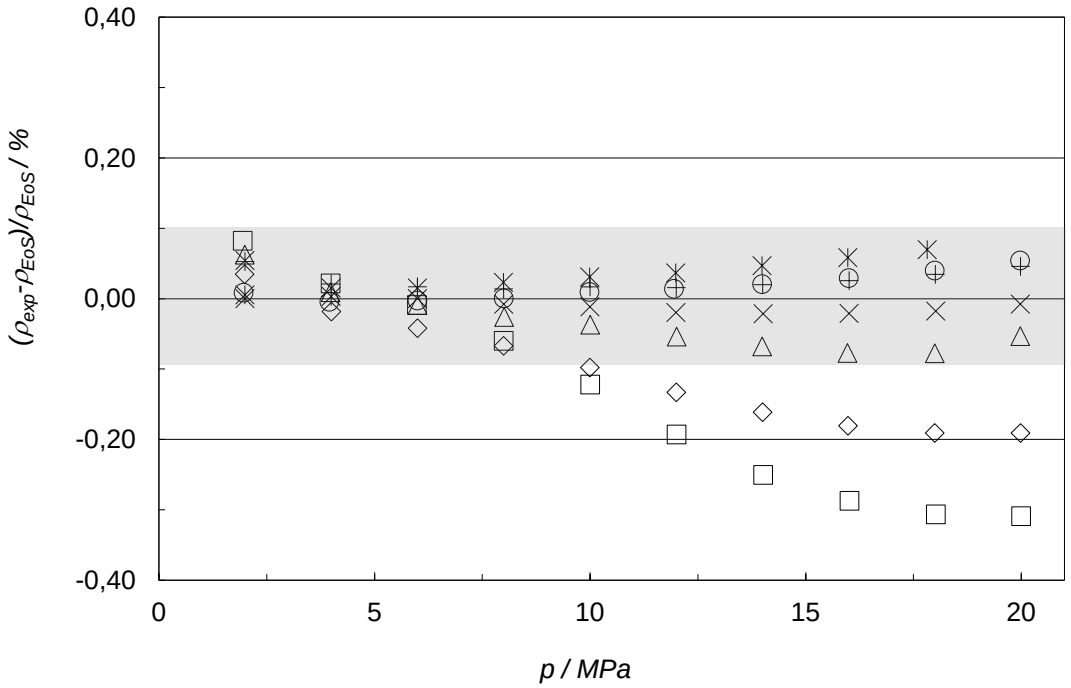

Figura 4.2. Desviaciones relativas porcentuales de los datos experimentales (p, ρ, T) para la mezcla (0.15 CO_2 + 0.85 N_2) respecto de las densidades ρ_{EoS} calculadas con la ecuación de estado GERG-2004, frente a la presión: □ 250 K; ◇ 275 K; △ 300 K; × 325 K; + 350 K; ○ 375 K; ✳ 400 K.

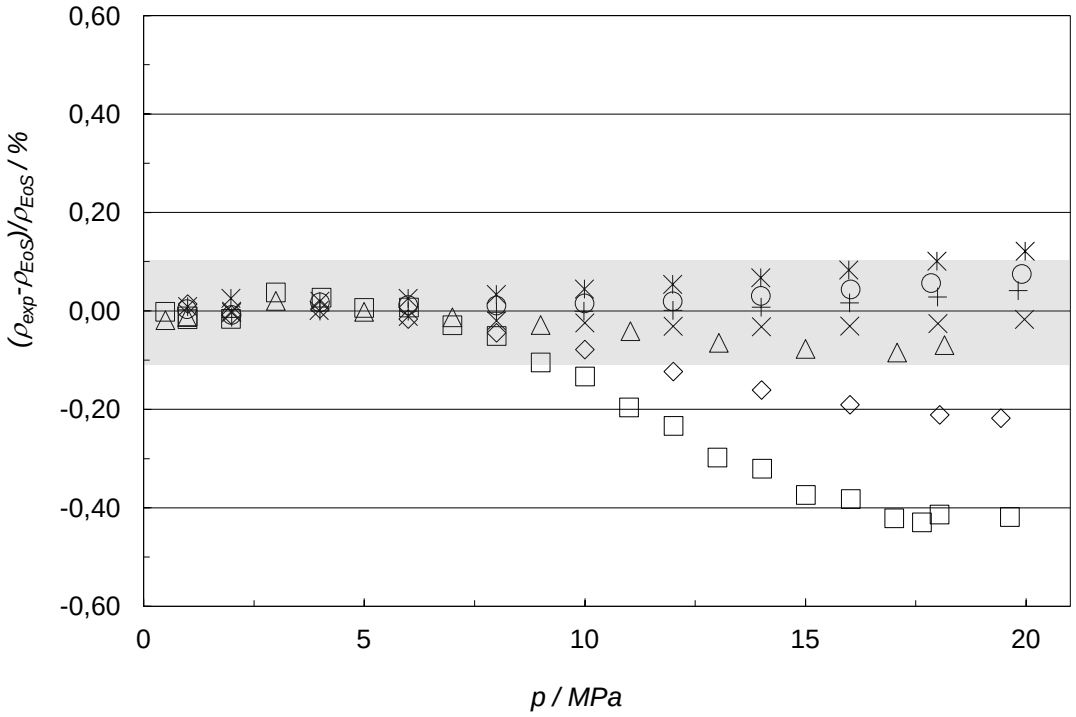

Figura 4.3. Desviaciones relativas porcentuales de los datos experimentales (p, ρ, T) para la mezcla (0.20 CO_2 + 0.80 N_2) respecto de las densidades ρ_{EoS} calculadas con la ecuación de estado GERG-2004, frente a la presión: □ 250 K; ◇ 275 K; △ 300 K; × 325 K; + 350 K; ○ 375 K; ✳ 400 K.

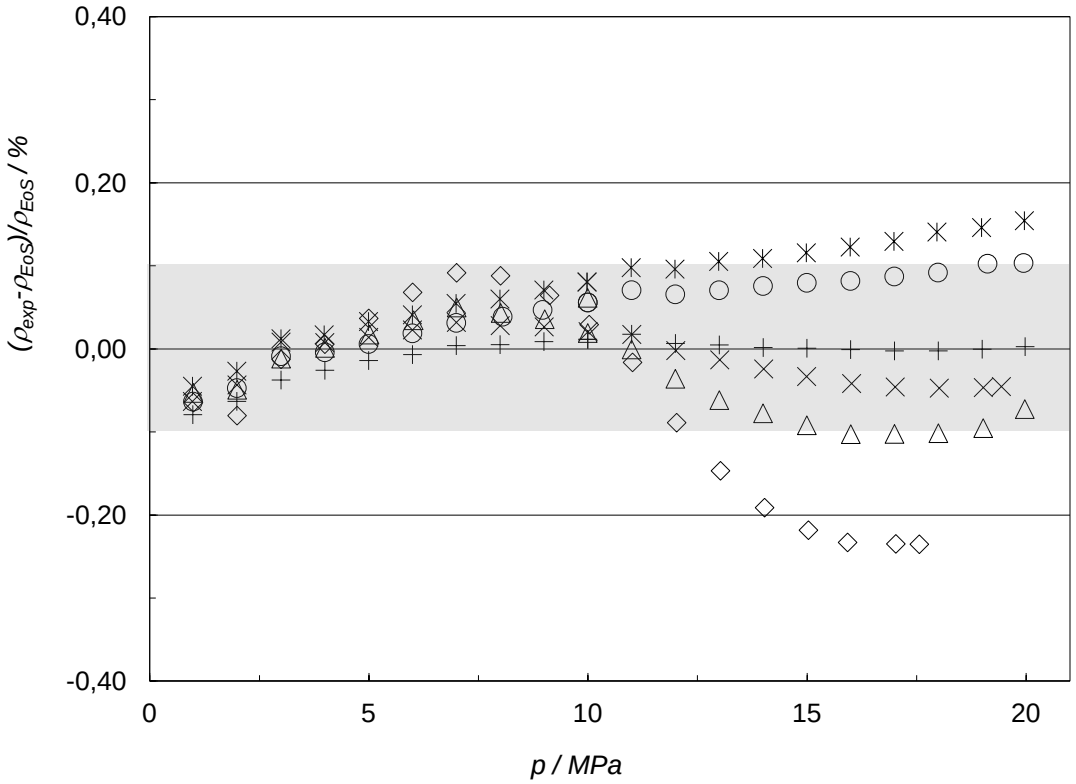

Figura 4.4. Desviaciones relativas porcentuales de los datos experimentales (p, ρ, T) para la mezcla (0.50 CO_2 + 0.50 N_2) respecto de las densidades ρ_{EoS} calculadas con la ecuación de estado GERG-2004, frente a la presión: ◇ 275 K; △ 300 K; × 325 K; + 350 K; ○ 375 K; ✳ 400 K.

Mientras que a presiones menores de 10 MPa las desviaciones relativas de los datos experimentales con respecto a las densidades calculadas mediante la ecuación de estado GERG-2004 se mantuvieron en una banda del 0.1% (coincidente con la incertidumbre estimada de la ecuación para estas mezclas), las desviaciones de las isotermas a bajas temperaturas y a altas presiones mostraron valores inesperadamente altos. Además, se observó que estas desviaciones eran crecientes con el contenido en dióxido de carbono de las mezclas, hasta el punto de que para la mezcla de composición x_{CO_2} = (0.50), las desviaciones correspondientes a las temperaturas T = 300 K y 400 K eran mayores que 0.1% para presiones superiores a 14 MPa.

En la comparación de los datos experimentales de la mezclas de composición x_{CO_2} = (0.10, 0.15) con otros datos de la literatura, se observaron similares desviaciones para altas presiones. Los datos de densidad publicados por Brugge et al. (3) a bajas presiones se mostraron más cercanos a la ecuación de estado debido a que la incertidumbre de los datos de densidad presentados en esta tesis es mayor a bajas presiones. En el caso de la comparación entre resultados para mezclas de composición x_{CO_2} = (0.50) se observaron también similares desviaciones tanto a altas como a bajas presiones.

4.3. COEFICIENTES SEGUNDO Y TERCERO DEL VIRIAL

Los datos experimentales *(p, ρ, T)* de las mezclas estudiadas en este capítulo se utilizaron para ajustar los coeficientes de la ecuación del virial de segundo orden para cada composición e isoterma.

Los valores obtenidos fueron comparados con los coeficientes calculados mediante la ecuación de estado GERG-2004, mostrando mayores divergencias para la mezcla de composición x_{CO_2} = (0.50) a bajas temperaturas, como cabía esperar.

4.4. DISCUSIÓN DE RESULTADOS

Los datos experimentales de densidad presentados en este trabajo para cuatro mezclas de nitrógeno y dióxido de carbono con composiciones x_{CO_2} = (0.10, 0.15, 0.20 y 0.50) en el rango de temperatura (250 – 400) K a presiones de hasta 20 MPa mostraron interesantes resultados a bajas temperaturas y altas presiones.

Mientras que los datos experimentales a bajas presiones mostraban un significante acuerdo con la ecuación de estado GERG-2004, las desviaciones relativas con respecto a ésta de los datos a bajas temperaturas y altas presiones se manifestaron mayores de lo esperado. Se pudo observar que las dichas desviaciones eran crecientes con el contenido en dióxido de carbono de la mezcla y a menores temperaturas, alcanzando valores de hasta 0.40% para la mezcla de x_{CO_2} = (0.20) a 20 MPa y 250 K

Los coeficientes de la ecuación del virial de segundo orden, calculados para cada isoterma y composición, mostraron diferencias importantes, como cabía esperar, con los coeficientes calculados con la ecuación de estado GERG-2004 a bajas temperaturas y para la mezcla de mayor contenido en dióxido de carbono.

BIBLIOGRAFÍA

1. KUNZ, O. et al. The GERG-2004 Wide-Range Reference Equation of State for Natural Gases and Other Mixtures*. GERG Technical Monograph Fortschr*, 2007.

2. ISO 6142:2011 - *Preparation of Calibration Gas Mixtures - Gravimetric Method.* , ISO draft.

3. BRUGGE, H.B. et al. Experimental Cross Virial Coefficients for Binary Mixtures of Carbon Dioxide with Nitrogen, Methane and Ethane at 300 and 320 K*. Physica A: Statistical Mechanics and its Applications*, 1989, vol. 156, no. 1. pp. 382-416.

CAPÍTULO 5

MEDIDAS DE MEZCLAS DE NITRÓGENO Y MONÓXIDO DE CARBONO

5.1. INTRODUCCIÓN

La importancia del estudio de mezclas de nitrógeno y monóxido de carbono viene, no sólo de la relación de sus componentes con los nuevos combustibles alternativos, sino también de la gran escasez de datos de densidad para estas mezclas, de las cuales sólo existen 343 datos experimentales *(p, ρ, T)* para una única composición (x_{CO} = 0.03).

En este capítulo se presentan 223 datos experimentales de densidad de dos mezclas de nitrógeno y monóxido de carbono con composiciones x_{CO} = (0.05, 0.10) en la fase gaseosa a temperaturas entre (250 – 400) K y a presiones de hasta 20 MPa. Los datos experimentales se comparan con las densidades calculadas con la ecuación GERG-2004 (1). Se dan también los coeficientes segundo y tercero del virial ajustados para los datos *(p, ρ, T)* presentados.

Las mezclas gaseosas fueron preparadas en el Centro Español de Metrología (CEM) mediante el método gravimétrico descrito en el Capítulo 4 y sus composiciones fueron comprobadas mediante cromatografía.

Las instalaciones del laboratorio se acondicionaron con un nuevo sistema de extracción de aire y un detector de monóxido de carbono debido a la alta toxicidad de las mezclas estudiadas.

5.2. DATOS EXPERIMENTALES Y COMPARACIÓN CON LOS DATOS DE LA LITERATURA

Los datos experimentales de densidad presentados en esta tesis se encuentran en el Apéndice B y las desviaciones relativas de éstos con respecto a la ecuación de estado GERG-2004 se representan en las Figuras 5.1 y 5.2.

Se pudo observar que todas las desviaciones se encontraban en una banda del 0.05%, mostrando una afinidad significante entre los datos experimentales y la ecuación de estado. Las desviaciones se mostraron independientes de la temperatura y ligeramente mayores para la mezcla de mayor concentración en monóxido de carbono.

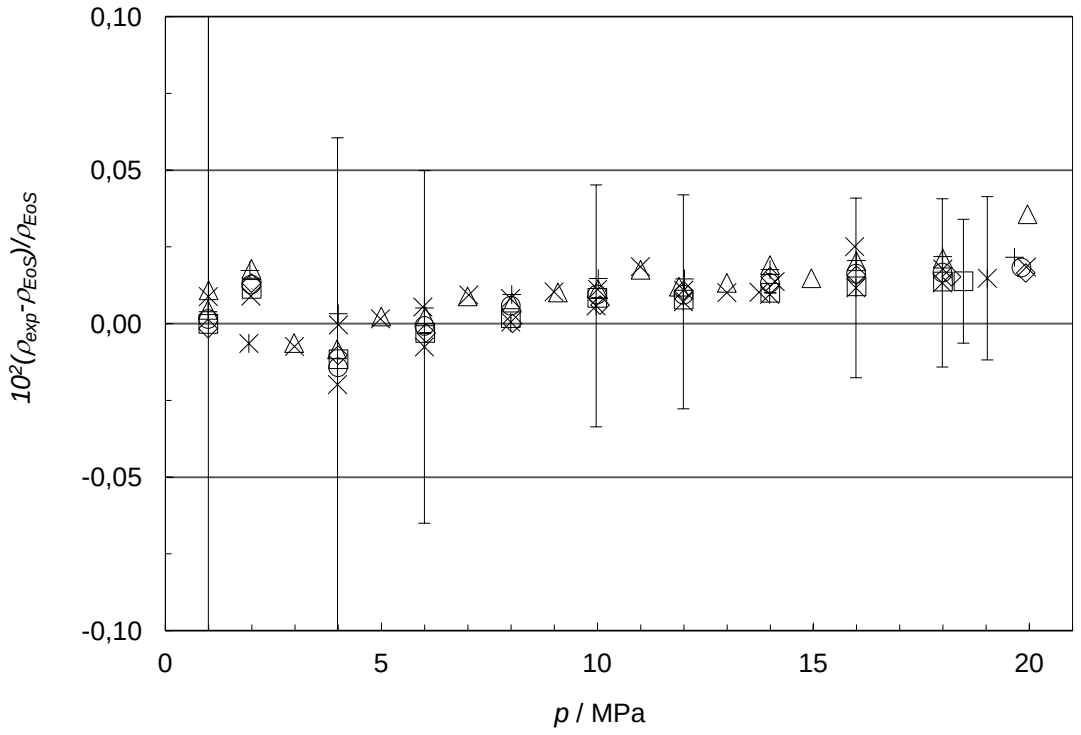

Figura 5.1. Desviaciones relativas porcentuales de los datos experimentales (p, ρ, T) para la mezcla (0.05 CO + 0.95 N_2) respecto de las densidades ρ_{EoS} calculadas con la ecuación de estado GERG-2004, frente a la presión: □ 250 K; ◇ 275 K; △ 300 K; × 325 K; + 350 K; ○ 375 K; ✳ 400 K. Las barras de error representan la incertidumbre expandida (k=2) en densidad.

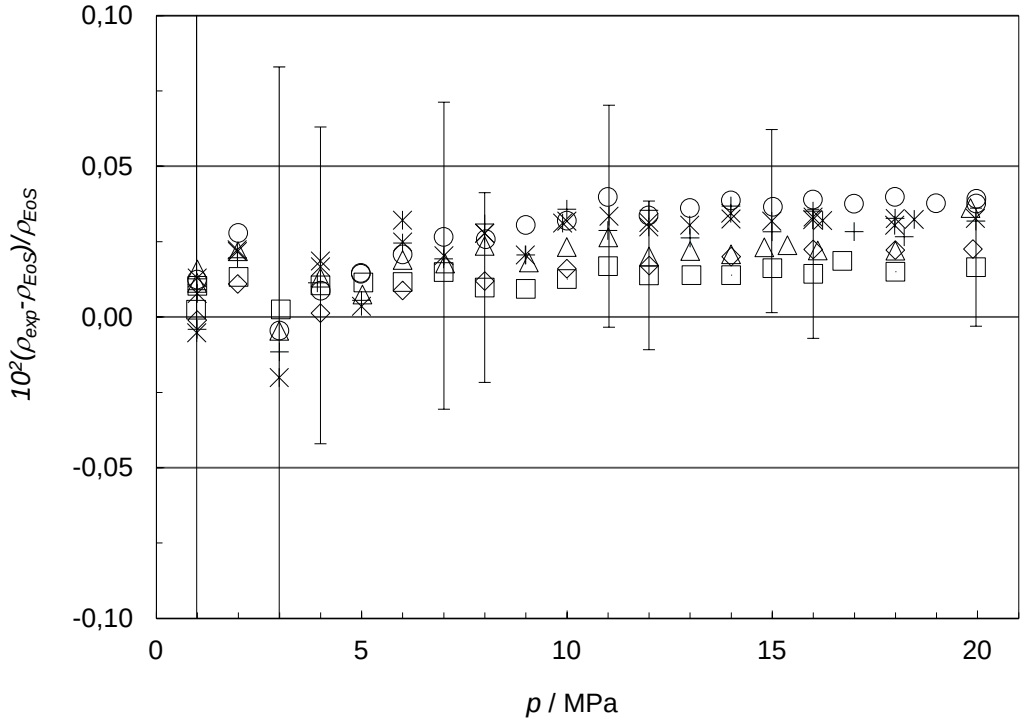

Figura 5.2. Desviaciones relativas porcentuales de los datos experimentales (p, ρ, T) para la mezcla (0.10 CO + 0.90 N_2) respecto de las densidades ρ_{EoS} calculadas con la ecuación de estado GERG-2004, frente a la presión: □ 250 K; ◇ 275 K; △ 300 K; × 325 K; + 350 K; ○ 375 K; ✳ 400 K. Las barras de error representan la incertidumbre expandida (k=2) en densidad.

Esto último también se observó al comparar los datos presentados aquí con las densidades publicadas por Jaeschke et al. (2) para una mezcla con una composición de x_{CO} = (0.03).

5.3. COEFICIENTES SEGUNDO Y TERCERO DEL VIRIAL

Los datos experimentales de densidad presentados se utilizaron para ajustar el segundo y tercer coeficiente de la ecuación del virial de segundo orden, para cada composición e isoterma.

Los valores obtenidos mostraron pequeñas desviaciones respecto de los coeficientes del virial calculados con la ecuación de estado GERG-2004, menores de 0.5 $cm^3 \cdot mol^{-1}$ y de 150 $(cm^3 \cdot mol^{-1})^2$ para B y C, respectivamente.

5.4. DISCUSIÓN DE RESULTADOS

Los datos (p, ρ, T) presentados en este trabajo para dos mezclas de nitrógeno y monóxido de carbono con composiciones x_{CO} = (0.05, 0.10) en el rango de temperatura (250 – 400) K a presiones de hasta 20 MPa se mostraron muy cercanos a las densidades calculadas mediante la ecuación de estado GERG-2004, encontrándose las desviaciones relativas en una banda menor de 0.05%.

Si bien se observó un ligero aumento de las desviaciones relativas en la mezcla con mayor contenido en monóxido de carbono, la alta incertidumbre, en comparación, de dichos datos, impidió confirmar una relación entre la capacidad de estimación de la ecuación de estado y el contenido en monóxido de carbono.

BIBLIOGRAFÍA

1. KUNZ, O. et al. The GERG-2004 Wide-Range Reference Equation of State for Natural Gases and Other Mixtures*. GERG Technical Monograph Fortschr*, 2007.

2. JAESCHKE, M. et al. *The GERG Databank of High Accuracy Compressibility Factor Measurements, GERG Technical Monograph.* , 1997.

CAPÍTULO 6

MEDIDAS DE UNA MEZCLA DE METANO Y DIÓXIDO DE CARBONO

6.1. INTRODUCCIÓN

Las mezclas gaseosas compuestas de metano y dióxido de carbono son las mezclas binarias cuyo comportamiento termodinámico ha sido más estudiado, por detrás de las mezclas de metano con nitrógeno y etano, dado su gran interés en la industria gasista. Sin embargo, a pesar del gran número de datos experimentales de densidad para estas mezclas, menos de la mitad fueron utilizados en el desarrollo de la ecuación de estado GERG-2004, bien por falta de fiabilidad o de precisión.

En este capítulo se presentan datos experimentales de densidad de una mezcla de metano y dióxido de carbono de composición $x_{\mathrm{CO_2}}$ = (0.20) en el rango de temperaturas (250 – 400) K a presiones de hasta 20 MPa. Estas medidas forman parte del proyecto de investigación ENG01 GAS, financiado por EURAMET y la Comisión Europea (1), para la caracterización de combustibles gaseosos alternativos.

La mezcla gaseosa fue preparada en el Centro Español de Metrología (CEM) y su composición fue comprobada mediante cromatografía.

6.2. DATOS EXPERIMENTALES Y COMPARACIÓN CON LOS DATOS DE LA LITERATURA

Los datos experimentales de densidad presentados en este capítulo para una mezcla de metano y dióxido de carbono se encuentran en el Apéndice C y las desviaciones relativas de éstos con respecto a la ecuación de estado GERG-2004 se representan en la Figura 6.1.

Las desviaciones relativas de los datos experimentales con respecto a las densidades calculadas con la ecuación de estado GERG-2004 se encuentran dentro de una banda del 0.05% para temperaturas superiores a 250 K, que es menor que la incertidumbre estimada de la ecuación para la densidad de estas mezclas, que es de un 0.1%. Sin embargo, las desviaciones observadas a 250 K a presiones entre 8 y 12 MPa alcanzaron valores mayores de lo esperado.

Los datos experimentales mostrados para T = 250 K fueron comparados con las densidades medidas por Hwang et al. (2) de una mezcla de composición x_{CO_2} = (0.29) y

a temperaturas T = (280, 260) K, respectivamente. A pesar de que las mezclas diferían en composición de la aquí estudiada, la comparación sirvió para confirmar la existencia de desviaciones relativas inusuales a bajas temperaturas y presiones medias.

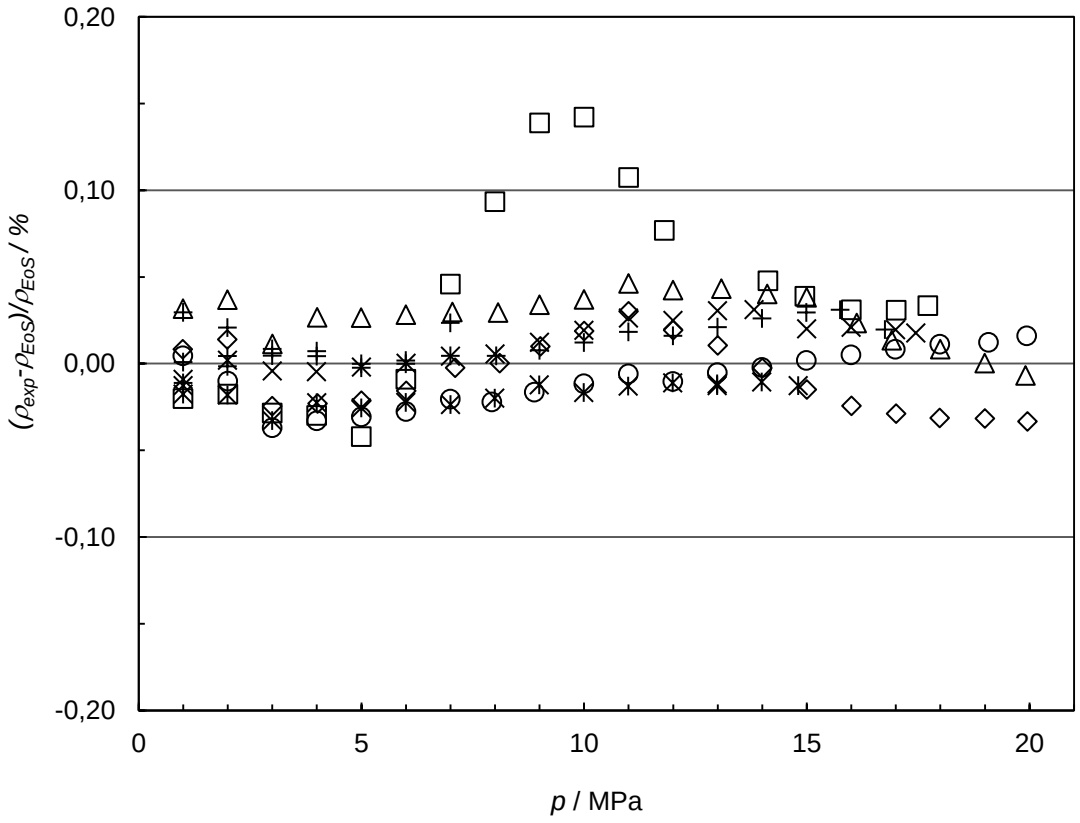

Figura 6.1. Desviaciones relativas porcentuales de los datos experimentales *(p, ρ, T)* para la mezcla (0.20 CO_2 + 0.80 CH_4) respecto de las densidades ρ_{EoS} calculadas con la ecuación de estado GERG-2004, frente a la presión: □ 250 K; ◇ 275 K; △ 300 K; × 325 K; + 350 K; ○ 375 K; ✳ 400 K.

6.3. DISCUSIÓN DE RESULTADOS

Los datos experimentales *(p, ρ, T)* presentados en este capítulo para una mezcla de metano y dióxido de carbono con composición x_{CO_2} = (0.20) en el rango de temperatura (250 – 400) K a presiones de hasta 20 MPa mostraron desviaciones relativas respecto de la ecuación de estado GERG-2004 menores del 0.05% para temperaturas mayores de 250 K. Sin embargo, en la isoterma de 250 K se pudo observar un aumento notable de las desviaciones de los datos experimentales a presiones entre 8 y 12 MPa. Los datos experimentales de esta isoterma fueron comparados con los medidos por otros autores para una mezcla similar a bajas temperaturas, confirmándose la existencia de mayores desviaciones en el rango medio de presión a esas temperaturas.

BIBLIOGRAFÍA

1. HALOUA, F. et al. *Caloric Quantities and Density Measurement of Non-Conventional Gases*, 2011.

2. HWANG, C.A et al. Densities of Carbon Dioxide + Methane Mixtures from 225 K to 350 K at Pressures Up to 35 MPa*. Journal of Chemical and Engineering Data*, 1997, vol. 42, no. 5. pp. 897-899.

CAPÍTULO 7

CONCLUSIONES Y LÍNEAS FUTURAS

7.1. CONTRIBUCIONES CIENTÍFICAS DE LA TESIS

Esta tesis se enmarca en el campo de la determinación de propiedades termodinámicas de mezclas binarias de gases componentes de combustibles alternativos. En este capítulo se enumeran las principales contribuciones científicas de esta tesis y se proponen posibles líneas de investigación a partir del trabajo realizado.

Mejora de la incertidumbre de medida del densímetro de flotador sencillo.

Como se concluyó en el capítulo 3, las incertidumbres de medida de cada magnitud del punto de estado (presión, densidad y temperatura) fueron reducidas satisfactoriamente gracias a las modificaciones realizadas en el equipo. La incertidumbre en temperatura fue reducida de forma significativa en todo el rango de trabajo del densímetro. La incertidumbre de la presión en el rango de bajas presiones fue reducida considerablemente para compensar la pérdida de precisión de la balanza a presiones bajas. Finalmente, la incertidumbre de la densidad fue también reducida, especialmente a bajas densidades. El análisis de incertidumbre se confirmó como una metodología excelente para detectar las principales fuentes de incertidumbre del densímetro y para la mejora efectiva de la incertidumbre de medida. Además, este análisis puede ser también utilizado para futuras mejoras de la incertidumbre.

La automatización del funcionamiento del densímetro de flotador sencillo.

El programa de control y adquisición de datos desarrollado antes de comenzar las medidas de densidad optimizó el tiempo requerido para la medida de cada isoterma y aumentó el número de datos experimentales medidos para cada mezcla. La interfaz de usuario facilita la realización de las medidas gracias al entorno gráfico de programación de VEE Agilent. Además, la flexibilidad del programa permite realizar fácilmente modificaciones para adaptar el programa de control a nuevas condiciones de operación.

Contribución a la actual base de datos de mezclas binarias de componentes presentes en el biogás y otros combustibles gaseosos alternativos.

Los datos de densidad de mezclas binarias de dióxido de carbono y nitrógeno, monóxido de carbono y nitrógeno, y de metano y dióxido de carbono, presentados en esta tesis, contribuyen de forma significativa a la actual base de datos experimentales de densidad de mezclas binarias.

La importancia de los nuevos datos presentados para mezclas de dióxido de carbono y nitrógeno viene de su gran precisión, que confirma las inesperadas desviaciones relativas respecto de la ecuación de estado GERG-2004, observadas a bajas temperaturas y altas presiones. Además, se concluyó que dichas desviaciones eran crecientes con el contenido en dióxido de carbono para las mezclas estudiadas.

Por otro lado, el gran interés de los nuevos datos de densidad de mezclas de monóxido de carbono y nitrógeno se basa en la importante falta de datos fiables para estas mezclas. Los nuevos datos publicados en esta tesis extienden el rango de temperaturas de los datos de densidad existentes previamente para estas mezclas, y corresponden a dos nuevas composiciones.

Finalmente, los datos experimentales de densidad presentados para una mezcla de metano con dióxido de carbono contribuyen a la base de datos con datos de alta calidad. Estos datos experimentales se mostraron en acuerdo con la ecuación de estado, exceptuando los datos medidos a bajas temperaturas y presiones medias, que mostraron grandes desviaciones.

Chequeo de la capacidad de estimación de la ecuación de estado de referencia para gas natural y otras mezclas relacionadas

La capacidad de estimación de la ecuación de estado GERG-2004, cuyas funciones de partición y parámetros de mezcla fueron ajustados con los datos experimentales existentes hasta la fecha, se probó con los nuevos datos experimentales de las mezclas estudiadas en esta tesis. Como ya se ha mencionado previamente, aunque la ecuación mostró una estimación muy buena de las densidades de mezclas de monóxido de

carbono y nitrógeno, se observó que las densidades estimadas en el caso de las mezclas de dióxido de carbono y nitrógeno diferían significativamente de los datos experimentales a temperaturas bajas y presiones altas.

7.2. LÍNEAS DE INVESTIGACIÓN FUTURAS

El trabajo presentado en esta tesis abre las puertas a futuras líneas de investigación, puesto que éste empezó como la continuación de un estudio previo realizado con el densímetro, y sienta las bases para nuevas líneas de trabajo en la determinación de densidades de mezclas gaseosas relacionadas con los combustibles alternativos. Como ejemplo, el rango de trabajo de densímetro puede ampliarse y la precisión de sus medidas puede ser aun mejorada. Además, existe una falta de datos experimentales de densidad de mezclas binarias que contengan componentes de combustibles alternativos. En esta sección se exponen algunas de las líneas inmediatas para una continuación de esta tesis.

Ampliación del rango de de trabajo en temperaturas del densímetro

El rango de trabajo en temperaturas del densímetro de flotador sencillo abarca desde los 250 K hasta los 400 K. El límite superior de este rango viene condicionado por las máximas temperaturas admitidas por los materiales utilizados en la celda de medida, el aislamiento y el de las conexiones de las sondas PRT-25. A pesar de que la ampliación de este límite superior supondría tan sólo cambios mínimos en el equipo, ésta es de poco interés dada la relativamente amplia disponibilidad de datos experimentales a temperaturas altas. Sin embrago, el límite inferior en temperatura del densímetro está condicionado principalmente por la capacidad refrigeradora del baño termostático utilizado como termostatizador primerio de la celda de medida. Por ello, la sustitución de este baño termostático por otro con mejores características técnicas podría ampliar el rango de trabajo del densímetro a bajas temperaturas. Esta modificación sería de gran interés puesto que muchos de los datos experimentales de densidad de gases están disponibles para temperaturas mayores de 260 K, lo cual indica que hay una gran falta de datos a menores temperaturas. Bajo esta modificación del rango de trabajo del densímetro sería necesario tener en cuenta dos consideraciones: la disponibilidad de un fluido refrigerador para el baño termostático

capaz de operar en el nuevo rango de temperaturas extendido, y la posibilidad de que se produzcan condensaciones parciales de algunos gases a las temperaturas más bajas.

Reducción de la incertidumbre de medida

Una de las conclusiones obtenidas tras realizar el análisis de incertidumbre para el densímetro fue que el volumen del flotador era la principal fuente de incertidumbre a altas densidades. El volumen del flotador, calibrado en el Centro Español de Metrología (CEM), tiene una incertidumbre relativamente alta. Distintos autores han conseguido valores menores de la incertidumbre del volumen del flotador mediante otros métodos de calibración. Por esta razón, una nueva calibración del volumen del flotador aumentaría la precisión de los datos experimentales de densidad a altas densidades, lo cual sería de gran interés si nuevas mezclas de mayor peso molecular fueran estudiadas.

El error en la transmisión de la fuerza inducido por el efecto del fluido no fue considerado en ninguna de las medidas publicadas en esta tesis dado que su valor era despreciable respecto de la incertidumbre en densidad de los datos experimentales. Sin embargo, si fueran estudiadas nuevas mezclas gaseosas con una alta susceptibilidad magnética o la incertidumbre de medida en densidad se redujera, el término del error en la transmisión de la fuerza debido al comportamiento magnético del fluido cobraría peso. En este caso, el efecto específico del fluido debería ser evaluado para corregir los datos experimentales de densidad.

Preparación in situ de mezclas gaseosas

Desde el punto de vista de la accesibilidad a nuevas mezclas binarias o ternarias para las medidas de densidad, el desarrollo de un sistema para la preparación in situ de mezclas gaseosas sería de gran interés. Los pros y contras del nuevo sistema deberían ser evaluados, puesto que a pesar de que la incertidumbre en la composición de las mezclas sería mayor que la de las mezclas estudiadas en esta tesis y la nueva instalación requeriría de una inversión inicial alta, el nuevo sistema permitiría preparar mezclas de cualquier composición deseada de forma rápida.

Medida de nuevas mezclas binarias y ternarias

Como se mencionó al comienzo de esta sección, la línea de investigación más importante sería la contribución a la actual base de datos de propiedades termofísicas con nuevos datos experimentales de densidad de alta precisión de mezclas binarias y ternarias compuestas de componentes mayoritarios de combustibles alternativos. Respecto a esta línea ya se mencionó, en el capítulo 1, la falta apreciable de datos de mezclas de monóxido de carbono y dióxido de carbono y de mezclas con oxígeno.

Una línea de investigación interesante sería la medida de mezclas ternarias de componentes presentes tanto en biocombustibles como en gas natural. En este caso se debería prestar especial atención a la incertidumbre en composición de cada componente ya que ésta sería una de las principales fuentes de incertidumbre de la densidad.

Mezclas sintéticas de biogás

Siguiendo la propuesta de investigación anterior, el número de componentes se podría extender hasta las mezclas multicomponente para simular la composición real de muestras de biogás o gas de síntesis. El estudio de estas mezclas tendría el principal objetivo de evaluar la ecuación de estado cuando ésta predice las propiedades de mezclas de varios componentes. El uso de mezclas sintéticas simulando biogás o gas de síntesis estaría justificado por la posible afectación del densímetro producida por impurezas de las muestras reales.